



**Design of Novel Tetrahedrally Chelating Ligands for
the Selective Extraction of Zinc.**

by

Andrew G. Smith

A thesis submitted to

The University of Edinburgh

for the Degree of Doctor of Philosophy

in the Faculty of Science and Engineering.

Department of Chemistry

The University of Edinburgh

The Joseph Black Building

Kings Buildings

EH9 3JJ

March 2000



Contents

	Page
Abstract.....	xi
Preface and Declaration.....	xiii
Acknowledgements.....	xiv
Abbreviations	xv
List of compounds.....	xix

Chapter 1 Introduction.	Page
1.1 Objectives	2
1.2 Zinc production.....	4
1.2.1 Raw materials	4
1.2.2 Early history of zinc isolation.....	6
1.2.3 Origins of zinc smelting.....	6
1.2.4 Industrial production of zinc.....	7
1.2.5 Uses and consumption of zinc.....	7
1.3 Current zinc extraction technology.....	9
1.3.1 Pre-treatment of raw materials.....	10
1.3.2 Fossil fuel reduction and distillation.....	11
1.3.3 Roast/leach process with electrowinning	15
1.3.4 Zinc electrolysis.....	19
1.3.5 Comparison of the two processes.....	22
1.4 Hydrometallurgical solvent extraction (SX).....	25
1.4.1 Copper recovery by solvent extraction.....	26

1.4.1.1	Extraction circuit	26
1.4.1.2	Mass balance	28
1.4.1.3	Commercial copper extractants	30
1.4.1.4	Advantages of solvent extraction	33
1.4.2	Zinc recovery by solvent extraction	34
1.4.2.1	Extractant criteria	35
1.4.2.2	Zinc selective extractants	36
1.5	Summary.....	43
1.6	References.....	44

Chapter 2	Ligand design.	Page
2.1	Objectives	48
2.2	Factors effecting the stability of metal-ion complexes.....	48
2.2.1	Nature of the metal ion: oxidation state and electron configuration	50
2.2.2	Nature of the ligand: hard-soft / acid-base theory	54
2.2.3	Chelate effect.....	55
2.3	The role of zinc(II) ions in biology.....	61
2.3.1	Catalytic roles	63
2.3.1.1	Human carbonic anhydrase (II).....	63
2.3.1.2	Carboxypeptidase A and thermolysin.....	64
2.3.1.3	Alkaline phosphatase.....	65
2.3.1.4	Alcohol dehydrogenase	66
2.3.2	Structural roles.....	67

2.3.2.1	Superoxide dismutase.....	67
2.3.2.2	Zinc fingers.....	68
2.3.3	Summary.....	69
2.4	Cambridge crystallographic database survey (CSD).....	70
2.4.1	Description of search procedure.....	72
2.4.2	Zinc(II) complexes in the CSD.....	73
2.4.2.1	Four coordinate zinc complexes.....	75
2.4.2.2	Five coordinate zinc complexes.....	78
2.4.2.3	Six coordinate complexes.....	81
2.4.3	Nickel(II) complexes in the CSD.....	82
2.4.4	Iron(III) complexes in the CSD.....	84
2.4.5	Summary of the CSD survey.....	87
2.5	Conclusions.....	89
2.6	References.....	92

Chapter 3	Pyridone chemistry.	Page
3.1	Introduction.....	96
3.2	Preparation and characterisation of N-benzyl-3-hydroxy- 2(1H)-pyridinethiones and pyridinones.....	100
3.2.1	NMR Spectroscopy.....	103
3.2.2	Mass spectroscopy.....	105
3.3	Preparation and characterisation of metal complexes.....	105
3.3.1	NMR spectroscopy.....	106
3.3.2	Mass spectroscopy.....	108

3.3.3	Electronic absorption spectroscopy.....	109
3.4	Crystallographic characterisation	110
3.4.1	Ligands	114
3.4.1.1	N-Benzyl-3-hydroxy-2(1H)-pyridinethione.....	114
3.4.1.2	N-Benzyl-3-hydroxy-2(1H)-pyridinone.....	116
3.4.1.3	Comparison of ligands.....	119
3.4.2	Metal complexes.....	120
3.4.2.1	Bis(N-benzyl-3-hydroxy-2(1H)-pyridinethionato) zinc(II).....	120
3.4.2.2	Bis(N-benzyl-3-hydroxy-2(1H)-pyridinethionato) copper(II).....	125
3.4.2.3	Bis(N-benzyl-3-hydroxy-2(1H)-pyridinethionato) nickel(II).(methanol)	127
3.4.2.4	Tris(N-benzyl-3-hydroxy-2(1H)-pyridinethionato) cobalt(III).bis(methanol)	128
3.4.2.5	Bis(N-benzyl-3-hydroxy-2(1H)-pyridinonato) copper(II).bis(ethanol).....	130
3.4.2.6	Poly((bis(N-benzyl-3-hydroxy-pyridinonato)tetra- (acetato)tri-zinc(II)).....	134
3.5	Comparison of pyridinethionato complexes.....	137
3.6	Comparison of pyridinethionato and pyridinonato copper complexes	140
3.7	Conclusions.....	140
3.8	Experimental.....	142

3.8.1	Pyridinethione and pyridinone ligands.....	142
3.8.2	Complexes of pyridinethiones and pyridinones.....	146
3.9	References.....	153

Chapter 4 Bidentate thiopyrazolone chemistry. Page

4.1	Introduction.....	157
4.2	Preparation and characterisation of pyrazol-5-thiones and pyrazol-5-ones.....	161
4.2.1	NMR spectroscopy.....	167
4.2.2	Mass spectroscopy.....	174
4.3	Preparation and characterisation of metal complexes.....	174
4.3.1	NMR spectroscopy.....	176
4.3.2	Mass spectroscopy.....	176
4.4	Crystallographic characterisation.....	177
4.4.1	Ligands.....	177
4.4.1.1	Comparison of 4- <i>t</i> -butyl, 4-cyclohexyl, 4- <i>t</i> - butylphenyl and 4-nitrophenylaldenamine-1-phenyl-3- methyl-pyrazol-5-thiones.....	178
4.4.2	Metal complexes.....	186
4.4.2.1	Structural effects of <i>t</i> -Bu, Ph and 4- <i>t</i> -BuPh imino substituents on the zinc(II) complexes.....	193
4.4.2.2	Structural effects of <i>t</i> -Bu, Ph and 4- <i>t</i> -BuPh imino substituents on the cobalt(II) complexes.....	202

4.4.2.3	Bis(1-phenyl-3-methyl-4-phenylaldimino-pyrazol-5-thiolato)nickel(II)	206
4.4.2.4	Bis(1-phenyl-3-methyl-4-(4- <i>t</i> -butylphenylaldimino)-pyrazol-5-ato)zinc(II)	212
4.4.2.5	Continuous symmetry measures.....	215
4.5	Solvent extraction of Zn(II), Co(II), Ni(II) and Cu(II).....	218
4.5.1	Factors affecting the “S-curve” shape	219
4.5.1.1	Solubility determination of zinc(II) complexes.....	220
4.5.1.2	Metal hydrolysis at high pH.....	224
4.5.2	Stoichiometry of the extracted metal species	227
4.5.3	Effect of the ligand substituents on the extraction selectivity and “strength”	231
4.5.3.1	Extractant acidity.....	235
4.5.3.2	Extractant solubility.....	237
4.5.3.3	Coordination geometry and stability of metal complexes.....	239
4.6	Preparation and characterisation hydrazono-pyrazol-5-thiones ..	241
4.6.1	NMR spectroscopy	242
4.6.2	Mass spectroscopy.....	244
4.7	Preparation and characterisation of metal complexes	244
4.7.1	NMR spectroscopy	245
4.7.2	Mass spectroscopy.....	245
4.8	Crystallographic characterisation	245

4.8.1	Bis(1-phenyl-3-methyl-4-phenylazo-pyrazol-5-thiolato) zinc(II).....	245
4.9	Solvent extraction of Zn(II), Co(II), Ni(II) and Cu(II) with 1-phenyl-3-methyl-4-phenylazo-pyrazole-5-thiones.....	250
4.10	Conclusions.....	252
4.11	Experimental.....	254
4.11.1	Solvent extraction.....	254
4.11.1.1	Single metal extraction.....	255
4.11.1.2	Multi-metal extraction.....	257
4.11.2	Synthesis.....	258
4.11.2.1	Pyrazol-5-thione and pyrazol-5-one ligands	258
4.11.2.2	Complexes of pyrazol-5-thiones and pyrazol-5-ones...	268
4.11.2.3	Hydrazono-pyrazol-5-thiones ligands	273
4.11.2.4	Complexes of hydrazono-pyrazol-5-thiones	277
4.12	References.....	279
 Chapter 5 Tetradentate thiopyrazolone chemistry.		Page
5.1	Introduction.....	286
5.2	Preparation and characterisation of pyrazol-5-thiones	287
5.2.1	NMR spectroscopy	289
5.2.1	Mass spectroscopy.....	290
5.3	Preparation and characterisation of metal complexes	290
5.3.1	NMR spectroscopy	292
5.3.2	Mass spectroscopy.....	292

5.4	Crystallographic characterisation	293
5.4.1	Ligands	293
5.4.1.1	Comparison of <i>trans</i> -1,2-cyclohexyl and n-butyl bridging groups	293
5.4.2	Complexes	299
5.4.2.1	(Bis(1,3-dimethyl-pyrazol-5-thiolato)-4- <i>o</i> - xylyldialdimino)zinc(II)	300
5.4.2.2	n-Butyl and <i>o</i> -xylyl bridged nickel(II) complexes	303
5.4.2.3	Comparison of nickel(II) complexes	309
5.5	Conclusions.....	311
5.6	Experimental.....	312
5.6.1	Pyrazol-5-thiones.....	312
5.6.2	Complexes of pyrazol-5-thiones.....	318
5.7	References.....	322

Chapter 6	Page
Conclusions and further work.....	325

Appendix	Page
I Magnetic Susceptibility of [Fe(5-H) ₃] (12)	329
II Chemicals and instrumentation.....	332
III Crystallographic data for N-benzyl-3-hydroxy-2(1H)- pyridinethione and N-benzyl-3-hydroxy-2(1H)-pyridinone and their metal complexes.....	334

IV	Crystallographic data for bidentate pyrazol-5-thiones and their metal complexes	338
V	Crystallographic data for tetradentate pyrazol-5-thiones and their metal complexes.....	345
VI	Solvent extraction data	348
	References.....	365

Abstract

Conventional methods for the recovery of zinc from primary and secondary sources have economical and environmental drawbacks. An alternative approach to the recovery of zinc could be based on a hydrometallurgical process using a leach-solvent extraction-electrowinning flowsheet analogous to that which has proven very successful for copper recovery. A key requirement for such a new process is the development of a reagent capable of selectively extracting Zn^{2+} ions at low pH (< 2) away from impurities, primarily Fe^{3+} . This thesis describes the design, synthesis and evaluation of such reagents.

The technology of existing zinc-recovery processes and the chemistry of two zinc extractants, a dithiophosphoramidate and di(2-ethylhexyl)phosphoric acid are summarised in Chapter 1. Chapter 2 reviews the coordination chemistry of zinc and proposes that in order to maximise the stability of the zinc complexes and to discriminate against other transition metal ions, ligands which favour tetrahedral geometry will be required.

The influence of donor atom types on the stability of zinc complexes is considered in Chapter 3, based on a series of 3-substituted pyridin-2-ones. A detailed study of N-benzyl-3-hydroxy-2(1H)-pyridinethione and N-benzyl-3-hydroxy-2(1H)-pyridinone, with $[\text{OS}]^-$ and $[\text{O}_2]^-$ donor sets respectively, and their complexes with Zn^{2+} , Cu^{2+} , Ni^{2+} , Co^{3+} and Fe^{3+} reveals that a range of coordination geometries can be achieved but that the rigidity of the chelate arms forces a chelate angle close to 90° , indicating the ligands preference for O_h or D_{4h} geometries. This ligand type, based on a 5-membered chelate ring, is unlikely to show selectivity for Zn^{2+} ions.

A range of bidentate monoanionic ligands with [NS]⁻ donor sets derived from 4-imino-substituted 5-thiopyrazolones are described in Chapter 4. The ligands show keto-enol tautomerism and ¹H NMR spectroscopy indicates that the ligands adopt the enamine-thione tautomer in solution. The crystallographic study of four ligand derivatives and nine complexes with Zn²⁺, Co²⁺ and Ni²⁺ reveals the structural influence of the imino substituent. The zinc and cobalt complexes are isostructural and display a geometry approaching that for a perfect tetrahedron, whereas the nickel complex is highly distorted from its preferred D_{4h} geometry. The steric volume of the imino substituents greatly affects the stability and geometry of the complexes. The solvent extraction strength follows the order Cu²⁺ > Zn²⁺ > Co²⁺ > Ni²⁺ with a range of different substituted ligands and disagrees with the Irving-Williams stability series but rather correlates with the propensity of the metal ions to adopt a tetrahedral geometry. Chapter 5 describes a number of di-anionic tetradentate thiopyrazolone derivatives (H₂L) with a predisposition towards tetrahedral geometry, that were prepared to further increase the stability on complexation to zinc.

Pyrazolone based extractants have been shown to have potential for the recovery of divalent metals from sulfate media, but no candidates examined to date have sufficient “strength” to function in a circuit analogous to the existing copper recovery process.

Acknowledgements

During the last three years spent at Edinburgh University many people have made valuable contributions to my project and more recently in writing my thesis. I would like to thank my supervisor Professor Peter Tasker for the help and numerous discussions without which my time at Edinburgh would have undoubtedly been much harder. I am also in great debt to Dr. David White whose endless ideas and knowledge have contributed enormously my development as a chemist. In addition I would like to thank Dr. Domenico Cupertino, Mr. John Cambell, Mrs. Sue Owens and Dr. Aid Bisson, at Avecia, for their advice and assistance during the 3 months spent in the laboratories at Blackley. I would also like to thank the current and ex-members to the group especially Dr. Jeremy Holmes and Miss Lucy Emeleus who were there right back at the beginning and Dr. Paul Lovett whose amusing jokes may never be repeated. In addition, I offer my thanks again to Dr. David White and to Drs Tim Higgs and Hamish Millar for advise and proof reading my thesis.

I am extremely grateful to Mr. John Millar and Mr. Wesley Kerr for the NMR analysis, to Mr. Alan Taylor and Mr. Harry Mackenzie for the mass spectrometry, to Miss Lorna Eades for the elemental analysis and to Dr. Simon Parsons, Dr. Steve Harris and Mr. Andy Parkin for the numerous crystal structure determinations.

I would like to thank Avecia for funding my PhD and their financial assistance that gave me the opportunity to present a poster at the American Chemical Society Conference held in Boston, September 1998.

Finally, and most importantly, I would especially like to thank Lorna for always being there and making the last four years very special.

Abbreviations

2-EtHex	2-ethylhexyl
2,3-Hopo	2,3-dihydroxypyridine
β	complex formation constant
δ	chemical shift
Δ	delta
Δ_o	octahedral crystal field splitting parameter
ϵ	extinction coefficient
ϕ	trigonal twist angle
Λ	lambda
θ (X-ray)	θ circle diffraction angle
θ	dihedral angle
θ_c	cone angle
λ	wavelength
μ_{so}	spin only magnetic moment
μ (X-ray)	absorption coefficient
μm	micrometre
μmol	micro molar
ν (IR)	wavenumber
χ	electronegativity
%	percentage
°	degree
°C	degree Centigrade
$\Delta\rho$ (X-ray)	residue electron density in difference electron density map
ΔH	heat of formation
ΔH°	standard heat of formation
ΔG°	Gibbs free energy
ΔS°	standard entropy
Å	Angstrom
AAS	Atomic Absorption Spectrometer

av.	average
biph	2,2'-biphenyl
bz	benzyl
br	broad
B.P.	boiling point
<i>ca.</i>	<i>circa</i>
CEN	centriod
CFSE	crystal field stabilisation energy
ch.	chapter
CIF	computer information file
<i>cis</i>	<i>cisoid</i>
cm ⁻¹	reciprical centimetre
cm ³	centimetre cubed
CSD	Cambridge Structural Database
CSM	continuous symmetry measure
Cy	cyclohexyl
d	doublet
D	distribution coefficient
D _c	crystal density
d ₆ -DMSO	deuterated dimethylsulfoxide
D _{4h}	square planar geometry
dd	doublet of doublets
decomp.	decomposed
dmbiph	2,2'-(6,6'-dimethyl)biphenyl
dm ³ mol ⁻¹ cm ⁻¹	decimetre cubed per mole per centimetre
DMF	dimethylformamide
d.p.	decimal places
E ^o	standard electrode potential
ed.	editor
edn.	edition
EIMS	electron impact mass spectroscopy
e.w.	electron withdrawing

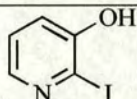
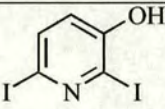
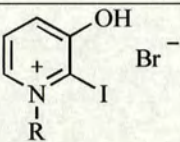
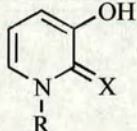
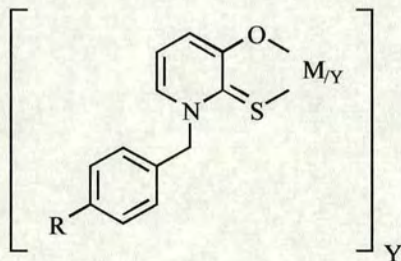
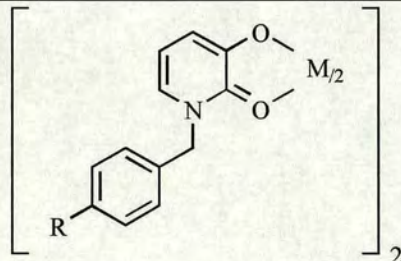
FABMS	fast atom bombardment mass spectroscopy
g	gram
g l ⁻¹	grams per litre
h	hour
Hal	halogen
HL	protonated mono-anionic ligand
H ₂ L	protonated di-anionic ligand
Hz	Hertz
I > 2σ(I)	intensity is greater than two times the standard deviation of the intensity peak
ICP-OES	Inductively Coupled Plasma-Optical Emission Spectrometer
<i>i</i>	<i>iso</i>
IR	infra-red spectroscopy
³ J _{HH}	three bond proton coupling constant
⁴ J _{HH}	four bond proton coupling constant
JK ⁻¹ mol ⁻¹	Joules per Kelvin per mole
K _a	acid dissociation constant
K _{extract}	extraction equilibrium constant
KDa	kilo Daltons
kg	kilogram
kJmol ⁻¹	kilo Joules per mole
L	ligand
Lit.	literature
m (IR)	medium
m (NMR)	multiplet
mm	millimetre
<i>m</i>	meta
mol	moles
mmol	milli moles
<i>m/z</i>	mass per unit charge
M	molar
<i>M</i>	molecular weight

max. dev.	maximum deviation
MJ	mega Joules
MJ kg ⁻¹	mega Joules per kilogram
ML ₂	bis bidentate metal complex
MHz	mega Hertz
min	minute
M.P.	melting point
nm	nanometre
NMR	nuclear magnetic resonance
no.	number
<i>o</i>	ortho
O _h	octahedral geometry
<i>p</i>	para
pH	negative logarithm (base ten) of the hydrogen ion concentration
pH _½	pH at which half the metal is extracted into the organic phase
pK _a	negative logarithm (base ten) of the acid dissociation constant
pp.	pages
ppm	parts per million
q	quartet
<i>R</i> (X-ray)	residual factor
<i>R</i>	Faraday constant
r.m.s	root mean square
R _{int}	independent reflections
s (IR)	strong
s (NMR)	singlet
s ⁻¹	per second
<i>sec</i>	secondary
sh	shoulder
SHE	standard hydrogen electrode
S _N 1	unimolecular nucleophilic substitution
t	triplet

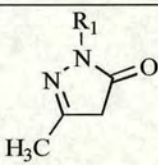
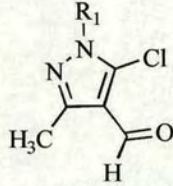
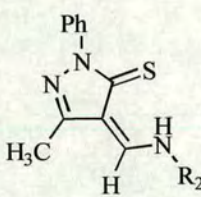
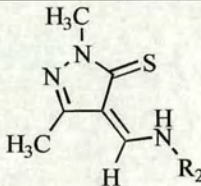
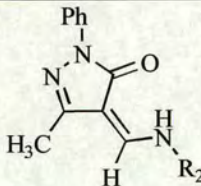
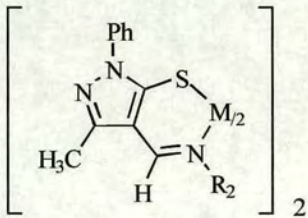
<i>t</i>	tertiary
T	temperature
T _d	tetrahedral geometry
THF	tetrahydrofuran
<i>trans</i>	<i>transoid</i>
U	crystal volume
UV	ultra violet
V	volts
vol.	volume
w	weak
wR(F ²)	weighted residual factor
Z	number of asymmetric units per unit cell

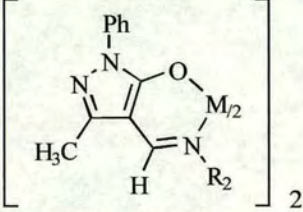
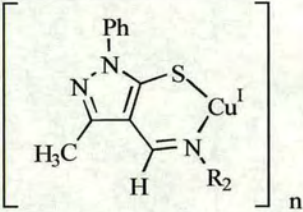
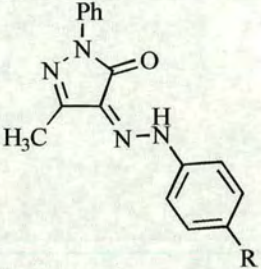
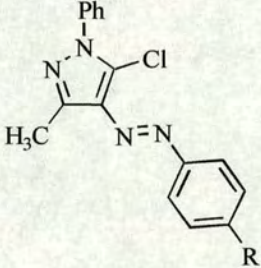
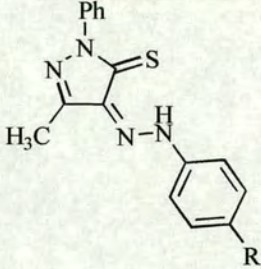
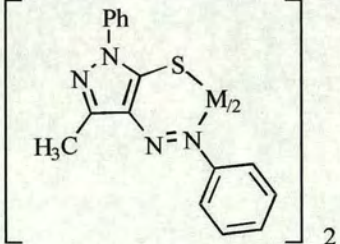
List of compounds

Pyridine-based compounds in Chapter 3.

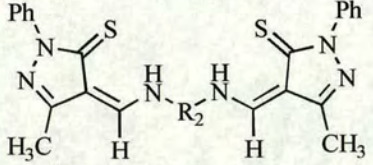
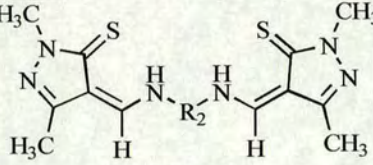
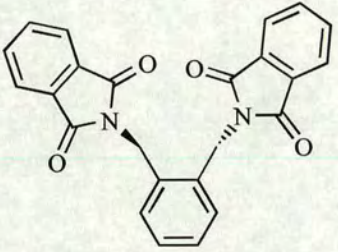
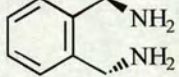
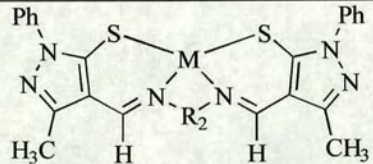
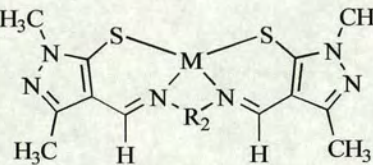
Compound	No.	Substituents
	1	
	2	
	3 4	R = CH ₂ C ₆ H ₅ R = CH ₂ C ₆ H ₄ C(CH ₃) ₃
	5 6 7	R = CH ₂ C ₆ H ₅ , X = S R = CH ₂ C ₆ H ₄ C(CH ₃) ₃ , X = S R = CH ₂ C ₆ H ₅ , X = O
	8 9 10 11 12 13 14 15	M = Zn, R = H, Y = 2 M = Cu, R = H, Y = 2 M = Ni, R = H, Y = 2 M = Co, R = H, Y = 3 M = Fe, R = H, Y = 3 M = Cu, R = C(CH ₃) ₃ , Y = 2 M = Ni, R = C(CH ₃) ₃ , Y = 2 M = Co, R = C(CH ₃) ₃ , Y = 3
	16	M = Cu, R = H
[Zn ₃ (7-H) ₂ (acetate) ₄] _n	17	

Pyrazolone-based compounds in Chapter 4.

Compound	No.	Substituents
	18	$R_1 = C_6H_5$
	19	$R_1 = CH_3$
	20	$R_1 = C(CH_3)_3$
	21	$R_1 = C_6H_5$
	22	$R_1 = CH_3$
	23	$R_2 = C(CH_3)_3$
	24	$R_2 = \text{cyclohexyl}$
	25	$R_2 = 2\text{-ethylhexyl}$
	26	$R_2 = C_6H_5$
	27	$R_2 = C_6H_4C(CH_3)_3$
	28	$R_2 = C_6H_4NO_2$
	29	$R_2 = 2\text{-ethylhexyl}$
	30	$R_2 = C_6H_4C(CH_3)_3$
	31	$R_2 = C_6H_4(C_9H_{19})$
	32	$R_2 = C_6H_4F$
	33	$R_2 = C_6H_4C(CH_3)_3$
	34	$M = Zn, R_2 = C(CH_3)_3$
	35	$M = Co, R_2 = C(CH_3)_3$
	36	$M = Zn, R_2 = C_6H_5$
	37	$M = Co, R_2 = C_6H_5$
	38	$M = Ni, R_2 = C_6H_5$
	39	$M = Zn, R_2 = C_6H_4C(CH_3)_3$
	40	$M = Co, R_2 = C_6H_4C(CH_3)_3$
	41	$M = Ni, R_2 = C_6H_4C(CH_3)_3$

	42	M = Zn, R ₂ = C ₆ H ₅
	43	M = Cu, R ₂ = C ₆ H ₄ C(CH ₃) ₃
	44 45	R = H R = C(CH ₃) ₃
	46 47	R = H R = C(CH ₃) ₃
	48 49	R = H R = C(CH ₃) ₃
	50 51	M = Zn M = Co

Pyrazolone-based compounds in Chapter 5.

Compound	No.	Substituents
	52	$R_2 = (\text{CH}_2)_2$
	53	$R_2 = (\text{CH}_2)_3$
	54	$R_2 = (\text{CH}_2)_4$
	55	$R_2 = \textit{trans}\text{-}1,2\text{-cyclohexyl}$
	56	$R_2 = (\text{CH}_2)_4$
	57	$R_2 = \textit{trans}\text{-}1,2\text{-cyclohexyl}$
	58	$R_2 = o\text{-CH}_2\text{C}_6\text{H}_4\text{CH}_2$
	59	
	60	
	61	$M = \text{Zn}, R_2 = \textit{trans}\text{-}1,2\text{-cyclohexyl}$
	62	$M = \text{Zn}, R_2 = (\text{CH}_2)_4$
	63	$M = \text{Ni}, R_2 = (\text{CH}_2)_4$
	64	$M = \text{Zn}, R_2 = \textit{trans}\text{-}1,2\text{-cyclohexyl}$
	65	$M = \text{Zn}, R_2 = o\text{-CH}_2\text{C}_6\text{H}_4\text{CH}_2$
	66	$M = \text{Ni}, R_2 = o\text{-CH}_2\text{C}_6\text{H}_4\text{CH}_2$

Chapter 1

Introduction

1.1 Objectives.

The objective of this project is to identify new, highly selective complexing agents for zinc which will find applications in novel processes to recover the metal from both primary sources (*i.e.* ore bodies) and secondary sources (*e.g.* effluents and by-products of galvanising operations).

All conventional methods of zinc recovery depend, at least in part, on pyrometallurgy for initial processing of the ore. An example is given by the roasting of zinc sulfide ores (Equation 1.1).



Roasting is used to generate calcine (ZnO) which is either reduced *in-situ* using fossil fuels (Section 1.3.2) or dissolved in acid to generate a solution from which the zinc is ultimately recovered by electrolysis (Section 1.3.3). Calcines are also produced pyrometallurgically from silicate and carbonate ores.

Pyrometallurgical processes are undesirable on both environmental and economic grounds. There are demands upon industry to eliminate harmful environmental emissions and calls for the need to lower the amount of fossil fuel consumed. Rather than considering improvements to existing processes leading to cleaner and less expensive adaptations, hydrometallurgical methods based on solvent extraction will be assessed. These were first pioneered in the nuclear fuels industry for the recovery of uranium¹ and are already in use for the extraction of copper.

New processes for the hydrometallurgical recovery of zinc can be based on the dissolution of the metal values into an acidic aqueous medium, mimicking the highly

successful copper operations (Section 1.4.1). The major focus of this thesis is the design of a “strong” and highly selective extractant capable of removing zinc from aqueous process streams, separating it from contaminants in a single step.

The “strength” of an extractant is usually defined by the pH range over which the metal value can be extracted into an organic phase and is labelled $\text{pH}_{1/2}$. For “pH-swing” extractants the stronger the extractant the lower the $\text{pH}_{1/2}$ (at which 50 % loading of the organic phase will occur).

A second strategy was also considered which is based on the design of a “weaker” and less selective extractant. This would be applicable in a solvent extraction process in which some impurities, most notably iron and copper, have previously been removed from the aqueous feed stream by other processes. Such a flowsheet can allow the zinc to be extracted at a higher pH at which precipitation of ferric iron would otherwise be a problem.

Zinc has a low economic value compared with other base metals² such as copper, cobalt, nickel, and manganese (Table 1.1).

	UK \$ / kg	USA \$ / kg
Zn	1.03	1.17
Cu	4.64	3.05
Ni	8.23	7.05 ^(a)
Mn	n/a	2.00

Table 1.1. Average consumer price of a selection of base metals in 1995. ^(a) No quote since 1987.

Zinc production using current technologies, both pyrometallurgical and electrochemical (Section 1.3.5) is complex and requires multiple steps for separation and purification. They require a high energy input and produce large amounts of waste products. The consumer price for zinc in 1995 was approximately 2.5 less than that of copper. Copper production by hydrometallurgical solvent extraction (\$0.77 per kg)³ is approximately half the price of production *via* pyrometallurgy. In order to develop a new process for zinc recovery with significantly lower production costs it would be logical to base it on the flowsheet which has been proven for copper (Section 1.4.1.1).

1.2 Zinc production.

Zinc is one of the less common elements. It is twenty-fourth in order of abundance and present in the Earth's crust at 76 ppm, slightly higher than that of copper at 68 ppm, and occurs only in a chemically combined state. It is approximately 500 times and 1000 times as abundant as the heavier group 12 elements, cadmium and mercury respectively.⁴ Zinc is a lustrous blue-white metal⁵ but in the presence of air it forms an inert oxide surface giving it a grey-white appearance.

1.2.1 Raw materials.

Zinc ores are widely distributed throughout the world with over 55 zinc minerals known. However only those listed (Table 1.2) have commercial importance.

Mineral	Composition	% Zinc	Impurities
sphalerite ^{(a),(b)}	ZnS	67.0	Metal sulfides Fe, Pb, Cd, Cu, As, Co, Hg, In, Tl, Ga, Ge.
smithsonite	ZnCO ₃	52.1	FeO, MnO, CuO, SiO ₂ , Fe ₂ O ₃ .
hemimorphite	Zn ₄ SiO ₇ (OH) ₂ .H ₂ O	54.2	Component of smithsonite.
willemite	Zn ₂ SiO ₄	58.5	FeO, MnO.
franklinite	(Zn,Fe,Mn)O. (Fe ₂ ,Mn ₂)O ₃	15-20	SiO ₂ , Al ₂ O ₃ , MgO
zincite	ZnO	80.3	FeO, Fe ₂ O ₃ .

Table 1.2. Commercially important zinc minerals.^{5,6} Zinc blende^(a) (cubic system), wurtzite^(b) (hexagonal system).

Zinc is a chalcophile, meaning that the predominant mineral forms in the Earth's crust are zinc sulfides. The sulfide-containing minerals have either a cubic structure, sphalerite (zinc blende), or the less common hexagonal structure wurtzite. The next most important forms of zinc are the silicates, willemite and hemimorphite, and the carbonates, smithsonite. The oxide mineral, zincite, is less common.⁶ Of these, sphalerite (most notably zinc blende) provides approximately 90 % of the zinc produced today. Zinc blende usually makes up 2-12 % of the mined ore. Oxidic ores are usually found in richer deposits and can comprise of 35 % of the ore body. These are most commonly carbonates (smithsonite and hemimorphite).⁵ Zinc minerals tend to be associated with those of other metals; the most common are zinc-lead and zinc-copper ores. Other minor metals are present such as Cd, In, Ge, and Tl, which are recoverable by-products of the zinc industry.

Secondary sources for zinc include the waste from the zinc production and using industries. They include zinc dusts, pyrometallurgical zinc residues, chemicals, zinc galvanising waste and scrap metal (die-casting and clippings).⁵

1.2.2 Early history of zinc isolation.

Zinc was first purified much later than other common metals such as iron. This is because the reduction temperature is higher than the boiling point of zinc (907 °C). Therefore when zinc is reduced with coal at high temperature zinc vapour is produced. Without suitable precautions the zinc vapour will escape into the atmosphere and re-oxidise to zinc oxide, making the isolation of zinc impossible. The preparation of alloyed zinc by smelting mixed ores does not require the isolation of zinc itself and is much more easily achieved. Zinc was first used in the alloy with copper, brass. The production of brass dates back as early as 8000 BC⁶ when copper was smelted from copper containing ores in the presence of the zinc ore smithsonite, Table 1.2.

The molten copper, in contact with zinc ore and carbon, reduced the zinc, which was absorbed by the molten copper resulting in the gold coloured brass alloy. Brass production works were developed in the Middle Ages, typically near deposits of smithsonite ($ZnCO_3$). This method of producing brass lasted into the 1800's.

1.2.3 Origins of zinc smelting.

Remains of zinc smelting operations in India^{4,6} confirm that zinc was produced prior to the 1300's. From India manufacture moved to China⁷ where coins containing 99 % zinc were cast during the Ming Dynasty (1368-1644). The smithsonite ore was

placed in clay jars, stacked in a pyramid, with coal between each. This was heated to evolve zinc vapour and when the cooled jars were broken open zinc metal was found at the centre. Zinc was imported from these areas to Europe as early as 1620 in the form of spelter, a less pure form of zinc.

jar as pyramid!

1.2.4 Industrial production of zinc.

Andreas Margraff, in Berlin, established the basic theory of zinc production in 1746 by distillation of smithsonite in sealed vessels. He later showed that zinc could be prepared from other zinc containing ores such as sphalerite, Table 1.2.

It was not until the 18th century that zinc was produced on a large scale in Bristol and Swansea. The first industrial smelting works was erected in Bristol⁴ in 1758 with a capacity of 200 tonnes per year. Zinc production reached the American continent in 1840 with the first smelter erected in Washington.⁴ Since then various types of smelter have been employed and these are discussed below (Section 1.3.2).

Zinc was produced from its oxidic ores for 500 years, but these are far less abundant than the sulfidic ores that dominate today. In the 1920's the roast/leach process with electrochemical deposition was introduced (Section 1.3.3) and is the major production technique for zinc today.

1.2.5 Uses and consumption of zinc.

The world consumption of zinc has risen from 500,000 metric tonnes⁸ in 1900 to 7.1 million metric tonnes⁹ in 1995. Since the 1970's there has been only a slow increase (Figure 1.1) and in the last ten years the market has remained fairly constant.

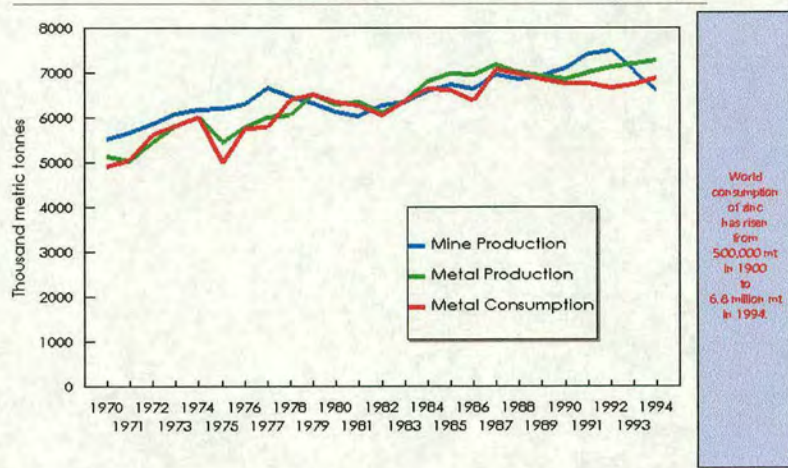


Figure 1.1. Zinc production and consumption: annual world totals⁸ 1970-1994.

Some of the largest markets^{4,5,6,8} for zinc (Figure 1.2) are in galvanising iron to protect against corrosion, in brass (coins), die-casting and the zinc-cadmium battery industry. By far the largest and most diverse of these is the anti-corrosion market, with 49 % of the market.

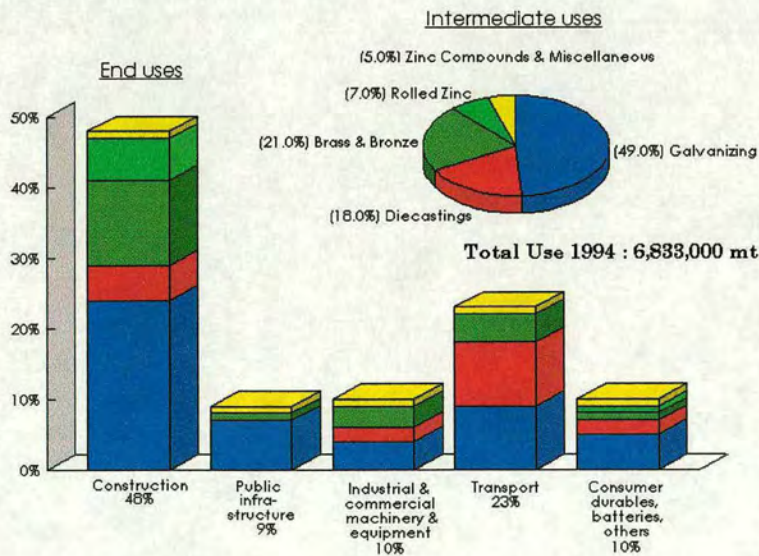


Figure 1.2. End use destination of zinc.⁸

Zinc, when applied to an iron surface as a film, produces a very stable oxide layer. It also sets up a galvanic cell that suppresses the oxidation of the iron. Even when the iron surface is exposed the “sacrificial” zinc is oxidised first while the iron remains unaffected.¹⁰

Zinc plating is used in many areas from galvanised buckets to engine parts. The most common plating process involves the application of molten zinc (hot dip galvanising). Immersion in the zinc bath at 450 °C causes the formation of a zinc-iron alloy at the surface interface on the steel, giving a very good adhesion of the zinc coating. Other galvanising processes^{10,11} include:

1. Film deposition of zinc from a zinc electrolyte (electrogalvanising).
2. Spraying with molten zinc.
3. Heating with powdered zinc (sherardizing).
4. Paint application containing powdered zinc.

1.3 Current zinc extraction technology.

Pyrometallurgy¹² or smelting¹³ involves the application of heat to reduce metals with simultaneous oxidation of a non-metal reducing agent, *e.g.* carbon.

At present there are two techniques that are employed for the recovery of zinc from minerals:

1. High temperature fossil fuel reduction, including purification *via* a distillation step (Section 1.3.2).
2. Roast/leach with electrochemical deposition (Section 1.3.3).

1.3.1 Pre-treatment of raw materials.

Both these conventional reduction processes require the zinc to be in the oxide form, thus an initial roasting of the sulfide, silicate or carbonate ore is involved. Before roasting, the zinc content must be increased as the mined ores are usually too low grade for economical pyrometallurgical treatment.

The zinc concentration of the ore is usually increased to between 40 and 60 % by three possible methods.⁷

1. Gravity separation of the milled ore by jigs and tables.
2. Flotation of complex ores where the ferrosilicon slurry floats and the heavy minerals sink.
3. Fire concentration, where fuel is used to volatilise the zinc in a Waelz kiln, which is immediately re-oxidised to crude zinc oxide.

The concentrated zinc ore is then roasted, in the presence of oxygen at approximately 900 °C converting the zinc sulfides (Equation 1.1), silicates and carbonates (Equation 1.2) to the oxide, calcine. At temperatures lower than this zinc sulfate forms (Equation 1.3) which is undesirable in the fossil fuel reduction process.⁵ Each percent of sulfur remaining in the calcine causes a 2 % loss in recovered zinc.⁷ However, if the roasted ore is to be used in the roast/leach process a small percentage of zinc sulfate produced at the roasting stage is desirable.



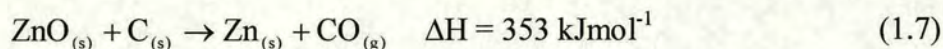
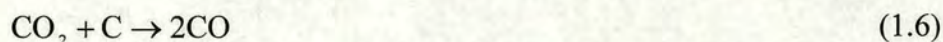
The sulfur dioxide produced in equation (1.1) is converted into sulfuric acid (Equation 1.4) and may be used in the leaching process described later (Section 1.3.3).

Early roasting furnaces, known as Wedge or Hegler roasters, contained a number of hearths through which the ore travelled. In the early 1950's flash roasters were developed in which no auxiliary heated was required with the finely divided ore burned in a large chamber in the presence of oxygen. The oxidation (Equation 1.1) of ZnS is very exothermic⁵ with high-grade sulfide ores, $\sim 5.0 \text{ MJkg}^{-1}$. In contrast zinc carbonate roasting (Equation 1.2) is endothermic and requires heating.

The following section describes the reduction of calcine by fossil fuels (section 1.3.2) and by dissolution in acid followed by electrolysis (section 1.3.3).

1.3.2 Fossil fuel reduction and distillation.

The calcine can be converted to metallic zinc by reduction with carbon in the absence of air. The reduction of zinc does not yield a pure metal and distillation is required to achieve chemical purity. It is thought that the overall reduction (Equation 1.7) proceeds *via* two steps, involving carbon monoxide in the first step (Equations 1.5 and 1.6).



The reaction is strongly endothermic such that 5.4 MJ of heat is required to produce 1 kg of zinc.⁶ In order to achieve complete reduction of the calcine and formation of carbon monoxide the temperature of the furnace must exceed 1000 °C. In general, an operating temperature of between 1000 and 1300 °C is maintained. It is important to remove traces of the carbon dioxide otherwise re-oxidation of the zinc vapour during condensation will occur.

Different furnace designs have been used for the reduction of calcine, which are listed below in chronological order.

1. Horizontal retort furnace.
2. Vertical retort furnace.
3. Electrothermal vertical retort furnace.
4. Imperial smelter (shaft furnace).

The first to be developed was the horizontal retort furnace,⁵ in 1800. This comprised of several hundred small horizontal retorts, containing the coal and the calcine, stacked several high and back to back to reduce heat loss. The retorts are slightly inclined towards the open end allowing any molten slag to drain to the cooler end. Heating for 24 hours using 2 kg of coal per 1 kg of zinc recovers approximately 80-85 % of the zinc.⁷ The molten zinc was collected at the slightly inclined front end in a condenser to which an additional condenser was attached for the collection of cadmium. The retorts need to be charged and discharged by hand which requires large amounts of manual labour under intense heat.

The development of the vertical retort made it possible to reduce zinc ores continuously and collect the resulting zinc vapour in large condensers. Two types of vertical retort were developed; (1) the “New Jersey Process” which was externally

heated using fossil fuel and (2) the “St. Joe Process” which used external electric heating. The ore and coal were pressed into briquettes and heated to just below the reduction temperature and then placed in the retort from the top. A condenser located directly above the furnace and maintained at 950 °C was used to condense lead vapour. The zinc vapour passed through and was collected in a separate condenser, maintained at 550 °C. Overall the process removes 96 % of zinc, a large improvement on the horizontal retort furnace. The resulting metallic zinc is approximately 98.5 % pure containing trace amounts of lead, iron, cadmium and copper.

These processes do not have the efficiency of a blast furnace in which the combustion of the fuel for heating takes place in the same chamber as the reduction of the oxide. Development of a blast furnace for the reduction of zinc in the 1950’s by the Imperial Smelting Co. (Imperial Smelting Process) overcame this inefficiency,

⁶ Figure 1.3.

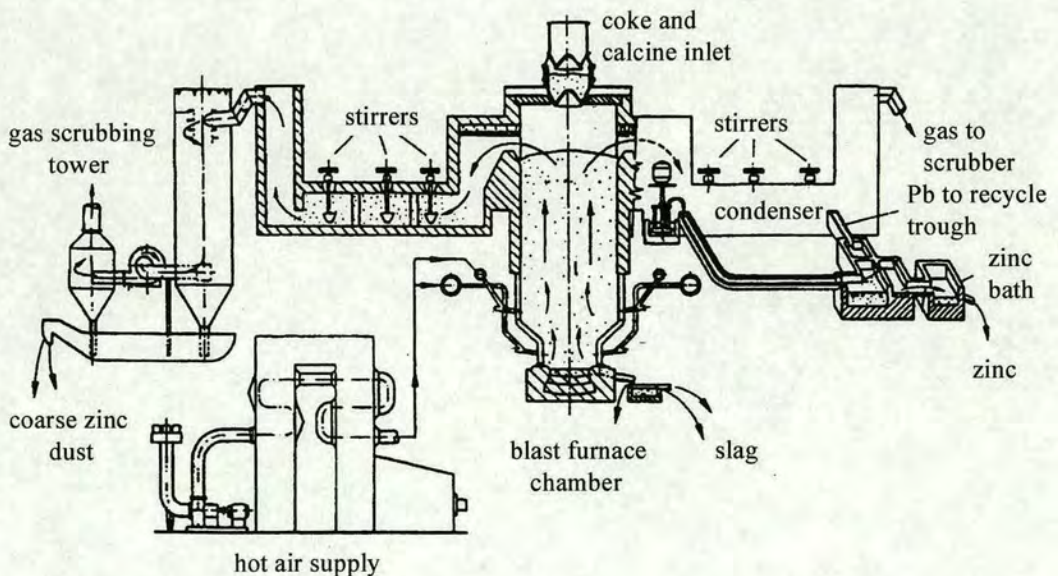


Figure 1.3. The Imperial Smelting blast furnace.⁶

Preheated air is passed into the reaction chamber containing calcine and reductant. The zinc vapour produced is rapidly cooled from 1100 °C to 550 °C by a spray of molten lead into which it dissolves so that re-oxidation is minimal. On further cooling to 440 °C the zinc separates out and floats to the surface to be collected over a weir, with a purity of 98.5 %. One advantage of this process is the ability to reduce ores with higher impurity levels and more complex compositions.

Purification of the impure zinc is achieved *via* distillation. The impurities in the crude zinc fall into two classes; those that have boiling points above (Pb, Cu and Fe) and below (Cd) that of zinc, Table 1.3. Consequently the distillation is a two step process, Figure 1.4.

Metal	B.P. (°C)
Cd	765
Zn	907
Pb	1751
Cu	2570
Fe	2750

Table 1.3. Boiling points of a selection of impurities in fossil fuel reduced zinc.

The molten zinc containing impurities passes from the melting pot (1) into the first fractionating column (2). The less volatile iron, lead and copper runs off into the liquating pot (7) while only zinc and cadmium distil over into the first condenser (3). Here the temperature is low enough for the zinc to condense while the cadmium remains as a vapour. Both the liquid zinc and the cadmium vapour then pass into the second fractionating column (4). The cadmium vapour moves up the column and

condenses in the cadmium condenser (5) and the zinc drains down the column into the refined metal pot (6). Here the pure zinc contains only a few thousandths of a percent of other metals.

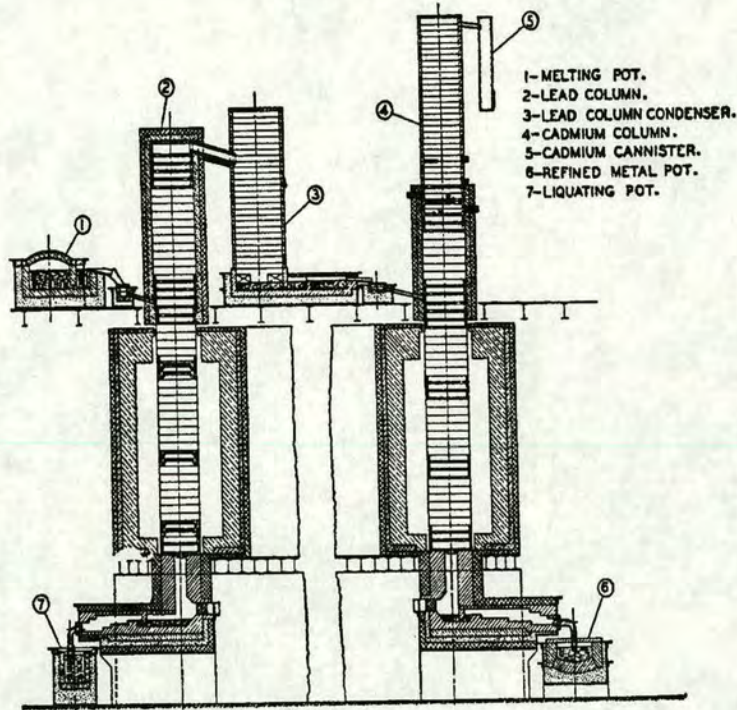


Figure 1.4. Schematic diagram for zinc distillation.⁷

1.3.3 Roast/leach process with electrowinning.

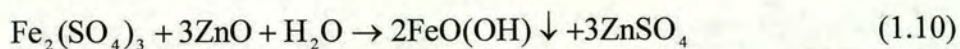
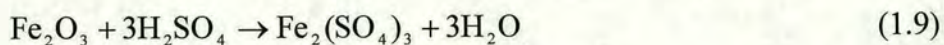
This process uses the same initial roasting of the zinc minerals as the fossil fuel reduction method, but the resulting calcine is then processed by dissolution in sulfuric acid. Electrolytic production of zinc from a sulfuric acid media accounts for 80 % of the current world production.⁶ To ensure rapid dissolution of the calcine a fine-grained structure is preferred, which is obtained by fluidised-bed roasting. In contrast to the fossil fuel reduction process described above, the formation of zinc sulfate as well as zinc oxide during roasting is beneficial for the second step in the

roast leach process. Conversion of the calcine to zinc sulfate (Equation 1.8) uses the sulfuric acid produced from the sulfur dioxide in the roasting step. Zinc sulfate formation in the roasting step is carefully controlled at 4 % to provide necessary sulfate to make up for the acid losses in the electrolytic cycle.⁷



Dissolution of the calcine by sulfuric acid also dissolves many other metals to make up the aqueous leach. Since electrodeposition of zinc from acidic solutions is thermodynamically less favourable than the liberation of hydrogen (E° for $\text{Zn}^{2+} / \text{Zn} = -0.762 \text{ V}$),¹⁴ efficient electrowinning depends on maintaining a high overpotential of hydrogen at the cathode, which in turn depends on high purity of the electrolyte, as discussed later (Section 1.3.4). Therefore, before the acid leach solution can be electrolysed the impurities present must be removed. Purification is achieved by a multiple step process, each removing a specific impurity.

Dissolution of iron also occurs during the acid leach (Equation 1.9). Iron is present as the largest impurity and is usually removed first, by precipitation as gelatinous oxyhydroxides. Calcine is added to the product of the acid leach, which dissolves producing more zinc sulfate while raising the pH. At $\text{pH} > 2.5$ the iron precipitates as oxyhydroxides (Equation 1.10).



Such oxyhydroxides are difficult to handle and dispose of. The precipitation of this gelatinous material causes arsenic, germanium and some zinc to be adsorptively coprecipitated giving unacceptable zinc yields of 85-88 %. Generation of more easily filtered iron residues improves the yield of zinc through less coprecipitation and can be achieved by precipitation of the iron as either (i) jarosite,¹⁵ $X[Fe_3(SO_4)_2(OH)_6]$, (ii) goethite,^{16,17} $FeO(OH)$ or (iii) hematite,¹⁷ Fe_2O_3 . Separation of iron as jarosite is the most common technique employed as part of the flow sheet in Figure 1.5.

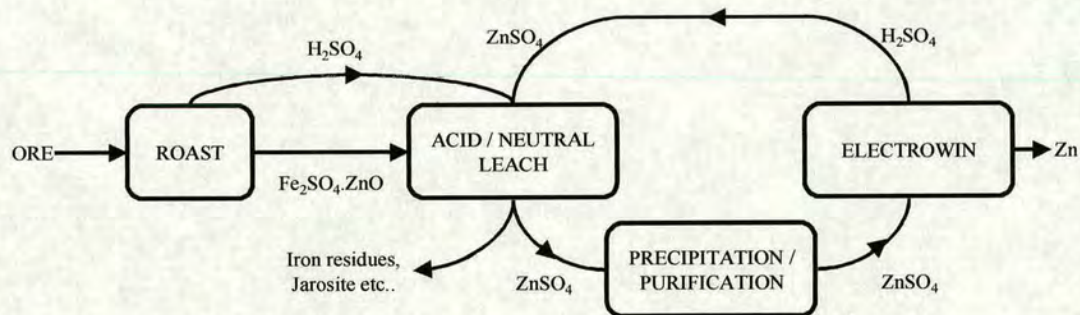


Figure 1.5. Schematic flowsheet for a roast/leach circuit to generate zinc by electrowinning.

Jarosites are Fe(III) compounds of the type $X[Fe_3(SO_4)_2(OH)_6]$ where X usually represents NH_4^+ which is precipitated by the addition of ammonium sulfate while adjusting the pH by the addition of calcine. This is usually⁵ carried out at 95 °C and pH 1.5 leading to a 96-98 % recovery of zinc with only a small amount of zinc reporting to the jarosite residue.¹⁵ Entrainment of zinc and heavy metals in the iron residues presents a serious environmental problem in their disposal.¹⁸

Other impurities still present after the precipitation of iron can be removed by various techniques:

1. Chemical precipitation.
2. Electrolytic deposition.
3. Cementation with zinc.

Chemical precipitation is mainly used for nickel and cobalt.⁶ Nickel is precipitated by dimethylglyoxime and cobalt by α -nitroso- β -naphthol, Figure 1.6.

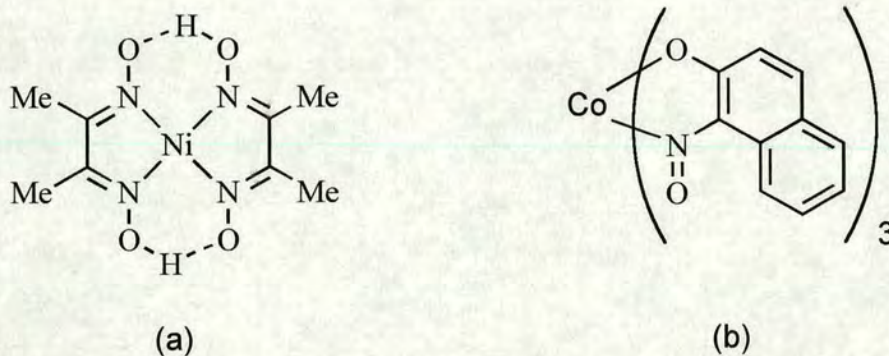


Figure 1.6. Nickel and cobalt complexes of (a) dimethylglyoxime¹⁹ and (b) α -nitroso- β -naphthol.^{20,21}

Both complexes are water insoluble and can be removed by filtration. The α -nitroso- β -naphthol forms a 3:1 neutral octahedral complex with cobalt coordinating *via* the N of the nitroso and the O function. It is not clear of the precise structural arrangement of the ligands, their ambidentate nature can give rise to linkage and / or geometrical isomers,²¹ although ¹³C nmr evidence²⁰ suggests the complex has facial geometry. As these reagents are expensive their use is only considered in cases where leach solutions contain very low levels of impurities. More easily electroplated metals can be removed by electrolysis, although this is a very energy expensive technique.

Alternatively, and most commonly, they are removed by cementation on zinc dust. This is based on the redox displacement of metal impurities in solution that are less electrochemically reactive than zinc. On contact with the high surface area of zinc dust the impurities are deposited and zinc in turn is dissolved producing more ZnSO₄, equation 1.11.



A large excess (5-10 fold) of zinc dust is used to ensure effective purification as it may form an inert surface covering.

1.3.4 Zinc electrolysis.

Electrolysis (Equation 1.12) has two major advantages over other reduction methods; there is no requirement for fossil fuels in effecting reduction, and no second purification step is needed to yield zinc of high purity.



Any new zinc-recovery process based on hydrometallurgy is likely to incorporate electrowinning of zinc in the flowsheet. This will set stringent demands on the purity of the electrolyte produced from a solvent extraction process (see Section 1.4.2), and consequently it is important to understand the requirements of conventional electrowinning technology.

Electrolysis of zinc is carried out using aluminium cathodes and lead anodes with the electrodes suspended vertically in a plastic (PVC) lined tank. The zinc collects at the cathodes and then is melted and cast into slabs.

The electrochemical reduction of zinc requires an extremely pure zinc electrolyte and relies on maintaining a high hydrogen overpotential. The potential required for zinc reduction⁵ on aluminium cathodes in a typical tankhouse is -2.35 V whereas that for hydrogen evolution from water is -2.4 V. Consequently if the hydrogen potential is reduced by as little as 0.05 V then hydrogen evolution is preferred to zinc deposition. The presence of impurities, even trace amounts can seriously impede or halt the deposition of zinc. The types of impurities fall into four different classes depending on their effect on the deposition of zinc.⁶ The potentials quoted are referenced with respect to the standard hydrogen electrode (SHE);

1. Impurities that are more electronegative than zinc, $E^{\circ}(M^{n+}/M) < -0.762$ V, *e.g.* K, Na, Mg, Al and Mn do not pose a significant problem. They do not interfere directly with the electrolytic process, but if their concentrations are too high the electrolyte viscosity increases and the diffusion of ions is affected.
2. Impurities whose standard reduction potentials lie between that of Zn^{2+} and H^+ , $E^{\circ}(M^{n+}/M) = -0.762$ to 0 V, and have a higher hydrogen overpotential than zinc are deposited as impurities in the zinc slab, *e.g.* Cd, Pb, Sn and Tl.
3. Impurities whose standard reduction potentials lie between Zn^{2+} and H^+ but have a lower hydrogen overpotential than zinc can also be deposited as impurities. However they easily re-dissolve

electrochemically and this redox behaviour significantly lowers the current efficiency and zinc yield. For this reason they are only tolerable in very low concentrations.

4. Impurities that are less electronegative than Zn^{2+} and H^+ , $E^{\circ}(M^{n+}/M) > 0$ V, *e.g.* Cu, Ge, Te, As, Sb and In. These lead to a reduction of the hydrogen overpotential and have disastrous effects on the deposition of zinc. Their deposition forms local elements on the cathode that lead to the dissolution of zinc and the evolution of hydrogen.

In practice it is difficult to assess the true effect of each impurity for they can exhibit synergism and are affected by physical factors such as temperature and electrolyte concentration.⁵ However, those that diminish the hydrogen overpotential and prevent zinc deposition are the biggest problem. As well as the impurity tolerances in the tankhouse (tankhouse limits, Table 1.4) their abundance, specific to each ore, in the leachate dictates which metals will pose the most significant problem in developing purification methods. A set of typical feed stream compositions is included in Table 1.4 together with the feed stream concentrations to tankhouse limit ratios. The latter define the metals for which effective selectivity across the circuit presents a particular challenge.

Arsenic, antimony, tellurium, selenium, germanium and copper pose a problem as a consequence of the very low tolerance which the electrolyte process has to these. Iron, in contrast, presents a problem largely because it will be delivered in the leachate at high concentrations and the selectivity for transport of zinc relative to iron across the circuit must be very high to maintain an acceptable current efficiency. This consideration will be a major factor in the design of a suitable solvent

extractant. Some technology to “polish” impurities from the electrolyte by taking a bleed of the electrolyte will also be needed for the development of a process but falls outside the scope of the work described in this thesis.

Metal	Feed Stream (FS) / ppm	Tankhouse Limit (THL) / ppm	Ratio (FS) : (THL)
Fe	34000	25.00	1360
Mg	2540	20000	<1
Mn	2500	4000	<1
As	1200	1.00	1200
Si	115	2500	<1
Cu	65	0.10	650
In	10	1.00	10
Cd	10	0.50	20
Ni	10	0.30	33
Co	10	0.30	33
Tl	10	0.10	100
Ge	10	0.05	200
Se	10	0.01	1000
Te	10	0.01	1000
Sb	10	0.001	10000

Table 1.4. Concentration and tankhouse limits of a zinc sulfate feed stream.²²

1.3.5 Comparison of the two processes.

In the past eighty years pyrometallurgy and hydrometallurgy have been in competition. The production of zinc, Table 1.5, and its graphical representation, Figure 1.7, show that the use of electrolytic processes, *i.e.* roast/leaching, has

increased significantly⁵ and now exceeds pyrometallurgical recovery methods due to lower costs and fewer environmental problems.

Production Process	Date of Commercialisation	Production %		
		1958	1968	1980
Horizontal retort (HR)	1800's	32	15	2
Vertical retort (VR)	1930	7	14	7
Electrothermal (EVR)	1936	3	4	4
Imperial smelting (IS)	1952	8	11	11
Total smelting (TS)	-	50	44	24
Roast/leach (RL)	1915	50	56	76

Table 1.5. Distribution of zinc production processes in non-communist countries.⁵

Decline of zinc smelting, by 26 %, in the period 1958-1980 occurred primarily because of the inability of older plants to meet the ever-tightening environmental standards or obtain sufficiently concentrated ores. The introduction of the more energy efficient, blast furnace type, imperial smelter acquired a proportion of the production market although this was not at the expense of the expanding electrolytic market.

Pyrometallurgy was most successful when high-grade sulfide ores were abundant. With exhaustion of such raw materials attention has turned to low-grade ores and to developing methods which can process these efficiently, *e.g.* hydrometallurgy. Pyrometallurgy has a number of disadvantages in comparison with the roast/leach process. Reduction to elemental zinc from calcine (Equation 1.7) is highly endothermic, requiring operating temperatures in excess of 1100 °C. This requires

large quantities of fuel that, in turn, generate large volumes of exhaust gases, CO, CO₂ and SO₂ (from sulfur contained in the fuel). Further refining, by distillation, again requires a high energy input. On a practical level, fossil fuel reduction is performed on a very large scale requiring an extensive capital input into development of large smelting sites. The capacity of these smelting sites is often so large that they will rapidly exhaust local ore bodies and have been sited to accept concentrates from distant mines, which leads to an increase in transportation costs. The waste materials produced, *i.e.* slags and metal residues, if present in sufficient quantities can be recovered by other smelting techniques or stored in relatively harmless piles without the danger of dissolution of toxic contaminants.

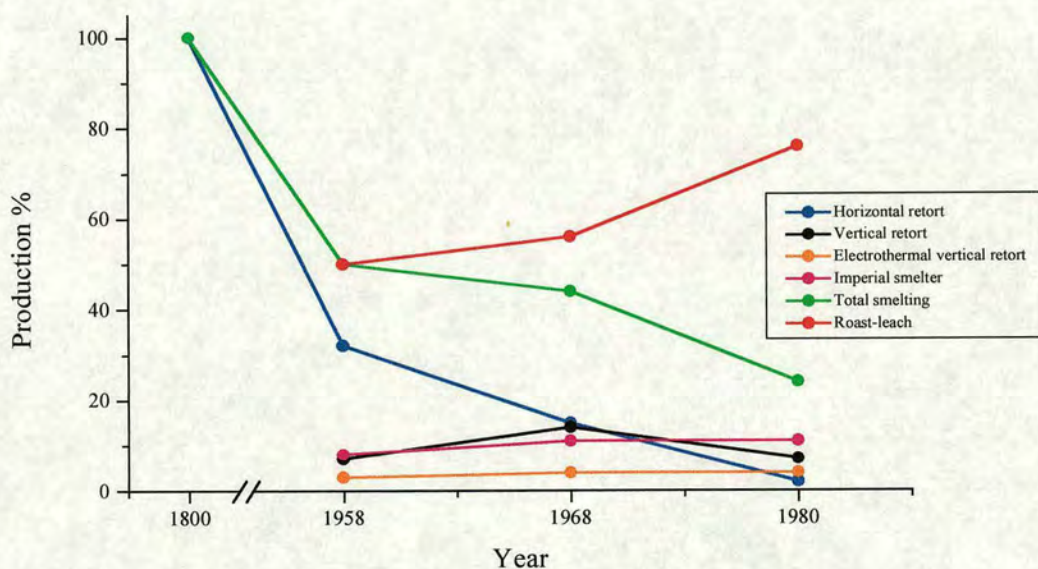


Figure 1.7. Graphical representation of the distribution of different types of zinc production processes in non-communist countries.

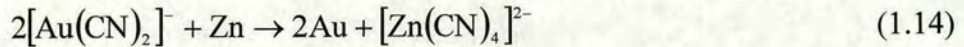
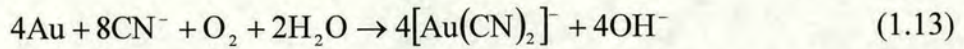
Conversely, roast/leaching methods require less capital input and can be used on a smaller scale. Dissolution in aqueous solutions at ambient temperatures without the

production of gases can be used for the treatment of low grade ores from which recovery by fossil fuel reduction would be impossible or economically non-viable. Purification of the impure leachate is usually performed at ambient temperatures. On occasions, for example during a hot leach step, the temperature may reach, at most, 95 °C. It is therefore a much less energy intensive process, even taking into account the large energy requirements of electrodeposition. The greatest disadvantage of the roast/leach process is the generation and disposal of iron residues, usually jarosite. They can create dust problems when dry and when wet release metal ions into the environment.

Both processes suffer the common disadvantages of a slow turnover rate, inherent of the complicated recovery processes. The development of a hydrometallurgical process involving solvent extraction analogous to that operating successfully for copper would overcome this. These successful copper operations are discussed below (Section 1.4.1).

1.4 Hydrometallurgical solvent extraction.

Hydrometallurgy is the extraction of metals *via* the dissolution in aqueous media (leaching) then recovery by either precipitation or electrodeposition of the metal value. It dates back to 1887 with the invention of the cyanidation process for treating gold ores,²³ which involves the dissolution of gold in a dilute sodium cyanide solution in the presence of air. Aerial oxidation in the presence of cyanide generates a gold(I) complex anion as in equation 1.13, from which the gold is precipitated by cementation with zinc (Equation 1.14).



In the 20th century hydrometallurgy has become well established and is used for the recovery of many metals such as uranium, copper, zinc, cobalt, nickel, vanadium and molybdenum. Modern day hydrometallurgical methods involving solvent extraction were developed during the Manhattan Project in the 1940's to produce extremely pure uranium for the use in the atomic bomb.¹ Solvent extraction is used to transfer the metal value from one liquid medium to another¹² (*i.e.* acidic leach solution to an organic solvent). Hence the distinction between the roast/leach process and a solvent extraction based process is that in the former the impurities are separated from the metal value using a series of steps, whereas the latter selectively removes the metal value in a single operation from the impurities in the leach solution.

1.4.1 Copper recovery by solvent extraction.

Since the mid-1960's solvent extraction has been applied on a commercial scale to the recovery of copper from aqueous solutions obtained from the leaching of oxidic copper ores with dilute sulfuric acid. The efficiency of the hydroxyoxime type extractants (Section 1.4.1.3) allows recovery from very low grade ores.

1.4.1.1 Extraction circuit.

A typical layout for a heap leach / solvent extraction / electrowinning plant for the recovery of copper from low grade ores or tailings is shown in Figure 1.8. The oxide ore is formed into a heap leach pad (1) and is sprayed with sulfuric acid, leaching the

metals into the “pregnant” leach solution which drains to a storage pond (2). From here the aqueous metal sulfate solution is fed to a mixer together with the extractant in a water-immiscible solvent, usually kerosene. The residence time in the mixer is typically two minutes, after which the mixture passes over a weir into the settling tank (3). As the mixture passes along the settler the two phases separate. The aqueous phase, the “raffinate”, is returned to the heap leach pad. The “pure” metal-loaded organic phase is fed into another mixer and “contacted” with a more highly acidic stripping solution which transfers the metal back into the aqueous phase. After settling (4) the regenerated organic extractant is recycled back to extraction and the “clean” aqueous phase containing the desired metal, the “advanced electrolyte”, passes into the electrowinning tankhouse (5).

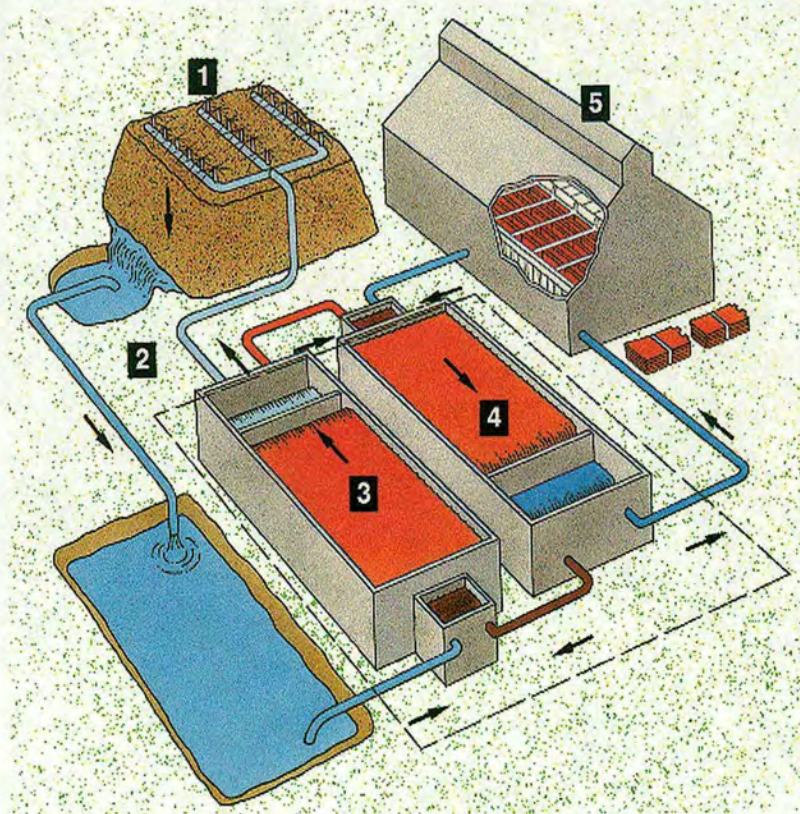


Figure 1.8. Solvent Extraction Plant For Copper Recovery.⁷

Normally two or three extraction and stripping steps are incorporated to ensure effective loading and stripping of copper. In addition to the purification of the copper-containing leach solution considerable concentration of the original copper content (1-3 gl^{-1}) is achieved during the solvent extraction process by using a high organic:aqueous ratio during stripping. This produces a sufficiently concentrated copper-containing electrolyte (30 gl^{-1}) for efficient electrowinning.¹²

Deposition of copper (Equation 1.15) occurs at stainless steel cathodes which are immersed in the metal sulfate solution.²⁴ Copper is stripped mechanically from the stainless steel cathodes and then melted into ingots or rods.



Oxygen is released at the lead anode (Equation 1.16) and the acid generated is recycled back to the stripping step, see Equation 1.20.



1.4.1.2 Mass balance.

The recycling of leachant, extractant and electrolyte in an idealised copper recovery circuit (Figure 1.9) is possible as a result of selectively transferring the desired metal by solvent extraction. This project focuses on the solvent extraction steps, highlighted in red, and the design of new extractants to be incorporated into an analogous circuit for zinc (Section 1.4.2).

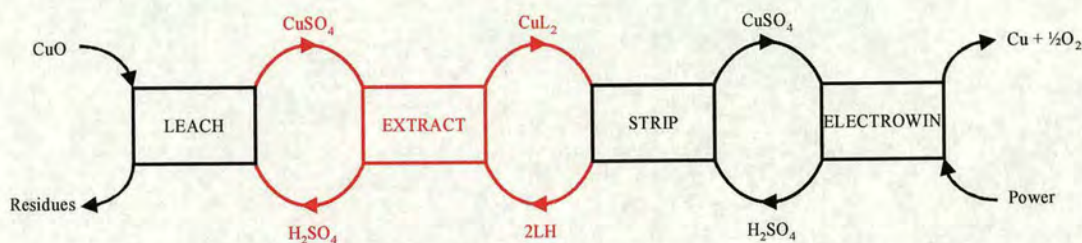


Figure 1.9. The Copper Solvent Extraction Circuit.

Examining the mass balance in such an idealised copper recovery circuit using equations (1.17) to (1.20) highlights the simplicity and efficiency of the process. A bar across the top of a term indicates species present in the organic phase. The use of an organic acid as the copper extractant ensures (Equation 1.18) that for every mole of copper transferred from the leach solution one mole of sulfuric acid is returned to leach. Consequently there is no net consumption of acid in the leach / extraction part of the circuit. The extractant is regenerated by reprotonation in stripping (Equation 1.19). The acid consumed in stripping is regenerated in the electrodeposition of copper (Equation 1.20). Summation of equations (1.17)-(1.20) implies that in such an idealised circuit the copper(II) oxide is split into its component elements (Equation 1.21) with only the consumption of electrical power in the tankhouse. Copper is driven through the process by maintaining a pH gradient across the circuit. In practice, the materials balance is less perfect. Since the water generated in leach (Equation 1.17) cannot be transferred to make up the water in the electrowinning (Equation 1.20).

Leach



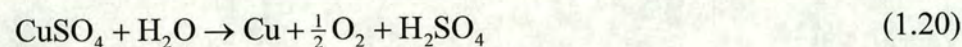
Extraction



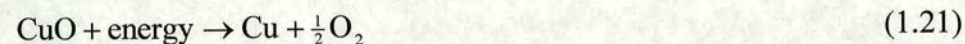
Stripping



Electrowinning



Overall



Also all the other metals leached must be accounted for. Iron is the major component in most low-grade ores processed in this way. As its concentration builds up in the recycled leach solution, a point is reached where it begins to precipitate as oxyhydroxides onto the leach pad. In practice, in such commercial operations, the high selectivity of the extractant ensures that iron “reports” to the leach residues, which can be returned to the mine.

1.4.1.3 Commercial copper extractants.

Industrial solvent extraction of copper was first commercialised in 1968 at the Bluebird Mine Arizona using the LIX 64 reagent,²⁵ Figure 1.10.

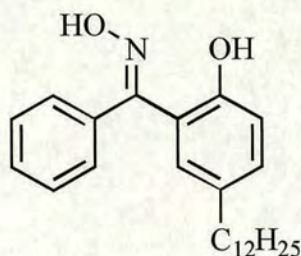


Figure 1.10. LIX 64: 2-Hydroxy-5-dodecylbenzophenone oxime.

Since then many variations on the oxime structure have been considered as extractants. All those currently used are based on phenolic oximes of the type shown in Figure 1.11.

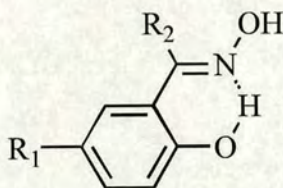


Figure 1.11. General structure of *para*-alkyl-phenolic oximes as copper extractants.

The two most widely used types²⁵ are (i) the ketoximes (where $R_2 = \text{Ph}$ or Me and $R_1 =$ long branched alkyl chain) and the aldoximes (where $R_2 = \text{H}$) which are manufactured by Henkel and classed as LIX reagents and (ii) the aldoximes manufactured by Avecia, an example of which is 5-nonyl salicylaldoxime (P50 where $R_2 = \text{H}$ and $R_1 =$ branched C_9H_{19}). The bulky alkyl chains at the *para*-position of the aromatic ring ensure that the extractant and its copper complex have high solubility in kerosene.

The extraction and stripping of copper is *via* a pH dependent exchange mechanism. For extraction to occur the ligand (HL) in equation (1.18) must lose a proton to form

the neutral copper complex. This must occur at $\text{pH} < 2$ because the pregnant leach solution must be maintained at a pH lower than 2.5 to ensure that no precipitation of iron(III) occurs in the plant (Section 1.4.2.1). A “pH-swing” in the stripping stage, using a stronger sulfuric acid solution, regenerates the protonated ligand and returns the copper to the aqueous phase. Measurement of the loading at different pH evaluates the “strength” of the extractant, which can be presented graphically as “S-curves” (Figure 1.12). From the S-curve, the $\text{pH}_{1/2}$ is obtained as the pH at which the extractant is 50 % loaded.

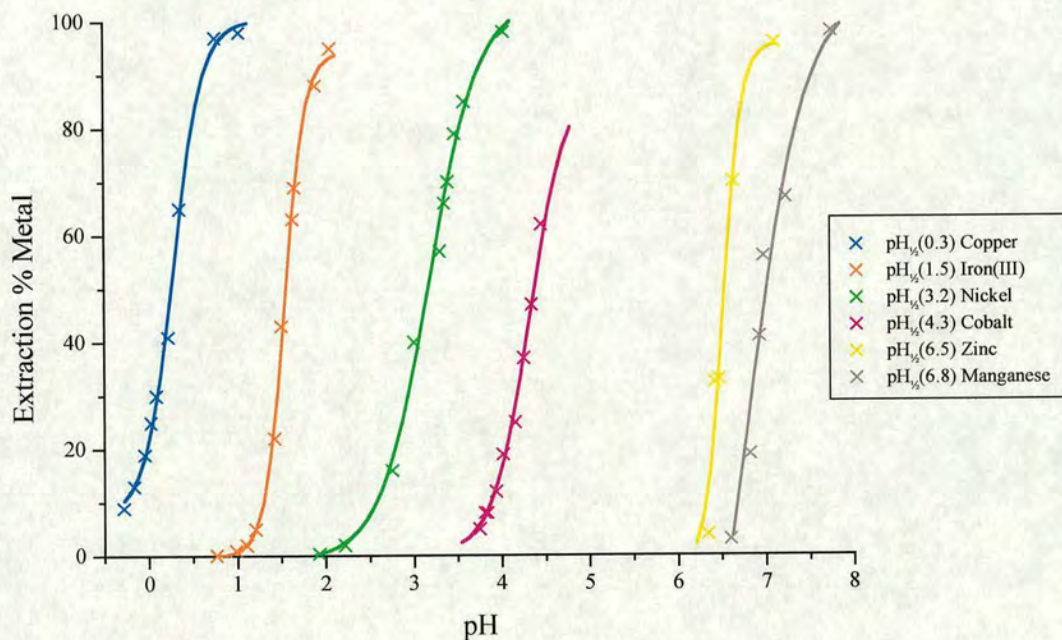


Figure 1.12. Selective extraction of metals using 0.1 M P50 oxime in kerosene (Escaid 100) and a 0.01 M metal sulfate feed at 20 °C.²²

Avecia’s P50 oxime has excellent selectivity for copper over iron(III) with a high loading capacity and possesses all the requirements needed for a successful

extractant. For divalent metals, extraction largely follows the Irving-Williams series ($\text{Mn} < \text{Fe} < \text{Co} < \text{Ni} < \text{Cu} > \text{Zn}$). The selectivity of these reagents for Cu(II) over Fe(III) is attributed to the special stability of the copper *trans* square planar complex which has the pseudo-macrocyclic structure formed by ligand-ligand hydrogen bonding in the complex, Figure 1.13. It has been proposed^{26,27} that ligand-ligand hydrogen bonding also occurs in the metal-free form of the phenolic oximes such as P50 oxime to form a dimer with a pre-organised N_2O_2 donor set (also see Figure 1.13).

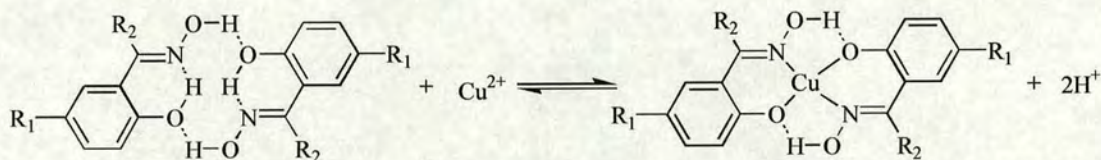


Figure 1.13. Pre-organisation and copper complexation of hydroxyoximes.

The dimer forms a cavity into which a copper(II) cation can fit. In addition to the two 6-membered chelate rings the complex is further stabilised by two 5-membered rings formed by hydrogen bonding of the oximic hydrogens to the phenolic oxygens of the adjacent ligand. In contrast, the tris(hydroxyoxime)iron(III) complex, although not fully characterised, is thought to be octahedral and less favourable hydrogen bonding arises.²⁸

1.4.1.4 Advantages of solvent extraction.

A flowsheet for zinc production analogous to that shown in Figure 1.9 can display advantages over the roast/leach process, Figure 1.5. Although both use

electrochemical reduction in the final stage of recovery the advantages arise from the unit operations of concentration and separation:

1. One step separation of the metal value from the impurities as opposed to the time consuming multi-stage removal of each impurity from the metal value to produce a pure electrolyte greatly simplifies the process and should reduce operating costs.
2. If iron reports to the heap leach residues as in the copper operations, the disposal of iron from production sites is much easier than in the existing zinc roast/leach circuits. Heap leach residues can be released to the mine sites.
3. Cost of metal production can be reduced through the recycling of materials. The process should be associated with a materials balance analogous to that in equations 1.17-1.21 if oxidic ores are used.

The following sections consider the applicability of the heap leach / solvent extraction / electrowinning flowsheet for processing zinc ores.

1.4.2 Zinc recovery by solvent extraction.

Presently there are no commercial extractants suitable for the recovery of zinc in a heap leach / solvent extraction / electrowinning flowsheet. Such a flowsheet is suited for the processing of oxidic ores, such as zincite. These contain many metal impurities specific to the individual ore body but a typical pregnant leach solution composition may be as shown in Table 1.4.

1.4.2.1 Extractant criteria.

An ideal extractant should fulfil a number of requirements to ensure that it will operate efficiently in a heap leach / solvent extraction / electrowinning circuit, Figure 1.14.



Figure 1.14. Extractant criteria for a heap leach / solvent extraction / electrowinning circuit.

The extractant must work on a “pH-swing” mechanism forming a neutral complex from which it can be regenerated on contact with a stronger acid. Consequently it must contain at least one acidic proton per ligand. Good zinc loading will be needed at $\text{pH}_{1/2} < 2.5$ to prevent the precipitation of iron(III) oxyhydroxides. In practice this will require a reagent $\text{pH}_{1/2} < 2.0$. It must be capable of selectively extracting zinc and discriminating against other key metals present in the feed stream, to meet the stringent requirements for a high purity zinc electrolyte. Iron poses a significant problem due to its extremely high concentration in feed streams (Table 1.4). Fast extraction and stripping kinetics are required to minimise the mixing time therefore

increasing the efficiency and turnover. Likewise good separation properties of the organic and aqueous phases and high solubility of the ligand and its metal complexes (copper operations are generally carried out using 0.1 M ligand in kerosene derived diluents) are required to minimise the entrainment of materials. Stability towards oxidation, UV light, temperature, hydrolytic decomposition and “poisoning” by the formation of extremely stable complexes with metal impurities are also important due to the recyclable nature of the process. Failure to fully address these requirements can lead to a continual and significant loss of reagent which requires replacing. Environment safety legislation also dictates non-toxicity of the extractant in its final composition in the diluent and during its synthesis. Due to the relatively low economic value of zinc an extractant which is cheap and therefore simple to make is required.

The purpose of this project is to identify novel extractants for the selective recovery of zinc, therefore only the criteria in red (Figure 1.14) will be focused on. One exception to this is the solubility of the extractants. This is not a primary concern, and studies on the ideal solubilising groups and their effect on the extractive properties will not be dealt with. However, the initial selectivity and strength of extractant can only be addressed if the ligand and its complexes are sufficiently soluble in the chosen organic phase.

1.4.2.2 Zinc selective extractants.

The ions close to zinc in the periodic table, which can be present in the aqueous feed stream, include Cu^{2+} , Ni^{2+} , Cd^{2+} , Co^{3+} and Fe^{3+} . The “normal” order of stability for complex formation defined by Irving and Williams,²⁹ for divalent transition metals

irrespective of the ligand type favours copper extraction ($Mn^{2+} < Fe^{2+} < Co^{2+} < Ni^{2+} < Cu^{2+} > Zn^{2+}$), Figure 1.15.

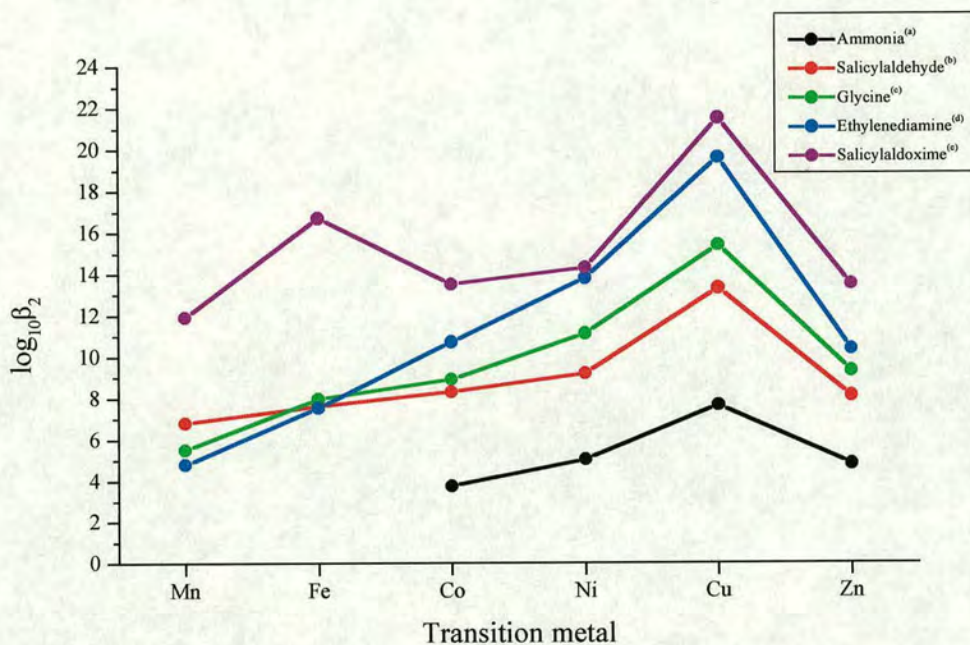


Figure 1.15. Successive stability constants of divalent transition metal complexes (a)-(d),²⁹ (e).³⁰ (a) 2 M NH_4NO_3 at 30 °C, (b) 50 % dioxane / water at 25 °C, (c) 0.1 M at 20 °C, (d) 1 M KCl at 30 °C, (e) 75 % dioxane / water at 25 °C.

A potential extractant for zinc must deviate from the usual stability order defined by Irving and Williams. Some ligands do not follow the expected order of complex stability across the 1st row transition metal series. Factors which can affect this include the coordination number of the complex, the steric constraints applied by the coordinating ligands and entropic factors (*e.g.* ligand denticity). These ‘anti’ Irving-Williams factors can be used to obtain favourable selectivity for different metals, in this case zinc, and will be addressed in detail in Chapter 2. However the stability of

Fe(III) complexes, which is not relevant to the Irving-Williams series, is usually greater than for Zn(II) complexes and poses a major problem.

At the outset of the project Avecia had developed an extractant L2083 for recovery of zinc from strong acidic feed streams which was based on a dithiophosphoramidate, Figure 1.16.

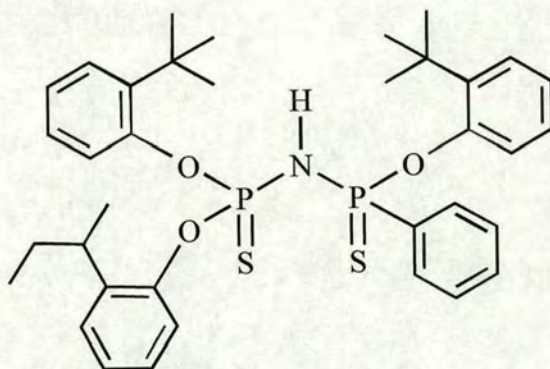


Figure 1.16. Avecia's proposed dithiophosphoramidate zinc extractant (L2083).

The dithiophosphoramidate fulfils many of the criteria outlined above. The extractant operates as a bidentate mono-anionic ligand and is easily deprotonated ($pK_a \sim 3$). It has excellent selectivity for zinc over iron(III) due to its inability to form stable, neutral octahedral FeL_3 complexes. This is due to the cumulative effects of (1) the steric hindrance around the metal centre provided by the bulky phenyl and phenoxy groups, and (2) the ligands "soft" donor atom set [2S] with which "hard" acids such as Fe^{3+} disfavour coordination. Asymmetry is incorporated into L2083, which greatly improves its solubility in kerosene, by the *sec*- and *t*-butyl phenoxy groups.³¹ It forms a six membered chelate ring through the sulfur donor atoms [4S]²⁻ with zinc to form a neutral tetrahedral complex.

The donor set $[S_4]^{2-}$ presented by bulky dithiophosphoramides strongly favours tetrahedral geometry in divalent first row transition metals; L2083 shows high affinity for both zinc(II) ($pH_{1/2} = 0.5$) and cobalt(II) ions ($pH_{1/2} = 2.7$), Figure 1.17.

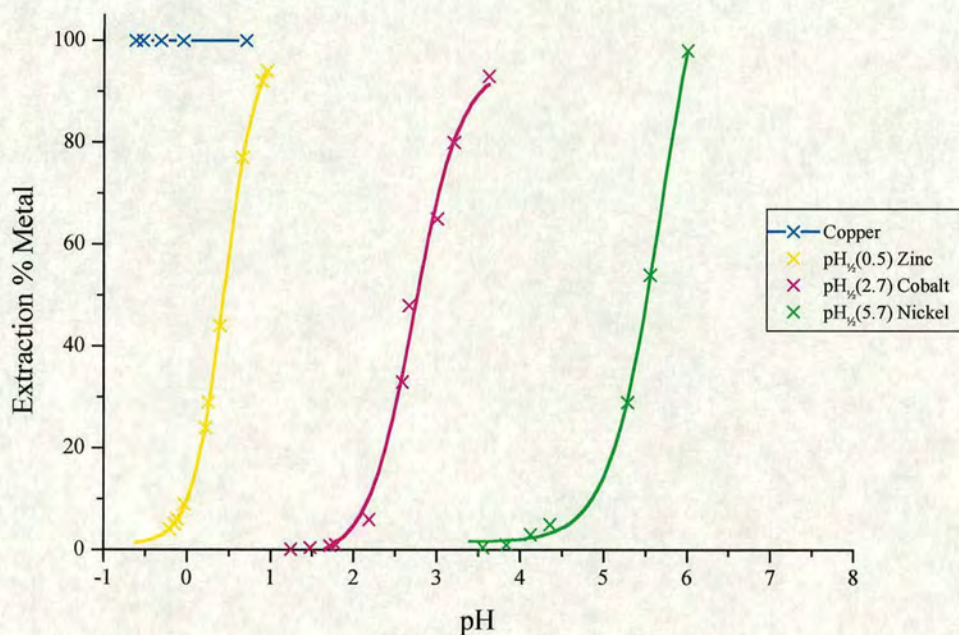


Figure 1.17. Extraction of Cu(II), Zn(II), Co(II) and Ni(II) from 0.01 M sulfate feeds using 0.1 M L2083 in kerosene (Escaid 100) at 25 °C.²²

Nickel(II) is only weakly extracted ($pH_{1/2} = 5.7$). This can be attributed to the relatively unfavourable tetrahedral coordination environment that L2083 imposes on it. For this d^8 metal ion CFSE favours square planar (D_{4h}) or octahedral (O_h) geometries over tetrahedral.

However there are some associated economic and stability concerns surrounding its use commercially. Its relatively high molecular weight (RMM = 666) means that a large weight of extractant is required per gram of zinc extracted. This means that

solutions that have a high zinc-loading capacity will have a very high extractant to diluent mass ratio and therefore be very viscous. L2083 is expensive to manufacture and as zinc has a relatively low value (\$0.56 per lb *c.f.* \$0.88 per lb for copper)³² this will reduce the profitability of a zinc recovery process based on solvent extraction. Under certain conditions L2083 has been found to be unstable in UV light and decomposes. With many of the possible operating sites being located in equatorial regions equipment will have to be designed to avoid exposure to sunlight if acceptable reagent lifetimes are to be achieved. Poisoning by copper reduces the life expectancy of L2083. Copper is complexed so strongly, Figure 1.17, that subsequent stripping can only be achieved with strong hydrochloric acid. However under these conditions the extractant undergoes considerable degradation.

The combination of high manufacturing cost, loss of extractant through copper poisoning and UV decomposition and a low zinc transfer efficiency as a result of the high molecular weight means that dithiophosphoramides may not prove to be commercially viable.

Zinc can be extracted from less acidic feed streams using extractants based on organophosphorus acids, Figure 1.18.



Figure 1.18. Weak extractants based on (a) phosphinic and (b) phosphoric acids.

The application of bis(2,4,4-trimethylpentyl)phosphinic acid (Cyanex 272) and di(2-ethylhexyl)phosphoric acid (D2EHPA) has been considered for the recovery of several base metals. The D2EHPA reagent has found commercial application in the separation of cobalt from nickel³³ and of zinc from copper³⁴ and cadmium.^{35,36} The extraction mechanism is more complicated than that of the extractants described previously. The organophosphorus ligands are known to dimerise when dissolved in low polarity aliphatic and aromatic hydrocarbons³⁷, *e.g.* kerosene, forming a stable 8-membered ring *via intermolecular hydrogen bonds*, Figure 1.19.

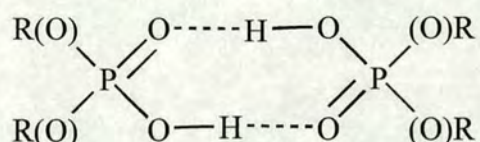


Figure 1.19. Organophosphorus acid dimerisation.

Hydrogen bonding between protonated and deprotonated ligands in metal complexes results in the formation of a wide variety of extracted metal species. With a sufficient excess of the organophosphorus acid neutral metal complexes are formed that are associated with the protonated ligand (ZnL_2 and $ZnL_2 \cdot 3HL$ for zinc(II), $CuL_2 \cdot HL$ and $CuL_2 \cdot 5HL$ for copper(II), $FeL_3 \cdot 2HL$ for iron(III), $CoL_2 \cdot HL$ and $Co_2L \cdot 4HL$ for cobalt(II) and $NiL_2 \cdot 3HL$ and $NiL_2 \cdot 6HL$ for nickel(II) respectively).³⁶ Many other studies have reported different metal species, their nature effected by the diluent concentration and the aqueous medium (SO_4^{2-} , NO_3^- , ClO_4^-).³⁸ However, when large amounts of metal ions are present in the organic phase and a lower ratio of extractant to metal is approached polymeric complexes can occur.³³ Careful control of the extractant, diluent and metal content complicate the recovery

procedure. The selective extraction of divalent metals using Cyanex 272³⁷ and D2EPHA^{39,40} are similar. The order of extraction ($\text{pH}_{1/2}$ given in brackets) for 1st row transition metals from a sulfuric acid media is:

Cyanex 272 Fe(III)(1.2) > Zn (2.0) > Mn (3.8) > Cu (4.0) > Co (4.3) > Ni (6.2)

D2EPHA Fe(III)(1.3) > Zn (2.0) > Mn (2.7) > Cu (2.9) > Co (3.7) > Ni (4.1)

Clearly they show no correlation with the Irving-Williams series for the stability constants of octahedral divalent complexes. Iron(III) forms strong complexes with chelating ligands which produce the donor atom set $[\text{O}_6]^{6-}$, e.g. 1,2-dihydroxybenzene⁴¹ ($\log\beta_3 = 44.2$). The order of divalent metals would suggest a correlation with the propensity of the metal ions to adopt a tetrahedral geometry that is favoured by such bulky ligands.³³ D2EPHA is the proposed extractant for use in the "Modified Zincex Process", for the recovery of zinc from secondary zinc residues.³⁴ It is based on the solvent extraction circuit where upon the iron content has previously been removed by cementation. Zinc is selectively extracted over copper but iron(III) traces remaining in the aqueous stream are strongly co-extracted. However, the rate of extraction and stripping of iron(III) is slow compared to that of zinc, therefore the iron(III) can be removed after zinc stripping by treating a bleed with strong hydrochloric acid to avoid iron build-up in the organic solvent. In comparison, the extraction series for the dithiophosphoramides show far stronger extraction for zinc and almost no extraction of iron(III). However the incorporation of the donor atom set $[\text{S}_4]^{2-}$ favours the strong and irreversible extraction of copper.

The design of a new extractant for the recovery of zinc will need to address both the problems associated with the dithiophosphoramides and with the organophosphorus acids. These include the development of a “strong” and highly selective extractant capable of discriminating over both copper and iron(III) at an acceptably low pH for the circuit. The methodology for identification of possible ligand types is described in Chapter 2.

1.5 Summary.

This chapter outlines the potential advantages of utilising the existing (copper) solvent extraction technologies for the recovery of zinc. As a suitable extractant that matches the criteria, outlined in Section 1.4.2.1, is currently unavailable Chapter 2 will consider the design features to obtain a suitably “strong” and selective zinc reagent. It considers the coordination environment of the zinc(II) ion and the factors affecting its coordination and geometries. It attempts to identify ligand systems that have the potential strength as zinc extractants and the properties that could provide discrimination against other key metals. Chapters 3, 4 and 5 present the results on these types of ligand systems.

1.6 References.

1. F. Habashi, *A Textbook Of Hydrometallurgy*, ed. F. Habashi, Métallurgie Extractive Québec, 1993, ch.1, pp.3-11.
2. *Metal Statistics 1985-1995*, ed. World Bureau of Metal Statistics, Ware, England, 83rd edn., 1996, pp.461-495.
3. M. Soderstrom, personal communication, Avecia.
4. R.H. Prince, *Encyclopaedia Of Inorganic Chemistry*, ed. B.R. King, Wiley, Exeter, England, 1994, vol.8, pp.4434-4450.
5. Kirk-Othmer, *Encyclopaedia Of Chemical Technology*, Wiley-Interscience, NY, 3rd edn., 1984, vol.24, pp.807-850.
6. F. Habashi, *Handbook of Extractive Metallurgy*, Wiley-VCH, Mortenbach, Germany, 1997, vol.2, pp.641-681.
7. M.C Sneed, R.C. Brasted, *Comprehensive Inorganic Chemistry*, D. Van Nostrand Company Inc., 1955, vol.4, pp.9-33.
8. <http://www.iza.com>, International Zinc Association webpage.
9. *Metal Statistics 1985-1995*, ed. World Bureau of Metal Statistics, Ware, England, 83rd edn., 1996, pp.34-36.
10. C.J. Slunder, W.K. Boyd, *Zinc: Its Corrosion Resistance*, Zinc Development Association, London, 1st edn., 1971, ch.1, pp.11-18.
11. N.N Greenwood, A. Earnshaw, *Chemistry Of The Elements*, Pergamon Press, Oxford, 4th edn., 1989, ch.29, pp.1395-1422.
12. Kirk-Othmer, *Encyclopaedia Of Chemical Technology*, Wiley-Interscience, NY, 3rd edn., 1980, vol.9, pp.739-767.

13. *Oxford Dictionary Of Chemistry*, ed. J. Daintith, Oxford University Press, Oxford, 3rd edn., 1996, p.446.
14. N.N. Greenwood, A. Earnshaw, *Chemistry of the Elements*, Pergamon Press, Oxford, 4th edn., 1989, pp.498.
15. R.V Pammenter, C.J. Haigh, *Extraction Metallurgy '81*, Institute of Mining and Metallurgy, London, 1981, pp.379-392.
16. P.T. Davey, T.R. Scott, *Hydrometallurgy*, 1976, **2**, 25.
17. J.M. Cigan, T.S. Mackay, T.J. O'Keefe, *Lead-Zinc-Tin '80*, ed. J.E. Dutrizac, AIME, New York, 1979, pp.532-564.
18. J.E. Dutrizac, G.B. Harris, *Iron Control and Disposal: Second International Symposium on Iron Control in Hydrometallurgy*, Ottawa, Canada, 1996.
19. L.E. Godycki, R.E. Rundle, *Acta. Crystallogr.*, 1953, **6**, 487.
20. J. Charalambous, G. Soobramanien, *Inorg. Chim. Acta.*, 1982, **60**, 150.
21. L.A. Epps, K. Wiener, R.C. Stewart, L.G. Marzilli, *Inorg. Chem.*, 1977, **16**, 2663.
22. D. Cupertino, personal communication, Avecia.
23. F. Habashi, *A Textbook Of Hydrometallurgy*, ed. F. Habashi, Métallurgie Extractive Québec, 1993, ch.9, pp.194-221.
24. F. Habashi, *A Textbook Of Hydrometallurgy*, ed. F. Habashi, Métallurgie Extractive Québec, 1993, ch.25, pp.637-639.
25. J. Szymanowski, *Hydroxyoximes and Copper Hydrometallurgy*, CRC Press, London, 1993, ch.2, Part A, pp.14-60.
26. P.A. Tasker, *XXVIII International Conference On Coordination Chemistry*, Gera, 1990, 104.
27. A. E. Koziol, Z. Kostarkiewicz, *Pol. J. Chem.*, 1984, **58**, 569.

28. J. Szymanowski, *Hydroxyoximes and Copper Hydrometallurgy*, CRC Press, London, 1993, ch.3, Part A, pp.104-115.
29. H. Irving, R.J.P. Williams, *J. Chem. Soc.*, 1953, 3192.
30. K. Burger, I. Egyed, *J. Inorg. Nucl. Chem.*, 1965, **27**, 2361.
31. D. Cupertino, *Metals Extraction Products Business*, 2nd International Technical Conference, University Of Edinburgh, 1996.
32. <http://www.metalbulletin.com>, 19th Oct 1999 - 19th Jan 2000 (3 month average).
33. M.J. Nicol, C.A. Flemming, J.S. Preston, *Comprehensive Coordination Chemistry*, ed. G. Wilkinson, Pergamon Press, Oxford, 1st edn., 1987, vol.6, ch.63, pp.779-835.
34. G. Diaz, D. Martin, *Resour. Conserv. Recycl.*, 1994, **10**, 43.
35. G. Owusu, *Hydrometallurgy*, 1998, **47**, 205.
36. A.K. Nayak, P.K. Mishra, C.R. Panda, V. Chakravorty, *Ind. J. Chem. Tech.*, 1995, **2**, 111.
37. Y. Nagaosa, Y. Binghue, *Talanta*, 1997, **44**, 327.
38. N.B. Devi, K.C. Nathsarma, V. Chakravorty, *Hydrometallurgy*, 1997, **45**, 169.
39. F. Habashi, *A Textbook Of Hydrometallurgy*, ed. F. Habashi, Métallurgie Extractive Québec, 1993, ch.21, pp.407-497.
40. J.S. Preston, *Hydrometallurgy*, 1983, **10**, 187.
41. A.M. Nardillo, *J. Inorg. Nucl. Chem.*, 1981, **43**, 620.

Chapter 2

Ligand Design

2.1 Objectives.

The design of a solvent extractant for the selective complexation of zinc over other metals requires that a number of properties are incorporated into the ligand.

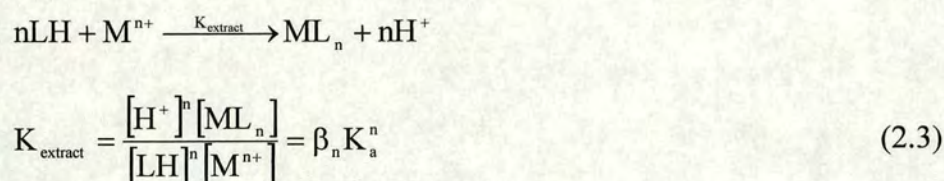
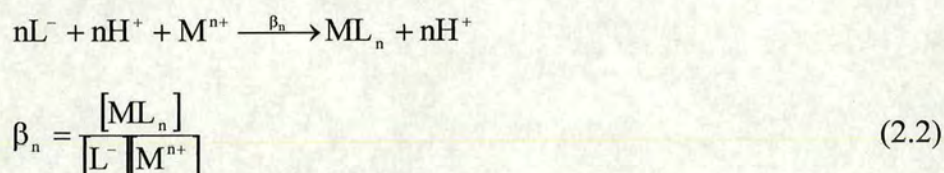
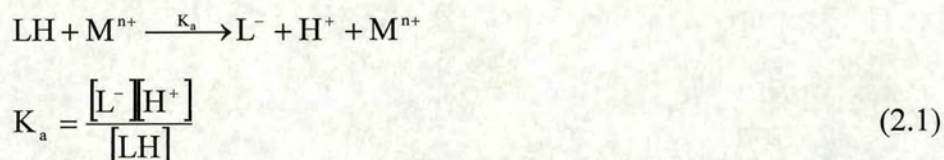
This chapter outlines the factors affecting the stability of a metal complex (Section 2.2). The wide variety of coordination geometries that the zinc(II) ion adopts in nature (Section 2.3) and in crystallographically characterised small molecule complexes contained within the Cambridge Structural Database (Section 2.4) are considered in order to gain an understanding of the common coordination geometries of zinc(II) with different donor atom types and ligand systems which give high thermodynamic stability. The criteria for the extractant, outlined in section 1.4.2.1, will be considered throughout this chapter to eliminate ligand systems that would produce zinc complexes unlikely to be extracted into an organic phase, for example those leading to charged complexes.

The questions to be addressed are, firstly, what would be the most suitable coordination number for the complex and, secondly, what would be the most suitable coordination geometry? The design of ligands to favour these will then be considered.

2.2 Factors affecting the stability of metal-ion complexes.¹⁻³

The proposed solvent extraction relies on a pH gradient across the system (Section 1.4) to transfer the metal value through the extraction and stripping stages to the tankhouse for the final reduction to the metal. Utilisation of the pH gradient mechanism dictates that the extractant must have at least one acidic proton which can be removed on complexation of the ligand to a metal. Formation of a neutral

extractable complex involves an equilibrium between the protonated ligand (HL), metal cations (M^{n+}), protons (H^+) and the complex (ML_n). The equilibrium constant, K_{extract} , involved in the formation of this extractable complex (Equation 2.3) can be expressed in terms of the acid dissociation constant of the ligand, K_a , (Equation 2.1) and the overall formation constant of the metal complex, β_n , (Equation 2.2).



Thus, the formation of the neutral extractable complex of a divalent metal (Equation 2.4) is dependent on the square of the ligand's acidity constant as well as the overall stability of the complex.



A “strong” extractant readily dissociates to provide conjugate anions (L⁻) which form stable metal complexes (ML₂). In general terms ligands which have high acid dissociation constants will provide conjugate anions which are relatively poor Lewis bases and thus will not form particularly stable metal complexes. The problem of obtaining “strong” extractants effectively requires identifying ligands which display a high “selectivity” for metal cations over protons and therefore will have a high value of K_{extract} . To obtain this “strength” the ligand must have features which ensure that the metal complex is favoured over the “proton complex”. The use of chelating ligands with cavities that match metal ion radii and which provide special bonding modes to the metal cations, *e.g.* hydrogen bonds, can contribute to this.

Selectivity is also key to metal recovery processes and the ligand must therefore be able to form a more stable complex with the metal value compared to the impurities present. The numerous factors that influence the thermodynamic stability of the metal complexes can be considered in terms of (1) the properties of the metal ion, *e.g.* oxidation state and electronic configuration, and (2) the properties of the ligand, *e.g.* types and disposition of donor atoms.

2.2.1 Nature of the metal ion: oxidation state and electron configuration.⁴

Transition metal complexes can adopt a range of oxidation states (I-VIII) although those of (II) and (III) are most common. The electronic configuration of the metal ion usually determines the coordination geometry of the complex. The most stable geometry usually prevails, except in instances where properties of the ligand prevent adoption of the favoured coordination and geometry, *e.g.* steric constraints. An explanation of preferences for particular geometries is most easily given using the

crystal field theory. The bonding between the central metal (where the d-orbital electrons in the metal have no role in bonding) and its ligands is assumed to be purely electrostatic (σ -bonds), due either to the attraction between oppositely charged ions or between the metal cation and the negative ends of dipolar molecules. For example, the geometries adopted by Ni^{2+} compounds (electronic configuration $[\text{Ar}]3d^8$) are commonly 4- and 6-coordinate square planar and octahedral compounds respectively. They both benefit from an increase in crystal field stabilisation energy (CFSE). Therefore the design of a ligand for selective extraction of nickel could be based on selecting features which promote O_h or D_{4h} geometries.

Unlike many of the transition metals zinc always has an oxidation state of (II) in coordination compounds, with the electronic configuration $[\text{Ar}]3d^{10}$. The presence of a full d-shell means that there is no CFSE contribution to impose a preferred geometry on the complex. A balance between optimising metal-ligand bond energies and minimising ligand repulsion energies thus determines the observed coordination environment of the complex.

The questions highlighted at the beginning of this chapter of what would be the most suitable coordination number and coordination geometry for the complex require amplification.

As mentioned in Section 2.2, the flowsheet requires the formation of a neutral extractable complex in an equilibrium controlled by a “pH-swing”. Given the divalent nature of zinc, this greatly restricts the number of types of ligand which could be used, especially if only homoleptic complexes can be formed (it greatly simplifies the operation process if only one ligand type is present in the extractant formulation). Monodentate mono-anionic ligands cannot be used if the coordination

number exceeds two because the complex will carry an anionic charge (see Table 2.1). Bidentate mono-anionic ligands can be used if the resulting complex has a coordination number of four. Tridentate mono-anionic ligands can only be used to generate a neutral complex if the coordination number is 6. Tetra-, penta- or hexadentate ligands must be capable of existing in a di-anionic form and must lead to complexes with coordination numbers four, five and six respectively.






Coord. No.	Geometry	Ligand Denticity					
		Mono-	Bi-	Tri-	Tetra-	Penta-	Hexa-
6		×	×	✓	×	×	✓
5	 or 	×	×	×	×	✓	×
4	 or 	×	✓	×	✓	×	×

Table 2.1. Coordination numbers and geometries which can be adopted by divalent metal ions in neutral complexes with mono-anionic bidentate and tridentate ligands and di-anionic tetra-, penta- and hexadentate ligands.

A process based on the extraction of an octahedral zinc complex would entail the use of either a mono-anionic tridentate ligand or a di-anionic hexadentate ligand to produce a charge neutral complex. An extractant capable of complexing zinc(II) in an octahedral geometry would strongly favour the formation of iron(III) complexes. Although the complex formed would be positively charged, and not be extractable

into a hydrocarbon phase, it could result in the effective loss of extractant and reduction in circuit efficiency, and therefore would be prudent to avoid.

Extraction based upon the formation of a homoleptic 5-coordinate neutral zinc complex can only be achieved using a di-anionic pentadentate extractant. Such a ligand is likely to be more expensive to manufacture than a bidentate ligand. The ease of forming irregular geometries between trigonal-bipyramidal and square-pyramidal and the possibility of solvation of the exposed coordination site, leading to the formation of a 6-coordinate complex, may also mean that the selectivity may not be sufficiently good.

An extractant based upon the formation of a 4-coordinate neutral zinc complex could be based upon either a mono-anionic bidentate ligand or a di-anionic tetradentate ligand, with the manufacturing costs most probably favouring the more simple bidentate ligand. Both square planar and tetrahedral geometries are observed for 4-coordinate transition metal complexes. For zinc, however, a lack of CFSE results in the ligands adopting the least sterically constraining positions around the metal centre. Therefore tetrahedral geometry is usually always preferred, except in the circumstances where a square planar arrangement is imposed due to ligand constraints. In contrast copper(II) and nickel(II) benefit from an increase in CFSE when a square planar geometry is adopted. This difference in preferred coordination geometry in bis-bidentate complexes may provide a means of gaining selectivity for zinc. By designing bidentate ligands with sufficiently bulky substituents it should be possible to prevent the formation of highly stable copper(II) and nickel(II) complexes by forcing the geometry to distort from planarity. An additional advantage of using bulky bidentate ligands would be in disfavouring the formation of a stable octahedral

iron(III) complex by preventing the binding of three ligands around the iron(III) cation.

2.2.2 Nature of the ligand: hard-soft / acid-base theory.

The donor atom type in the ligand will affect the stability of the resulting metal complex. The Lewis acid-base concept defines the metal as the acid (electron pair acceptor) and the ligand, containing the donor atom(s), as the base (electron pair donor). Acids and bases have been categorised^{5,6} as being either “hard” (class a), “soft” (class b) or borderline. Hard acids tend to be highly charged ions of electropositive elements and are not easily polarisable, *e.g.* Co^{3+} , Cr^{3+} , and Al^{3+} . They tend to form stable (through primarily electrostatic interactions) complexes with hard bases that in turn tend to be small and electronegative, *e.g.* R_3N , O^{2-} and F^- . Metals with a lower oxidation state are softer than the corresponding metal with a higher oxidation state. They tend to form stable complexes with less electronegative and more easily polarisable ligands, *e.g.* I^- , through primarily covalent interactions. Such ligands often have empty π^* orbitals capable of accommodating charge from the metal d-orbitals by π -back bonding, *e.g.* R_3P , CO , CN^- , RS^- . Many divalent 1st row transition metals, including zinc, are classed as borderline and can have an affinity for hard and soft donor atom types alike, Table 2.2.

Hard	Borderline	Soft
Acids		
H ⁺ , Li ⁺ , Na ⁺ , K ⁺ , Be ²⁺ , Mg ²⁺ , Ca ²⁺ , BF ₃ , Al ³⁺ , Sc ³⁺ , Ti ⁴⁺ , VO ²⁺ , Cr ³⁺ , Fe ³⁺ , Co ³⁺	Fe ²⁺ , Co ²⁺ , Ni ²⁺ , Cu ²⁺ , Zn ²⁺ , Rh ³⁺ , R ₃ C ⁺ , Pb ²⁺ , Sc ²⁺	Cu ⁺ , Ag ⁺ , Au ⁺ , Cd ²⁺ , Hg ²⁺ , Pt ²⁺ , Pt ⁴⁺ , MnO ₂ , Pd ²⁺
Bases		
NH ₃ , RNH ₂ , N ₂ H ₄ , H ₂ O, OH ⁻ , O ²⁻ , ROH, RO ⁻ , CO ₃ ²⁻ , SO ₄ ²⁻ , ClO ⁴⁻ , F ⁻ , Cl ⁻	PhNH ₂ , N ₃ ⁻ , N ₂ , Br ⁻ , SO ₃ ²⁻ , imines	H ⁻ , R ⁻ , C ₂ H ₄ , C ₆ H ₆ , CN ⁻ , CO, SCN ⁻ , R ₃ P, R ₂ S, RSH, RS ⁻ , I ⁻

Table 2.2. Classification of some hard and soft acids and bases.^{7,8}

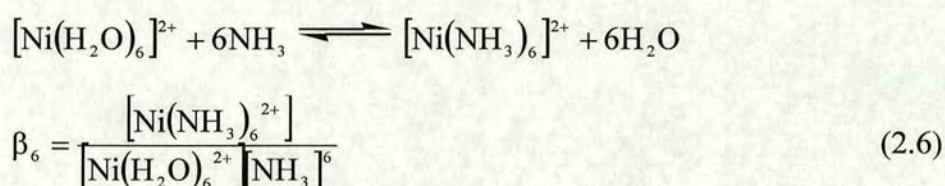
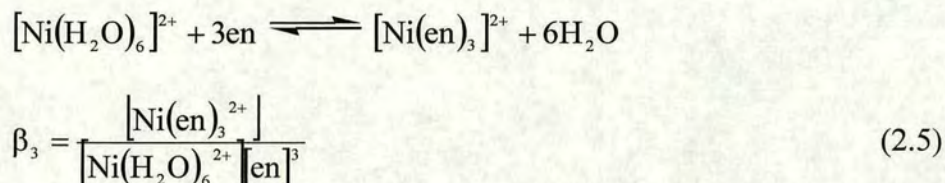
From this table it can be seen that in the design of a solvent extractant for a hard metal cation such as Fe³⁺ might utilise hard base ligands such as phenolates or alkoxides. However, from the hard-soft / acid-base concept, the identification of an appropriate donor atom types for a potential zinc extractant is less clear and a different approach is needed. Two simple approaches can be taken;

1. Biomimetic approach – use the donor atom types found in very stable zinc-containing proteins and metalloenzymes, Section 2.3.
2. Observation of the most commonly adopted coordination numbers and geometries in small molecule complexes in the Cambridge Structural Database (CSD), Section 2.4.

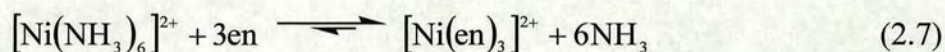
2.2.3 Chelate effect.^{1-3,7,9}

Experimentally it is observed that complexes of chelating ligands are more stable than those of comparable monodentate ligands.¹⁰ For example, the stability constant

for the complexation of Ni^{2+} by ethylenediamine (en, $\text{NH}_2\text{CH}_2\text{CH}_2\text{NH}_2$) ($\log\beta_3 = 18.3$), equation 2.5, is larger than for complexation by six NH_3 ($\log\beta_6 = 8.6$), equation 2.6.



As a consequence of the chelate effect it is thermodynamically favourable for six NH_3 ligands to be replaced by three en ligands, equation 2.7.



The increased stability of $[\text{Ni}(\text{en})_3]^{2+}$ compared to $[\text{Ni}(\text{NH}_3)_6]^{2+}$ can be understood by considering differences in the enthalpy (ΔH°) and entropy (ΔS°) of the complex formation in the system. The equilibrium constant is related to the standard free energy (ΔG°) of the reaction, equation 2.8.

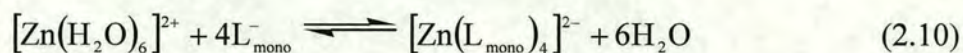
$$\Delta G^\circ = -RT \ln K \quad (2.8)$$

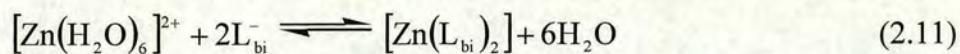
When large values of K are encountered the reaction proceeds to the right and has a large negative value of ΔG° . The standard free energy is also related to the temperature and changes in enthalpy and entropy, equation 2.9.

$$\Delta G^\circ = \Delta H^\circ - T\Delta S^\circ \quad (2.9)$$

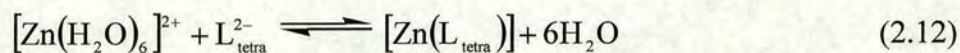
A reduction in the free energy ($\Delta G^\circ = -54 \text{ kJmol}^{-1}$) by the displacement of NH_3 by the bidentate ethylenediamine ligands, equation 2.7, is a result of a favourable change in the enthalpy and entropy terms. A change in enthalpy of reaction ($\Delta H^\circ = -29 \text{ kJmol}^{-1}$) contributes to approximately half of this, which could be attributed to the nickel-nitrogen bond being stronger in $[\text{Ni}(\text{en})_3]^{2+}$ than in $[\text{Ni}(\text{NH}_3)_6]^{2+}$. However, it could also be that there is less strain energy required in forming the en complex because the $\text{N}\cdots\text{N}$ repulsion energies have already been partly overcome in the synthesis of en. The remaining change in free energy is accounted for by an increase in the entropy as four species are converted into seven species ($\Delta S^\circ = 88 \text{ JK}^{-1}\text{mol}^{-1}$) and differences in solvation of the species.

A favourable chelate effect can be utilised to increase the metal complex stability and therefore enhance its solvent extraction. For example the extraction of zinc(II) ions using a bidentate ligand compared to that of comparable monodentate ligands is expected to be associated with a larger entropy of reaction, equations 2.10 and 2.11, although the actual entropies of reaction will also depend on the level of solvation of the species.





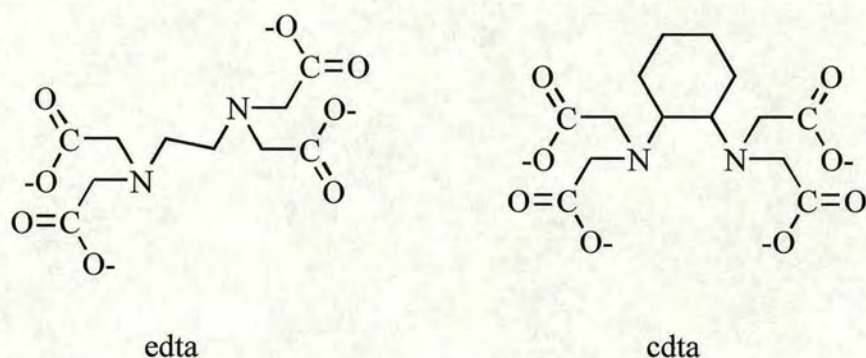
A further increase in entropy of reaction is expected with the use of a tetradentate ligand, equation 2.12.



The design of the ligand is highly important to the stability of the complex. It is not solely dependent on its denticity (entropy), but also on its capability of providing and/or adopting the most thermodynamically stable geometry. A ligand will adopt a conformation that is most sterically and energetically favourable, *i.e.* to reduce the electrostatic repulsion between donor atoms. However a considerable geometrical arrangement of the ligand, to a more highly strained conformation, is usually required on complexation to a metal. By designing a ligand in which the donor atoms are fixed closely to the arrangement required in the metal complex the electrostatic repulsions can be, to an extent, overcome. Thus the design of highly pre-organised ligands, which display the appropriate geometry, can also lead to an increase in the stability of the metal complex.

The significance of pre-organisation of donor sets can be exemplified by comparing ethylenediaminetetraacetate (EDTA) and cyclohexyldiaminetetraacetate (CDTA), Figure 2.1. For example, the hexadentate ligand, EDTA, forms very stable complexes with Cu^{2+} and Fe^{3+} . The flexible ethylene bridge allows the free ligand to adopt a less strained skew geometry and reduce the *intra*-electrostatic repulsions

between its carboxylate groups. On complexation it must therefore undergo a conformational rearrangement to a more strained geometry.



		EDTA	CDTA
Cu(II)	logK	18.7	21.9
Fe(III)	logK	25.0	30.0

Figure 2.1. Stability constants for Cu^{2+} and Fe^{3+} with EDTA and CDTA.¹¹

However, if the ethylene bridge is replaced by a less flexible cyclohexyl unit, as in CDTA, the nitrogen atoms are held in a *trans* position, close to the arrangement required in the metal complex. The electrostatic repulsions between the nitrogen donors has been overcome in the synthesis of the ligand and higher stability constants with both Cu^{2+} and Fe^{3+} are observed compared to EDTA.

The size of a chelate ring also affects the stability of the metal complex. In general, those which contain 5- and 6-membered chelate rings, are the most common^{11,12} and the most stable. In the case of unsaturated 5- and 6- membered rings in which resonance occurs, the atoms are approximately coplanar, Figure 2.2. Above a ring size of six the stability of complexes generally decreases due to an increase in the ring strain, which can invoke puckering of the chelate to overcome the strain.



Figure 2.2. Unsaturated 5- and 6-membered coplanar chelate rings.

The distance between the donor atoms in the chelate, which is partly dependent on the size of the ring, and the metal-donor bond lengths are key in influencing the size of the donor-metal-donor angle (X-M-X). For a tetrahedral complex the ideal donor-metal-donor angle, from one apex (X) through the centroid (M) to another apex, is 109.5° , Figure 2.3.

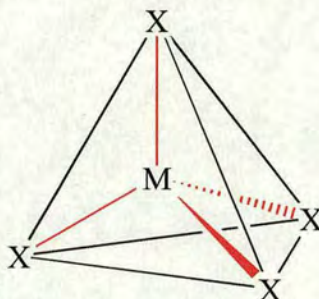


Figure 2.3. An illustration of a tetrahedron and tetrahedral geometry.

For planar 5- and 6-membered chelates the sum of the angles round each ring is 540° and 720° respectively. If the donor-metal-donor angle is ideally 109.5° then the average remaining angle around the chelate is 107.8° for the 5-membered ring and 122.1° for the 6-membered ring. Clearly those in the 6-membered ring are closer to the ideal 120° for sp^2 hybridisation in a planar ring and therefore on this basis a 6-membered ring would be best suited for adopting a tetrahedral geometry. There are of course other factors such as (1) the ionic radius of the metal ion and its effect on

the donor-metal-donor angle and (2) the size of the ring, if any, which is annealed to the chelate ring, but in general this is a good guide.

2.3 The role of zinc(II) ions in biology.

Zinc is the second most abundant trace metal in humans. A human body weighing approximately 70 kg contains around 2-3 g of zinc.¹³ There are over 100 known zinc-containing enzymes in living systems, but of these only a few have been structurally characterised, Table 2.3. The biological role of zinc(II) falls into two categories; (1) where it acts as a catalytic centre in a metalloenzyme and (2) where it is a structural component in a protein.¹³ As zinc is generally strongly bonded in these systems it is useful to know what donor atom types and dispositions are involved. A biomimetic approach could then be used for the design of extractants for zinc.

	Mass kDa	Lig 1	Lig 2	Lig 3	Lig 4	Biological Function	Ref
Carbonic anhydrase (II)	28-30	His	His	His	H ₂ O	CO ₂ hydration	[13]
Carboxypeptidase A	34	His	His	η^2 -Glu	H ₂ O	Peptide hydrolysis	[14]
Thermolysin	34.6	His	His	η^1 -Glu	H ₂ O	Peptide hydrolysis	[15]
Alkaline phosphatase	2 x 47	His His	His η^1 -Asp	η^2 -Asp μ -Asp	H ₂ O H ₂ O	Phosphate ester hydrolysis	[13]
Alcohol dehydrogenase	2 x 40	His Cys	Cys Cys	Cys Cys	H ₂ O Cys	Oxidation of alcohols	[16]
Superoxide dismutase	2 x 16	His	His	μ -His	η^1 -Asp	Disproportionation of superoxide	[16]
Zinc fingers	-	His	His	Cys	Cys	DNA binding	[13]

Table 2.3. Some structurally characterised Zn(II)-containing biomolecules.

An enzyme is a protein that catalyses a biochemical reaction and a metalloenzyme is one that contains a metal as the catalytic centre.¹⁷ Zinc(II) acts as a Lewis acid, lowering the pK_a of coordinated water and promoting the loss of a proton to leave a coordinated hydroxide, which in turn acts as a strong nucleophile in associated mechanistic pathways. Alternatively, the coordinated water molecule can exchange rapidly with a substrate, a property of the kinetic lability of ligands in zinc complexes which is attributed to the lack of preference for a given coordination number. However the zinc itself must not be lost from the protein. The ready formation of low coordination number sites, which are more acidic than high coordination number sites, together with the ease of deformation and accessibility of 4-, 5- and 6-coordination numbers throughout the catalytic cycle, are features that benefit the presence of zinc in the catalytic centre.^{13,17} Perhaps the most important feature is the lack of redox chemistry (E^0 for $Zn^{2+}/Zn = -0.762$ V as no other cationic forms of zinc are accessible)¹⁸, where the presence of a redox active metal could promote reactions deleterious to the host. As mentioned above zinc(II) is a borderline metal with respect to hardness and has an affinity for N, O and S donor atoms. Consequently it is therefore commonly found coordinated to histidines (His), glutamates (Glu), aspartates (Asp) and cysteines (Cys), Figure 2.4, or solvent bound (H_2O), in proteins.¹⁶

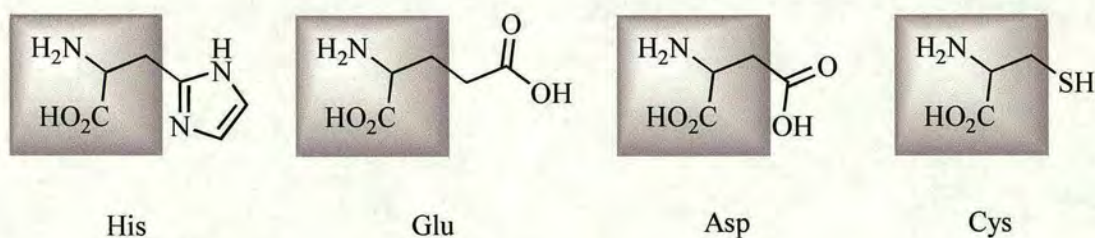


Figure 2.4. The amino acid residues found coordinated to zinc in nature.

Two histidines (His-94 and His-96) are bound *via* the N(4) atom on the imidazole ring whereas one (His-119) is bound *via* the N(2) atom. All appear to be bonded equally strongly, with similar bond lengths, the differences in bonding modes are probably dictated by the steric constraints of the protein folding.

2.3.1.2 Carboxypeptidase A and thermolysin.

Carboxypeptidase A, Figure 2.6(a), and thermolysin, Figure 2.6(b), both hydrolyse peptides and esters. Carboxypeptidase hydrolyses C-terminal amino acids from peptides in mammals whereas thermolysin hydrolyses bacterial peptide sequences. Although the amino acid sequences and the overall structures of carboxypeptidase A and thermolysin are unrelated, the active sites of these two metalloenzymes are remarkably similar¹⁵ as are their proposed mechanistic pathways.¹⁹

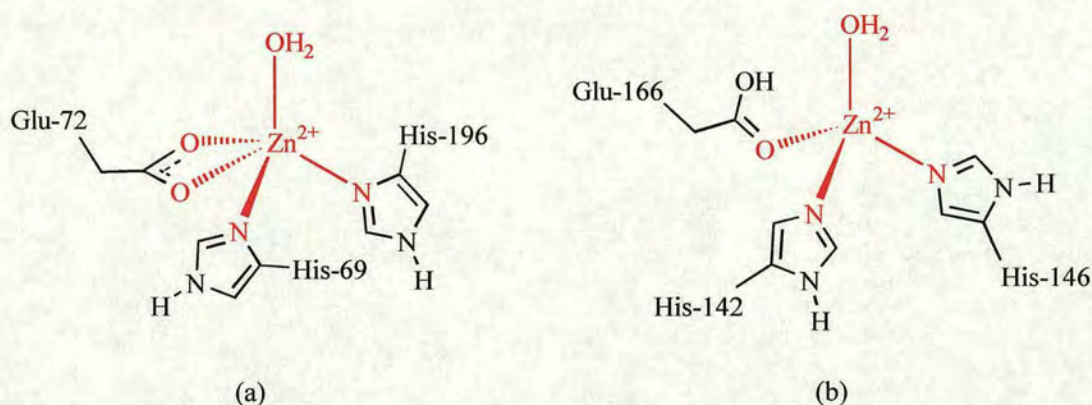


Figure 2.6. Representations the active sites in (a) carboxypeptidase A and (b) thermolysin.

The zinc(II) ion in carboxypeptidase A is coordinated to two histidine residues (His-69 and His-196), a bidentate glutamate (Glu-72) residue and a water molecule,

weakly bound, in a distorted pentacoordinate geometry.²⁰ In thermolysin the zinc(II) ion is also bound to two histidines (His-142 and His-146), a glutamine (Glu-166) and a water molecule. However the glutamate residue is bound in a monodentate fashion forming a distorted tetrahedral arrangement at the active site.

2.3.1.3 Alkaline phosphatase.

Alkaline phosphatase (AP) catalyses the hydrolysis of phosphate esters.¹⁶ The most studied AP is the enzyme from *E. Coli* and is an example of a tri-nuclear metalloenzyme, Figure 2.7. It is bilobal in structure with identical subunits, each containing three metal binding sites. In the example discussed here each site contains two zinc(II) ions and one magnesium ion, although in some enzymes all three are zinc.

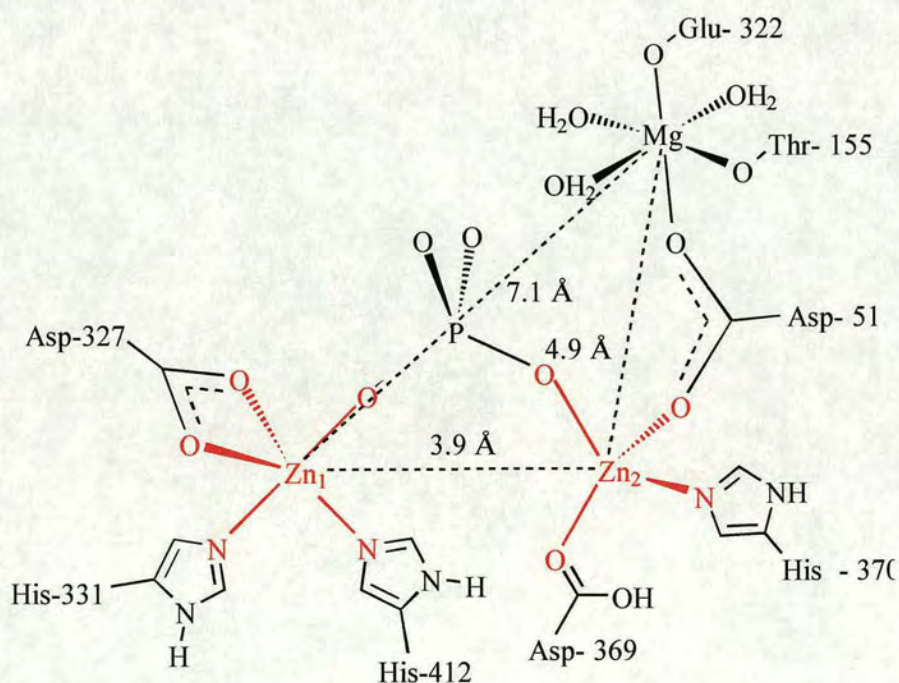


Figure 2.7. Representation of active site of the metalloenzyme alkaline phosphatase from *E. Coli*.

The first zinc ion (Zn_1) is pentacoordinated to two histidine residues (His-331 and His-412), a bidentate aspartate (Asp-327) and a bridging phosphate ester. It is best described as pseudotetrahedral with both oxygen atoms of the chelating Asp-327 occupying one apex. The second zinc ion (Zn_2) is ligated to one imidazole residue (His-370), one monodentate aspartate (Asp-369), a bridging phosphate ester and a bridging aspartate (Asp-51) also in a distorted tetrahedral array. The two zinc sites are separated by 3.9 Å. In the native AP the bridging phosphate ester positions would be occupied with coordinating water molecules.

2.3.1.4 Alcohol dehydrogenase.

Alcohol dehydrogenase (ADH) is one of a class of oxidoreductases. It catalyses the oxidation of primary alcohols to aldehydes. Liver alcohol dehydrogenase (LADH), Figure 2.8, consists of two polypeptide units each containing two zinc(II) ions. In LADH zinc plays the role of both the catalytic centre and a component of the structural framework. The zinc at the catalytic site is coordinated to one histidine (His-167), two thiolato cysteine residues (Cys-46 and Cys-174) and a water molecule. The other zinc is bound to four cysteine residues (Cys-97, Cys-100, Cys-103 and Cys-111) and is deep within the enzyme where it is inaccessible to water.¹⁶

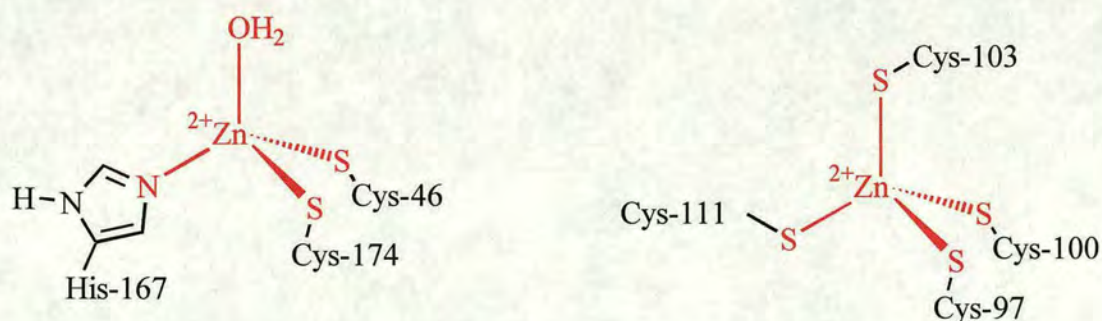


Figure 2.8. Representation of the zinc binding motifs in LADH.

2.3.2 Structural roles.

Zinc(II) ions can also have a purely structural role within proteins. Three examples are superoxide dismutase¹⁵ and “zinc finger” proteins¹³ and alcohol dehydrogenase.

2.3.2.1 Superoxide dismutase.

Bovine erythrocyte superoxide dismutase (BESOD) contains two identical subunits held together by hydrophobic interactions. The active site, Figure 2.9, contains two metals, copper and zinc.

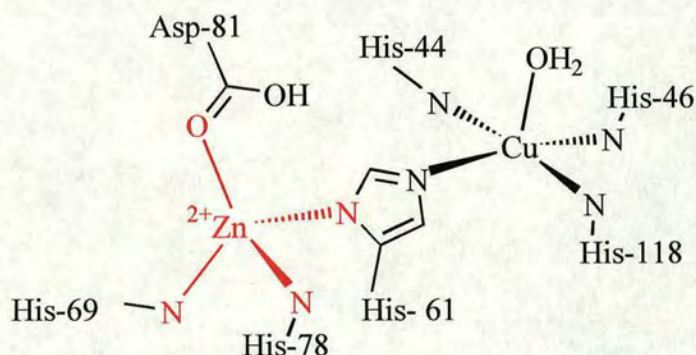


Figure 2.9. Representation of the structural role of zinc in BESOD.

The copper ion is the catalytic site and has a distorted square pyramidal geometry, coordinated to four histidine residues (His-44, His-46, His-61 and His-118) and a water molecule at the apical position. One of the histidine residues (His-61) bridges to the zinc(II) ion. Together with two other histidine residues (His-69 and His-78) and a monodentate aspartate (Asp-81) the zinc ion is four coordinate with distorted tetrahedral geometry. The Cu-Zn separation is ~ 5.4 Å.¹³ The copper acts as the redox centre for the disproportionation of superoxide while the zinc appears to play a

purely structural role, removal of which leads to loss of thermal stability and denaturing of the enzyme.²⁰

2.3.2.2 Zinc fingers.

Zinc(II) ions can provide a structural centre to direct the folding of proteins. DNA-binding metalloproteins, or “zinc fingers”, play an important role in controlling the transcription of RNA. The zinc binds along the amino acid oligomer with distorted tetrahedral geometry, causing the protein to fold defining the 3-dimension α -helical loop, Figure 2.10(a). These “zinc fingers” lie in the major groove of DNA. Three types of protein folds have been identified, (a) the zinc fingers, (b) the zinc twists and (c) the zinc clusters.

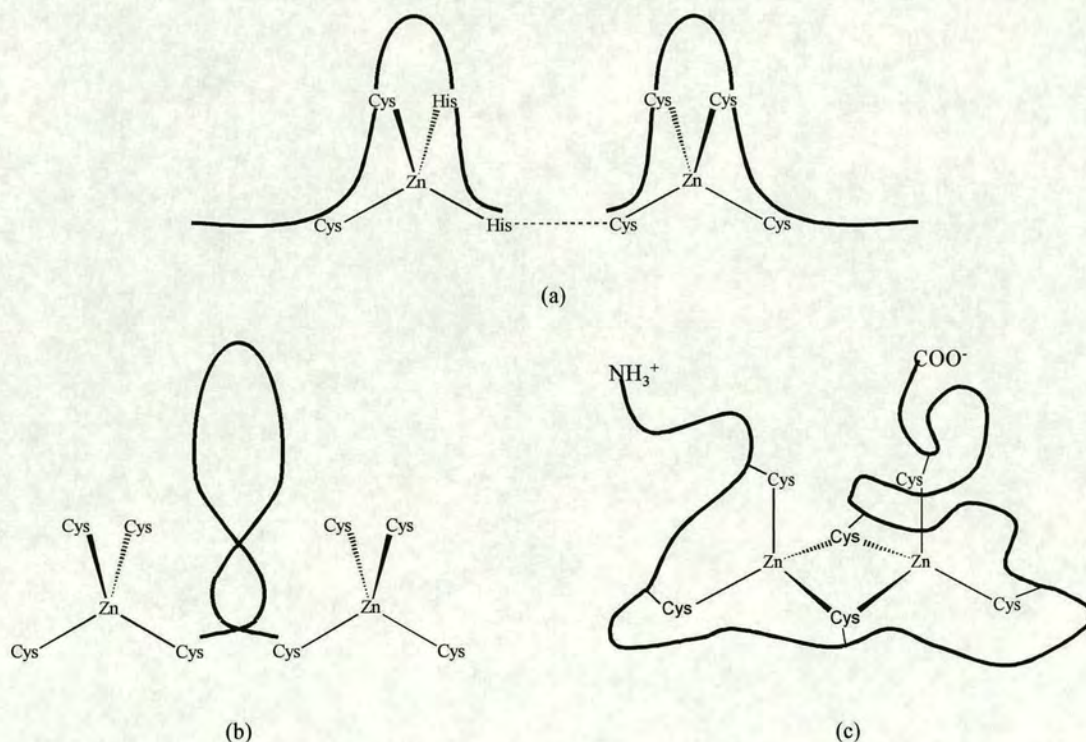


Figure 2.10. Representation of (a) zinc fingers, (b) zinc twists and (c) zinc clusters.¹³

In transcription factor IIIA (TFIIIA) the zinc(II) ion binds to two imidazole histidines and two thiolato cysteines to form zinc fingers. In yeast transcription factor GAL4 two zinc ions are tetrahedrally coordinated to six cysteine residues, two of which are bridging (Zn-Zn distance = 3.5 Å). The structural motif of the glucocorticoid receptor (Glu Rec) also contains two zinc ions that tetrahedrally ligate to four cysteine residues and are separated by 13 Å.¹³

2.3.3 Summary.

As discussed above, zinc can play important structural as well as catalytic roles in proteins. One major feature that distinguishes these two roles is that an open coordination position is always present at a catalytic zinc site but is absent at a structural site. There are other differences between the ligand types within these two classes of zinc proteins. A distinct donor atom type pattern is seen, Table 2.3. Where the zinc ion occupies a catalytic site nitrogen and oxygen donor based ligands are most common, the inner sphere compositions shown here are of the type [Zn(His)₃(OH₂)], [Zn(His)₂(Glu)(OH₂)], [Zn(His)₂(Asp)(OH₂)] and [Zn(His)(Cys)₂(OH₂)]. For structural sites the compositions of [Zn(Cys)₄] and [Zn(Cys)₂(His)₂] are observed. Both catalytic and structural sites have a tendency to adopt a distorted tetrahedral coordination sphere. For catalytic zinc, one of the coordination sites is occupied by a water molecule, which either functions directly in the catalytic reaction and/or is easily replaced by a substrate. They can undergo rapid ligand exchange of both the bound substrate and the water molecule, *e.g.* HCA(II). In doing so the coordination sphere easily fluctuates from four to five or six during substrate binding. In structural sites the distorted tetrahedral coordination

is derived from protein bound ligands, *i.e.* does not bind substrates or water molecules, in which the donor atoms are commonly nitrogen or sulfur. The presence of more than two cysteine ligands and the absence of a coordinated water molecule reduces the likelihood that the coordination sphere might expand beyond four, thus precluding the potential use of such zinc centres for substrate binding.

From a structural stability perspective this evidence might suggest that ligands containing either sulfur or sulfur / nitrogen donor atom sets would best provide zinc complex stability rather than oxygen or oxygen / nitrogen donor atom sets. However the choice of sulfur and nitrogen donating amino acids in Nature is not only to provide coordinative stability but also to preferentially select zinc and discriminate against other trace metals available to biological systems, *e.g.* copper and nickel disfavour tetrahedral coordination.

For our purposes in defining appropriate donor sets for “strong” and selective extractants it would appear more appropriate to use the “zinc fingers” type sites. Donor sets which favour 5-coordinate structures will lead to difficulties in ensuring that homoleptic complexes are formed unless a di-anionic pentadentate molecule is used (see Table 2.1). Also ligands, particularly simple bidentate systems, containing anionic oxygen donors are likely to bond very strongly to iron(III), forming 3:1 complexes.

2.4 Cambridge structural database survey.

The wealth of structural information available in the Cambridge Structural Database²¹ (CSD) has been analysed to help identify ligands that show potential as extractants with a preference for tetrahedral coordination. It has been used to

classify transition metal complexes in terms of the angles that describe their coordination geometry, *e.g.* square planar and tetrahedral 4-coordinate complexes, (Figure 2.11).

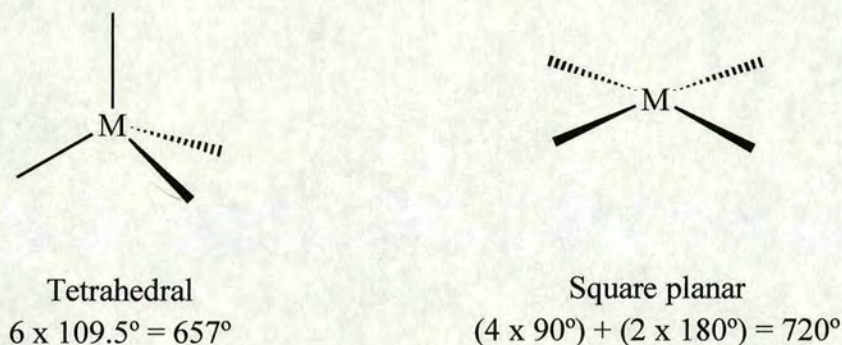


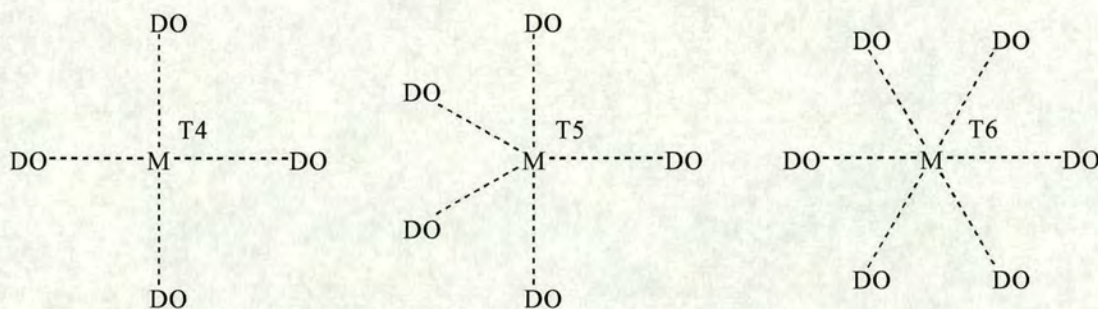
Figure 2.11. An illustration of the six donor-metal-donor angles that define the geometry around a central metal ion in a 4-coordinate complex.

For perfect tetrahedral geometry the sum of the donor-metal-donor angles is expected to be 657° , and for perfect square planar geometry, 720° . However, it is often found that the sum of the angles observed is not either of these two values. This is because complexes that are described as square planar are often neither perfectly square nor planar, while complexes that are described as tetrahedral can also exhibit severe distortions. The aim of this survey is therefore to identify tetrahedrally selective ligands rather than perfectly tetrahedral complexes.

The search has been divided into three categories, zinc(II), nickel(II) and iron(III). The CSD contains over 197,000 crystal structures, of which 10,807 contain either Zn (1793), Fe (4669), or Ni (4345) in mononuclear complexes.

2.4.1 Description of search procedure.

The metal complex structures involving zinc(II), nickel(II) and iron(III) were extracted from the CSD using the QUEST program in separate searches. The first step was to subdivide each set by the coordination number of the complex. This was achieved by employing the following procedure:



1. Specify the metal (M).
2. Specify the donor atom type (DO) to represent generic donor atoms (N, O, S, or any halogen).
3. Connect the DO's to the metal (M) using *Any bond* type.
4. In the *2D Constraints menu* select *Total coordination no.* (TX, X = 4, 5 or 6).
5. In the *3D Constraints menu* define all angles and all bonds using the *Parameter* command.
6. Specify a mononuclear complex using the *Search* menu then selecting *Formula* and applying the parameter *4m1* which indicates that complexes containing only one atom from the 1st transition metal row will be selected.

7. For iron only, specify the oxidation state by selecting the **NAME* parameter in the *Search* menu and applying the constraint *iron(iii)*.

Such searches allow the number of 4-, 5-, and 6-coordinate structures for each metal with either N, O, S or halogens as donors to be determined. Searches were carried out for each coordination number to separate the results into specific donor atom sets, e.g. DO = [S₄], [S₂N₂].

2.4.2 Zinc(II) complexes in the CSD.

In order to test the assumption that the absence of any CFSE for zinc(II) with its d¹⁰ configuration leads to a preference to adopt 4-coordinate tetrahedral geometries was investigated by looking at the distribution and composition of 4-, 5-, and 6-coordinate zinc complexes. This revealed that there are also many examples of 5- and 6-coordinate zinc complexes in the CSD. The distribution of the sum of the angles that define the 4-, 5- and 6-coordinate zinc systems, Figure 2.12, demonstrate a clear separation of each coordination number.

The sum of the six angles that describe the 4-coordinate species range between 640-720°. The 10 angles that describe 5-coordinate species sum to between 940-1080°, whereas the 15 angles that describe 6-coordinate species range between 1500-1620°. The frequency of structures for each coordination number implies that 4-coordinate species are the most commonly represented in the CSD. However it is found that many of the structures are represented more than once, e.g. [ZnCl₄]²⁻ and [Zn(H₂O)₆]²⁺. Other factors also contribute to the relative frequency of a particular donor atom set or ligand type, which include; (1) scientific interest, (2) ease of ligand and metal complex synthesis and (3) ease of crystallisation. Therefore the abundance

of a particular donor atom set or ligand type is not an indication of the stability of the associated metal complex.

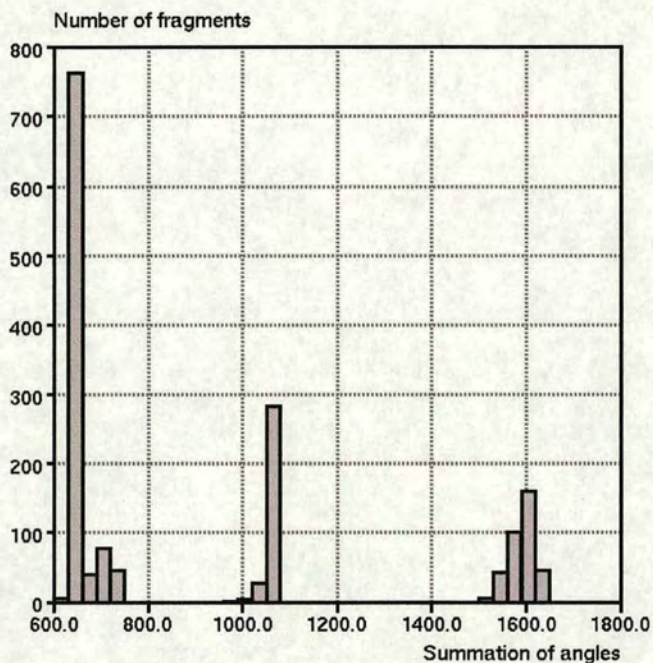


Figure 2.12. Summation of the angles that describe 4-, 5- and 6-coordinate mononuclear zinc structures where the donor atoms represent N, O, S or any halogen.

Less emphasis was placed upon the 5- and 6-coordination surveys simply because they are not candidates for ligand systems (see Section 2.2.1) although the distribution of donor atom sets within these surveys can be compared against those of the 4-coordinate results.

2.4.2.1 Four coordinate zinc complexes.

The occurrence of 4-, 5- and 6-coordinate zinc(II) complexes with donor atom sets containing any combination of nitrogen, oxygen sulfur or halogen is graphically represented in Figure 2.13.

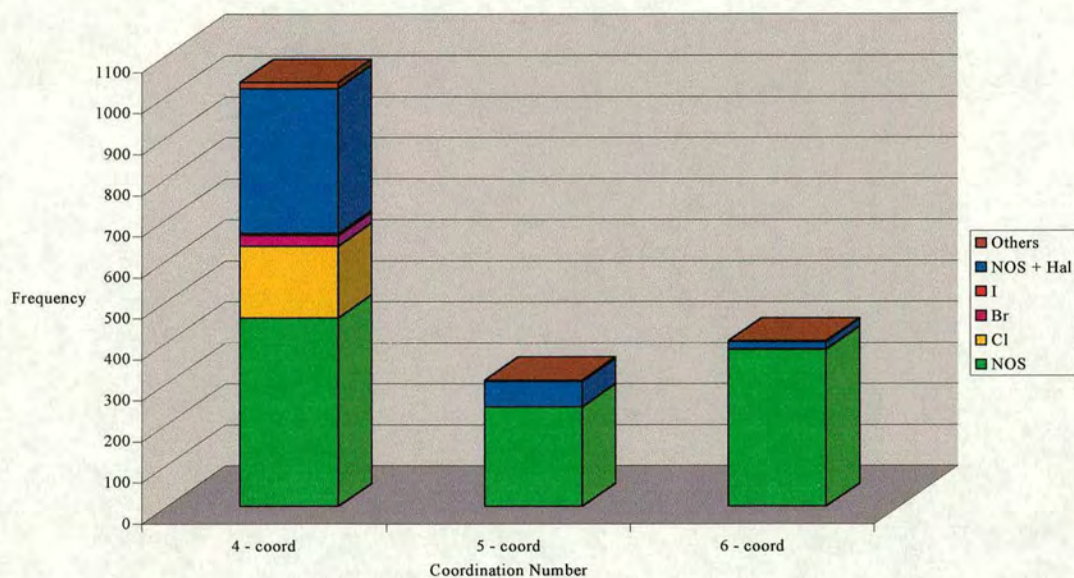


Figure 2.13. The occurrence of mononuclear ZnX_Y complexes in the CSD where X is any combination of N, O, S or halogen and Y = 4, 5, or 6.

The structures of greatest interest are those with a donor atom set comprising of either N, O or S which form simple neutral complexes. These were selected for further analysis. Those that contained any halogen donors, mainly of the type $[ZnCl_4]^{2-}$, or formed a charged species have not been considered further.

A more detailed analysis of the 4-coordinate structures, Figure 2.14, reveals the donor atom combinations present.

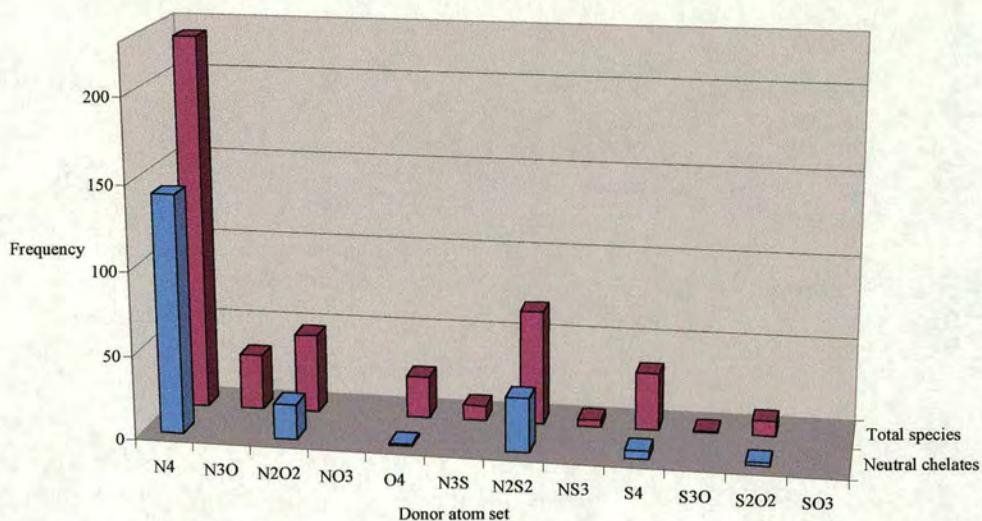


Figure 2.14. Distribution of 4-coordinate ZnX_4 ($X = N, O, S$) complexes.

In total the CSD contains 453 $ZnN_XO_Y S_Z$ ($X + Y + Z = 4$) structures, approximately half of which are charged species and/or comprise of monodentate ligands (228). The donor atom sets that are not represented at all in the CSD are $[NO_3]$ and $[SO_3]$, whereas those of $[N_3O]$, $[NO_3]$, $[N_3S]$, $[S_3O]$, $[SO_3]$ are not represented as neutral polydentate compounds. Those that do form neutral polydentate compounds ($[N_4]$, $[N_2S_2]$, $[N_2O_2]$, $[S_4]$, $[S_2O_2]$ and $[O_4]$) are dominated by the $[N_4]$ donor atom set.

Inspection of the total angle distribution of the $[N_4]$ and the other represented donor atom sets, Figure 2.15, reveals that $[N_4]$ species ($>680^\circ$), without exception, belong to the macrocyclic porphyrin family, which forces D_{4h} symmetry. The other donor atom sets are only present in the tetrahedral configuration that usually predominates in 4-coordinate zinc structures.

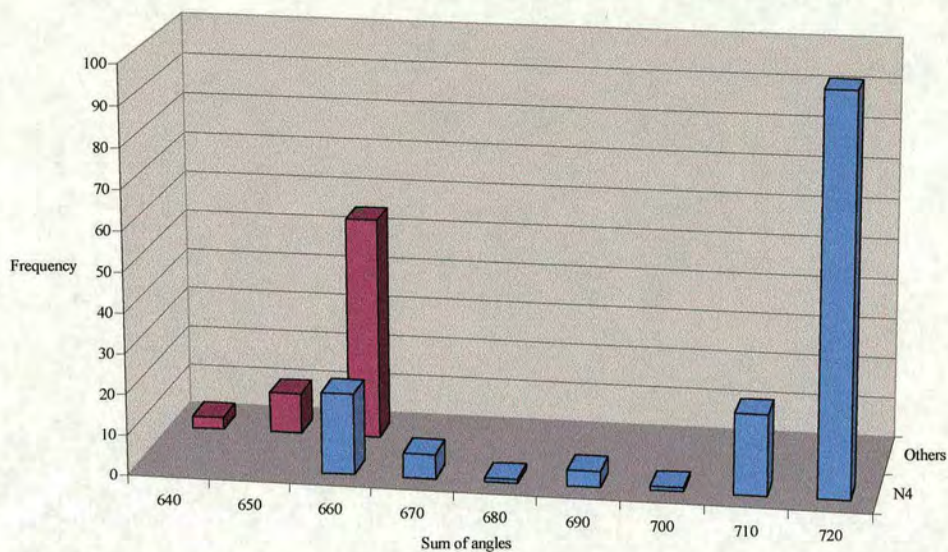


Figure 2.15. Total angular distribution of donor atom sets of 4-coordinate zinc compounds.

The ligands that give zinc complexes with geometries close to tetrahedral and form neutral bis-bidentate complexes are summarised in Figure 2.16. The topological tree diagram at the top of Figure 2.16 denotes the number of donor atoms present and their arrangement in the ligand backbone.²² In this bidentate case there is only one fundamental way of arranging the donor atoms, linear. As expected for the zinc(II) complexes (see Section 2.2.2) the selection of bidentate ligands (Figure 2.16) contain N, O, and S donor atoms and shows no obvious donor atom type preference. The predominant metal chelate ring size contains 6-members, which is proposed to favour tetrahedral configurations (Section 2.2.3), although examples of 5-membered chelate rings are present, as is one example of a 4-membered chelating ligand, dithiocarboxylate.

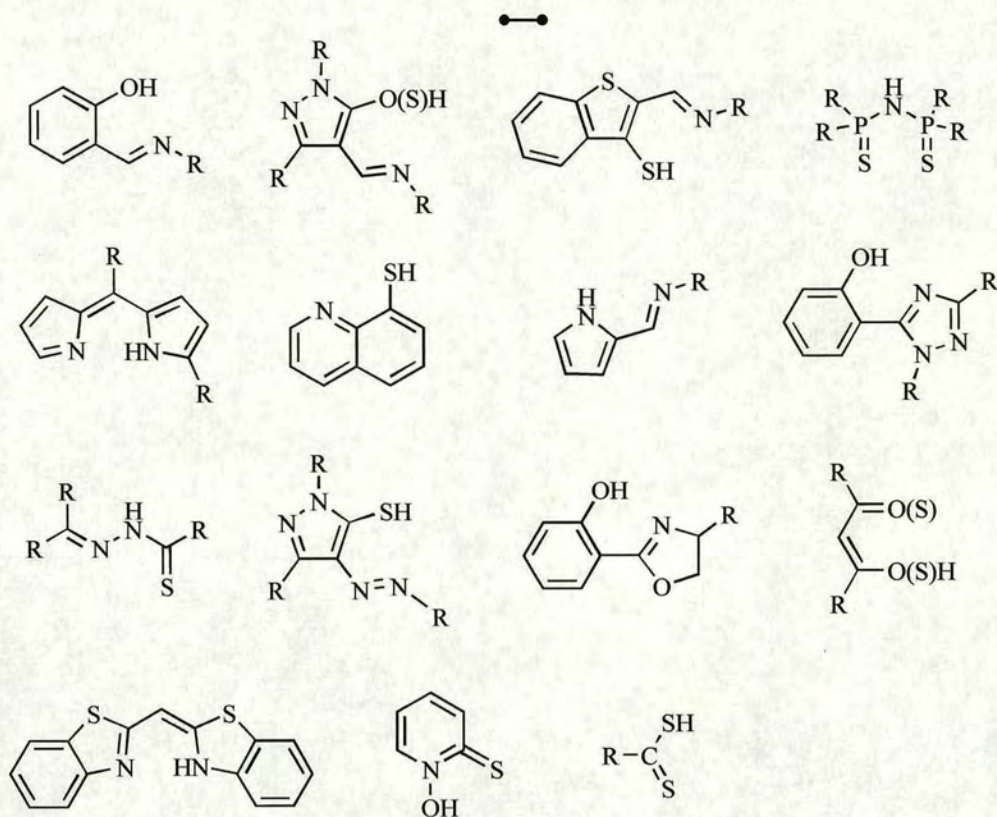


Figure 2.16. Ligands identified that tetrahedrally coordinate zinc(II) to give neutral complexes.

2.4.2.2 Five coordinate zinc complexes.

The search for 5-coordinate zinc structures, Figure 2.13, gave 308 mononuclear species with the formula ZnX_5 ($X = N, O, S, \text{Hal}$). Of these, 232 complexes (Figure 2.17) are distributed between the donor atom sets containing nitrogen, oxygen or sulfur, most of which are charged species and/or are comprised of monodentate ligands.

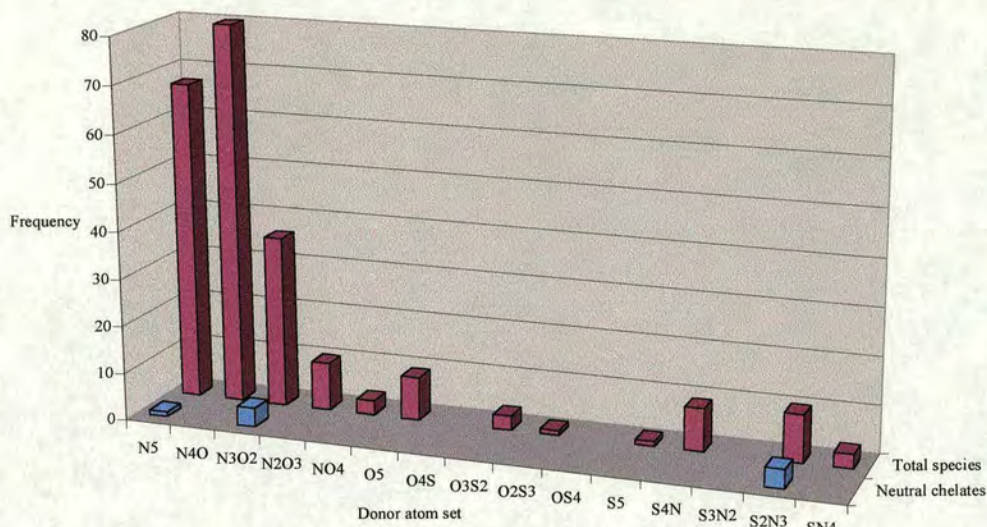


Figure 2.17. Distribution of 5-coordinate ZnX_5 ($X = N, O, S$) complexes.

Ligands containing nitrogen and oxygen donors are widespread, whereas few examples are provided in which sulfur is incorporated in the coordination sphere. Neutral complexes containing pentadentate ligands are represented by only a few examples, Figure 2.18.

There is an increasingly large number of ways in which the donor atoms could be arranged on the ligand backbone as the number of donor atoms present increases. However only three are observed in the pentadentate di-anionic zinc(II) complexes in the CSD, those with a linear arrangement being most common. The observed coordination geometry is somewhat dependent upon the saturation of the ligand. The unsaturated ligands first prepared by Sacconi and Bertini²³ that are derived from salicylaldehyde and triamines (top right) and the related ligands (top middle) form structures intermediate between trigonal-bipyramidal and square-pyramidal. The fully saturated ligands (top left) offer more flexibility and generally can accommodate coordinated solvent to form a 6-coordinate metal complex.²⁴ The

branched tripodal ligand (bottom left) and the cyclic porphyrin (bottom right) both complex with a square pyramidal configuration but readily adopt an octahedral configuration with a coordinated solvent molecule.

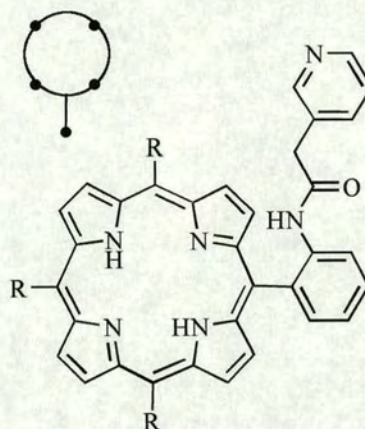
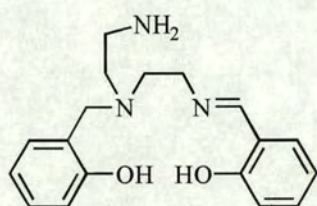
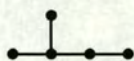
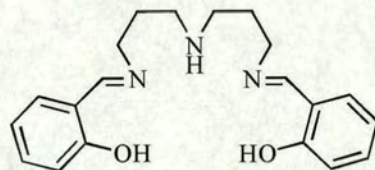
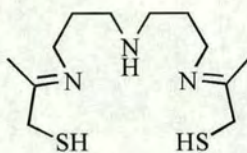
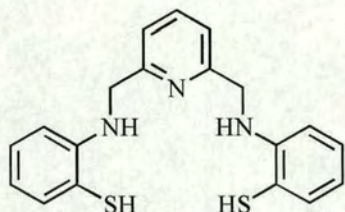


Figure 2.18. Neutral polydentate 5-coordinate zinc complexes.

2.4.2.3 Six coordinate zinc complexes.

A trend similar to 5-coordinate structures is observed for 6-coordinate zinc(II) compounds, Figure 2.20.

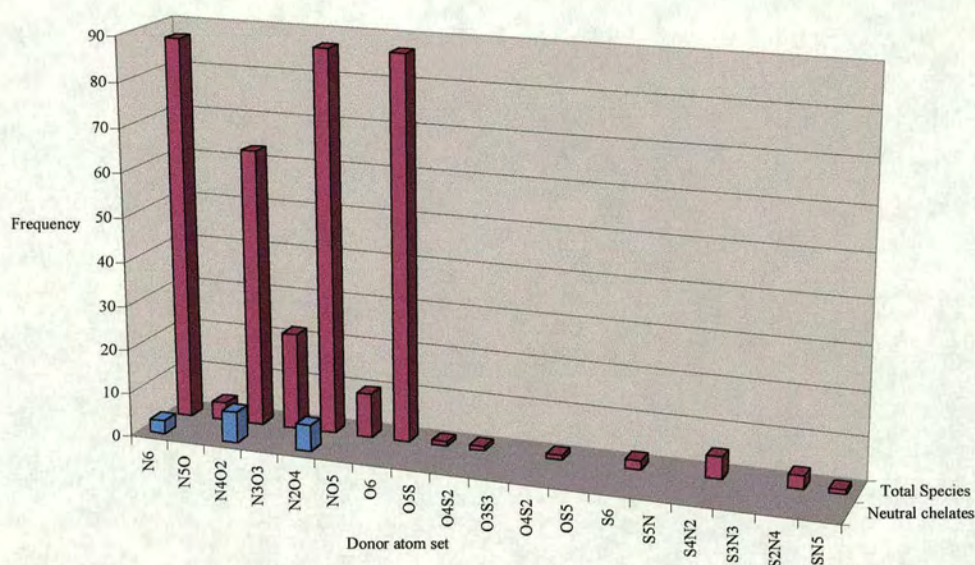


Figure 2.20. Distribution of 6-coordinate ZnX_6 ($X = N, O, S$) complexes.

Of the 374 $ZnN_XO_Y S_Z$ ($X + Y + Z = 6$) structures in the CSD most have a donor atom set containing nitrogen and oxygen atoms. In many cases the coordination number six is acquired through the coordination of solvent molecules, *e.g.* H_2O or pyridine, or anions, *e.g.* acetate and nitrate. Three donor atom sets, *i.e.* $[N_6]$, $[N_4O_2]$ and $[N_2O_4]$, Figure 2.21, are observed in neutral zinc complexes.

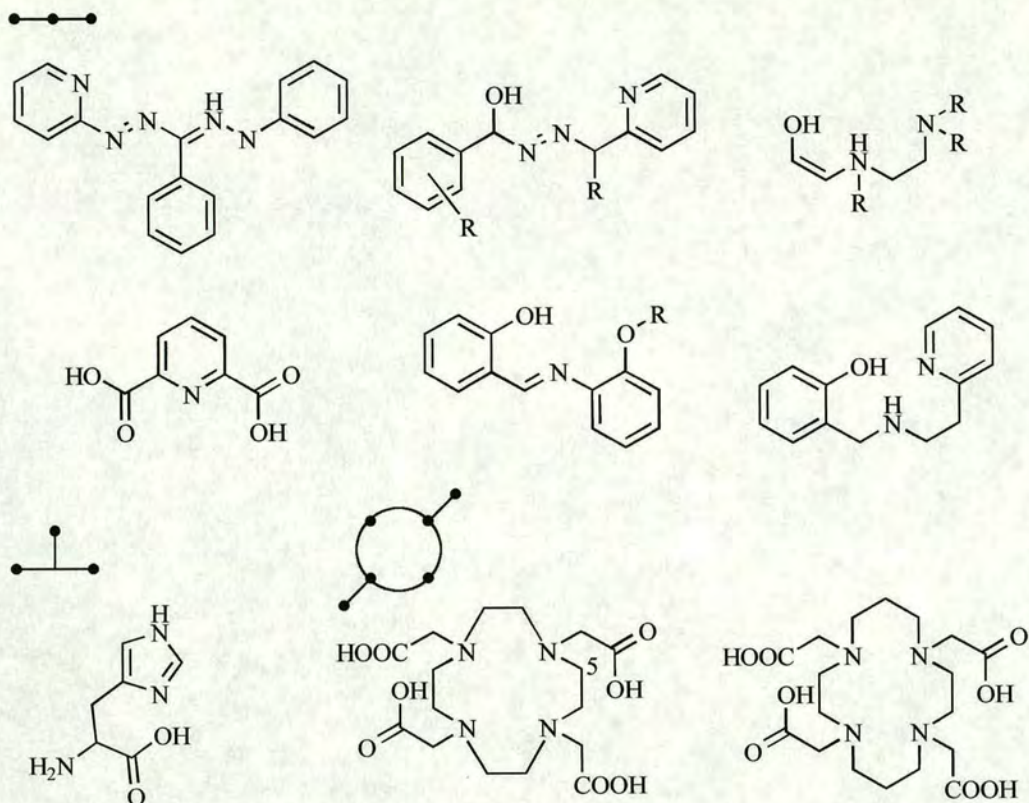


Figure 2.21. Ligands which form neutral polydentate 6-coordinate zinc complexes.

The most commonly observed structures contain tridentate ligands with 5-membered chelate rings. These are expected to favour octahedral geometry (Section 2.2.3).

2.4.3 Nickel(II) complexes in the CSD.

The identification of L2083 as a selective zinc(II) extractant (see Section 1.4.2.2) was based²⁵ on the observation that “simple” dithiophosphoramides (*e.g.* $\text{Ph}_2\text{P}(\text{S})\text{NHP}(\text{S})\text{Ph}_2$) give stable tetrahedral complexes of nickel(II). Tetrahedral nickel(II) is a relatively unusual coordination environment, with D_{4h} and O_h geometry being considerably more stable. Consequently it was assumed²⁵ that ligands which impose tetrahedral geometry on nickel(II) are likely to favour very stable zinc complexes by providing its favoured geometry.

This logic has been exploited in this project in identifying other types of ligands which may show a high affinity for zinc(II) ions. A search of the CSD was performed²⁶ of all known 4-coordinate bis-bidentate complexes of nickel(II). This has been extended to incorporate tetradentate ligands, Figure 2.22.

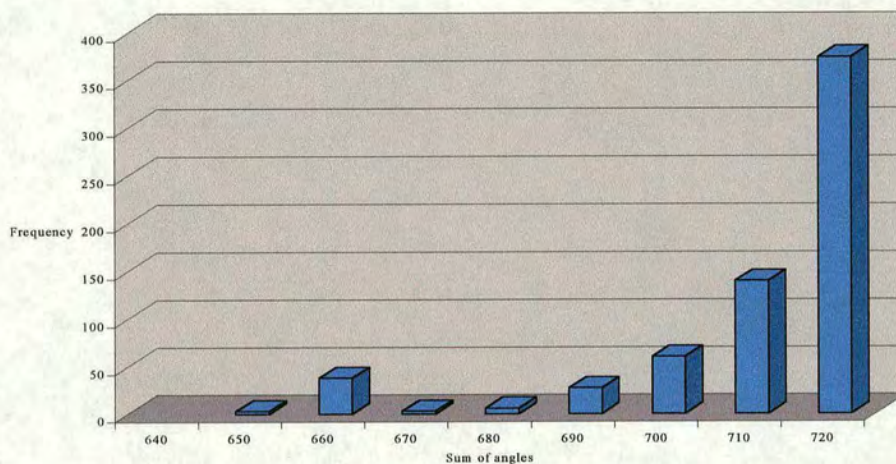


Figure 2.22. Angular distribution of 4-coordinated bis-bidentate and mono-tetradentate NiX_4 ($X = N, O, S$) complexes.

The majority were, as expected, square planar. However, approximately forty structures (Figure 2.23) display tetrahedral geometry, Figure 2.23.

The most common feature of ligands giving tetrahedral nickel(II) complexes are nitrogen and / or sulfur donors and 6-membered chelate rings. The ligand type that occurs most frequently is the thiopyrazolone (top left, Figure 2.23), which provides a $[N_2S_2]^{2-}$ donor set on deprotonation giving a 6-membered chelate ring.

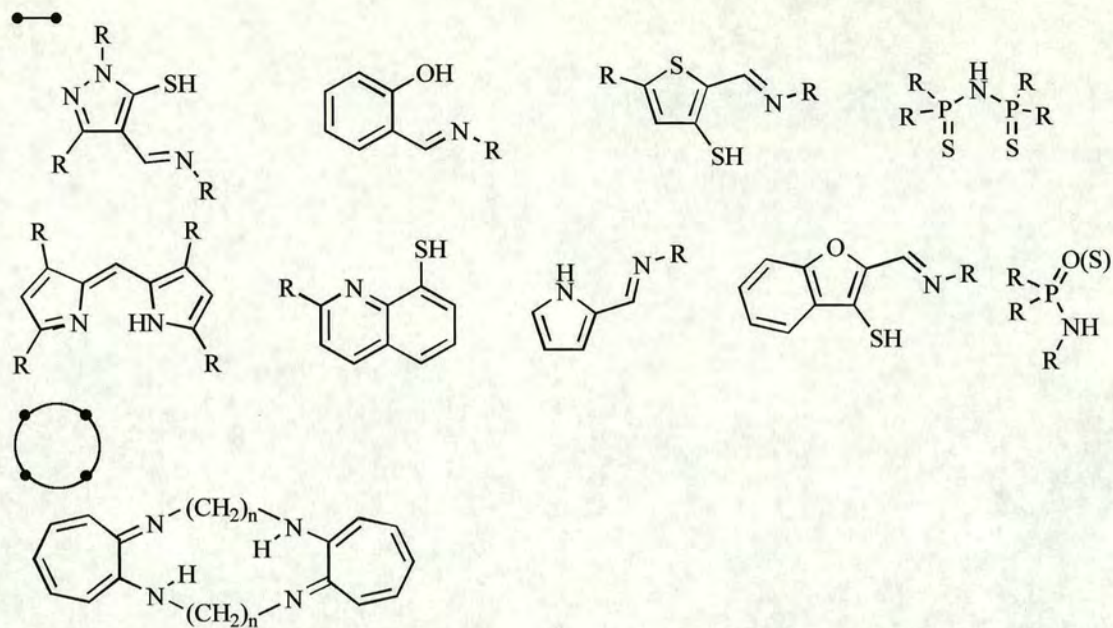


Figure 2.23. Polydentate ligands giving tetrahedral nickel(II) complexes.

2.4.4 Iron(III) complexes in the CSD.

For the successful recovery of zinc in the extraction process, outlined in Section 1.4.1.1, the extractant is required to discriminate against iron(III). This section attempts to identify the structural properties observed in the chelating ligands of stable octahedral complexes present in the CSD. This will be useful in ensuring that these are extended to the design criteria of the potential zinc extractant. The CSD contains 321 mononuclear FeX_6 ($X = \text{N}, \text{O}, \text{S}$) complexes of which 81 are neutral complexes of polydentate ligands, Figure 2.24.

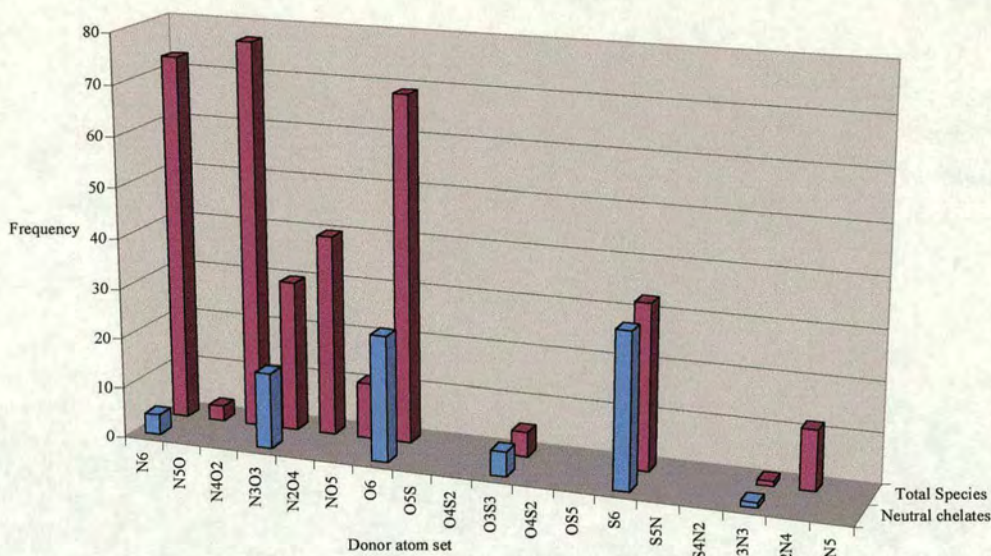


Figure 2.24. Distribution of 6-coordinate FeX_6 ($X = \text{N}, \text{O}, \text{S}$) complexes.

A hard metal cation such as Fe^{3+} , as expected (Section 2.2.2), commonly forms complexes with ligands containing hard base donor atoms, *e.g.* oxygen. Examples of complexes using softer polydentate ligands containing sulfur donor atoms are relatively uncommon, with the exception of the dithiocarbamates which provide a $[\text{S}_6]^{2-}$ donor set after deprotonation giving a 4-membered chelate ring, Figure 2.25. The examples of neutral polydentate iron(III) complexes in the CSD are represented most frequently by linear bidentate ligands but also by tripodal hexadentate ligands. This survey gives an indication of the types of ligands which are found to form 3:1 neutral complexes with iron(III). However the complexes reported in the CSD only represent a fraction of the known octahedral iron(III) complexes, those for which it has been possible to grow crystals.

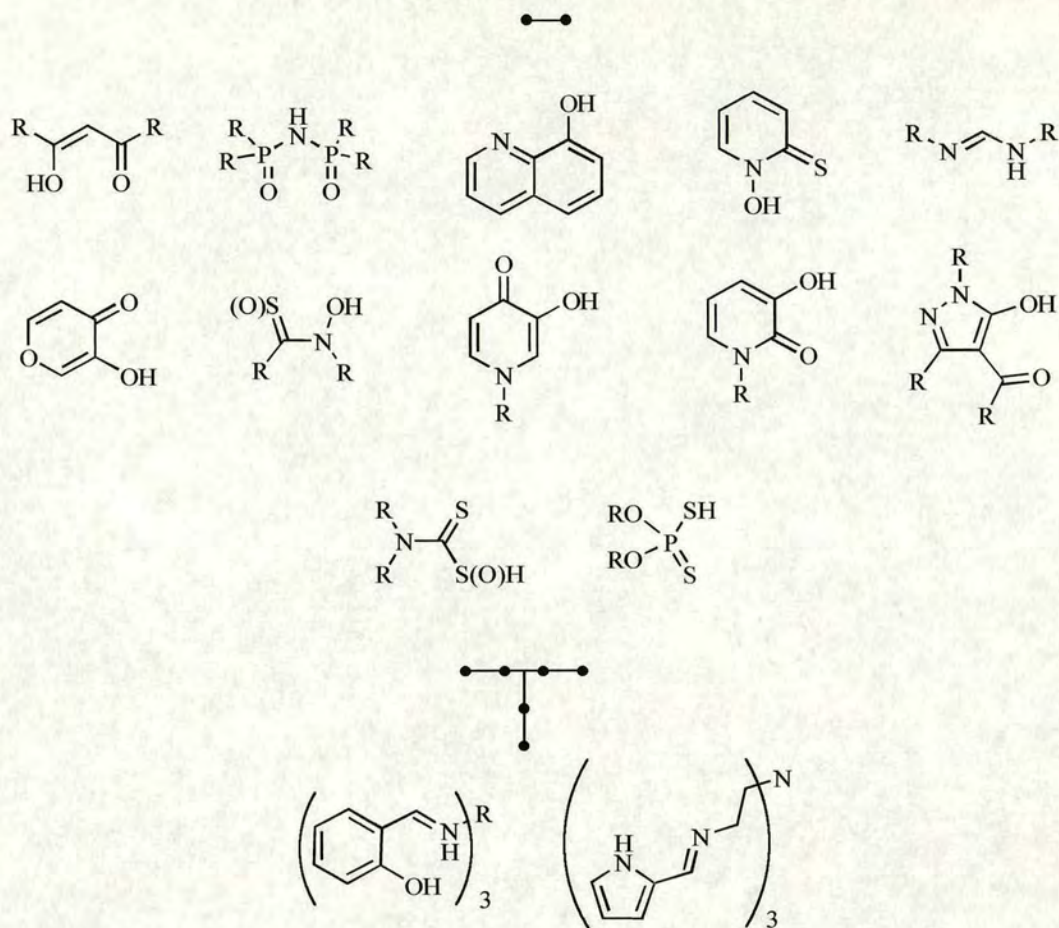


Figure 2.25. Ligands identified as forming stable octahedral iron(III) complexes.

Some of the ligands presented here (second row, first four, Figure 2.25) are closely related to the polydentate iron transport agents, siderophores, which have a high affinity for sequestering iron and forming extremely stable octahedral neutral complexes. The siderophores are low-molecular weight compounds produced by micro-organisms to facilitate the uptake and transport of iron(III).²⁷ They fall into two categories²⁸ with the most common functional groups being; (1) hydroxamate ligands, *e.g.* ferrichromes and ferrioxamines, and (2) catecholate ligands, *e.g.* enterobactin, Figure 2.26.

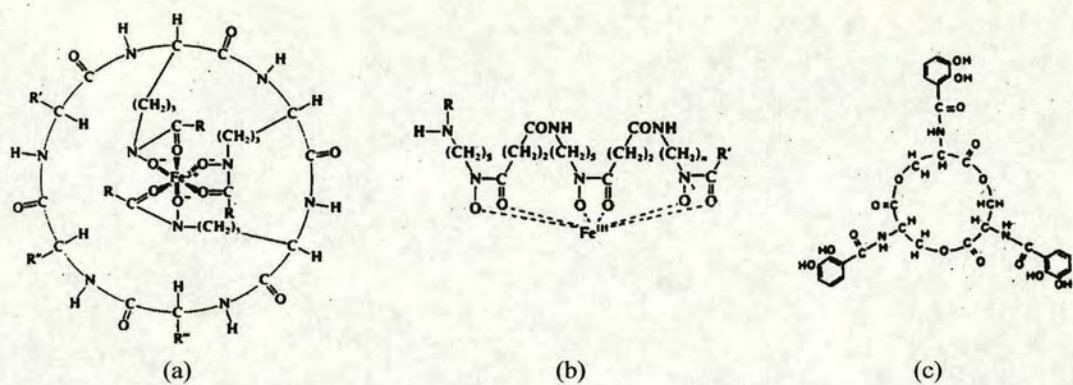


Figure 2.26. Structures²⁸ of (a) cyclic ferrichromes, (b) linear ferrioxamines and (c) enterobactin.

There are more than 300 naturally occurring siderophores which have been isolated and characterised.²⁹ Current research continues to design more effective sequestering agents, modelled after enterobactin, for the use in the treatment of human iron overload. Of all the natural and man-made compounds so far investigated, the one that binds iron the most strongly under physiological conditions is enterobactin with an $[O_6]^{6-}$ donor set. Enterobactin employs three catecholate ligands to encapsulate iron(III) with an overall stability constant³⁰ (K_F) $\sim 10^{49}$.

2.4.5 Summary of the CSD survey.

As expected, the 4-coordinate tetrahedral zinc structures are well represented in the CSD by N, O and S donors. There is a shift from 4-coordinate through to 6-coordinate zinc complexes when sulfur donors are replaced by oxygen; 4-coordinate complexes generally have $[S_4]$, $[N_2S_2]$, $[N_4]$ donor sets whereas 6-coordinate complexes are all mixed nitrogen and oxygen systems $[N_xO_y]$. A decrease in the

chelate ring size from 6- to 5-membered accompanies higher coordination numbers (5 or 6) around the zinc ion.

Approximately half of the examples of bidentate ligand types which were found to form neutral 4-coordinate zinc(II) complexes were also found to coordinate with nickel(II) in a tetrahedral geometry (first 7 examples, Figure 2.16) with a similar preference for nitrogen and/or sulfur donor atoms. Similarly, some of the bidentate zinc complexing ligands (top 4 ligands, Figure 2.25) are also found to form 3:1 octahedral complexes with iron(III). However, the complexes observed containing similar ligand types differ in the choice of donor atoms. Whereas the zinc complexes generally contain soft anionic sulfur donor atoms, these are replaced by the more favourable oxygen donors in the iron examples, *e.g.* dithiophosphoramides, quinolinethiols, thio- β -diketones, Figure 2.25.

From the survey, the promotion of a 4-coordinate tetrahedral geometry that favours stable zinc complexes and actively disfavours octahedral iron(III) complexes should benefit from using a 6-membered chelate ring comprising of nitrogen and/or sulfur donors. Some examples of bidentate ligands that qualify on these two assumptions and are capable of deprotonation to form neutral 2:1 complexes are displayed in Figure 2.27. These ligands also provide the opportunity to disfavour the formation of 6-coordinate complexes by incorporating sterically hindering groups preventing 3:1 complex formation.

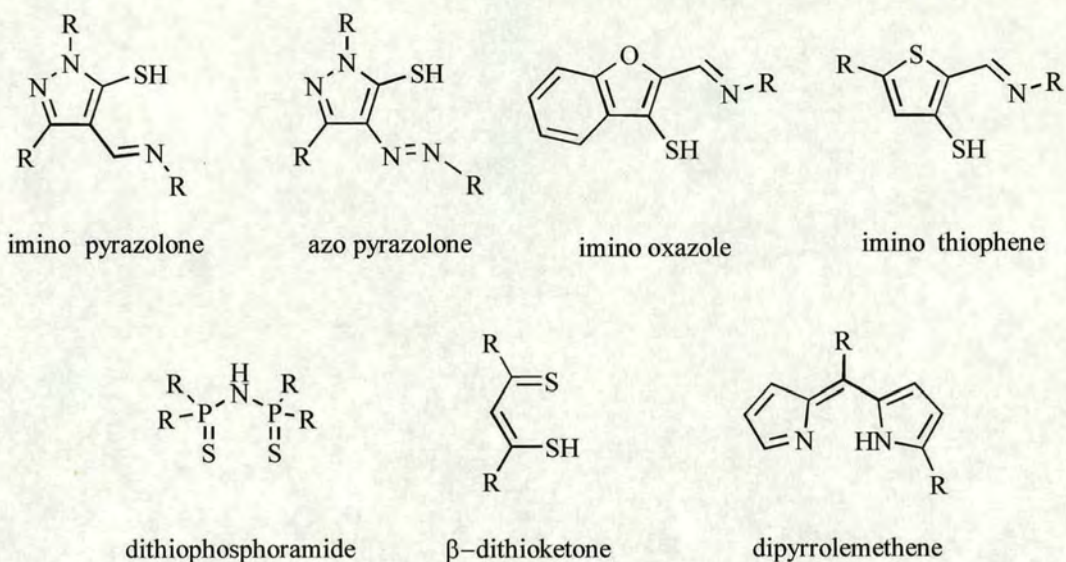


Figure 2.27. Ligands identified as possible selective zinc extractants.

2.5 Conclusions.

The criteria outlined in Section 1.4.2.1, as defined by Avecia at the outset, for a successful extraction candidate underlie the properties which are thought to be necessary in the initial design of a successful extractant. This project focuses on those criteria that require the reagent to be highly selective for Zn^{2+} over Fe^{3+} (and preferably other transition metals, most importantly Cu^{2+}) and also operate at $pH_{1/2} < 2$. The other criteria are of less importance to this project and will be considered in further development work at Avecia.

The design of an extractant for the selective complexation of zinc(II) discriminating against other transition metals is complicated. Many factors contribute; (1) the coordination number and geometrical configuration of the complex, (2) the donor atom types, (3) the denticity of the ligand, (4) chelate ring size and (5) the ligand pK_a .

Factors 1-4 have been considered in Sections 2.2-2.4 above. It has been rationalised that a process based on the formation of 4-coordinate neutral tetrahedral complexes incorporating bidentate ligands will provide the best opportunity to gain the maximum selectivity over Fe^{3+} and other transition metals while maintaining a minimal manufacturing cost. The surveys of the zinc containing metalloenzymes (Section 2.3) and the small molecule complexes in the CSD (Section 2.4) indicate that maximum “strength” of an extractant might be obtained by the incorporation of nitrogen and/or sulfur donor atoms. This would also benefit an increase the selectivity over Fe^{3+} , which prefers harder donor atoms.

The pK_a of the ligand is also important for the operation of a pH-dependent extraction equilibrium (see Section 1.4.1.2) and to generate neutral, hydrocarbon soluble, zinc complexes. By increasing the maximum overall stability constant (K_{extract}) of the zinc complex the “strength” and selectivity of extraction can be maximised. This depends on the acidity of the ligand (K_a) and the formation constant (β_n) of the complex formed (see Equation 2.3). How acidic the ligand must be for optimal zinc extraction is uncertain. An increase in K_{extract} is expected as the acidity of the ligand increases, ultimately leading to a lower extraction pH. However a consequence of the high acidity is the formation of a weaker deprotonated conjugate base, resulting in the formation of a less stable metal complex. If the relative loss in complex stability is greater than the increase in ligand acidity then the overall effect would be a “weaker” extractant, operating at a higher pH. In addition because of the $[\text{H}^+]^n$ term in the equilibrium constant expression, high acidity will also favour the extraction of high valent metals such as Fe^{3+} which might possibly have detrimental repercussion in the selectivity of Zn^{2+} over Fe^{3+} .

Of those bidentate ligands short-listed as possible extraction candidates (Figure 2.27) the dithiophosphoramides were not considered as they have previously been studied at Avecia, and were found not to fulfil all the necessary criteria (see Section 1.4.2.2). It was decided that an extractant based upon the imino-thiopyrazolones and azo-thiopyrazolones (which were also the most abundant in the CSD) would provide the greatest opportunity for potential derivatisation and consequent study of the effect of different substituents on the strength and selectivity. The results of this study are discussed in Chapter 4.

They also lend themselves to the relatively simple synthesis of di-anionic tetradentate ligands based on two bidentate thiopyrazolone units linked *via* a bridge between the nitrogen donors, (see Chapter 5). This provides the opportunity to further increase the stability of the extracted zinc complex by incorporating in to the design of the ligand, by the careful selection of the bridging group, a tetrahedral predisposition of the donor atoms and therefore potentially increasing the “strength” of the extractant.

2.6 References.

1. F.A Cotton, G. Wilkinson, *Advanced Inorganic Chemistry*, Wiley-Interscience, New York, 5th edn., 1988, ch.2, pp.35-83.
2. N.N. Greenwood, A. Earnshaw, *Chemistry of the Elements*, Pergamon Press, Oxford, 4th edn., 1989, ch.19, pp.1060-1101.
3. R.J. Angelici, *Inorganic Biochemistry*, ed. G.L. Eichhorn, Elsevier, Amsterdam, 1973, vol.1, ch.2, pp.63-101.
4. B.M. Mahan, R.J. Myers, *University Chemistry*, Addison-Wesley, California, 4th edn., 1987, ch.16, pp.800-856.
5. S. Arhland, J. Chatt, N.R. Davies, *Quart. Rev. (London)*, 1958, **12**, 265.
6. R.G. Pearson, *J. Am. Chem. Soc.*, 1963, 3533.
7. M.J. Winter, *d-Block Chemistry*, ed. J. Evans, Oxford University Press, Bath, 3rd edn., 1996, ch.2, pp.7-22.
8. J.J.R. Frausto da Silva, R.J.P. Williams, *The Biological Chemistry of the Elements*, Clarendon Press, Oxford, 1991, ch.2, pp.23-70.
9. D. Nicholls, *Complexes and First-Row transition Elements*, ed. P. Sykes, Macmillan, Hong Kong, 5th edn., 1988, ch.3, pp.17-33.
10. L.G. Sillen, A.E. Martell, *Stability Constants of metal – ion complexes*, Chem. Soc., Spec. Publ. No.17, London, 1964.
11. A.E. Martell, R.D. Hancock, *Metal complexes in Aqueous Solutions*, ed. J.P. Fackler Jr., Plenum Press, New York, 1996, ch.30, pp.63-95.
12. H. Diehl, *Chem. Rev.*, 1937, **21**, 39.
13. D.E. Fenton, *Bioinorganic Chemistry*, ed. J. Evans, Oxford University Press, NY, 2nd edn., 1997, ch.6, pp.60-80.

14. B.Y. Aylett, *Comprehensive Inorganic Chemistry*, Pergamon Press, Oxford, 1973, vol.3, ch.30, pp.187-328
15. B.W. Matthews, *Acc. Chem. Res.*, 1988, **21**, 333.
16. S.J. Lippard, J.M. Berg, *Principles of Bioinorganic Chemistry*, University Science Books, California, 1994, ch.10, pp.257-281.
17. I. Bertini, H.B. Gray, S.J. Lippard, J.S. Valentine, *Bioinorganic Chemistry*, University Science Books, California, 1994, ch.2, pp.37-106.
18. N.N. Greenwood, A. Earnshaw, *Chemistry of the Elements*, Pergamon Press, Oxford, 4th edn., 1989, pp.498.
19. W.R. Kester, B.W. Matthews, *J. Biol. Chem.*, 1977, **252**, 7704.
20. D.C. Rees, M. Lewis, W.N. Lipscomb, *J. Mol. Biol.*, 1983, **168**, 367.
21. F.H. Allen, O. Kennard, R. Taylor, *Acc. Chem. Res.*, 1983, **16**, 146.
22. D.St.C. Black, A.J. Hartshorn, *Coordination Chemistry Reviews*, Elsevier, Amsterdam, 1973, **9**, 219.
23. L. Sacconi, I. Bertini, *J. Amer. Chem. Soc.*, 1966, **88**, 5180.
24. D.St.C Black, I.A McLean, *Aust. J. Chem.*, 1971, **24**, 1391.
25. J. Cambell, R.F. Dalton, P.H. Quan, EP 0573182A1, 1993.
26. Work carried out by Dr. M. Charlton, Blackley, Avecia, 1997.
27. R.C.Scarrow, P.E. Riley, K. Abu-dari, D.L. White, K.N. Raymond, *Inorg. Chem.*, 1985, **24**, 954.
28. D.E. Fenton, *Bioinorganic Chemistry*, ed. J. Evans, Oxford University Press, NY, 2nd edn., 1997, ch.2, pp.10-20.
29. T.R. Ward, A. Lutz, S.P. Parel, J. Ensling, P. Gutlich, P. Buglyo, C. Orvig, *Inorg. Chem.*, 1999, **38**, 5007.

30. L.D. Loomis, K.N. Raymond, *Inorg. Chem.*, 1991, **30**, 906.

Chapter 3

Pyridone Chemistry

3.1 Introduction.

This chapter considers the synthesis, characterisation and crystallographic structures of two ligands based on, 3-hydroxy-2(1H)-pyridinethione and 3-hydroxy-2(1H)-pyridinone, Figure 3.1, and a range of their complexes with 1st row transition metals (Fe^{3+} , Co^{3+} , Ni^{2+} , Cu^{2+}) and Zn^{2+} .

The aim of the work described was initially to provide additional experimental evidence (Chapter 2) to determine the ligand donor atom preferences of zinc(II). The 2,3-disubstituted pyridine ligand was envisaged as offering a wide range of monoprotic donor atom combinations comprising of nitrogen, oxygen and sulfur within the heterocyclic framework, in order to ascertain those that showed the highest affinity for the complexation and stabilisation of the zinc(II) ion. The different combinations of donor atoms on the heterocyclic core framework (Figure 3.1) demonstrate the multiplicity of arrays that could potentially be made.

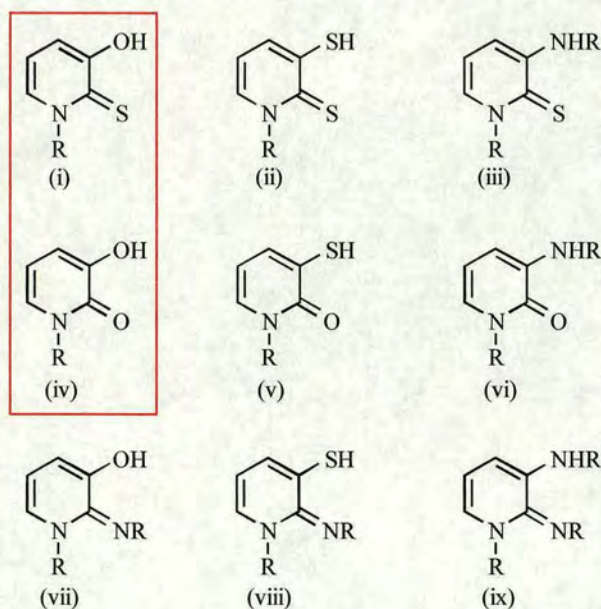


Figure 3.1. Possible donor atom combinations based on 3-hydroxy-2(1H)pyridones (R = benzyl, 4-*t*-butyl-benzyl).

For a number of reasons which are outlined below, only (i) and (iv), highlighted in red, were successfully synthesised. With the exceptions of (i) and (iv) examples of these structures are not present in the literature and many of the related compounds are also rare. Those containing a thiol group, *i.e.* (ii), (v) and (viii), are only represented by 3-thiol-2(1H)-pyridinethione, 3-thiol-2(1H)-pyridinone and 9-thiol-pyrido-(1,2-a)-pyrimidin-4-one respectively, Figure 3.2. They are potentially unstable towards oxidative coupling to form disulfides, in the presence of air, due to the relatively low bond dissociation energy of the S-H bond.¹ In addition to this the thiolate anion, generated upon deprotonation, is a powerful nucleophile and can lead to further reaction to form sulfide bridges.

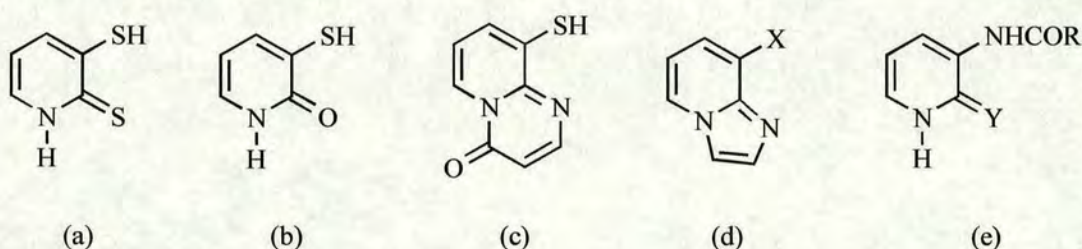


Figure 3.2. (a) 3-thiol-2(1H)-pyridinethione,^{1,2} (b) 3-thiol-2(1H)-pyridinone,³ (c) 9-thiol-pyrido-(1,2-a)-pyrimidin-4-one,⁴ (d) 8-hydroxy-imidazo-(1,2-a)-pyridine⁵ where X = OH and 8-acetamidoimidazo-(1,2-a)-pyridine⁶ where X = NHCOCH₃, (e) 3-(2'-chlorobenzoyl)amino(thio)pyridin-2-one⁷ where Y = O, (S) and R = C₆H₅Cl.

The multitude of examples in the literature related to the structures of (vii) and (ix) with NO and N₂ donor atom sets, respectively, all comprise of an additional 5- or 6-membered ring annelated to the pyridine ring, *e.g.* the commonly occurring imidazo-(1,2-a)-pyridine system, Figure 3.2(d), although there are no examples

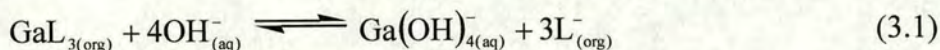
containing non-cyclised imines at the 2-position. Likewise there are many examples of compounds related to the structures of (iii) and (vi) all of which comprise of an amide at the 3-position, Figure 3.2(e).

The two ligands made, (i) and (iv), clearly do not provide a wide enough range of donor atom variables to draw rigorous conclusions about the donor atom preferences of zinc(II). However from the metal complexes of these two ligands (Section 3.4 to 3.7) some conclusions about the two donor atom sets [OS] and [O₂] and their apparent compatibility with a range of different metals can be elucidated. The crystal structures reported, in this chapter, provide an insight to the required metal coordination environment and the geometrical disposition of the donor atoms around the metal centre which should favour the selective complexation of zinc over other metals.

Hydroxy-pyridinones have been used in chelation therapy for the removal from the body of excess iron resulting from repeated blood transfusions and iron poisoning.⁸ Their use has resulted from an effort to design more effective sequestering agents based on the naturally occurring enterobactin, a catecholate containing siderophore (microbial iron transport agent).⁹ Other possible uses of hydroxy pyridinones are in the chelation of ions with a high charge to ionic radius ratio which exhibit chelation preferences similar to that of iron.¹⁰ For example, treatment of victims with plutonium contamination¹¹ and the sequestration of tumour imaging radionuclides such as gallium and indium utilised in magnetic resonance imaging.¹²

The related pyridinethiones (iv) discussed here are a class of heterocyclic thione developed for the solvent extraction of group(III) metals. They are particularly useful for the selective extraction of gallium from an aqueous acidic solution

containing aluminium in large excess.¹³ Subsequent stripping of the gallium by contacting the loaded organic solution with an aqueous alkaline solution separates it from all other metals that may have been co-extracted, e.g. copper, zinc and silver, Equation 3.1. Extraction is very selective and high purity gallium is recovered (99.9999 %) which is suitable for use in the manufacturing of semiconductors.¹⁴



The trivalent Al^{3+} cation with its relatively small ionic radius, Table 3.1, is classed as a hard Lewis acid (Section 2.2.2) and tends to form complexes with hard bases. In contrast the Ga^{3+} cation is less electropositive, has a much larger ionic radius and is classed as a softer Lewis acid.

Property	Al	Ga	Zn
Electronic configuration	Ne[3s ²]	Ar[3d ¹⁰ 4s ² 3p ¹]	Ar[3d ¹⁰ 4s ²]
Ionic radius / Å (6-coord.)	0.53 ^(a)	0.62 ^(a)	0.60 ^(b) (T _d)
Electronegativity (χ)	1.6	1.7	1.6

Table 3.1. Physical and atomic properties of Al, Ga and Zn. ^(a) Oxidation state (III).¹⁵ ^(b) Oxidation state (II).¹⁶

Consequently the incorporation of a soft base donor atom such as sulfur facilitates Ga^{3+} selectivity. The Zn^{2+} cation has some similar features to those of the Ga^{3+} cation. Although zinc will only form a divalent 4-coordinate complex its tetrahedral

ionic radius is comparable to that of trivalent Ga³⁺ and both contain an identical core of electrons, *i.e.* [Ar]3d¹⁰.

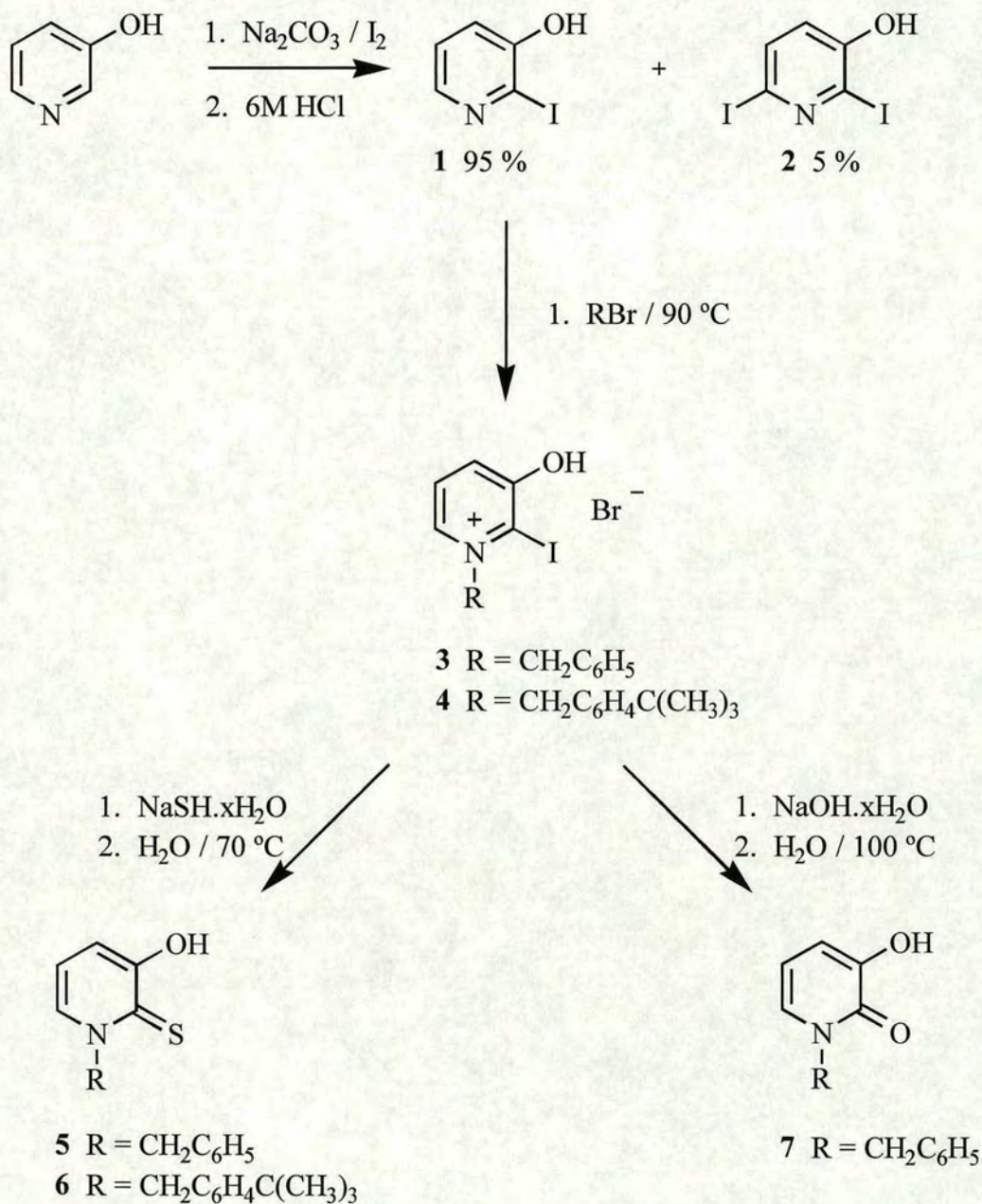
3.2 Preparation and characterisation of N-benzyl-3-hydroxy-2(1H)-pyridinethiones and pyridinones.

There are a number of literature methods for producing both N-benzyl-3-hydroxy-2(1H)-pyridinethiones (**5**), its N-4-*t*-butyl-benzyl derivative (**6**) and N-benzyl-3-hydroxy-2(1H)-pyridinone (**7**), some which are discussed below. The general method used here involves the commercially available starting material 3-hydroxypyridine for the production of both the OS and the O₂ analogues in a 3-step procedure, Scheme 3.1. Although not optimised, the overall yield of the reaction scheme is high at ~70 % for **5** and **6** and ~65 % for **7**.

The halogenation of 3-hydroxypyridine has been well documented. One possible method is direct halogenation with bromine^{17,18,19} in 10 % NaOH or in dry pyridine.^{20,21} Iodination under similar conditions^{20,22,23,24} affords 3-hydroxy-2-iodopyridine in approximately 65 % yield. Here we use a slight modification of this method using sodium carbonate as the base instead of NaOH which increases the yield to ~95 %.²⁵ Electrophilic aromatic substitution of 3-hydroxypyridine affords 3-hydroxy-2-iodopyridine (**1**) with 3-hydroxy-2,6-diiodopyridine (**2**) produced as a minor by-product.

The ratio of mono-, di- and tri-iodinated products obtained is dependent on the stoichiometry of the 3-hydroxypyridine, iodine and sodium carbonate used.²⁵ When a ratio of 1:1:2 is used, mono-substitution at the 2-position predominates and the 2,6-disubstituted compound **2** is formed as a minor by-product. It has been

determined that although the α - and γ -positions (w.r.t. the OH-group) are activated by the *o*- and *p*-directing hydroxyl group, substitution at the α -position dominates and in addition overwhelmingly at the 2-position.^{20,24,26,27}



Scheme 3.1. Synthetic procedure for N-benzyl-3-hydroxy-2(1H)-pyridinethiones and N-benzyl-3-hydroxy-2(1H)-pyridinones.

The second step in the synthetic pathway is electrophilic addition at the pyridine nitrogen, which yields the quaternary pyridinium salt. Simple alkylation is achieved by heating alkyl iodides under pressure in DMF.^{21,28} Alternatively, direct heating of methyl toluene sulfonate with 3-hydroxy-2-bromo-pyridine^{17,19} affords the methyl pyridinium toluene sulfonate. An example of the method employed here is the heating of 3-hydroxy-2-iodo-pyridine (**1**) in the absence of solvent with a two fold excess of benzyl bromide to afford the N-benzyl-3-hydroxy-2-iodo-pyridinium bromide (**3**) and the 4-*t*-butyl-benzyl derivative (**4**).²³ Competing O-alkylation does not occur when the hydroxy function is not deprotonated because the nitrogen, with its lone pair of electrons, is considerably more nucleophilic. The minor amount of di-substituted impurity (**2**) present does not undergo electrophilic addition. The increased bulkiness of the iodine in the 2- and 6-positions prevents the approach of the carbocation.²⁸ This is confirmed by the unsuccessful attempted benzylation of 6-methyl-3-hydroxy-2-iodo-pyridine under the same conditions. The proposed S_N1 type N-alkylation mechanism means that the choice of alkylating agent is confined to those which can form a stable carbocation, *i.e.* resonance stabilised or tertiary halides, and secondly can approach the pyridine nitrogen without steric hindrance. In addition electrophiles containing β -hydrogens cannot be used because they can react by the competing β -elimination pathway resulting in hydrogen abstraction and formation of the corresponding alkene, Figure 3.3.

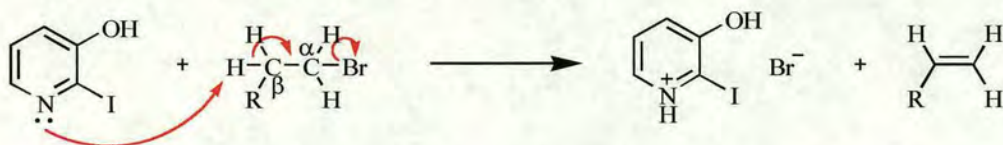
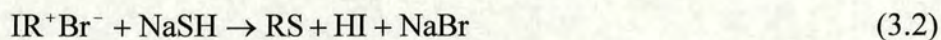


Figure 3.3. β -Elimination pathway of alkanes containing β -hydrogens.

The final step is the formation of the pyridinethiones **5** and **6** or the pyridinone **7** via nucleophilic substitution of the iodine using either sodium hydrogen sulfide⁸ or sodium hydroxide in water respectively, Equation 3.2.



Previous methods for preparing simple N-alkyl-3-hydroxy-2(1H)-pyridinethiones²⁸ and 3-hydroxy-2(1H)-pyridinethiones^{21,27} use potassium hydrogen sulfide in either propylene glycol or DMF at 80 °C. Nucleophilic substitution at C-2 is facilitated by its relatively electropositive character and further enhanced by its close proximity to the quaternary ring nitrogen and the good leaving group characteristics of the iodine.

3.2.1 NMR spectroscopy.

Full experimental characterisation is given in Section 3.8. The ¹H NMR spectra of the ligands **5**, **6** and **7** were recorded in d₆-DMSO and are in agreement with the expected structure, Figure 3.4.

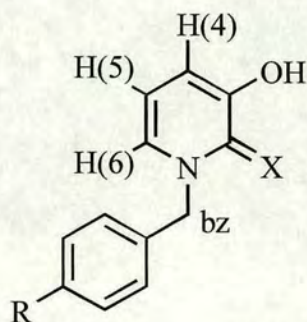


Figure 3.4. ¹H NMR proton labelling of the ligands (a) **5** where X = S, R = H, (b) **6** where X = S, R = *t*-butyl, (c) **7** where X = O, R = H.

The benzylic protons (bz) in the pyridinethiones **5** and **6** and pyridinone **7** appear as singlets at 5.8 ppm and 5.0 ppm respectively indicating that they are able to freely rotate in solution. Replacement of oxygen for sulfur at C-2 results in a downfield shift of the benzylic (~0.8 ppm) and pyridine based protons (~0.4-0.7 ppm) which is expected due to the higher shielding effect of the oxygen compared to that of sulfur. The hydroxyl protons appear as sharp singlets suggesting a slow rate of exchange on the NMR time scale. This is attributed to strong intramolecular S··H and O··H hydrogen bonding.

The ^{13}C NMR of the ligands **5** and **7** were recorded in d_6 -DMSO and assigned according to the labelling in Figure 3.5.

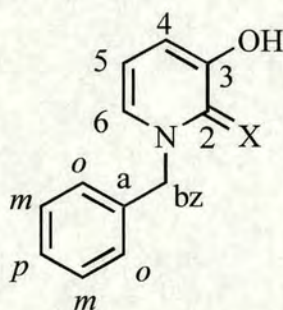


Figure 3.5. ^{13}C NMR labelling of the ligands (a) **5** where X = S, (b) **7** where X = O.

The assignment of signals for the pyridine based C-4 / C-5 carbons on ligand **5** and the *ortho* (*o*) and *meta* (*m*) aromatic carbons on both ligands **5** and **7** has not been possible as these overlap, Table 3.2. Where C-4 and C-5 are distinguishable, in **7**, C-4 has been assigned the larger chemical shift based on the greater deshielding of H(4) in the proton spectra. The assignment of the quaternary signal for C-2 was based upon the downfield shift when oxygen is replaced with sulfur. This

replacement also results in a similar downfield shift for C-5, C-6 and bz, *ca.* proton spectra.

Ligand	Chemical shift (δ) / ppm									
	2	3	4	5	6	bz	a	<i>o</i>	<i>m</i>	<i>p</i>
5	168.15	154.36	113.06-113.93		133.49	59.21	135.74	127.81-127.91		128.70
7	147.02	157.89	114.80	105.49	128.26	51.41	137.49	127.63-127.80		128.64

Table 3.2. Assignment of ^{13}C NMR resonances in d_6 -DMSO for HL (5) and HL (7).

3.2.2 Mass spectroscopy.

The EI spectrum of 3-hydroxy-2-iodopyridine (1) is consistent with the expected structure. The molecular ion in the positive FAB spectrum of N-benzyl-3-hydroxy-2-iodopyridinium bromide (3) and the 4-*t*-butyl-benzyl derivative (4) was absent with m/z 312 attributed to the pyridinium cation. The EI spectrum of the ligands 5, 6 and 7 are in agreement with the expected structure. Fragments m/z 91 and m/z 147 are indicative of the presence of benzyl and 4-*t*-butyl-benzyl respectively on the nitrogen of the pyridine ring.

3.3 Preparation and characterisation of metal complexes.

The complexes $[\text{Zn}(\mathbf{5-H})_2]$ (8), $[\text{Cu}(\mathbf{5-H})_2]$ (9), $[\text{Ni}(\mathbf{5-H})_2]$ (10), $[\text{Co}(\mathbf{5-H})_3]$ (11) and $[\text{Fe}(\mathbf{5-H})_3]$ (12) were prepared by the addition of a hot methanol solution of the appropriate metal(II) acetate hydrate to a hot methanol solution of the ligand (HL) N-benzyl-3-hydroxy-2(1H)-pyridinethione (5), Figure 3.6. The complexes $[\text{Cu}(\mathbf{6-H})_2]$ (13), $[\text{Ni}(\mathbf{6-H})_2]$ (14), $[\text{Co}(\mathbf{6-H})_3]$ (15) and $[\text{Cu}(\mathbf{7-H})_2]$ (16) were prepared by a similar procedure.

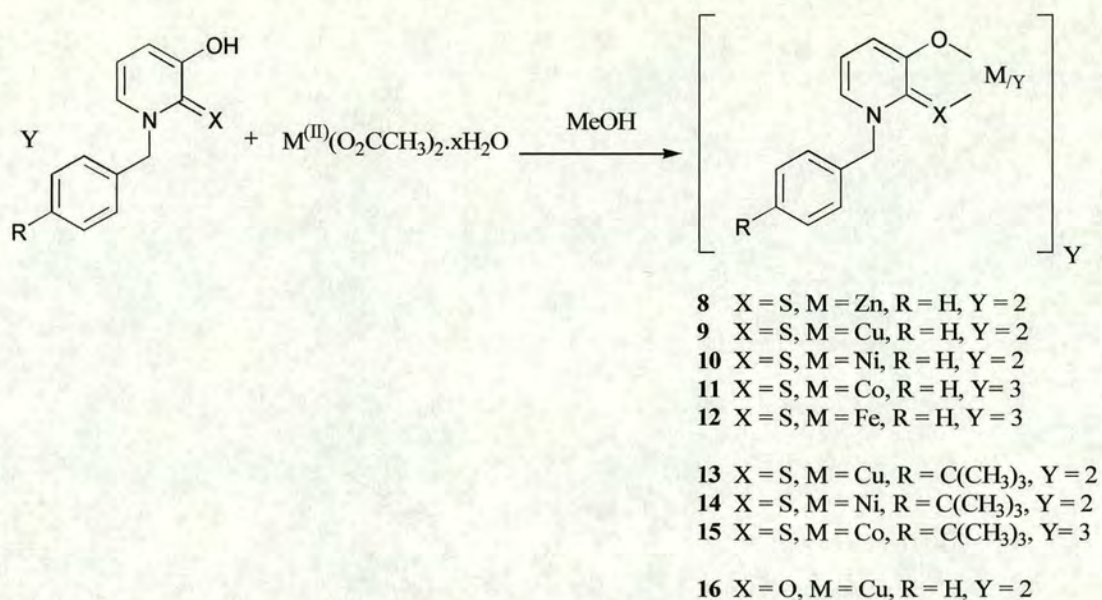


Figure 3.6. Synthesis of metal complexes $[M(L)_Y]$. $M = Zn^{2+}$, Cu^{2+} , Ni^{2+} ($Y = 2$), $M = Co^{3+}$, Fe^{3+} ($Y = 3$), $L =$ pyridinethiones (**5**) and (**6**) and pyridinone (**7**).

It was not possible to prepare the bis-pyridinonato complex $[Zn(\mathbf{7-H})_2]$ by a procedure analogous to that for **8** using a 1:2 (metal:ligand) ratio, as described above. The preparation of a zinc complex of ligand **7** was achieved by using an approximately 4.5 fold excess of zinc acetate based on that needed to form a ML_2 complex. The characterisation of the complex, by X-ray crystallography (Section 3.4.2.6), and supported by 1H NMR and elemental analysis revealed that this was an acetate bridged polymeric species consisting of the trimeric repeating unit $[Zn_3(O_2CCH_3)_4(\mathbf{7-H})_2]$ (**17**).

3.3.1 NMR spectroscopy.

The 1H NMR spectra obtained in $CDCl_3$ of $[Zn(\mathbf{5-H})_2]$ (**8**), $[Ni(\mathbf{5-H})_2]$ (**10**) and $[Ni(\mathbf{6-H})_2]$ (**14**) are similar to those of their component ligands. Deprotonation of the ligand upon metal complex formation is consistent with the absence of the hydroxyl

proton singlet in the spectra. The sharpness of the spectra for **10** and **14** indicate that they are diamagnetic and square planar around the nickel centre (Section 3.4.2.3). A singlet for the benzylic protons indicates free rotation of this substituent. In the case of the $[\text{Co}(\mathbf{5}\text{-H})_3]$ (**11**) and $[\text{Co}(\mathbf{7}\text{-H})_3]$ (**15**) the sharpness of the peaks indicate octahedral coordination around a diamagnetic low-spin d^6 cobalt(III) centre (Section 3.4.2.4). The benzylic protons appear as an “ab” quartet (~ 5.6 ppm), attributed to the magnetic inequivalence of the two protons with the inclusion of a chiral cobalt centre, Figure 3.7.

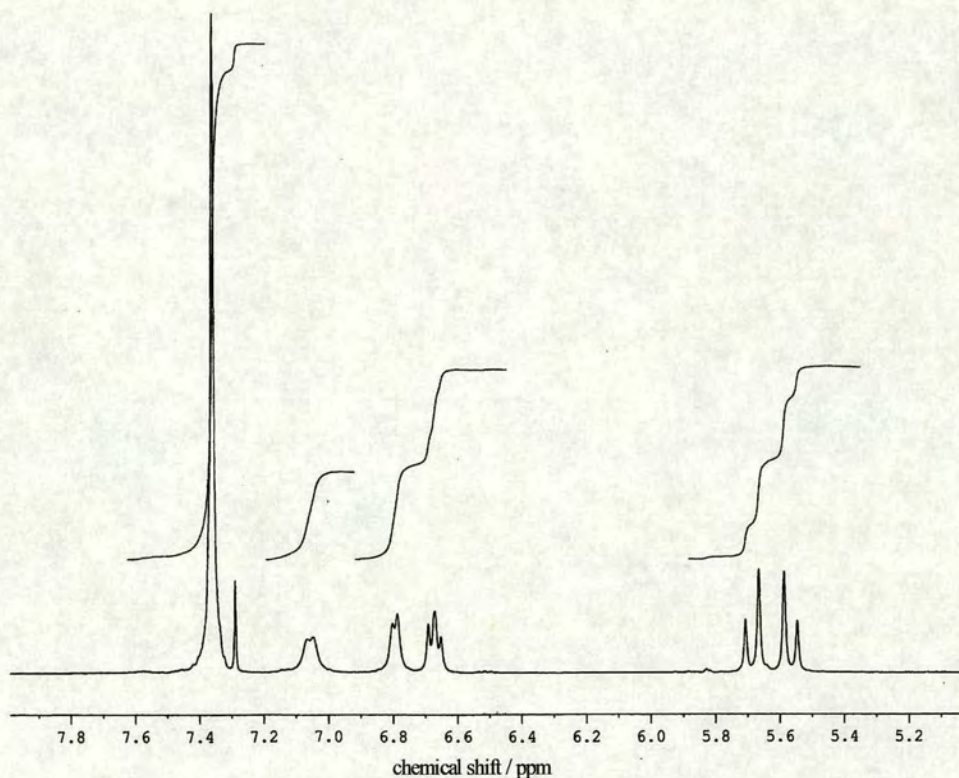


Figure 3.7. The ^1H NMR (200 MHz) spectrum of tris(N-benzyl-3-hydroxy-2(1H)-pyridinethionato)cobalt(III) (**11**).

The spectra of the polymer $[\text{Zn}_3(\text{O}_2\text{CCH}_3)_4(\mathbf{7}\text{-H})_2]_n$ (**17**) was obtained by the dissolution in hot d_6 -DMSO over a period of approximately 30 min, during which some breakdown of the polymeric structure (Section 3.4.2.6) is likely to have occurred. The spectrum is similar to that of **8** but also includes a singlet at 1.8 ppm associated with the bridging acetates, with an integral appropriate for the proposed trimeric structure.

3.3.2 Mass spectroscopy.

The positive FAB spectra of complexes **8-11**, **13**, **14** and **16** with the generalised molecular formula $[\text{M}(\text{L})_2]$ and **11**, **12** and **15**, $[\text{M}(\text{L})_3]$, show the molecular ion peaks associated with $[\text{M}(\text{L})_2(\text{H})]^+$ and $[\text{M}(\text{L})_3(\text{H})]^+$ respectively. The fragmentation patterns of these complexes clearly indicates the successive loss of ligand units (L). For $[\text{M}(\text{L})_2]$ complexes the fragmentation peaks assigned are associated with the $[\text{M}(\text{L})]^+$ and $[\text{L}]^+$ species. Those for the $[\text{M}(\text{L})_3]$ complexes are assigned $[\text{M}(\text{L})_2]^+$, $[\text{M}(\text{L})]^+$ and $[\text{L}]^+$. The fragments m/z 91 and m/z 147 which are indicative of the presence of benzyl and 4-*t*-butyl-benzyl, as seen in **5**, **6** and **7** are also present. Ion peaks greater than the molecular ion are present in all the FAB spectra. These have been tentatively assigned to the $[\text{M}_2(\text{L})_3]^+$ and $[\text{M}_2(\text{L})_4]^+$ species for $[\text{M}(\text{L})_2]$ and $[\text{M}(\text{L})_3]$ complexes respectively and are thought to arise as a product of the FABMS technique and not of the synthetic procedure. This is based on the element analysis evidence (Section 3.8) for the complexes and a mixed FAB spectrum, of a sample prepared by the grinding together the cobalt complexes **11** and **15**, which are comprised of ligands **5** and **6** respectively. A fragment, m/z 547, present in this

spectrum is representative of $[M(\mathbf{5})(\mathbf{6})]^+$ which can only have been created in the mass spectrometer.

3.3.3 Electronic absorption spectroscopy.

The electronic spectra of the **5** and the metal complexes $[\text{Zn}(\mathbf{5-H})_2]$ (**8**), $[\text{Cu}(\mathbf{5-H})_2]$ (**9**), $[\text{Ni}(\mathbf{5-H})_2]$ (**10**), $[\text{Co}(\mathbf{5-H})_3]$ (**11**) and $[\text{Fe}(\mathbf{5-H})_3]$ (**12**) were obtained in chloroform at ambient temperature. Several spectra were determined for each metal complex at different concentrations, ranging between 1 mmol and 10 μmol , in order to observe electronic transitions over a range of intensities. The ligand and each metal complex absorb at a wavelength in the range of 265 and 375 nm, Table 3.3. The extinction coefficient, ϵ ($\text{dm}^3 \text{mol}^{-1} \text{cm}^{-1}$), calculated indicates an electronic transition based on the molecular orbital associated with the ligand.

Compound	$\lambda_{\text{max}} / \text{nm}$ ($\epsilon_{\text{max}} / \text{dm}^3 \text{mol}^{-1} \text{cm}^{-1}$)				
HL 5	284 (11600)	363 (15100)			
$[\text{Zn}(\mathbf{5-H})_2]$ (8)	281 (13100)	364 (30400)			
$[\text{Cu}(\mathbf{5-H})_2]$ (9)	263 (14000)	327 sh (12900)	390 (37800)	592 sh (270)	831 (60)
$[\text{Ni}(\mathbf{5-H})_2]$ (10)	267 (34000)	316 (21900)	392 sh (8700)	466 (14400)	726 (50)
$[\text{Co}(\mathbf{5-H})_3]$ (11)	268 (49600)	313 (19100)	407 (23000)	432 (22500)	656 sh (70)
$[\text{Fe}(\mathbf{5-H})_3]$ (12)	285 (24000)	374 (33200)	489 (7900)	587 (7800)	

Table 3.3. Electronic absorption maxima of HL (**5**) and its metal complexes **8-12** dissolved in CHCl_3 at ambient temperature. Extinction coefficients are given in parenthesis and (sh) denotes that the absorption appears as a shoulder.

The extinction coefficients for the absorptions above 375 nm are associated with charge-transfer (CT) transitions. The expected d-d transitions within the metal based orbitals for square planar [Cu(**5-H**)₂] (**9**) and [Ni(**5-H**)₂] (**10**) complexes were observed at 831 (60) and 726 (50) respectively. Only one of the expected two d-d transitions (¹A_{1g}→¹T_{1g} and ¹A_{1g}→¹T_{2g}) was seen for the low spin [Co(**5-H**)₂] complex, 656(sh) (70), due to masking from the more intense charge-transfer bands. The cobalt spectra displays two very similar bands, 404 (24000) and 432 (23100) that could be associated with the two different ligand environments around the octahedral chiral cobalt centre.

As expected the high spin [Fe(**5-H**)₂] (**12**) complex (magnetic susceptibility measurement, Appendix I) does not display a d-d transition, which is consistent with the high spin d⁵ ground state.

3.4 Crystallographic characterisation.

The metal complexes **8-16** adopt a diverse range of stereochemistries with the pyridine based ligands **5** and **7**. The same is true for the metal complexes of the pyrazolone based ligands (Chapter's 4 and 5). Two methods are used for the interpretation and comparison of these structures. They include the relatively simple consideration of the dihedral and chelate angles and a fully quantitative analysis, *i.e.* continuous symmetry measure (CSM).

The CSM is a fully quantitative method of measuring the stereochemistry.²⁹ The method is based upon the idea that perfect symmetry is rarely attainable. It quantitatively expresses how much of a given symmetry there is in any (distorted)

structure with respect to any ideal group symmetry, *e.g.* T_d and D_{4h} , with a single parameter (CSM) defined by equations 3.3 and 3.4.

$$\text{CSM} = \min \frac{\sum_{k=1}^N |Q_k - P_k|^2}{\sum_{k=1}^N |Q_k - Q_o|^2} \times 100 \quad (3.3)$$

where Q_o is the coordinate vector of the centre of gravity of a point in the investigated structure.

$$Q_o = \frac{1}{N} \sum_{k=1}^N Q_k \quad (3.4)$$

The amount of a given symmetry in a structure is a function of the minimal distance that the vertices have to undergo to attain the defined perfect symmetry, *i.e.* when $\text{CSM} = 0$ then the structure is deemed to have perfect symmetry around the metal cation. Thus, in a given structure composed of N vertices (4-coordinate species, $N = 4$), the vertex coordinates of the structure $\{Q_k, k = 1, 2, \dots, N\}$ are related to the vertex coordinates of the defined perfect symmetry $\{P_k, k = 1, 2, \dots, N\}$. This gives a value for $|Q - P|^2$ with the units of length squared. To avoid size effects, the size of the original structure is normalised to the distance from its centre of mass, which is placed at the origin relative to all vertices. Therefore the degree of symmetry for a range of structures, with an equal number of vertices can be directly compared. For example the calculated T_d and D_{4h} symmetry measures, Table 3.4, for the copper complexes **9** and **16** (Sections 3.4.2.2 and 3.4.2.5 respectively) indicate a comparable

degree of square planarity. However complex **16** has a smaller tetrahedral component compared to that of **9**. This is presumably explained by its non-planar conformation (dihedral angle = 162.8°) compared to 180° for **9**.

Complex	T _d	D _{4h}
[Cu(5-H) ₂] (9)	33.81	0.71
[Cu(7-H) ₂] (16)	27.72	0.70

Table 3.4. Continuous symmetry measurements for bis(N-benzyl-3-hydroxy-2(1H)-pyridinethiones(ones)) copper(II) complexes, **9** and **16**.

The continuous symmetry method provides a “global” view of the geometry of the complexes it describes. However, it does not satisfactorily relate the defined geometry to the chelate angle and donor atom “bite” distance parameters that are well understood by coordination chemists. More importantly these structural features are readily controlled in ligand design by variation of the backbone of simple chelates and this can be used to tune the strength and selectivity of complex formation by matching the coordination requirements of the metal ion.

The structures here are represented in figures with atomic displacement ellipsoid plots generated from XP.³⁰ The estimated standards deviations for *inter*- and *intra*-atomic distances that are not classified as formal bonds were calculated using PLATON,³¹ and the crystallographic data for the structures are summarised in Appendix III. The fractional coordinates and thermal parameters of the crystal structures can be obtained from the crystallographic information files (CIF's) stored electronically on CD and located on the inside back cover of this thesis.

The dihedral angle (θ) between the coordination planes defined by the ligands in the 2:1 complexes were calculated using XP as the angle between the perpendiculars from the planes, A-M-B and C-M-D (where A, B are the donors of chelate ring 1 and C, D are the donor set of chelate ring 2). In all cases for the structures in this thesis the two chelating ligands are identical, *e.g.* A = C and B = D, and therefore a distinction can be made between *cis* and *trans* configurations of donor atoms. A dihedral angle of 0° denotes a perfectly planar *cis* arrangement of donor atoms. As θ increases the geometry moves away from planarity but still tends towards *cis* geometry below the value of 90° . Dihedral angles greater than 90° are classified as having distorted *trans* geometry and the perfectly planar *trans* arrangement of donor atoms has a dihedral an angle of 180° , Figure 3.9.

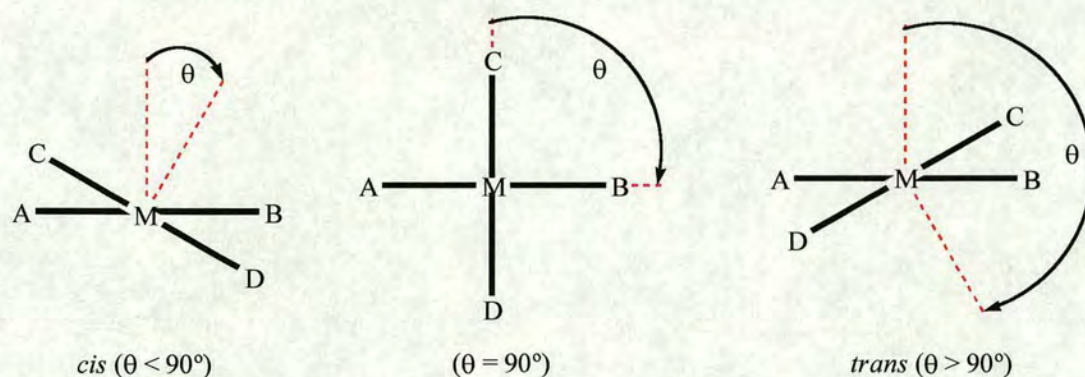


Figure 3.9. Illustration of the distinction between *cis* and *trans* dihedral angles when A = C and B = D, *e.g.* O₂S₂ donor set. The intersecting perpendicular of the planes A-M-B and C-M-D are shown in red.

The atoms are labelled according to whether the structure contains any symmetry. Three situations arise for the structures contained in this thesis:

1. The atoms of the first ligand in each structure are labelled with the suffix (A). In the remaining ligands the atoms are labelled with the suffix (B) [and (C) in the exceptional case of the 3:1 complex with cobalt] when they are not related by crystallographic symmetry.
2. When crystallographic symmetry relates ligands the second ligand is labelled with the suffix (‘).
3. For the tetradentate pyrazolone compounds (Chapter 5) when there is a crystallographic relationship within the ligand the two halves are labelled (A) and (A’). If there is no crystallographic relationship the two halves are labelled (A) and (B).

The exception to these rules is the zinc polymer (**17**), see Figure 3.22 for atom labelling.

3.4.1 Ligands.

3.4.1.1 N-benzyl-3-hydroxy-2(1H)-pyridinethione.

Large colourless needle like crystals of **5** were grown by recrystallisation from hot ethanol. The ligand crystallises in a monoclinic lattice with space group $P2_1/n$ (no.14). The asymmetric unit in the crystal structure consists of one ligand, Figure 3.10. In the solid state the ligands are arranged as dimers with the inversion centre situated at the centre of the donor atom “cavity”, the second ligand related by inversion symmetry (-x, -y, -z). Strong *intra*- and *intermolecular* S⋯H hydrogen bond interactions are present and lie within the typical range of O-H⋯S hydrogen bonds,³² Table 3.5.

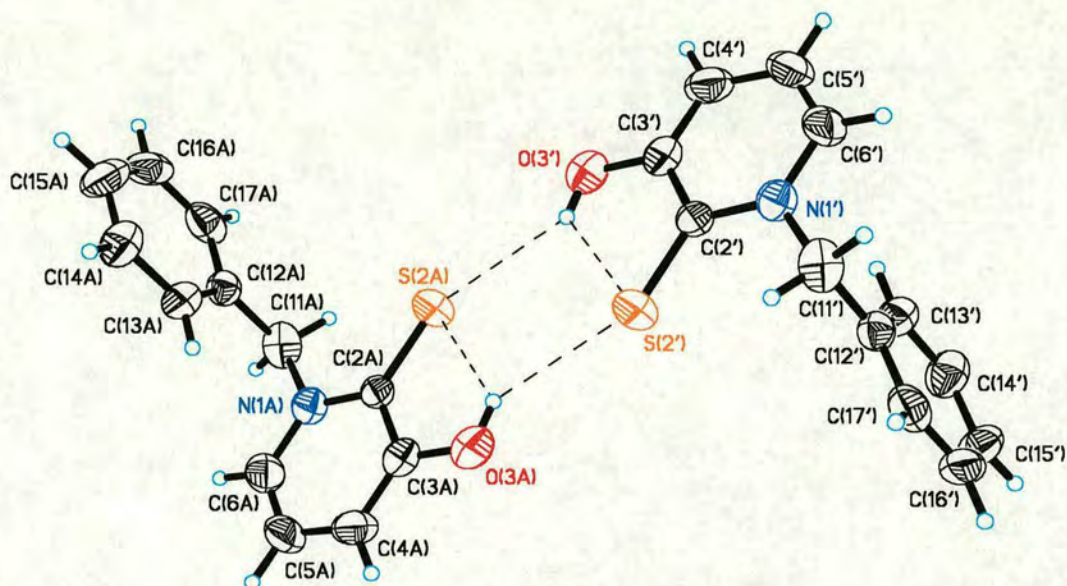


Figure 3.10. The structure of N-benzyl-3-hydroxy-2(1H)-pyridinethione (**5**) showing the hydrogen bonding between two asymmetric units. Atomic displacement ellipsoids are displayed at the 50 % probability level.

The two pyridine rings lie close to the O_2S_2 plane (r.m.s deviation from plane, 0.0885 Å, max. dev. H(3') = 0.1667 Å) in a dimer arrangement with similar donor atoms *trans* to each other.

	D–H \cdots A	D–H (Å)	H \cdots A (Å)	D \cdots A (Å)	D–H \cdots A (°)	Symmetry
HL (5)	O(3)–H(3) \cdots S(2)	0.830(4)	2.366(3)	2.918(3)	124.5(3)	—
	O(3)–H(3) \cdots S(2')	0.830(4)	2.923(3)	3.498(3)	140.80(13)	-x, -y, -z
HL (7)	O(3)–H(3) \cdots O(2)	0.8302	2.3254	2.7601(17)	113.20	—
	O(3)–H(3) \cdots O(2')	0.8302	1.9280	2.6705(17)	148.35	1-x, 1-y, -z

Table 3.5. Hydrogen bond interactions for N-benzyl-3-hydroxy-2(1H)-pyridinethione (**5**) and N-benzyl-3-hydroxy-2(1H)-pyridinone (**7**). Estimated standard deviations are given in parentheses. D = donor and A = acceptor.

Selected bond lengths and angles are listed in Table 3.7. The alternating C-C bond lengths in the pyridine ring and the bond lengths involving C(2)-S(2) and C(3)-O(3), which are typical of double and single bond characters respectively, confirm this resonance form. As might be expected, the benzyl carbon atom lies close to the pyridine least square plane and the torsion angles at the N(1)-C(2) and N(1)-C(6) bonds are close to 180° (torsions 1 and 2, Table 3.6). The phenyl rings are approximately perpendicular to the pyridine unit giving torsion angles of 85.3(4) and 14.4(5)° (torsions 3 to 6, Table 3.6).

	Torsion	HL (5)	HL (7)
1	C(3)-C(2)-N(1)-C(11)	178.3(3)	179.66(14)
2	C(5)-C(6)-N(1)-C(11)	177.5(4)	178.75(14)
3	C(2)-N(1)-C(11)-C(12)	85.3(4)	75.97(17)
4	C(6)-N(1)-C(11)-C(12)	91.6(4)	105.35(16)
5	N(1)-C(11)-C(12)-C(13)	14.4(5)	161.28(17)
6	N(1)-C(11)-C(12)-C(17)	168.6(3)	20.3(2)

Table 3.6. Selected torsion angles (°) for HL 5 and 7. Esd's calculated using PLATON.

3.4.1.2 N-benzyl-3-hydroxy-2(1H)-pyridinone.

Crystals of the ligand 7 were grown from 1-butanol as colourless blocks in the monoclinic system with space group P2₁/c (no.14). The asymmetric unit in the crystal structure consists of one ligand, Figure 3.11.

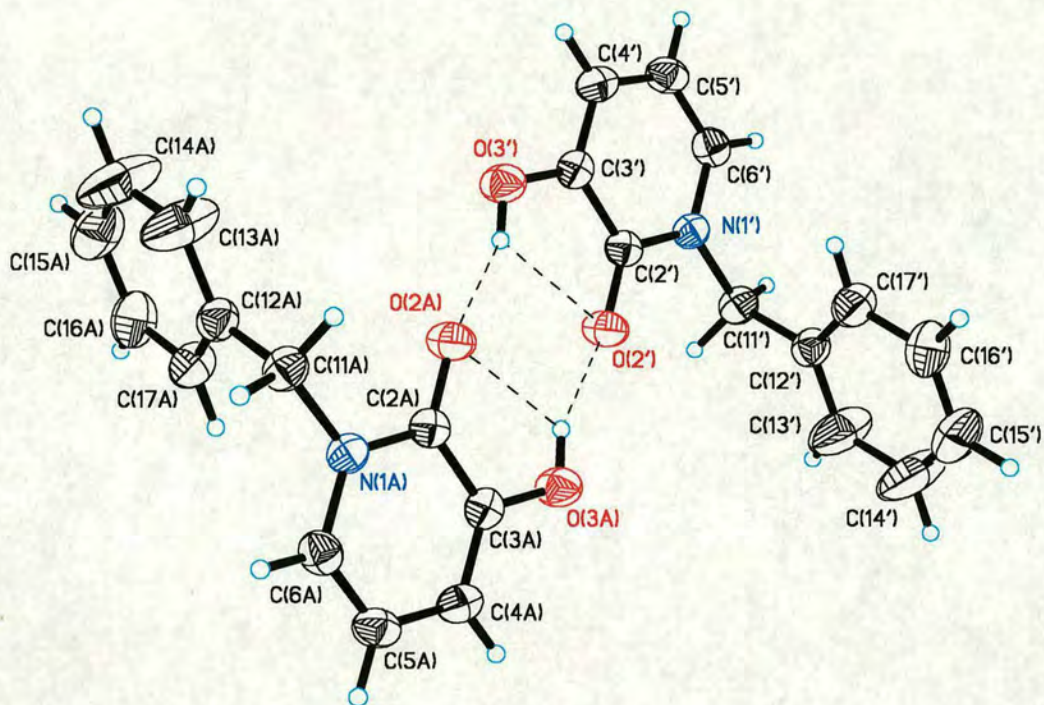


Figure 3.11. The structure of N-benzyl-3-hydroxy-2(1H)-pyridinone (**7**) showing the hydrogen bonding between to asymmetric units. Atomic displacement ellipsoids are displayed at the 50 % probability level.

It forms a centrosymmetric dimer, with the second ligand related to the first by inversion symmetry ($1-x, 1-y, -z$) via strong *intermolecular* hydrogen bonds, Table 3.5, with the oxygen carbonyl donor atoms arranged in a *trans* configuration, analogous to that of **5**. *Intramolecular* hydrogen bond interactions are also seen, although weaker (~ 0.4 Å longer). The two pyridine rings lie close to the O_4 plane (r.m.s. deviation from plane, 0.0775 Å, max. dev. $O(2), O(2') = 0.1792$ Å). The phenyl ring is rotated, to a lesser extent than in **5**, and consequently is less perpendicular to the pyridine ring (torsions 3 to 6), Table 3.6. It is structurally similar to the published N-butyl-3-hydroxy-2(1H)-pyridinone (2,3-Hopo),¹² Table 3.7.

	HL (5)	HL (7)	2,3-Hopo
N(1)-C(6)	1.361(5)	1.374(2)	1.383(2)
N(1)-C(2)	1.366(4)	1.374(2)	1.373(2)
N(1)-C(11)	1.463(4)	1.469(2)	1.460(3)
S(O)(2)-C(2)	1.678(3)	1.2448(18)	1.242(2)
C(2)-C(3)	1.434(5)	1.442(2)	1.432(2)
O(3)-C(3)	1.350(4)	1.3520(18)	1.352(2)
C(3)-C(4)	1.360(5)	1.358(2)	1.349(2)
C(4)-C(5)	1.383(5)	1.407(2)	1.406(3)
C(5)-C(6)	1.344(6)	1.346(2)	1.331(3)
S(O)(2)-C(2)-C(3)	120.6(3)	123.28(14)	123.5(2)
O(3)-C(3)-C(2)	117.3(3)	117.82(14)	117.0(2)

Table 3.7. Bond lengths (Å) and angles (°) calculated for N-benzyl-3-hydroxy-2(1H)-pyridinethione (**5**), N-benzyl-3-hydroxy-2(1H)-pyridinone (**7**) and N-butyl-3-hydroxy-2(1H)-pyridinone (**2,3-Hopo**).¹²

3.4.1.3 Comparison of ligands.

The bite distance in **5** (S \cdots O) is larger than that in **7** (O \cdots O) by approximately 0.16 Å, Table 3.8. This can be attributed to the thione C(2)-S(2) bond being longer (~0.43 Å) longer than the C(2)-O(2) carbonyl bond and also to a lesser extent by the slightly greater single bond character of the C(2)-C(3) of **5** compared to that of **7**, Figure 3.12.

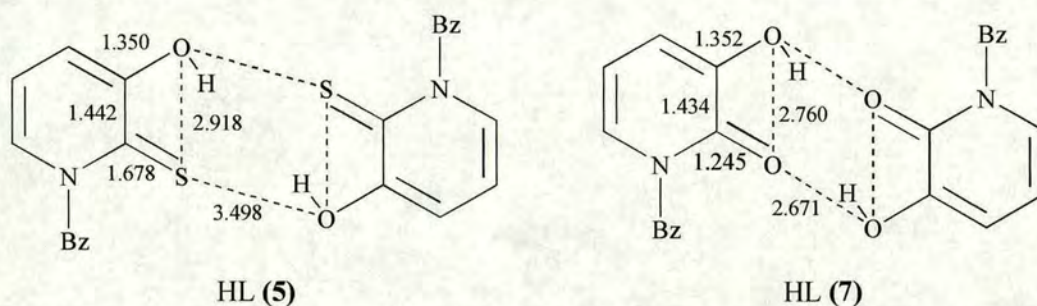


Figure 3.12. Comparison of bond lengths (Å) for the chelate rings of N-benzyl-3-hydroxy-2(1H)-pyridinethione (**5**) and N-benzyl-3-hydroxy-2(1H)-pyridinone (**7**).

	HL (5)	HL (7)
S(O)(2A) \cdots O(3A)	2.918(3)	2.7601(17)
S(O)(2A) \cdots O(3')	3.498(3) ^(a)	2.6705(17) ^(b)
S(O)(2A) \cdots S(O)(2')	4.241(2) ^(a)	3.2200(17) ^(b)
O(3A) \cdots O(3')	4.848(4) ^(a)	4.3739(19) ^(b)

Table 3.8. Donor atom distances for ligands **5** and **7**. Related by inversion symmetry

^(a) -x, -y, -z, ^(b) 1-x, 1-y, -z.

In contrast the carbon-hydroxy bond length C(3)-O(3) is the same in **5** and **7**, Table 3.7. The *intramolecular* S \cdots H contact in **5** is much shorter (~0.6 Å) than the

intermolecular S \cdots H contact, Table 3.5. Consequently the O₂S₂ donor set in the dimer is elongated with the *intermolecular* O \cdots S distance of the parallelogram being approximately 0.6 Å longer than the *intramolecular* distance. The opposite is observed in **7**, where the *intramolecular* hydrogen bond (O \cdots H) is longer (~0.4 Å) resulting in the O₄ donor set approximating to a rhombus. The reversal of the relative hydrogen bond strength is partly a consequence of the rigidity of the chelate arms. The parallelogram and rhombus arrays are such that the diagonal O(3A) \cdots O(3') is the longer, allowing the cavity to accommodate the volume occupied by the hydrogen atoms. The distortion is greater in **7** due to the closer proximity of the two ligands to each other. The larger bite distance of **5**, coupled with the inflexibility of the chelate ring, should allow it to accommodate a larger metal cation in contrast to the smaller bite distance of **7**.

3.4.2 Metal complexes.

The crystallographic data are summarised in Appendix III.

3.4.2.1 Bis(N-benzyl-3-hydroxy-2(1H)-pyridinethionato)zinc(II).

Colourless block crystals of [Zn(**5-H**)₂] (**8**), grown from methanol, have the space group P2₁/c (no.14). The asymmetric unit contains a single [Zn(**5-H**)₂] molecule in which the zinc(II) cation lies at the centre of a highly distorted tetrahedral O₂S₂ donor set, Figure 3.13.

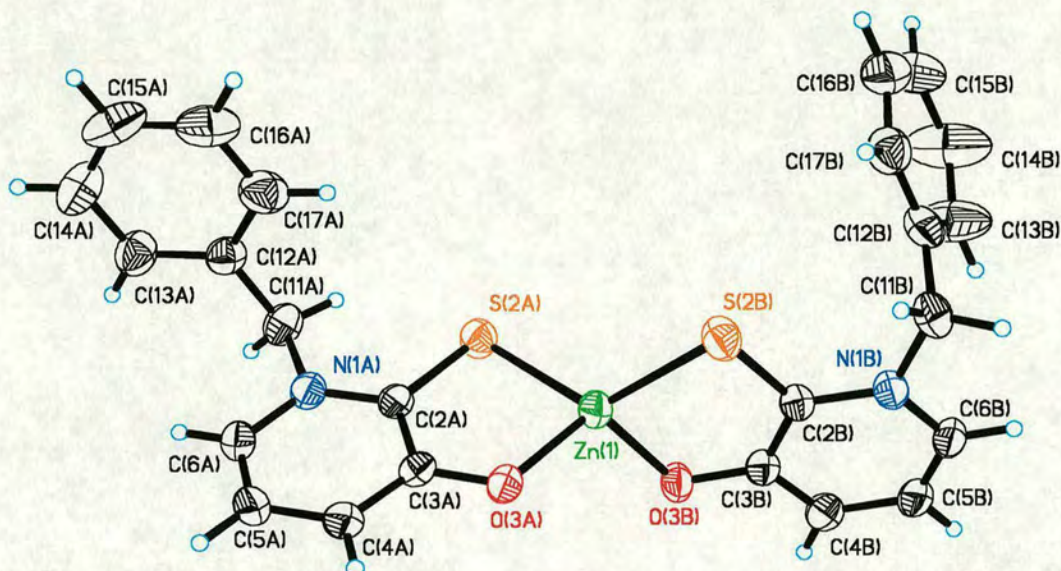


Figure 3.13. The structure of bis(N-benzyl-3-hydroxy-2(1H)-pyridinethionato) zinc(II) (**8**) showing atomic displacement ellipsoids at the 50 % probability level.

The distortion of the O₂S₂ donors from tetrahedral geometry is evident from the marked variation of the bond angles about the zinc(II) atom (range from 89.14(5)° to 124.25(6)°) and the dihedral angle of 83.8° between the Zn, O, S planes which deviates considerably from the ideal value of 90°, Table 3.9. The chelating O-Zn-S angles (89.14(5) and 90.12(5)°) are much smaller than the ideal value for tetrahedral geometry as a consequence of the rigidity and limited bite of the ligand.

	[Zn(5-H) ₂] (8)		[Cu(5-H) ₂] (9) ^(a)		[Ni(5-H) ₂].MeOH (10)		[Co(5-H) ₃].2MeOH (11)		
	L(A)	L(B)	L(A)	L(°)	L(A)	L(B)	L(A)	L(B)	L(C)
M(1)-S(2)	2.3149(9)	2.2931(8)	2.2669(9)	2.2669(9)	2.155(3)	2.157(3)	2.251(2)	2.226(2)	2.215(2)
M(1)-O(3)	1.9469(17)	1.9546(17)	1.919(2)	1.919(2)	1.881(3)	1.868(4)	1.939(3)	1.915(3)	1.932(3)
S(2)-M(1)-O(3)	89.14(5)	90.12(5)	88.23(6)	88.23(6)	90.29(11)	90.47(11)	87.54(9)	88.84(9)	89.11(10)
S...O	3.002(2)	3.016(2)	2.924(2)	2.924(2)	2.868(5)	2.865(5)	2.906(3)	2.907(3)	2.917(3)
S(2A)-M(1)-O(3B)	121.86(6)		91.77(6)		173.78(9)				
S(2B)-M(1)-O(3A)	124.25(6)		91.77(6)		176.96(9)				
S(2A)-M(1)-S(2B)	124.11(3)		180.0		92.13(9)				
O(3A)-M(1)-O(3B)	109.76(7)		180.0		87.31(14)				
θ	83.8		180 ^(b)		6.0 ^(b)				

Table 3.9. Metal-donor bond lengths (Å), angles (°), chelate bite distances (Å) and dihedral angles (θ °) defined by the chelates, together with the remaining bond angles at the metal in [Zn(5-H)₂] (8), [Cu(5-H)₂] (9), [Ni(5-H)₂].MeOH (10) and [Co(5-H)₃].2MeOH (11). ^(a) The two ligands are related by inversion symmetry (-x, -y, -z).

On complexation to zinc the C-S bonds lengths within the ligand increase by ~ 0.05 Å to 1.727(2) and 1.731(2) Å whereas the C-O bonds lengths decrease by ~ 0.04 Å to 1.313(3) and 1.310(3) Å, Table 3.10, suggesting that π -delocalisation is enhanced by metal chelation.

The ZnO_2S_2 coordination sphere is the one of the least common of all possible combinations of $\text{ZnN}_x\text{O}_y\text{S}_z$ ($x + y + z = 4$) with only nine examples out of 453 structures present in the current CSD release, September 1999, (Section 2.4.2.1). Of the nine examples, the greatest of relevance for comparison here is the $[\text{ZnL}_2]$ complex of the OS chelating ligand 1-hydroxy-4-methyl-2(1H)-pyridinethione,³³ Figure 3.14.

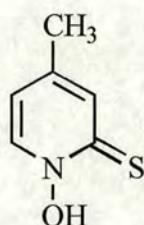


Figure 3.14. The structure of 1-hydroxy-4-methyl-2(1H)-pyridinethione.

The bond lengths and angles within the chelate ring are similar to those in $[\text{Zn}(\mathbf{5-H})_2]$ (**8**), producing a chelate angle of 88.7° , with the exception the C-N and N-O distances. The inclusion of the pyridine nitrogen in the chelate ring produces a decrease by ~ 0.07 Å in the C-N bond length compared to C(2)-C(3) in **8** and an increase of ~ 0.04 Å in the N-O distance compared to and C(3)-O(3) in **8**.

	HL (5)	[Zn(5-H) ₂] (8)		[Cu(5-H) ₂] (9) ^(a)		[Ni(5-H) ₂].MeOH (10)		[Co(5-H) ₃].2MeOH (11)		
	L(A)	L(A)	L(B)	L(A)	L(*)	L(A)	L(B)	L(A)	L(B)	L(C)
C(2)-S(2)	1.678(3)	1.727(2)	1.731(2)	1.711(3)	1.711(3)	1.722(4)	1.716(4)	1.721(4)	1.723(4)	1.709(4)
C(2)-C(3)	1.434(5)	1.437(3)	1.434(3)	1.424(4)	1.424(4)	1.421(6)	1.421(5)	1.416(6)	1.428(5)	1.448(6)
C(3)-O(3)	1.350(4)	1.313(3)	1.310(3)	1.310(3)	1.310(3)	1.311(5)	1.324(3)	1.310(4)	1.302(5)	1.297(5)
N(1)-C(6)	1.361(5)	1.361(3)	1.363(3)	1.356(4)	1.356(4)	1.368(5)	1.360(5)	1.365(6)	1.361(5)	1.374(6)
N(1)-C(2)	1.366(4)	1.358(3)	1.361(3)	1.367(4)	1.367(4)	1.363(5)	1.352(5)	1.371(5)	1.356(5)	1.352(5)
N(1)-C(11)	1.463(4)	1.491(3)	1.480(3)	1.471(4)	1.471(4)	1.458(5)	1.486(5)	1.465(6)	1.476(5)	1.475(5)
C(3)-C(4)	1.360(5)	1.382(3)	1.384(3)	1.391(4)	1.391(4)	1.391(5)	1.386(5)	1.388(6)	1.390(6)	1.387(6)
C(4)-C(5)	1.383(5)	1.391(4)	1.378(4)	1.390(5)	1.390(5)	1.387(6)	1.392(5)	1.386(6)	1.388(6)	1.385(6)
C(5)-C(6)	1.344(6)	1.348(4)	1.359(4)	1.357(5)	1.357(5)	1.362(6)	1.364(6)	1.335(7)	1.357(6)	1.365(7)
M(1)-S(2)-C(2)	—	92.96(8)	92.48(8)	94.59(10)	94.59(10)	95.91(6)	96.04(15)	95.0(2)	95.01(14)	95.8(2)
S(2)-C(2)-C(3)	120.6(3)	120.68(18)	121.21(17)	119.5(2)	119.5(2)	117.6(3)	117.5(3)	118.6(3)	118.4(3)	118.2(3)
O(3)-C(3)-C(2)	117.3(3)	120.3(2)	120.5(2)	119.1(3)	119.1(3)	118.5(4)	118.5(3)	119.3(4)	118.9(4)	119.(4)
M(1)-O(3)-C(3)	—	116.78(15)	115.68(15)	118.36(18)	118.36(18)	117.7(3)	117.6(3)	117.6(3)	118.2(3)	117.3(3)

Table 3.10. Selected bond lengths (Å) and angles (°) in the HL (5) and in the chelate units of its complexes [Zn(5-H)₂] (8), [Cu(5-H)₂] (9), [Ni(5-H)₂].MeOH (10) and [Co(5-H)₃].2MeOH (11). ^(a) The two independent ligands are crystallographically related by inversion symmetry (-x, -y, -z).

3.4.2.2 Bis(N-benzyl-3-hydroxy-2(1H)-pyridinethionato)copper(II).

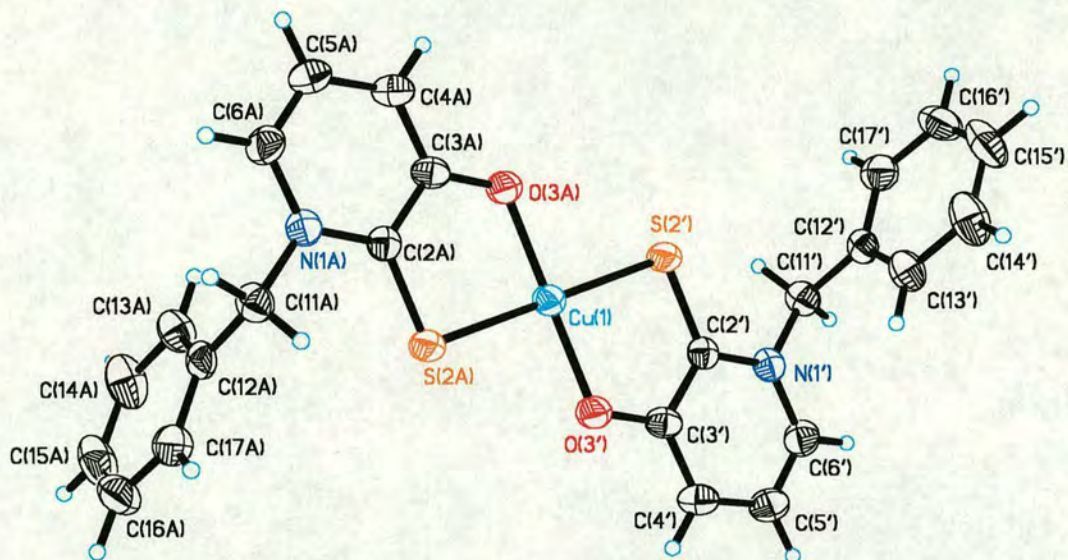


Figure 3.15. The structure of bis(N-benzyl-3-hydroxy-2(1H)-pyridinethionato)copper(II) (**9**) showing two asymmetric units related by inversion symmetry. Atomic displacement ellipsoids are displayed at the 50 % probability level.

Red plate-like crystals of $[\text{Cu}(\mathbf{5-H})_2]$ (**9**), grown in methanol, have the space group $P2_1/n$ (no.14). The asymmetric unit consists of one half of a $[\text{Cu}(\mathbf{5-H})_2]$ complex in which the metal is positioned on a crystallographic inversion centre, the other half related to it by inversion symmetry $(-x, -y, -z)$, Figure 3.15.

The CuS_2O_2 coordination sphere is relatively uncommon with only six reported structures out of 1658 $\text{CuN}_x\text{O}_y\text{S}_z$ ($x + y + z = 4$) entries in the CSD (September 1999). The structure of $[\text{Cu}(\mathbf{5-H})_2]$ (**9**) is closely related to that of *trans* bis(6-methyl-3-hydroxy-2(1H)-pyridinethionato)copper(II).bis(dimethylformamide) previously reported,³⁴ Figure 3.16.

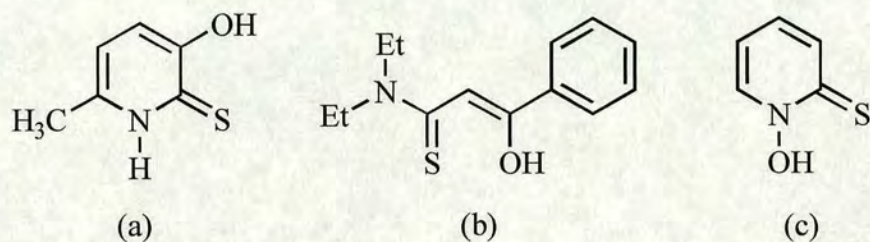


Figure 3.16. The structure of ligands (a) 6-methyl-3-hydroxy-2(1H)-pyridinethione, (b) N,N-diethyl-2-benzoylthioacetamide and (c) 1-hydroxy-2(1H)-pyridinethione.

The coordination around the copper centre of **9** is perfectly planar, with the chelate angle (88.23(6) Å) of the ligand ideally suited to this geometry. The complex has a *trans* geometry, which is typical amongst the limited number of CuS₂O₂ coordination spheres characterised with only one nearly planar *cis* structure reported for copper³⁵ of the bidentate N,N-diethyl-2-benzoylthioacetamide ligand, Figure 3.16(b). However the crystal structure of this complex contains two symmetry independent molecules. One molecule shows a nearly planar *cis*-arrangement of the donor set with a dihedral angle of 5.2° whereas the other has a perfectly planar *trans* configuration.

The geometry is necessarily distorted from a square in **9** by the inequivalent Cu-S and Cu-O bond lengths, Table 3.9. Significant π -delocalisation is evident throughout the pyridine and chelate rings with the alternation in C-C bond lengths in the pyridine ring becoming less pronounced, Table 3.10, and both the pyridine and chelate rings close to planar (r.m.s. deviation from plane, 0.1496 Å, max. dev. O(3) = 0.3938 Å).

3.4.2.3 Bis(N-benzyl-3-hydroxy-2(1H)-pyridinethionato)nickel(II).(methanol).

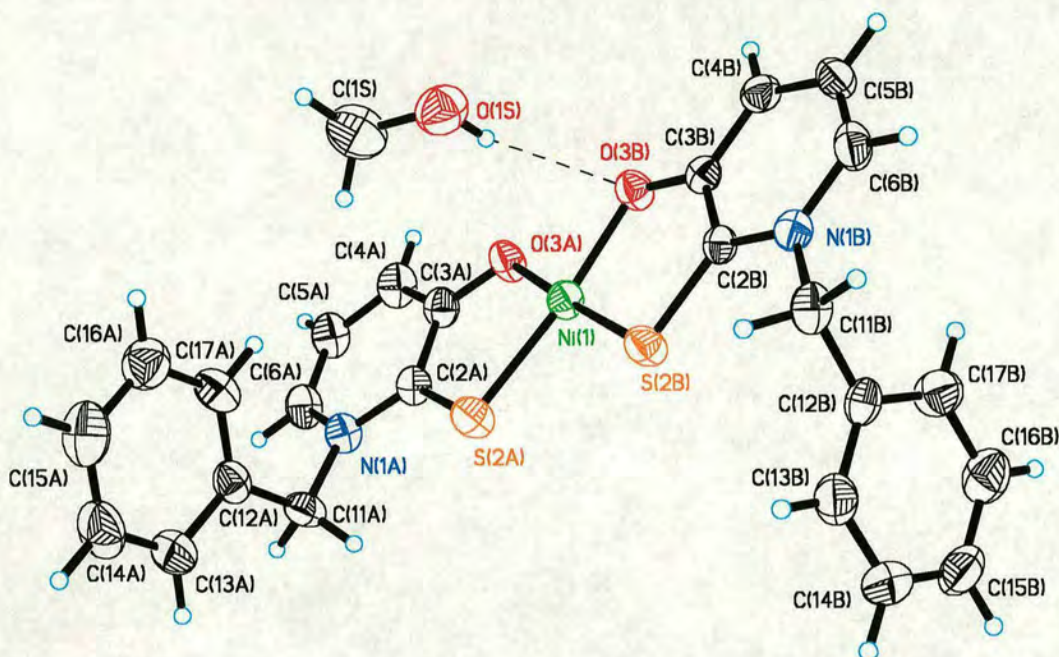


Figure 3.17. The structure of bis(N-benzyl-3-hydroxy-2(1H)-pyridinethionato)nickel(II) (**10**) showing atomic displacement ellipsoids at the 50 % probability level.

Yellow lath crystals of $[\text{Ni}(\mathbf{5-H})_2]\cdot\text{MeOH}$ (**10**), were grown from methanol and the space group determined to be $P\bar{1}$ (no.2). The asymmetric unit, Figure 3.17, contains a single $[\text{Ni}(\mathbf{5-H})_2]$ molecule hydrogen bonded to a methanol molecule of crystallisation, Table 3.12.

The NiS_2O_2 coordination sphere is the most common of the examples reported here. However, even in this case, of the 1596 $\text{NiN}_x\text{O}_y\text{S}_z$ ($x + y + z = 4$) structures in the CSD only 20 (1.3 %) contain the NiS_2O_2 unit. Two examples of direct relevance here are *trans*-bis(6-methyl-3-hydroxy-2(1H)-pyridinethionato)nickel(II).bis(DMF)³⁴ and *cis*-bis(1-hydroxy-2(1H)-pyridinethionato)nickel(II),³⁶ Figure 3.16(a) and (c). The ligands adopt a *cis* square planar geometry around the nickel centre in **10** and the

bond lengths in the chelating units are in good agreement with those in the closely related *trans*-bis(6-methyl-3-hydroxy-2(1H)-pyridinethionato)nickel(II) bis(DMF). The chelate angles O-Ni-S are 90.29(11) and 90.47(11)°, and are almost ideal for square planar geometry, Table 3.9. However, the geometry is necessarily distorted from a square by the inequivalent Ni-S and Ni-O bond lengths, Table 3.9. The molecule is further distorted from planarity with a dihedral angle of 6.0° between the S(2A)-Ni(1)-O(3A) and S(2B)-Ni(1)-O(3B) triangles producing a small distortion towards tetrahedral geometry. The S-Ni-S bond angle of 92.13(9)°, Table 3.9, exhibits a slight expansion of from the ideal square planar value of 90°. This accordingly compresses the opposite O-Ni-O angle to a value of 87.31(14)°.

3.4.2.4 Tris(N-benzyl-3-hydroxy-2(1H)-pyridinethionato)cobalt(III) bis(methanol).

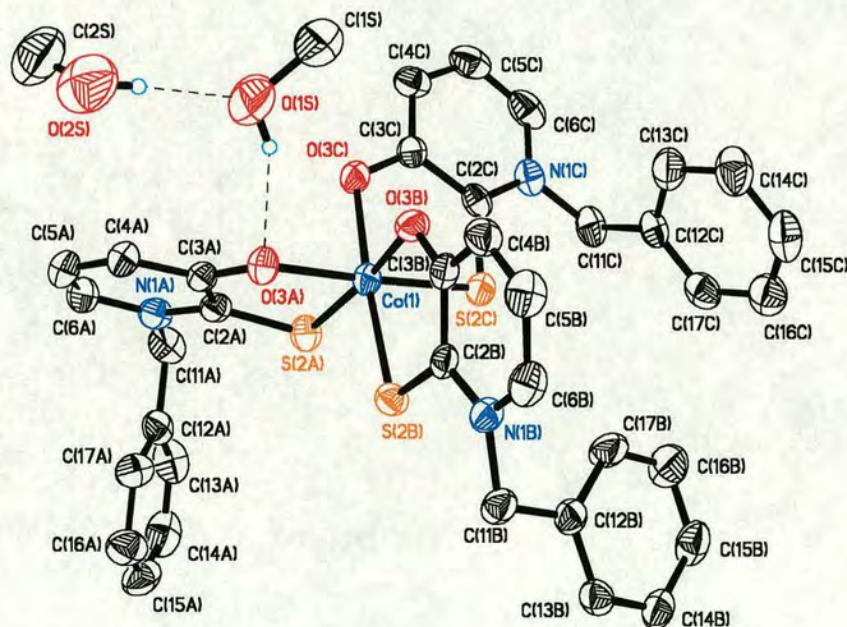


Figure 3.18. The structure of tris(N-benzyl-3-hydroxy-2(1H)-pyridinethionato)cobalt(III) (**11**) showing atomic displacement ellipsoids at the 50 % probability level.

Dark red lath crystals of $[\text{Co}(\mathbf{5-H})_3]\cdot 2\text{EtOH}$ (**11**), grown from methanol have the space group $P\bar{1}$ (no.2). The asymmetric unit contains a single $[\text{Co}(\mathbf{5-H})_3]$ molecule and two molecules of methanol, Figure 3.18. The complex is chiral with both enantiomers (Λ and Δ) occurring in the unit cell and related by a crystallographic inversion centre. One methanol is hydrogen bonded to O(3A) of a ligand A ($\text{O}\cdots\text{O}$ is 2.812(6) Å) and the second methanol, although disordered, forms a hydrogen bond to the oxygen of the first ($\text{O}\cdots\text{O}$ is 2.660(8) Å), Table 3.12. In each molecule the Co(III) ion is coordinated by three chelating N-benzyl-3-hydroxy-2(1H)-pyridinethione ligands. The geometry at the metal centre is close to octahedral, as expected for a low spin d^6 metal ion, Figure 3.19.

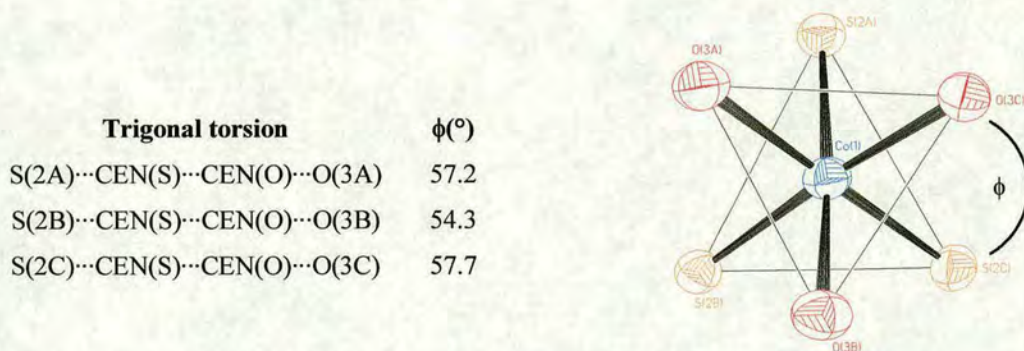


Figure 3.19. A representation of the Δ enantiomer of the chiral coordination sphere for $[\text{Co}(\mathbf{5-H})_3]$ (**11**) viewed along the idealised C_3 axis. The trigonal twist angle is obtained by averaging the three torsion angles defined by the centriods CEN(O) and CEN(S) of the two faces “normal” to the molecular pseudo- C_3 axis and the pairs of atoms composing of each chelate ring, *e.g.* S(2A) \cdots CEN(S) \cdots CEN(O) \cdots O(3A).

The three 5-membered chelate rings define a *cis* geometry giving a *facial* complex with approximate trigonal symmetry (trigonal twist angle is 56.4° , ideal O_h symmetry is 60°). The trigonal face defined by the O(3) atoms has shorter sides than

the trigonal face defined by the S(2) atoms, Table 3.11. Coupled with the shorter Co-O distances than the Co-S distances (av. ~ 0.41 Å shorter), Table 3.9, the oxygen trigonal face subsequently lies closer to the cobalt centre (~ 0.1 Å) leading to further distortion away from the ideal O_h geometry.

S(3A)⋯S(3B)	3.238(2)	O(3A)⋯O(3B)	2.643(4)
S(3B)⋯S(3C)	3.077(2)	O(3B)⋯O(3C)	2.667(4)
S(3C)⋯S(3A)	3.254(2)	O(3C)⋯O(3A)	2.711(5)

Table 3.11. O⋯O and S⋯S distances defining the trigonal faces of the coordination sphere for the $[\text{Co}(\mathbf{5-H})_3] \cdot 2\text{MeOH}$ (**11**) complex.

The CoO_3S_3 coordination sphere is one of the least common observed in cobalt(III) chemistry. Of the 1938 $\text{CoN}_x\text{O}_y\text{S}_z$ ($x + y + z = 6$) structures in the CSD only 8 CoO_3S_3 are presented. Those which are of most direct relevance contain the OS chelating ligand 1-hydroxy-2(1H)-pyridinethione,^{13,37-39} Figure 3.16(c), all of which share the common *facial* geometry.

The limited bite of the ligand also gives rise to a small distortion from octahedral geometry with chelate angles ranging from $87.54(9)^\circ$ to $89.11(10)^\circ$, Table 3.9.

3.4.2.5 Bis(N-benzyl-3-hydroxy-2(1H)-pyridinonato)copper(II).bis(ethanol).

Green tablet like crystals of $[\text{Cu}(\mathbf{7-H})_2] \cdot 2\text{EtOH}$ (**16**), grown in ethanol have the space group $P2_1/n$ (no.14). The asymmetric unit contains a single $[\text{Cu}(\mathbf{7-H})_2]$ molecule and two associated molecules of ethanol, Figure 3.20.

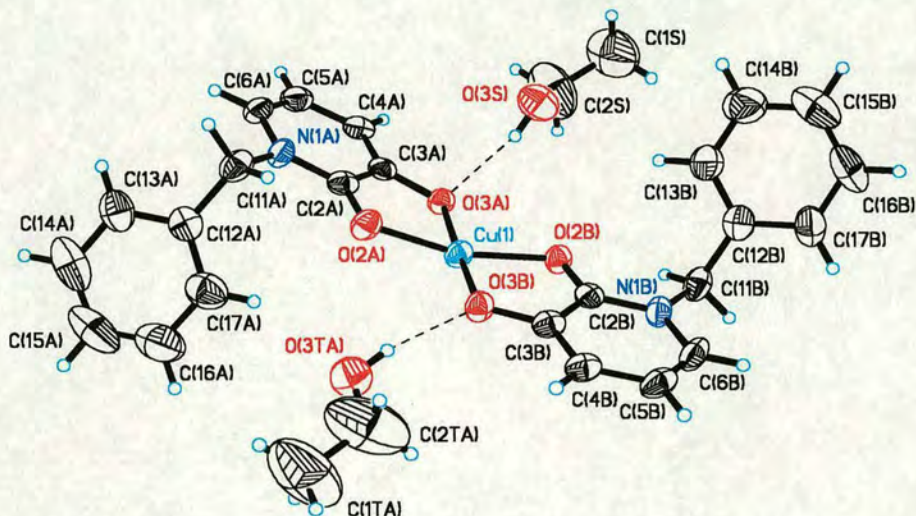


Figure 3.20. The structure of bis(*N*-benzyl-3-hydroxy-2(1*H*)-pyridinonato)copper(II) (**16**) showing atomic displacement ellipsoids at the 50 % probability level.

Both O(3A) and O(3B) are hydrogen bonded to ethanol molecules. One ethanol is hydrogen bonded to ligand A (O(3A)⋯O(3S) 2.813(6) Å). The second ethanol is hydrogen bonded to ligand B (O(3B)⋯O(3TA) 2.801(9) Å), Table 3.12. It is generated by the symmetry operation 1-*x*, -*y*, -*z* and exhibits disorder about C(1TA) and C(2TA), both positions 50 % partially occupied.

	D-H⋯A	D-H (Å)	H⋯A (Å)	D⋯A (Å)	D-H⋯A (°)
[Ni(5-H) ₂] (10)	O(1M)-H(1M)⋯O(3B)	0.8307	2.2929	3.080(6)	158.38
[Co(5-H) ₂] (11)	O(1M)-H(1M)⋯O(3A)	0.83(4)	2.03(4)	2.812(6)	157(6)
	O(2M)-H(2M)⋯O(1M)	0.83(5)	1.84(4)	2.660(8)	170(4)
[Cu(7-H) ₂] (16)	O(3S)-H(3S)⋯O(3A)	0.8298	2.0008	2.813(6)	165.90
	O(3T)-H(3T)⋯O(3B) ^(a)	0.8288	1.9906	2.801(9)	165.79

Table 3.12. Hydrogen bond interactions of molecules of solvent for [Ni(**5-H**)₂].MeOH (**10**) [Co(**5-H**)₂].2MeOH (**11**) and [Cu(**7-H**)₂].2EtOH (**16**). ^(a)

Generated by the symmetry operation 1-*x*, -*y*, -*z*.

Selected bond lengths and angles for HL (**7**) and complex (**16**) are listed in Table 3.13 for comparison. The ligands adopt a distorted square planar geometry with a *trans* configuration around the copper(II) centre, O(3A)-Cu(1)-O(3B) and O(2A)-Cu(1)-O(2B) are 177.25(14)° and 162.85(14)° respectively, producing a dihedral angle between the O-Cu-O chelates of 162.8°.

On complexation the two C-O distances become more similar. The pyridone C-O bond lengths are equivalent (an increase of ~ 0.04 Å upon complexation) whereas the formal C-O single bond distances are different, 1.348(6) Å and 1.325(6) Å. The O-Cu-O chelate angles, 85.39(14) and 85.40(14)°, are smaller than that dictated by perfect square planar geometry and are a consequence of the smaller bite of the O...O chelate (2.629(5) Å).

The molecules assemble in discrete dimeric units in the crystal lattice with two close molecular contacts between O(3) and Cu(1), 2.505(3) Å, in each molecule forming a square-based pyramidal coordination around each copper centre, Figure 3.21.

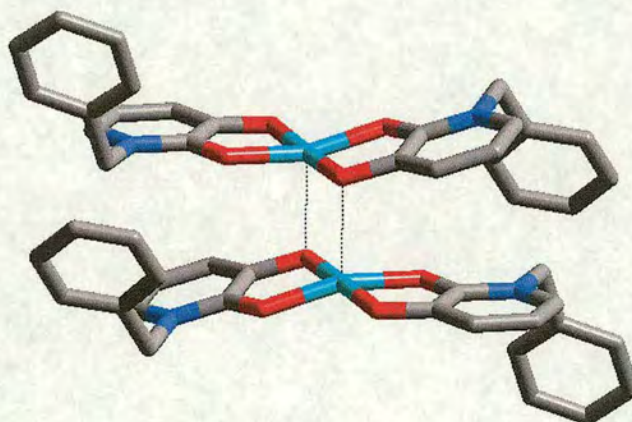


Figure 3.21. A representation of the dimerisation of [Cu(**7-H**)₂].2EtOH (**16**) molecules in the solid state, using CERIOUS.⁴²

	HL (7)	[Cu(7-H) ₂].2EtOH (16)	
	L(A)	L(A)	L(B)
C(2)-O(2)	1.2448(18)	1.280(5)	1.283(5)
C(2)-C(3)	1.442(2)	1.433(7)	1.435(7)
C(3)-O(3)	1.350(18)	1.348(6)	1.325(6)
Cu(1)-O(2)	—	1.945(3)	1.959(3)
Cu(1)-O(3)	—	1.930(3)	1.919(3)
N(1)-C(6)	1.374(2)	1.374(6)	1.378(6)
N(1)-C(2)	1.374(2)	1.341(6)	1.353(6)
N(1)-C(11)	1.469(2)	1.483(6)	1.473(6)
C(3)-C(4)	1.358(2)	1.362(6)	1.369(7)
C(4)-C(5)	1.407(2)	1.402(7)	1.398(7)
C(5)-C(6)	1.346(2)	1.354(7)	1.344(7)
Cu(1)-O(2)-C(2)	—	109.8(3)	108.9(3)
O(2)-C(2)-C(3)	123.28(14)	119.7(5)	119.5(4)
O(3)-C(3)-C(2)	117.82(14)	114.5(4)	115.1(4)
Cu(1)-O(3)-C(3)	—	110.4(3)	110.9(3)
O(2)-Cu(1)-O(3)	—	85.40(14)	85.39(14)

Table 3.13. Selected bond lengths (Å) and angles (°) in HL (7) and in the chelating units of [Cu(7-H)₂].2EtOH (16).

3.4.2.6 Poly((bis(N-benzyl-3-hydroxy-pyridinonato)tetra(acetato)tri-zinc(II)).

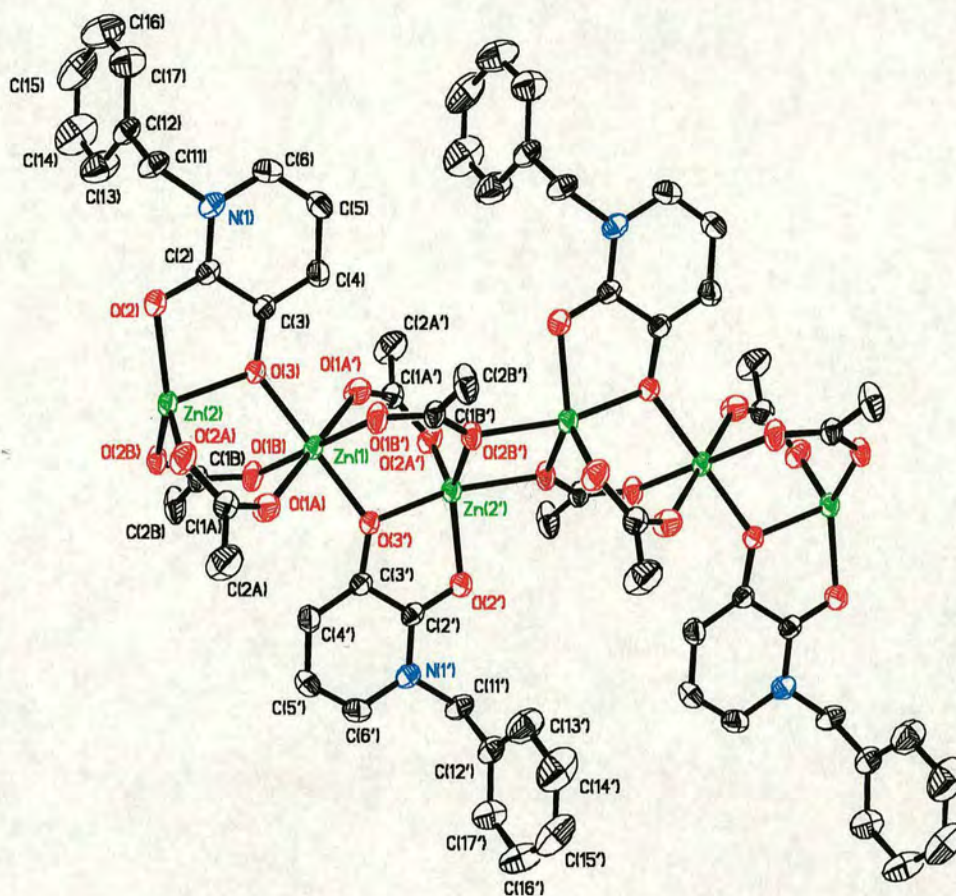


Figure 3.22. The structure of $[Zn_3(7-H)_2(O_2CCH_3)_4]_n$ (**17**), poly((bis(N-benzyl-3-hydroxy-pyridinonato)tetra(acetato)tri-zinc(II)), showing the bonding between two unit cells each consisting of two asymmetric units. Atomic displacement ellipsoids are displayed at the 50 % probability level. Hydrogen atoms are omitted for clarity.

Colourless block crystals of $[Zn_3(7-H)_2(O_2CCH_3)_4]_n$ (**17**) were obtained by crystallisation in methanol and were determined to be in space group $P\bar{1}$ (no.2). The structure is composed of infinite one-dimensional chains with a minimum repeating unit of $[Zn_3(7-H)_2(O_2CCH_3)_4]$, Figure 3.22. The unit cell contains three zinc ions, one with octahedral geometry and two with distorted square-based pyramidal

geometries, that are linked (Zn(1)⋯Zn(2); 3.3492(17) Å and Zn(2)⋯Zn(2'); 3.2602(17) Å) by two bridging acetates and a N-benzyl-3-hydroxy-2(1H)-pyridinonato ligand. In this space group the asymmetric unit consists of half the translational repeating unit that forms the trimer unit cell in which Zn(1) lies on an inversion centre.

In contrast to the simple bidentate mode seen in the simple [ML₂] species described previously, in this structure the ligand (7) displays two modes of complexation. The pyridone O(2) and the formally anionic O(3) donor atoms complex in a bidentate fashion and occupy two coordination sites of the distorted square-based pyramidal zinc ion, Zn(2), producing a chelate angle of 80.19(10) Å. In addition the O(3) atom occupies a coordination site of the octahedral zinc ion, Zn(1), similar to a binuclear bridging phenolate. The Zn(1)-O(3) and Zn(2)-O(3) bonds are the same length within experimental error, Table 3.14.

The two acetate bridges in the asymmetric unit provide the remainder of coordination sites around each zinc ion and display a different mode of complexation to each other. One forms a bidentate bridge between Zn(1) and Zn(2) (Zn(1)-O(1A) and Zn(2)-O(2A) are 2.131 and 1.968 Å respectively) reflecting the double and single bond character of the acetate C(1A)-O(1A) and C(1A)-O(2A) distances, 1.241 Å and 1.271 Å respectively. The second acetate is trinucleating, linking the 5- and 6-coordinate zinc ions in one asymmetric unit and the 5-coordinate zinc ion in the adjacent asymmetric unit, related by the symmetry operation (1-x, -y, -z). As with the first bidentate acetate the “carbonyl” O(1B) atom (C(1B)-O(1B); 1.227 Å) complexes to the 6-coordinate zinc ion forming a longer bond (Zn(1)-O(1B); 2.094 Å) than O(2B) to the 5-coordinate zinc ion (Zn(2)-O(2B); 2.032 Å), Table 3.14.

Zn(1) coordination		Zn(2) coordination	
Zn(1)-O(3)	2.033(2)	Zn(2)-O(2)	2.042(3)
Zn(1)-O(3') ^(a)	2.033(2)	Zn(2)-O(3)	2.032(2)
Zn(1)-O(1A)	2.131(3)	Zn(2)-O(2A)	1.968(2)
Zn(1)-O(1A') ^(a)	2.131(3)	Zn(2)-O(2B)	2.032(2)
Zn(1)-O(1B)	2.094(2)	Zn(2)-O(2B') ^(b)	2.119(2)
Zn(1)-O(1B') ^(a)	2.094(2)	Zn(2') ^(b) -O(2B)	2.119(2)
O(3)-Zn(1)-O(3') ^(a)	180.0	O(2)-Zn(2)-O(3)	80.19(10)
O(1A)-Zn(1)-O(1A') ^(a)	180.0	O(2A)-Zn(2)-O(3)	101.58(11)
O(1B)-Zn(1)-O(1B') ^(a)	180.0	O(2A)-Zn(2)-O(2B)	112.08(11)
O(3)-Zn(1)-O(1A)	90.11(10)	O(3)-Zn(2)-O(2B)	97.02(9)
O(3') ^(a) -Zn(1)-O(1A') ^(a)	90.11(10)	O(2A)-Zn(2)-O(2)	115.13(11)
O(3)-Zn(1)-O(1B)	88.35(10)	O(2B)-Zn(2)-O(2)	132.30(11)
O(3') ^(a) -Zn(1)-O(1B') ^(a)	88.35(10)	O(2A)-Zn(2)-O(2B') ^(b)	96.70(11)
O(3)-Zn(1)-O(1B') ^(a)	91.65(10)	O(3)-Zn(2)-O(2B') ^(b)	161.71(10)
O(3') ^(a) -Zn(1)-O(1B)	91.65(10)	O(2B)-Zn(2)-O(2B') ^(b)	76.52(9)
O(3)-Zn(1)-O(1A') ^(a)	89.89(10)	O(2)-Zn(2)-O(2B') ^(b)	91.48(10)
O(3') ^(a) -Zn(1)-O(1A)	89.89(10)		
O(1A)-Zn(1)-O(1B)	91.48(11)		
O(1A') ^(a) -Zn(1)-O(1B') ^(a)	91.48(11)		
O(1A)-Zn(1)-O(1B') ^(a)	88.52(11)		
O(1A') ^(a) -Zn(1)-O(1B)	88.52(11)		
Chelate ring		Acetate bridges	
C(2)-O(2)	1.273(4)	O(1A)-C(1A)	1.241(4)
C(2)-C(3)	1.443(4)	O(2A)-C(1A)	1.271(5)
C(3)-O(3)	1.321(4)	C(1A)-C(2A)	1.500(6)
O(2)-C(2)-C(3)	120.8(3)	O(1B)-C(1B)	1.227(4)
C(2)-O(2)-Zn(2)	111.3(2)	O(2B)-C(1B)	1.296(4)
O(3)-C(3)-C(2)	113.5(3)	O(2B)-Zn(2') ^(b)	2.119(2)
C(3)-O(3)-Zn(2)	113.8(2)	C(1B)-C(2B)	1.550(5)

Table 3.14. Selected bond lengths (Å) and angles(°) for poly((bis(N-benzyl-3-hydroxy-pyridinonato)tetra(acetato)tri-zinc(II)) (**17**). ^(a) Generated by inversion symmetry (-x, -y, -z). ^(b) Generated by symmetry operation 1-x, -y, -z.

The O(2B) atom bridges the 5-coordinate zinc centres, with Zn(2)-O(2B) and Zn(2')-O(2B), 2.032 and 2.119 Å respectively. The longer, and therefore weaker, Zn-O bond between unit cells offers a mode for the “cracking” of the polymer on dissolution which correlates well with the observed integral in the ¹H NMR assigned to the unit cell (Section 3.3.1).

3.5 Comparison of pyridinethionato complexes.

The metal centres in the complexes [Zn(**5-H**)₂] (**8**), [Cu(**5-H**)₂] (**9**), [Ni(**5-H**)₂] (**10**) and [Co(**5-H**)₃] (**11**) all adopt a different stereochemistry with HL (**5**) under the same preparative conditions (Section 3.3). The cobalt(II) acetate precursor is oxidised to cobalt(III) to form the more thermodynamically stable low spin d⁶ octahedral complex **11** as opposed to a cobalt(II) 4-coordinate complex which would not benefit from the greater CFSE.

The zinc(II) complex (**8**) adopts a pseudo-tetrahedral geometry with a dihedral angle of 83.8° that is attributed to the affinity of zinc(II) to adopt a tetrahedral coordination geometry. The rigid bite size of the ligand restricts the chelate angle (av. ~89.6°) to that more commonly observed in square planar complexes.

The nickel complex **10** adopts a *cis*-square planar geometry in contrast to the *trans* geometry adopted by the copper complex **9**.

The observed variation in the metal-donor distances correlates well with the ionic radii, Figure 3.23. The bite distances in the ligand also increase in the same order. This would be expected if the ligand is to subtend angles of *ca.* 90 ° at the metal when the donor-metal lengths increase.

Ionic radius / Å	Ni(II)(0.49) < Co(III)(0.545) < Cu(II)(0.57) < Zn(II)(0.60)
Bite distance	Ni(II) < Co(III) < Cu(II) < Zn(II)
Average M-O	Ni(II) < Cu(II) < Co(III) < Zn(II)
Average M-S	Ni(II) < Co(III) < Cu(II) < Zn(II)

Figure 3.23. A comparison of the metal-donor distances and the bite distance of the complexes $[\text{Zn}(\mathbf{5-H})_2]$ (**8**), $[\text{Cu}(\mathbf{5-H})_2]$ (**9**), $[\text{Ni}(\mathbf{5-H})_2]\cdot\text{MeOH}$ (**10**) and $[\text{Co}(\mathbf{5-H})_3]\cdot 2\text{MeOH}$ (**11**) with their ionic radii.⁴¹ $\text{Ni}^{2+}(\text{D}_{4h}) = 0.49 \text{ \AA}$, low spin $\text{Co}^{3+}(\text{O}_h) = 0.545 \text{ \AA}$, $\text{Cu}^{2+}(\text{D}_{4h}) = 0.57 \text{ \AA}$ and $\text{Zn}^{2+}(\text{T}_d) = 0.60 \text{ \AA}$.

The similarity of the Cu(II) and Co(III) ionic radii is probably responsible for the discrepancy in the variations of the M-O distances which also may be associated with the copper complex adopting a *trans* structure.

The *cis* and *trans* geometries are associated with quite different distortions from a square S_2O_2 donor atom set. These result from the M-S bonds being significantly longer than the M-O bonds. The *cis* nickel complex **10** has its longest donor-donor contact between the *cis*-sulfur atoms, forming a trapezium. In contrast the donor set in the copper complex is elongated along the sulfur-sulfur axes to form a parallelogram, Figure 3.24.

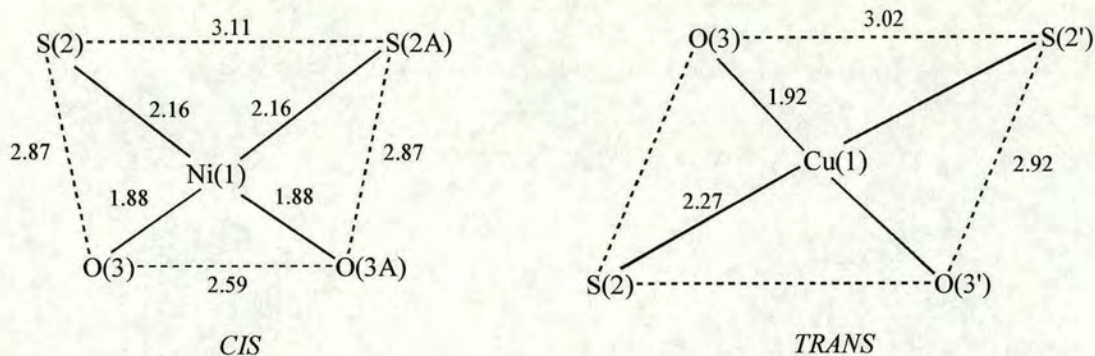


Figure 3.24. Stereochemistry around the nickel and copper centres for complexes $[\text{Cu}(\mathbf{5-H})_2]$ (**9**) and $[\text{Ni}(\mathbf{5-H})_2]$ (**10**).

The Cu-S and Cu-O bonds are longer than the Ni-S and Ni-O bond lengths (~ 0.11 and ~ 0.05 Å respectively). An increase (~ 0.08 Å) is expected by consideration of the square planar ionic radii of Cu^{2+} (0.57 Å) compared to that of Ni^{2+} (0.49 Å).⁴¹ The metal-sulfur bonds in complex **9** are slightly longer (~ 0.03 Å) than this, which could be attributed to the *trans*-effect.⁴² The sulfur atom is thought to have a greater π -acceptor character than the oxygen and therefore removes most π -electron density away from the metal. This reduces the electron density most at the coordination site directly opposite, *i.e.* *trans*. With two sulfur atoms *trans* to each other they are in direct competition and will receive less π -donation compared to if they were *cis*. Consequently they form a slightly longer and less stable M-S bond. The metal-oxygen bond lengths in complex **9** are slightly shorter (~ 0.03 Å) than the expected increase based on the ionic radii of Cu^{2+} and Ni^{2+} which is expected considering the *trans*-effect.

	[Zn(5-H) ₂] (8)	[Cu(5-H) ₂] (9) ^(a)	[Ni(5-H) ₂] (10)	[Cu(7-H) ₂] (16)
S(O)(2A)···O(3A)	3.002(2)	2.924(2) ^(a)	2.868(5)	2.629(5)
S(O)(2B)···O(3B)	3.016(2)	2.924(2) ^(a)	2.865(5)	2.629(5)
S(O)(2A)···O(3B)	3.736(2)	3.015(2) ^(a)	4.018(7)	2.834(5)
S(O)(2B)···O(3A)	3.752(2)	3.015(2) ^(a)	4.037(7)	2.845(5)
O(3A)···O(3B)	3.191(2)	3.838(3) ^(a)	2.589(5)	3.848(5)
S(O)(2A)···S(O)(2B)	4.0706(14)	4.5338(15) ^(a)	3.105(5)	3.860(5)

Table 3.15. Non-bonded distances between donor atoms in the coordination sphere for [Zn(5-H)₂] (8), [Cu(5-H)₂] (9), [Ni(5-H)₂].MeOH (10) and [Cu(7-H)₂].2EtOH (16). ^(a) Related by inversion symmetry (-x, -y, -z) consequently the ligand B is labelled “prime”.

3.6 Comparison of pyridinethionato and pyridinonato copper complexes.

The copper complex **9**, discussed above, is elongated along the sulfur-sulfur axes to form a parallelogram, Figure 3.24. Replacement of the sulfur donors with oxygen to produce an O₄ donor atom set has a noticeable affect on the complexation of copper, complex **16**. The bis-pyridinato copper complex **16** still adopts a *trans* configuration but is no longer planar, exhibiting a dihedral angle of 162.8°. The bite distance (O(2)···O(3), 2.629(5) Å) decreases (~0.3 Å) from that in complex **9**, Table 3.15, attributed to a shorter C-O than C-S (~0.43 Å) and is reflected in a decrease in the chelate angle (~2.8°) from 88.23 to 85.40°.

3.7 Conclusions.

The pyridinethione (**5**) and pyridinone (**7**) ligands define a variety of different coordination geometries with Zn²⁺, Cu²⁺, Ni²⁺ and Co³⁺. The adopted geometry in

each complex is a balance between that preferred by the metal and that imposed by the rigidity of the chelate ring.

The limited distance (O...S) of HL (**5**) is limited by the rigidity of the chelate units which subtends a chelate angle of approximately 90°, ideal for the formation of stable square planar and octahedral complexes. The steric influence of the benzyl group is minimal and therefore it is not possible to disfavour the formation of Fe³⁺ stable 3:1 octahedral complexes. The inclusion of two oxygen donor atoms in a pyridine analogue of catechol, HL (**7**), further restricts the already limited bite distance due to the reduction in length of the pyridone (C=O) bond compared to (C=S). The combination of; (i) a small bite distance and (ii) a hard donor set, disfavour the formation of the [Zn(**7-H**)₂] species, analogous to the bis-pyridinethionato zinc(II) complex (**8**), and instead a polymeric species is observed in which the coordination sites are bridged by acetates.

Since the geometrical features of the chelating units clearly do not match the preferred coordination geometry of zinc(II) it was judged that the original objective of probing the influence of the donor atom types on the stability of zinc(II) complexes using the series of ligands (i-ix), Figure 3.1, was unlikely to be effective. Attention was then focused on ligands that have a more pronounced tendency to favour the formation of tetrahedral 2:1 complexes (Chapter 4).

3.8 Experimental.

3.8.1 Pyridinethione and pyridinone ligands.

3-Hydroxy-2-iodopyridine (1).

Iodine (25.36 g, 0.1 mol) was added to a solution of 3-hydroxy-pyridine (9.50 g, 0.1 mol) and Na_2CO_3 (22.34 g, 0.21 mol) in water (250 cm^3) at ambient temperature and stirred for 20 h or until the iodine colouration had disappeared. Hydrochloric acid (6 M, 45 cm^3) was then added to precipitate the product until the effervescence, due to CO_2 evolution, ceased (\sim pH 3). The crude product was isolated by filtration and dried *in vacuo* (21.57 g, 97.6 %). Recrystallisation from EtOH / H_2O (1:1) gave pale yellow crystals. M.P. (decomp.) 168.5-170 °C (Lit. 176 °C²⁵); (Found: C, 27.52; H, 1.70; N, 6.43; EIMS m/z 221. $\text{C}_5\text{H}_4\text{INO}$ requires C, 27.18; H, 1.82; N, 6.34 %; M 221); ^1H NMR (d_6 -DMSO, 200 MHz): δ 7.13 (dd, $^3J_{\text{HH}}$ 8.0 Hz, $^4J_{\text{HH}}$ 1.8 Hz, 1H, H(4)), 7.20 (dd, $^3J_{\text{HH}}$ 8.0 Hz, $^4J_{\text{HH}}$ 4.3 Hz, 1H, H(5)), 7.83 (dd, $^3J_{\text{HH}}$ 4.3 Hz, $^4J_{\text{HH}}$ 1.8 Hz, 1H, H(6)), 10.7 (br s, 1H, OH). IR (cm^{-1} , KBr disk) 2723(w), 2575(w), 1558(m), 1454(m), 1301(m), 1189(m), 1122(m), 1077(w), 1046(m), 853(w), 794(m), 717(w), 668(m), 552(w).

N-Benzyl-3-hydroxy-2-iodopyridinium bromide (3).

A slurry of 3-hydroxy-2-iodopyridine (2.01 g, 9.1 mmol) and benzyl bromide (2.2 cm^3 , 18.5 mmol) was stirred at 90 °C for 2 h. The resulting oil was cooled and acetone (65 cm^3) added to produce a pale yellow precipitate that was isolated by filtration (2.82 g, 79.0 %) and then recrystallised from absolute ethanol. M.P.

(decomp.) 142-144 °C (Lit. (decomp.) 160-161 °C²³); (Found: C, 36.63; H, 2.50; N, 3.47; FABMS m/z 312. C₁₂H₁₁BrINO requires C, 36.77; H, 2.83; N, 3.57 %; M 392); ¹H NMR (d₆-DMSO, 200 MHz): δ 6.04 (s, 2H, CH₂), 7.17-7.49 (m, 5H, Ph), 7.79-8.01 (m, 2H, H(4, 5)), 8.91 (t, ³ J_{HH} 3.6 Hz, 1H, H(6)). IR (cm⁻¹, KBr disk) ν : 3414(br, m), 3063(s), 1581(m), 1490(m), 1460(s), 1432(m), 1316(s), 1200(s), 1156(m), 1058(m), 788(m), 744(m), 701(s).

N-4-*t*-butyl-benzyl-3-hydroxy-2-iodopyridinium bromide (4).

A slurry of 3-hydroxy-2-iodopyridine (14.96 g, 68 mmol) and 4-*t*-butyl benzyl bromide (20.5 cm³, 120 mmol) was stirred at 90 °C for 2 h. The resulting oil was cooled and acetone (100 cm³) added to produce a white precipitate that was isolated by filtration (18.19 g, 59.7 %) and then recrystallised from propan-2-ol. M.P. (decomp.) 180 °C; (Found: C, 42.58; H, 4.04; N, 3.13; FABMS m/z 368. C₁₆H₁₉BrINO requires C, 42.88; H, 4.27; N, 3.13 %; M 448); ¹H NMR (d₆-DMSO, 200 MHz): δ 1.26 (s, 9H, 3CH₃), 5.99 (s, 2H, CH₂), 7.13-7.46 ('ab' q, ³ J_{HH} 8.6 Hz, 4H, Ph), 7.80 (dd, ³ J_{HH} 8.5 Hz, ⁴ J_{HH} 1.4 Hz, 1H, H(5)), 7.94 (d, ³ J_{HH} 1.4 Hz, 1H, H(4)), 8.99 (dd, ³ J_{HH} 5.8 Hz, ⁴ J_{HH} 1.4 Hz, 1H, H(6)). IR (cm⁻¹, KBr disk) ν : 3412(br, m), 3056(s), 2962(s), 2868(s), 1612(w), 1571(m), 1516(w), 1485(m), 1460(s), 1432(m), 1393(w), 1365(m), 1316(s), 1267(s), 1198(s), 1157(m), 1058(m), 790(m), 774(m), 704(w).

N-Benzyl-3-hydroxy-2(1H)-pyridinethione (5).

N-benzyl-3-hydroxy-2-iodopyridinium bromide (5.012 g, 12.8 mmol) was added to a solution of NaSH.xH₂O (6.66 g, 0.12 mol) in water (100 cm³) and heated at 70 °C for

2 h. The green solid was collected by filtration and dried *in vacuo* (2.592 g, 93.3 %). This was recrystallised from ethanol to give pale green, X-ray grade, needles (2.491 g, 89.7 %). M.P. 90-91 °C; (Found: C, 66.10; H, 5.05; N, 6.39; EIMS m/z 217. $C_{12}H_{11}NOS$ requires C, 66.33; H, 5.10; N, 6.45 %; M 217); 1H NMR (d_6 -DMSO, 200 MHz): δ 5.83 (s, 2H, CH_2), 6.88 (dd, $^3J_{HH}$ 7.7 Hz, $^4J_{HH}$ 6.2 Hz, 1H, H(5)), 7.14 (dd, $^3J_{HH}$ 7.7 Hz, $^4J_{HH}$ 1.4 Hz, 1H, H(4)), 7.27-7.36 (m, 5H, Ph), 7.96 (dd, $^3J_{HH}$ 6.6 Hz, $^4J_{HH}$ 1.4 Hz, 1H, H(6)), 8.58 (s, 1H, OH). ^{13}C NMR (d_6 -DMSO, 250 MHz) δ : 59.21 (CH_2), 113.06 (CH, C-4 / C-5), 113.93 (CH, C-4 / C-5), 127.81 (CH, *o*-, *m*-, aromatic), 127.91 (CH, *o*-, *m*-, aromatic), 128.70 (CH, *p*-aromatic), 133.49 (CH, C-6), 135.74 (q, ipso aromatic), 154.36 (q, C-3), 168.15 (q, C-2). λ_{max} / nm ($CHCl_3$) 284 (ϵ / $dm^3 mol^{-1} cm^{-1}$ 11600), 363 (15100). IR (cm^{-1} , KBr disk) ν : 3112(m), 3052(w), 2960(w), 1626(m), 1547(m), 1498(m), 1468(s), 1454(m), 1436(s), 1372(m), 1219(m), 1168(m), 1117(m), 1065(s), 766(m), 740(m), 714(m), 695(m), 668(m), 645(m).

N-4-*t*-butyl-benzyl-3-hydroxy-2(1H)-pyridinethione (6).

N-4-*t*-Butyl-benzyl-2-iodopyridinium bromide (6.031 g, 13 mmol) was added to a solution of NaSH. \cdot xH $_2$ O (8.11 g, 140 mmol) in water (33 cm 3) and heated to 80 °C for 3 h. The solution was cooled and the precipitate isolated by filtration to give a yellow / green solid (3.39 g, 95.4 %) which was recrystallised from absolute ethanol to give yellow / green needles (3.06 g, 86.1 %). M.P. 126-128 °C; (Found: C, 70.21; H, 7.27; N, 5.29; EIMS m/z 273. $C_{16}H_{19}NOS$ requires C, 70.29; H, 7.00; N, 5.12 %; M 273); 1H NMR (d_6 -DMSO, 200 MHz): δ 1.24 (s, 9H, 3 CH_3), 5.79 (s, 2H, CH_2), 6.86 (dd, $^3J_{HH}$ 7.7 Hz, $^4J_{HH}$ 6.6 Hz, 1H, H(5)), 7.13 (dd, $^3J_{HH}$ 7.7 Hz, $^4J_{HH}$ 1.4 Hz, 1H,

H(4)), 7.22-7.39 ('ab' q, $^3J_{HH}$ 8.6 Hz, 4H, Ph), 7.96 (dd, $^3J_{HH}$ 6.6 Hz, $^4J_{HH}$ 1.4 Hz, 1H, H(6)), 8.58 (s, 1H, OH). IR (cm⁻¹, KBr disk) ν : 3095(m), 2963(s), 2866(m), 1626(m), 1544(m), 1516(m), 1468(s), 1431(s), 1364(m), 1285(s), 1198(m), 1168(m), 1117(m), 1059(s), 898(m), 799(s), 768(s), 714(m), 628(s).

N-benzyl-3-hydroxy-2(1H)-pyridinone (7).

N-benzyl-3-hydroxy-2-iodopyridinium bromide (1.493 g, 3.8 mmol) was added to a solution of NaOH.xH₂O (2.091 g, 52 mmol) in water (30 cm³) and heated at 100 °C for 4 h. The cooled solution was then acidified (pH 3) using 6M HCl. The precipitate was isolated by filtration and dried *in vacuo* to give a brown solid (0.642 g, 84.0 %). The crude product was then recrystallised from cyclohexane / EtOH to produce colourless crystals. X-ray grade crystallographic crystals were grown from hot 1-butanol. M.P. (decomp.) 140-141 °C; (Found: C, 71.73; H, 5.23; N, 6.86; EIMS *m/z* 201. C₁₂H₁₁NO₂ requires C, 71.63; H, 5.51; N, 6.96 %; *M* 201); ¹H NMR (d₆-DMSO, 200 MHz): δ 5.13 (s, 2H, CH₂), 6.12 (t, $^3J_{HH}$ 7.1 Hz, 1H, H(5)), 6.70 (dd, $^3J_{HH}$ 7.2 Hz, $^4J_{HH}$ 1.8 Hz, 1H, H(4)), 7.26 (dd, $^3J_{HH}$ 6.9 Hz, $^4J_{HH}$ 1.8 Hz, 1H, H(6)), 7.28-7.38 (m, 5H, Ph), 9.10 (s, 1H, OH). ¹³C NMR (d₆-DMSO, 250 MHz) δ : 51.41 (CH₂), 105.49 (CH, C-5), 114.80 (CH, C-4), 127.63 (CH, *o*-, *m*-, aromatic), 127.80 (CH, *o*-, *m*-, aromatic), 128.26 (CH, C-6), 128.64 (CH, *p*-aromatic), 137.49 (q, ipso aromatic), 147.02 (q, C-2), 157.89 (q, C-3). IR (cm⁻¹, KBr disk) ν : 3226(s), 3089(m), 3028(m), 2934(s), 1654(s), 1602(s), 1566(m), 1497(m), 1452(m), 1425(m), 1403(m), 1362(m), 1284(s), 1250(s), 1218(m), 1153(m), 1078(m), 781(m), 754(s), 716(s), 691(m).

6-Methyl-3-hydroxy-2-iodopyridine.

Iodine (35.06 g, 138 mmol) was added to a suspension of 6-methyl-3-hydroxy pyridine (15.008 g, 138 mmol) and Na₂CO₃ (30.073 g, 284 mmol) in water (400 cm³) and stirred at ambient temperature until the iodine colouration had disappeared. Hydrochloric acid (6 M, 62 cm³) was then added to precipitate the product until all the CO₂ evolution had ceased (approximately pH 3). The crude product was isolated by filtration and dried *in vacuo* (19.49 g, 60.1 %) and then recrystallised from EtOH / H₂O (1:1) to produce a beige crystalline powder. M.P. (decomp.) 191-193 °C; (Found: C, 30.76; H, 2.62; N, 5.98; EIMS *m/z* 235. C₆H₆INO requires C, 30.66; H, 2.57; N, 5.96 %; *M* 235); ¹H NMR (d₆-DMSO, 200 MHz): δ 2.31 (s, 3H, CH₃), 7.04 (s, 2H, H(4, 5)), 10.52 (br. s, 1H, OH). IR (cm⁻¹, KBr disk) ν: 2921(m), 2832(m), 2747(m), 2662(m), 2577(m), 1552(s), 1488(m), 1452(m), 1410(m), 1319(m), 1288(s), 1212(s), 1130(m), 1071(m), 830(s), 780(m), 771(m), 671(s).

3.8.2 Complexes of pyridinethiones and pyridinones.

Bis(N-benzyl-3-hydroxy-2(1H)-pyridinethionato)zinc(II) (8).

A solution of zinc(II) acetate dihydrate (0.180 g, 0.82 mmol) in methanol (2.5 cm³) was added to a solution of N-benzyl-3-hydroxy-2(1H)-pyridinethione (0.411 g, 1.89 mmol) in methanol (30 cm³). The mixture was shaken and left to stand. The deposited solid was collected by filtration to give the crude product (0.379 g, 92.8 %) and this was recrystallised from methanol to give pale yellow crystals (0.228 g, 55.8 %). X-ray crystallographic grade crystals were obtained by recrystallisation from hot methanol. M.P. 225-227 °C; (Found: C, 57.88; H, 3.84; N, 5.29; FABMS

m/z 499. $C_{24}H_{20}N_2O_2S_2Zn$ requires C, 57.89; H, 4.05; N, 5.63 %; M 498); 1H NMR ($CDCl_3$, 200 MHz): δ 5.76 (s, 4H, 2CH₂), 6.83 (dd, $^3J_{HH}$ 8.2 Hz, $^4J_{HH}$ 6.2 Hz, 2H, 2H(5)), 7.05 (dd, $^3J_{HH}$ 8.1 Hz, $^4J_{HH}$ 1.4 Hz, 2H, 2H(4)), 7.21 (dd, $^3J_{HH}$ 6.2 Hz, $^4J_{HH}$ 1.4 Hz, 2H, 2H(6)), 7.27-7.47 (m, 10H, 2Ph). λ_{max} / nm ($CHCl_3$) 281 ($\epsilon / dm^3 mol^{-1} cm^{-1}$ 13000), 364 (30400). IR (cm^{-1} , KBr disk) ν : 3074(m), 3039(m), 3006(m), 1592(m), 1548(m), 1496(m), 1441(s), 1416(s), 1328(s), 1290(s), 1117(m), 1082(m), 1064(s), 768(m), 738(m), 710(m), 693(m), 659(m), 635(m).

Bis(N-benzyl-3-hydroxy-2(1H)-pyridinethionato)copper(II) (9).

A solution of copper(II) acetate monohydrate (0.164 g, 0.82 mmol) in methanol (5 cm³) was added to a solution of N-benzyl-3-hydroxy-2(1H)-pyridinethione (0.405 g, 1.86 mmol) in methanol (30 cm³). The mixture was shaken and left to stand. The solid was isolated by filtration to give X-ray crystallographic grade red / brown crystals (0.379 g, 97.9 %). M.P. 269-275 °C; (Found: C, 58.23; H, 4.03; N, 5.46; FABMS m/z 495. $C_{24}H_{20}CuN_2O_2S_2$ requires C, 58.11; H, 4.06; N, 5.65 % M 496). λ_{max} / nm ($CHCl_3$) 263 ($\epsilon / dm^3 mol^{-1} cm^{-1}$ 14000), 327 (sh) 12900, 375(sh) (29300), 390 (37800), 592(sh) (270), 831 (60). IR (cm^{-1} , KBr disk) ν : ~3050(w), 1590(w), 1540(m), 1496(w), 1434(s), 1301(s), 1245(w), 1174(m), 1118(m), 1072(m), 804(w), 763(w), 737(w), 710(w), 696(w), 674(w).

Bis(N-benzyl-3-hydroxy-2(1H)-pyridinethionato)nickel(II).(methanol) (10).

A solution of nickel(II) acetate tetrahydrate (0.207 g, 0.83 mmol) in methanol (5 cm³) was added to a solution of N-benzyl-3-hydroxy-2(1H)-pyridinethione (0.404 g, 1.86 mmol) in methanol (30 cm³). The mixture was shaken and left to stand.

Yellow / brown crystals were deposited and collected by filtration (0.409 g, >95 %). X-ray crystallographic grade crystals were obtained by recrystallisation from hot methanol. M.P. 280 °C; (Found: C, 57.09; H, 4.67; N, 5.39; FABMS m/z 491. $C_{24}H_{20}N_2NiO_2S_2$ requires C, 57.38; H, 4.62; N, 5.35 %; M 491); 1H NMR ($CDCl_3$, 200 MHz): δ 5.45 (s, 4H, 2CH₂), 6.66 (dd, $^3J_{HH}$ 8.2 Hz, $^4J_{HH}$ 5.9 Hz, 2H, 2H(5)), 6.75 (dd, $^3J_{HH}$ 8.2 Hz, $^4J_{HH}$ 1.4 Hz, 2H, 2H(4)), 6.95 (dd, $^3J_{HH}$ 5.9 Hz, $^4J_{HH}$ 1.4 Hz, 2H, 2H(6)), 7.22-7.41 (m, 10H, 2Ph). λ_{max} / nm ($CHCl_3$) 267 (ϵ / $dm^3 mol^{-1} cm^{-1}$ 34000), 316 (21900), 392(sh), (8700), 466 (14400), 726 (50). IR (cm^{-1} , KBr disk) ν : ~3050(w), 1588(w), 1535(w), 1497(w), 1434(s), 1315(s), 1253(w), 1172(m), 1124(m), 1067(m), 756(m), 720(m), 700(m), 690(w).

Tris(N-benzyl-3-hydroxy-2(1H)-pyridinethionato)cobalt(III).bis(methanol) (11).

A solution of cobalt(II) acetate tetrahydrate (0.383 g, 1.5 mmol) in methanol (10 cm^3) was added to a solution of N-benzyl-3-hydroxy-2(1H)-pyridinethione (0.99 g, 4.6 mmol) in methanol (70 cm^3). The mixture was shaken and left to stand. Dark red crystals were deposited and collected by filtration (0.809 g, 68.1 %). X-ray crystallographic grade crystals were obtained by recrystallisation from hot methanol. M.P. 198-200 °C; (Found: C, 59.66; H, 4.51; N, 5.73; FABMS m/z 707. $C_{36}H_{30}CoN_3O_3S_3 \cdot 1.5CH_3OH$ requires C, 59.59; H, 4.80; N, 5.56 %; M 708); 1H NMR ($CDCl_3$, 200 MHz): δ 5.49-5.69 ('ab' q, $^2J_{HH}$ 14.7 Hz, 6H, 3CH₂), 6.64 (dd, $^3J_{HH}$ 8.1 Hz, $^4J_{HH}$ 6.2 Hz, 3H, 3H(5)), 6.77 (dd, $^3J_{HH}$ 6.2 Hz, $^4J_{HH}$ 1.1 Hz, 3H, 3H(4)), 7.03 (dd, $^3J_{HH}$ 8.1 Hz, $^4J_{HH}$ 0.9 Hz, 3H, 3H(6)), 7.29-7.47 (m, 15H, 3Ph). λ_{max} / nm ($CHCl_3$) 268 (ϵ / $dm^3 mol^{-1} cm^{-1}$ 49600), 313 (19100), 407 (23000), 432 (22500),

656(sh) (70). IR (cm^{-1} , KBr disk) ν : \sim 3050(w), 1586(w), 1528(w), 1497(w), 1436(s), 1314(s), 1240(w), 1173(w), 1113(m), 1065(m), 739(w), 697(w), 670(w), 638(w).

Tris(N-benzyl-3-hydroxy-2(1H)-pyridinethionato)iron(III) (12).

A solution of iron(II) acetate (0.062 g, 0.34 mmol) in methanol (2.5 cm^3) was added to a solution of N-benzyl-3-hydroxy-2(1H)-pyridinethione (0.234 g, 1.1 mmol) in methanol (25 cm^3). The mixture was shaken and left to stand. The deposited solid was collected by filtration yielding deep blue / red crystals (0.235 g, 92.3 %). This solid was then recrystallised from absolute ethanol (0.126 g, 49.6 %). M.P. 184-186 °C; (Found: C, 60.61; H, 4.34; N, 5.73; FABMS m/z 704. $\text{C}_{36}\text{H}_{30}\text{FeN}_3\text{O}_3\text{S}_3 \cdot 1.5\text{H}_2\text{O}$ requires C, 60.59; H, 4.38; N, 5.88 % M 705). $\lambda_{\text{max}} / \text{nm}$ (CHCl_3) 285 (sh) ($\epsilon / \text{dm}^3 \text{ mol}^{-1} \text{ cm}^{-1}$ 24000), 374 (33200), 489 (7900), 587 (7800). IR (cm^{-1} , KBr disk) ν : \sim 3050(m), 1590(m), 1534(w), 1497(w), 1457(m), 1433(s), 1414(m), 1304(s), 1174(w), 1114(m), 1068(m), 802(w), 733(w), 714(w), 696(w), 668(w), 633(w).

Bis(N-4-*t*-butyl-benzyl-3-hydroxy-2(1H)-pyridinethionato)copper(II) (13).

A solution of copper(II) acetate monohydrate (0.029 g, 0.14 mmol) in methanol (5 cm^3) was added to a solution of N-4-*t*-butyl-benzyl-3-hydroxy-2(1H)-pyridinethione (0.077 g, 0.28 mmol) in methanol (20 cm^3). The mixture was heated at reflux for 15 min with stirring then left to cool slowly. The precipitated solid was isolated by filtration yielding green / brown crystals (0.617 g, 71.9 %). M.P. 295 °C; (Found: C, 63.20; H, 5.86; N, 4.54; FABMS m/z 609. $\text{C}_{32}\text{H}_{36}\text{CuN}_2\text{O}_2\text{S}_2$ requires C, 63.18; H, 5.96; N, 4.61 %; M 608). IR (cm^{-1} , KBr disk) ν : \sim 3090(w), 2963(m),

1592(w), 1539(w), 1518(w), 1439(m), 1424(m), 1307(s), 1340(w), 1177(w), 1110(m), 1067(m), 798(w), 768(w), 716(w), 672(w), 625(w).

Bis(N-4-*t*-butyl-benzyl-3-hydroxy-2(1H)-pyridinethionato)nickel(II) (14).

A solution of nickel(II) acetate tetrahydrate (0.037 g, 0.15 mmol) in methanol (2 cm³) was added to a solution of N-4-*t*-butyl-benzyl-3-hydroxy-2(1H)-pyridinethione (0.083 g, 3.0 mmol) in methanol (20 cm³). The mixture was heated at reflux for 15 min with stirring then left to cool slowly. The crude product that precipitated was isolated by filtration to yield gold coloured crystals (0.073 g, 79.4 %) and then recrystallised from methanol. M.P. 300 °C; (Found: C, 63.74; H, 6.01; N, 4.55; FABMS *m/z* 602. C₃₂H₃₆N₂NiO₂S₂ requires C, 63.69; H, 6.01; N, 4.64 %; *M* 603); ¹H NMR (CDCl₃, 200 MHz): δ 1.29 (s, 18H, 6CH₃), 5.41 (s, 4H, 2CH₂), 6.64 (dd, ³*J*_{HH} 8.2 Hz, ⁴*J*_{HH} 5.9 Hz, 2H, 2H(5)), 6.74 (dd, ³*J*_{HH} 8.2 Hz, ⁴*J*_{HH} 1.3 Hz, 2H, 2H(4)), 6.94 (dd, ³*J*_{HH} 5.9 Hz, ⁴*J*_{HH} 1.3 Hz, 2H, 2H(6)), 7.17-7.46 (m, 8H, 2Ph). IR (cm⁻¹, KBr disk) ν: ~3090(w), 2964(m), 1541(w), 1431(s), 1309(s), 1244(w), 1180(w), 1112(m), 1066(m), 764(w), 714(w).

Tris(N-4-*t*-butyl-benzyl-3-hydroxy-2(1H)-pyridinethionato)cobalt(III) (15).

A solution of cobalt(II) acetate tetrahydrate (0.185 g, 0.74 mmol) in methanol (5 cm³) was added to a solution of N-4-*t*-butyl-benzyl-3-hydroxy-2(1H)-pyridinethione (0.61 g, 2.2 mmol) in methanol (70 cm³). The mixture was heated at reflux for 15 min with stirring then left to cool slowly. The solid was isolated by filtration to give a yellow / brown solid (0.596 g, 91.9 %). M.P. 192-194 °C; (Found: C, 63.15; H, 6.34; N, 4.45; FABMS *m/z* 875. C₄₈H₅₄CoN₃O₃S₃ 2H₂O requires C,

63.21; H, 6.41; N, 4.61 %; *M* 876); ¹H NMR (CDCl₃, 200 MHz): δ 1.29 (s, 27H, 9CH₃), 5.56 ('ab' q, ²*J*_{HH} 14.7, Hz, 6H, 3CH₂), 6.64 (dd, ³*J*_{HH} 8.0 Hz, ⁴*J*_{HH} 6.5 Hz, 3H, 3H(5)), 6.76 (d, ³*J*_{HH} 5.7 Hz, 3H, 3H(4)), 7.04 (d, ³*J*_{HH} 7.9 Hz, 3H, 3H(6)), 7.28-7.39 (m, 12H, 3Ph). IR (cm⁻¹, KBr disk) ν: 3092(w), 2962(m), 2868(w), 1588(m), 1529(m), 1435(s), 1311(s), 1269(w), 1232(w), 1203(w), 1173(m), 1111(m), 1062(s), 791(w), 757(w), 708(w), 670(w), 622(w).

Bis(N-benzyl-3-hydroxy-2(1H)-pyridinonato)copper(II).bis(ethanol) (16).

A solution of copper(II) acetate monohydrate (0.138 g, 0.69 mmol) in water (5 cm³) was added to a solution of N-benzyl-3-hydroxy-2(1H)-pyridinone (0.319 g, 1.6 mmol) in methanol (16 cm³). The mixture was heated at reflux for 15 min with stirring then left to cool slowly. The precipitate that formed was isolated by filtration to give green crystals (0.250 g, 78.0 %) which were then recrystallised from absolute ethanol to produce X-ray quality crystals (0.167 g, 52.2 %). M.P. 240-242 °C; (Found: C, 62.09; H, 4.38; N, 5.94; FABMS *m/z* 464. C₂₄H₂₀CuN₂O₄ requires C, 62.13; H, 4.34; N, 6.04 %; *M* 464). IR (cm⁻¹, KBr disk) ν: 3032(w), 1619(w), 1526(s), 1456(m), 1373(m), 1293(m), 1244(m), 1205(w), 1150(w), 1084(w), 866(w), 763(w), 745(w), 726(w), 700(w), 630(w).

Poly((bis(N-benzyl-3-hydroxy-pyridinonato)tetra(acetato)tri-zinc(II)) (17).

A solution of zinc(II) acetate dihydrate (0.304 g, 1.38 mmol) in methanol (10 cm³) was added in large excess to a solution of N-benzyl-3-hydroxy-2(1H)-pyridinone (0.119 g, 0.59 mmol) in methanol (10 cm³). The mixture was heated at reflux for 15 min with stirring then left to cool slowly. The solid that then deposited was isolated

by filtration to give colourless X-ray grade crystals (0.144 g, 58.6 %). M.P. 255 °C; (Found: C, 46.03; H, 3.52; N, 3.19. $C_{32}H_{32}N_2O_{12}Zn_3$ requires C, 46.15; H, 3.87; N, 3.36 %); 1H NMR (d_6 -DMSO, 200 MHz): δ 1.80 (s, 12H, 4CH₃), 5.22 (s, 4H, 2CH₂), 6.30 (t, $^3J_{HH}$ 7.0 Hz, 2H, 2H(5)), 6.48 (dd, $^3J_{HH}$ 5.7 Hz, $^4J_{HH}$ 1.3 Hz, 2H, 2H(4)), 6.96 (dd, $^3J_{HH}$ 6.6 Hz, $^4J_{HH}$ 1.5 Hz, 2H, 2H(6)), 7.26-7.75 (m, 10H, 2Ph). IR (cm⁻¹, KBr disk) ν : 3033(w), 1603(s), 1585(s), 1546(s), 1417(m), 1392(m), 1333(m), 1297(m), 1244(m), 1205(w), 1149(w), 1086(w), 1016(w), 935(w), 865(w), 748(w), 727(w), 702(w), 682(w), 669(w), 639(w), 618(w).

3.9 References.

1. K. Krowicki, *Pol. J. Chem.*, 1978, **52**, 2039.
2. S. Puig-Torres, C.H. Womack, G.E. Martin, K. Smith, *J. Heterocycl. Chem.*, 1982, **19**, 1561.
3. K. Smith, D. Anderson, I. Matthews, *J. Org. Chem.*, 1996, **61**, 662.
4. M. Imuta, H. Itani, H. Ona, Y. Hamada, S. Uyeo, T. Yoshida, *Chem. Pharm. Bull.* 1991, **39**, 663.
5. R. Rydzkowski, D. Blondeau, H. Sliwa, *Tetrahedron Lett.*, 1985, **26**, 2571.
6. E. Hand, W.W. Paudler, *J. Org. Chem.*, 1978, **43**, 2900.
7. M. Oklobdzija, G. Comisso, E. Decorte, T. Fajdiga, G. Gratton, F. Moimas, R. Toso, V. Sunjic, *J. Heterocycl. Chem.*, 1983, **20**, 1329.
8. R.C. Scarrow, K.N. Raymond, *Inorg. Chem.*, 1988, **27**, 4140.
9. R.C. Scarrow, P.E. Riley, K. Abu-dari, D.L. White, K.N. Raymond, *Inorg. Chem.*, 1985, **24**, 954.
10. K.N. Raymond, *Environmental Inorganic Chemistry*, ed. K.J. Irgolic, A.E. Martell, VCH, Florida, 1985, pp331-347.
11. K.N. Raymond, M.J. Kappel, V.L. Pecoraro, W.J. Harris, C.J. Carrano, F.L. Weitzel, P.W. Durbin, *Actinides in Perspective*, ed. N.M. Edelstein, Pergamon Press, Oxford, 1982, pp491-507.
12. S.M. Moerlein, M.J. Welch, K.N. Raymond, *J. Nucl. Med.*, 1982, **23**, 501.
13. European Patent 90306646.2, GB/12.07.89/GB, priority 8915959.
14. I.J. Polymear, *Chemistry of Aluminium, Gallium, Indium and Thallium*, ed. A.J. Downs, Blackie Academic & Professional Press, Glasgow, 1st edn., 1993, ch.2,

- pp81-110. K. Wade, A.J. Banister, *Comprehensive Inorganic Chemistry*, Pergamon, Oxford, 1st edn., 1973, vol.1, ch.12, pp993-1172.
15. N.N Greenwood, A. Earnshaw, *Chemistry Of The Elements*, Pergamon Press, Oxford, 4th edn., 1989, ch.7, pp.243-295.
16. R.D. Shannon, C.T. Prewitt, *Acta. Crystallogr.*, 1969, **B25**, 925.
17. A.R. Katritzky, J. Banerji, N. Dennis, J. Ellison, G.J. Sabongi, *J. Chem. Soc. Perkin I*, 1979, 2528.
18. K. Lewicka, E. Plazek, *Rocz. Chem.*, 1966, **40**, 405.
19. A.R. Katritzky, N.E. Grzeskowiak, *J. Chem. Res(M)*., 1981, **7**, 2345.
20. F. Broekman, H. Tendeloo, *Rec. Trav. Chim. Pays-Bas*, 1962, **81**, 107.
21. K. Undheim, V. Nordal, T. Knutt, *Het. Compd.*, 1969, **71**, 283.
22. O. Schickh, A. Binz, A. Schulz, *Ber. Dtsch. Chem. Ges.*, 1936, **69**, 2593.
23. B.R. Baker, F.J. McEnvoy, *J. Org. Chem.*, 1955, **20**, 118.
24. G. Clark, K. Deady, *Aust. J. Chem.*, 1981, **34**, 927.
25. V. Koch, S. Schnatterer, *Synthesis*, 1990, 497.
26. H.J. Den Hertog, F.R. Schepman, J. de Bruyn, J.E. Thyse, *Rec. Trav. Chim. Pays-Bas*, 1950, **69**, 1281.
27. K. Undheim, V. Nordal, K. Tyønneland, *Acta. Chem. Scand.*, 1969, **23**, 1704.
28. K. Undhiem, O. Tvieta Per, L. Borka, V. Nordal, *Acta. Chem. Scand.*, 1969, **23**, 2065.
29. M. Pinsky, D. Avnir, *Inorg. Chem.*, 1998, **37**, 5575.
30. G.M. Sheldrick, SHELXL-97, University of Gottingen, Germany, 1997.
31. A.L. Spek, *Acta. Crystallogr., Sect. A*, 1990, **46**, C34.
32. T. Steiner, *J. Chem. Soc., Chem. Commun.*, 1998, 411.

33. R. Xiong, B. Song, X. You, T.C.W. Mak, Z. Zhou, *Polyhedron*, 1996, **15**, 991.
34. J.A. Boyko, W.F. Furey Junior, R.A. Lalancette, *Acta. Crystallogr., Sect. C*, 1992, **48**, 1606.
35. R. Richter, J. Sieler, E. Ludwig, E. Uhlemann, L. Golic, *Z. Anorg. Allg. Chem.*, 1984, **513**, 114.
36. X. Chen, Y. Hu, D. Wu, L. Weng, B. Kang, *Polyhedron.*, 1991, **10**, 2651.
37. Y. Hu, L. Weng, L. Huang, X. Chen, D. Wu, B. Kang, *Acta. Crystallogr., Sect. C.*, 1991, **47**, 2655.
38. J. Xu, B. Kang, X. Chen, L. Huang, *Acta. Crystallogr., Sect. C*, 1995, **51**, 370.
39. V. Manivannan, S. Dutta, P. Basu, A. Chakravorty, *Inorg. Chem.*, 1993, **32**, 769.
40. Graphical display was obtained from Cerius² molecular modelling system under licence from Molecular Simulations Inc., San Diego, CA.
41. R.D. Shannon, *Acta. Crystallogr., Sect. A*, 1976, **32**, 751.
42. N.N Greenwood, A. Earnshaw, *Chemistry Of The Elements*, Pergamon Press, Oxford, 4th edn., 1989, ch.27, pp.1328-1363.

Chapter 4

Bidentate Thiopyrazolone Chemistry

4.1 Introduction.

This chapter reports the synthesis, characterisation and crystallographic structures of some ligands based on 1-substituted-3-methyl-4-(alkylaldenamine)-pyrazol-5-thiones and pyrazol-5-ones and 1-phenyl-3-methyl-4-phenylhydrazono-pyrazol-5-thione (Figure 4.1) and a selection of their complexes with some 1st row transition metals (Cu^{2+} , Co^{2+} , Ni^{2+} , Zn^{2+}). It also includes data on the solvent extraction on several of these ligands to assess their strength and selectivity towards these metals.



Figure 4.1. (a) 1-substituted-3-methyl-4-(alkylaldenamine)-pyrazol-5-thiones where $\text{X} = \text{S}$ and pyrazol-5-ones where $\text{X} = \text{O}$ and $\text{R}_1, \text{R}_2 =$ a range of alkyl and aromatic groups, (b) 1-phenyl-3-methyl-4-phenylhydrazono-pyrazol-5-thione(ones).

The enamine and hydrazono pyrazol-5-thiones were identified as fulfilling the criteria determined in Chapter 2;

1. They promote tetrahedral geometry.
2. They form neutral complexes.
3. They consist of a 6-membered chelate ring and a mixed nitrogen / sulfur donor set.

The primary aim of the work in this chapter was to develop and test these extractants (Section 4.5 and 4.9) for the selective complexation of zinc over other 1st row metals

(Cu, Co, Ni), under conditions which are directly relevant to the industrial hydrometallurgical solvent extraction process (Section 1.4.1.1). The secondary aim is to maximise the strength of these ligands for zinc while maintaining a high selectivity over cobalt and nickel by altering the substituents at R₁ and R₂ (Figure 4.1) to provide the optimal steric and electronic properties.

Since the early discovery of pyrazolin-5-ones by Knorr¹ in 1883, substituted pyrazoles have received much attention and been commercially exploited in a diverse number of areas including pharmaceuticals, dyes, photography and analytical reagents.² The most successful and commercially important use for substituted pyrazolin-5-ones is as dyes. They have been successfully employed for this purpose since the synthesis of the yellow dye tartrazine, Figure 4.2(a), by Ziegler in 1884 which is used as a colouring for foodstuffs.² Almost all pyrazolinone dyes have an arylazo group substituted at the 4-position, many of which contain two, three or four azo groups in the entire molecule. A tremendous variety of azo-dyes have been prepared, many of which are very complex, and their success can be partially attributed to excellent fastness to light and water (colour running). The fabric can be treated with either the parent azo-dye or dyes which are complexed to metals. Earlier pyrazolinone dyes were used to dye wool yellow. Complexation with different metals, *e.g.* Cr, Cu, Co, Pb, Ni and Fe results in the ability to dye almost any material any colour.

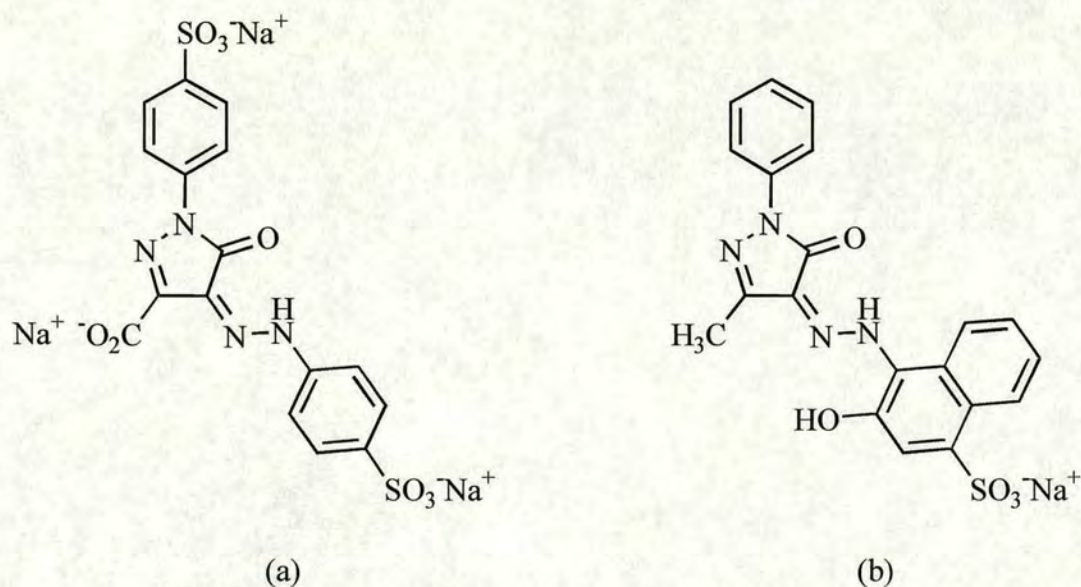


Figure 4.2. Examples of two azo-dyes (a) tartrazine and (b) Eriochrome Red B.

As a result of their metal chelating properties and intense colours they have also found application in the colourimetric analysis of metals. For example Eriochrome Red B, Figure 4.2(b), is used for the analysis of Be, Cd, Cu, Ga, Ni, Ti, V and Zn in addition to its use as a dye for wool, polyamides and leather.³

The most important use of pyrazolinones in photography is their utilisation as colour couplers.² For example the coupling reaction of a *p*-phenylenediamine developer, usually *p*-amino-*N,N*-diethylaniline, with 2-pyrazolin-5-ones in the presence of the oxidising agent, *e.g.* silver ions, forms magenta azomethine dyes, Figure 4.3.

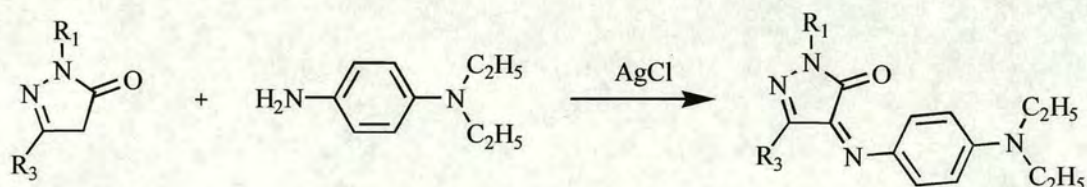


Figure 4.3. Oxidative coupling of 2-pyrazolin-5-one and *p*-amino-*N,N*-diethylaniline with silver chloride.

The film is coated with a substance that sensitises that surface to green light. A magenta colour appears during the development stage at those points where the silver halide has been exposed to green light. The conjugated azomethine has a very strong absorption band in the green region of the spectrum (510-560 nm) and can be reprinted as green.

More recently the utility of pyrazoles in agricultural processes has been realised. Some pyrazole derivatives which are structurally related to the commercially important systemic fungicide Carboxin show fungicidal activity of the same order against wheat, broad bean and cereal rusts,⁴ Figure 4.4.

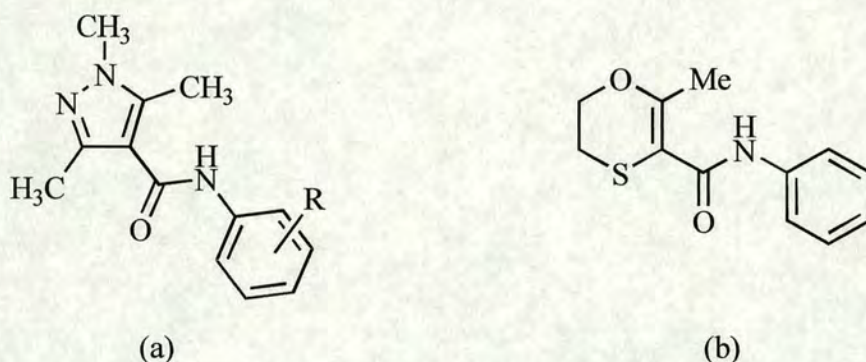


Figure 4.4. (a) 1,3,5-trimethyl-N-phenylpyrazole-4-carboxamide, R = H or *p*-CH₃ and (b) Carboxin.

Solvent extraction studies of various metals with 4-hydrazono-pyrazol-5-thiones and 4-hydrazono-pyrazol-5-ones in chloroform / water⁵ and benzene / water⁶ are present in the literature. Limited stability measurements of 4-substituted-hydrazono-pyrazol-5-ones with Cu, Co, Ni and Zn in 75 % dioxane and the effect of changing the alkyl substituents have also been reported.⁷⁻⁹ There is also an extensive body of literature on the solvent extraction of many metals using 4-acyl-pyrazol-5-one derivatives in

different solvent / water systems¹⁰⁻¹⁹ as well as 4-benzoyl-pyrazol-5-thiones and 4-thiobenzoyl-pyrazol-5-ones, Figure 4.5.

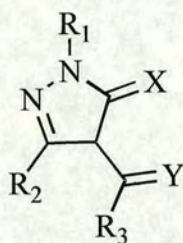
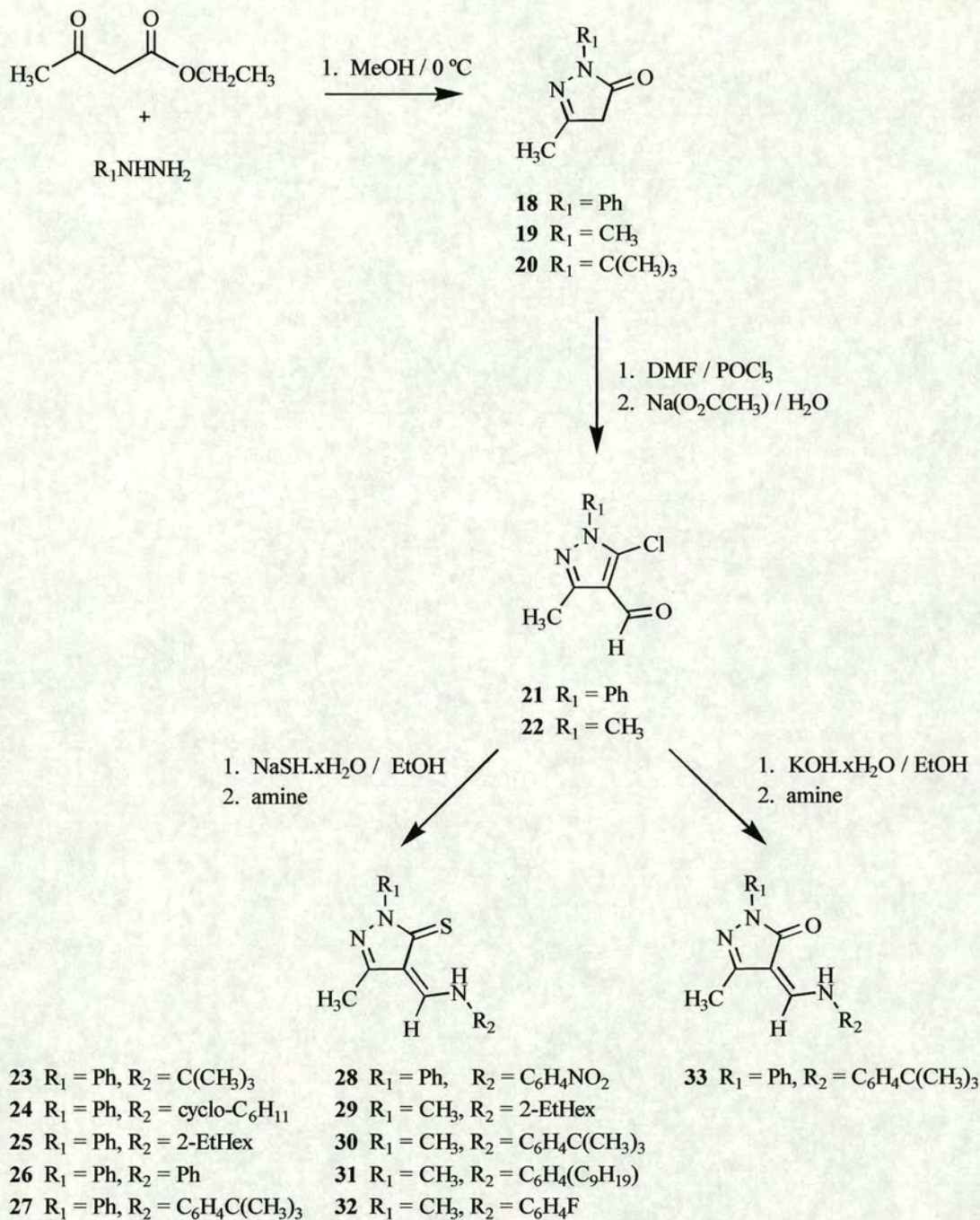


Figure 4.5. 4-Acyl-pyrazol-5-ones when X, Y = O. 4-Benzoyl-pyrazol-5-thiones when X = S, Y = O and R₃ = Ph. 4-Thiobenzoyl-pyrazol-5-ones when X = O, Y = S and R₃ = Ph.

However, to our knowledge there is no reported use of the 1,3-disubstituted-4-(alkylaldenamine)-pyrazol-5-thiones and pyrazol-5-ones as potential extractants. This is possibly due to the concern over the expected instability towards acid or base hydrolysis under the conditions necessary for pH-swing extraction process (Section 1.4).

4.2 Preparation and characterisation of pyrazol-5-thiones and pyrazol-5-ones.

The 1-substituted-3-methyl-4-(alkylaldenamine)-pyrazol-5-thiones (**23-32**) and the 1-phenyl-3-methyl-4-(4-*t*-butylphenylaldenamine)-pyrazol-5-one (**33**) NO-analogue were prepared *via* a three step synthetic procedure as outlined in Scheme 4.1.



Scheme 4.1. General 3-step synthetic procedure for 1-substituted-3-methyl-pyrazol-5-thiones and pyrazol-5-ones.

The preparation of 1-substituted-2-pyrazolin-5-ones (**18-20**) is well documented.^{20,21}

There are numerous procedures but the most straight-forward and frequently used

method is the condensation of a β -ketoester with a mono-substituted hydrazine, first exemplified by Knorr in 1883 by the reaction of ethylacetoacetate with phenylhydrazine.¹ The β -ketoester and hydrazine have been varied greatly and in general the yields are greatest (nearly quantitative) for small and simple substituents.²¹ A number of different reaction conditions are available in the literature. One possible method is to reflux an aqueous hydrazine solution with the β -ketoester.²² Acidic conditions can be employed using glacial acetic acid as the solvent.²³ Alternatively, the reagents can be refluxed in methanol²⁴ or ethanol.²⁵ Recently condensation has been achieved quantitatively and rapidly (~ 10 min) using microwave irradiation.²⁶ Here we use milder conditions involving the addition of the hydrazine to a cold (~ 0 °C) methanol solution of ethylacetoacetate to form the intermediate hydrazone²⁷ which undergoes ring closure when refluxed, Figure 4.6.

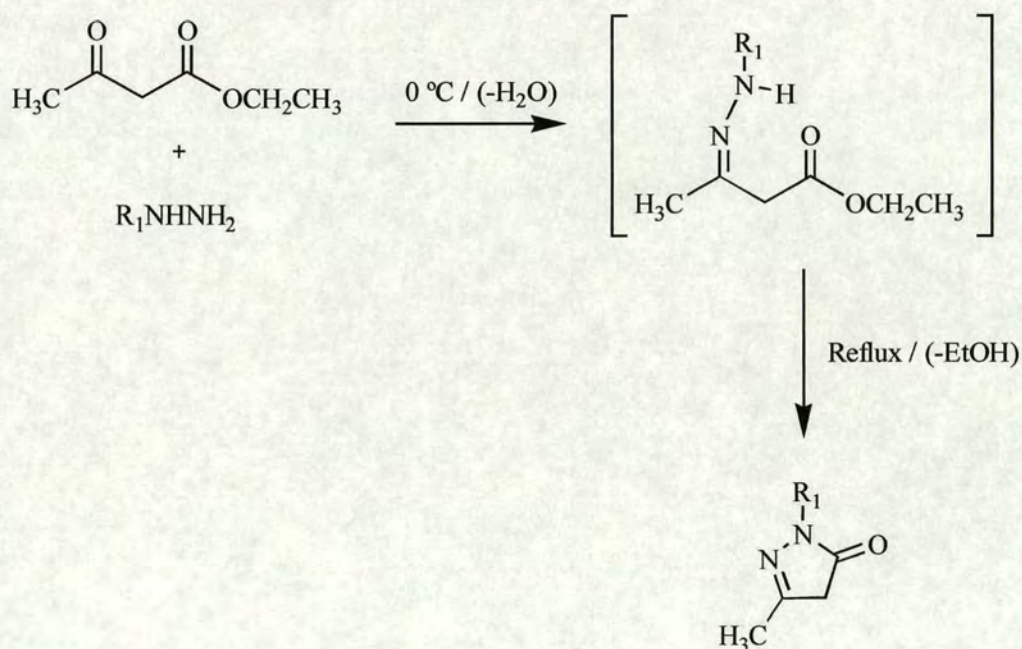


Figure 4.6. Formation of the hydrazone intermediate in the preparation of 1-substituted-3-methyl-2-pyrazolin-5-ones.

2-pyrazolin-5-one reported in the literature to effect the chloroformylation was 7:3:1.³⁴ In general, providing there is an excess of DMF and POCl₃ the chloroformylation will take place. Here the ratio of 2:2:1 was found to give the best yields (~63 % for **21** and ~52 % for **22**), although the reactions were not optimised.

The final step in the formation of the 1-substituted-3-methyl-4-(alkylaldenamine)-pyrazol-5-thiones (**23-32**) and pyrazol-5-one (**33**) involve two functional transformations that can either be performed as separate stages or simultaneously, both routes offering comparable yields. The one-pot method was used here because of its convenience. The previously described one-pot literature method³⁵ is *via* the nucleophilic substitution of the chlorine using a 1.0 M potassium hydrogen sulfide solution and condensation of the aldehyde using the appropriate amine, carried out in ethanol with refluxing. This method was modified slightly by introducing the nucleophile in the form of solid sodium hydrogen sulfide rather than an aqueous solution to dry ethanol in order to favour the imine condensation from which water is a by-product, Figure 4.8.

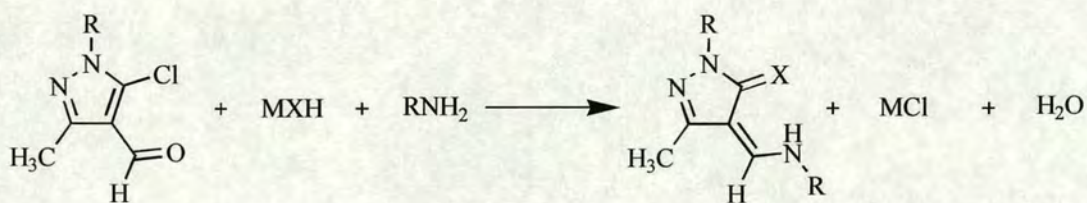


Figure 4.8. A balanced equation for the one-pot formation of the 1-substituted-3-methyl-4-(alkylaldenamine)-pyrazol-5-thiones(ones) (**23-33**) where M = Na, X = S and pyrazol-5-ones where M = K, X = O.

The pyrazol-5-one analogues can be prepared by the acylation of 1-phenyl-3-methyl-2-pyrazolin-5-one (**21**) *via* nucleophilic substitution at the C-4 position using an acyl chloride in the presence of Ca(OH)₂ suspended in dioxane.³⁶ This produces the Ca²⁺ complex which is decomposed under aqueous acidic conditions to produce the 4-acyl-pyrazol-5-one, which is then condensed with an amine. Alternatively, formylation at the C-4 position is carried out using the Vilsmeier-Haack reaction using stoichiometric quantities of POCl₃ and DMF, in contrast to the chloroformylation described above. However, due to the availability of the 5-chloro-3-methyl-4-pyrazolecarboxaldehydes, previously prepared, the method employed in the formation 1-phenyl-3-methyl-4-(4-*t*-butylphenylaldenamine)-pyrazol-5-one (**33**) was similar to that used for the formation of the pyrazol-5-thiones (**23-32**) by replacing NaSH with KOH.

The range of amines used were obtained commercially with the exception of the *p*-nonylaniline which was provided by Avecia (Appendix II).

The two-stage method was previously favoured in the literature, the first step being formation of the thiol *via* the nucleophilic substitution of the chlorine.³⁷ However, the formation and subsequent reaction of the 4-formyl-5-thiol-pyrazole prepared by this method is hindered by the instability of the β-thiolaldehyde towards oxidation and disulfide formation,^{38,39} in contrast to the stable 4-benzoyl-5-thiol-pyrazole.⁴⁰ Protection of the thiol with a *t*-butyl group using sodium *t*-butylthiolate in THF and sodium hydride at ambient temperature²⁹ produces the stable 5-*t*-butylthioether-3-methyl-4-formyl-pyrazole in good yields. The second step is the nearly quantitative formation of the imine by the condensation of the protected thiol-aldehyde with the appropriate amine in ethanol. Complexation of these protected ligands is then

achieved by the cleavage of the *t*-butyl protecting group with strong acid or by using Lewis acid metal ions,^{41,42} *e.g.* Cu(II) and Zn(II). The advantage of the one-pot method used here is that both steps are achieved with relative ease and it does not require the use of protecting groups to prevent disulfide formation.

4.2.1 NMR spectroscopy.

Full experimental characterisation is given in Section 4.11.2.1. The ¹H NMR of the ligands (**23-33**) and their synthetic precursors (**19-21**) were recorded in CDCl₃. 1,3-dimethyl-5-chloro-4-pyrazolecarboxaldehyde (**22**) was recorded in d₆-DMSO due to its low solubility in CDCl₃.

The 1-substituted-2-pyrazolin-5-ones can exist in three tautomeric forms, Figure 4.9. The tautomer adopted is dependent upon the external environment of the 2-pyrazolin-5-one.

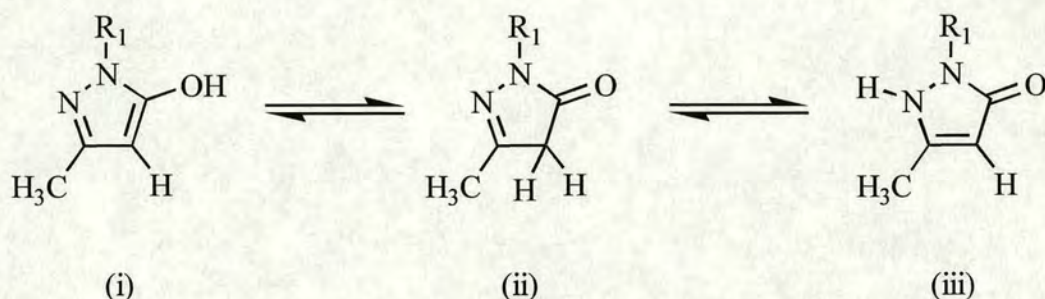


Figure 4.9. The tautomeric forms of 1-substituted-2-pyrazolin-5-ones; (i) OH-form, (ii) CH-form and (iii) NH-form.

It has been shown^{23,43} that in non-polar solvents, *e.g.* CHCl₃, they exist as the CH-tautomer (ii). In aqueous or polar solvents and in the solid state they exist as a

mixture of the OH and NH tautomers and form strong *intermolecular* hydrogen bonded networks in the solid state, Figure 4.10.

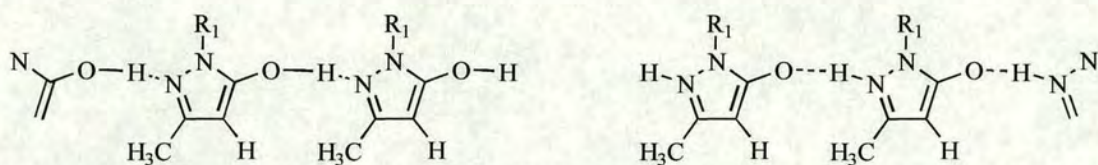


Figure 4.10. The solid state hydrogen bonded OH and NH networks.

The proton spectra of the 1-methyl (**19**) and the 1-*t*-butyl (**20**) 2-pyrazolin-5-ones are in agreement with the literature. They both display singlets at approximately 3.1 ppm demonstrating that they exist as the CH-tautomer in CDCl_3 . However in the solid state the IR spectra contain very broad stretches at approximately 2500 cm^{-1} and 1800 cm^{-1} (see Section 4.11.2) which are consistent with the expected hydrogen bonded NH and OH tautomers.

The pyrazol-5-ones and thiones (**23-33**) also exhibit keto-enol tautomerism with four possible tautomeric forms (Figure 4.11) similar to those described for the 2-pyrazolin-5-ones.

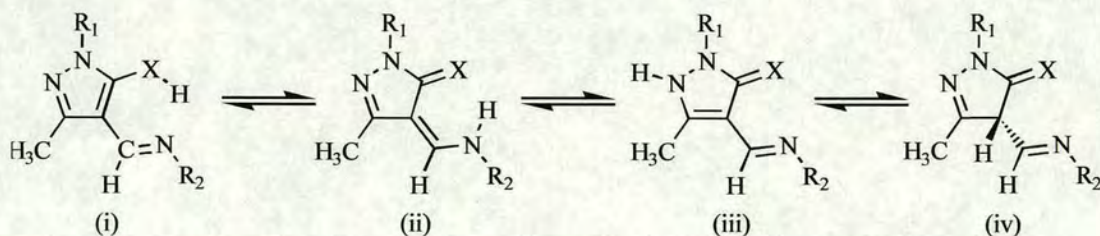


Figure 4.11. The tautomers of the pyrazol-5-thiones and pyrazol-5-ones where X = S or O; (i) imino-thiol(enol), (ii) enamine-thione(ketone), (iii) planar imino-thione(ketone), (iv) non-planar imino-thione(ketone).

The sulfur-containing ligands **23-32** exist as the enamine-thione tautomer (ii) in solution confirmed by the presence of NH resonance with a chemical shift in the range 12.65 ppm to 14.99 ppm. This is in agreement with the crystallographic evidence (Section 4.4) in which the acidic proton is located on the nitrogen of chelate ring. It is further confirmed by the presence of a doublet associated with the aldehydic proton (H-CN) coupled to the NH ($^3J_{HH} \sim 13$ Hz), which can only occur with the planar / non-planar tautomeric forms. In addition to the tautomeric equilibrium, the hydrogen bonded ring is delocalised with an equilibrium between two canonical forms, Figure 4.12.

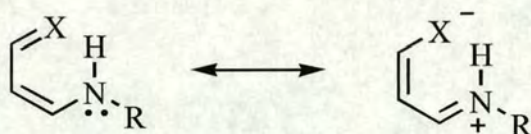


Figure 4.12. Resonance delocalisation in the hydrogen bonded ring of the enamine-thione tautomer.

The chemical shift of the NH proton is greatly affected by the inductive effect of the substituents R_1 and R_2 . The greatest shift downfield is observed when both R_1 and R_2 are aromatic, Table 4.1. As the electron withdrawing capacity of the R_2 substituent is decreased, *i.e.* increase in aliphatic character, an upfield shift in the NH resonance is observed which is expected due to greater shielding of the NH proton. This is also mirrored in the gradual upfield shift of signals for H-CN and, to a lesser extent for CH_3 .

	29	25	24	23	32	31	30	27	26	28
R ₁	Me	Ph	Ph	Ph	Me	Me	Me	Ph	Ph	Ph
R ₂	2-EtHex	2-EtHex	Cy	<i>t</i> -Bu	<i>o</i> -C ₆ H ₅ F	<i>p</i> -Ph(nonyl)	<i>t</i> -BuPh	<i>t</i> -BuPh	Ph	<i>p</i> -PhNO ₂
NH	12.65	13.06	13.16	13.43	14.35	14.41	14.42	14.81	14.84	14.99
H-CN	7.66	7.76	~7.85	~7.90	8.19	8.12	8.12	8.21	8.23	8.23
CH ₃	2.21	2.29	2.29	2.31	2.29	2.28	2.30	2.37	2.37	2.39

Table 4.1. The inductive effect of the R₁ and R₂ substituents on the chemical shift (ppm) of the NH, H-CN and CH₃ resonance's in CDCl₃. 2-ethylhexyl (2-EtHex), cyclohexyl (Cy).

Replacement of Ph with CH₃ at R₁, while keeping R₂ constant, *e.g.* between ligands **25** and **29** and ligands **27** and **30**, results in an upfield shift of the NH (0.4 ppm), H-CN (0.1 ppm) and CH₃ (0.07 ppm) signals. Replacement of sulfur at the C-5 position in ligand **27** by oxygen results in an upfield shift (~3.6 ppm) assigned to the NH proton which is attributed to the greater shielding effect of the oxygen. Whereas with the sulfur containing ligands this signal is relatively sharp, and in some cases resolved as a doublet, in **33** it is very broad suggesting a high rate of exchange on the NMR time scale. The aldehydic proton in **33** appears as a singlet, which is expected in on the basis of the reduced coupling with the NH proton due to the proposed fast rate of exchange.

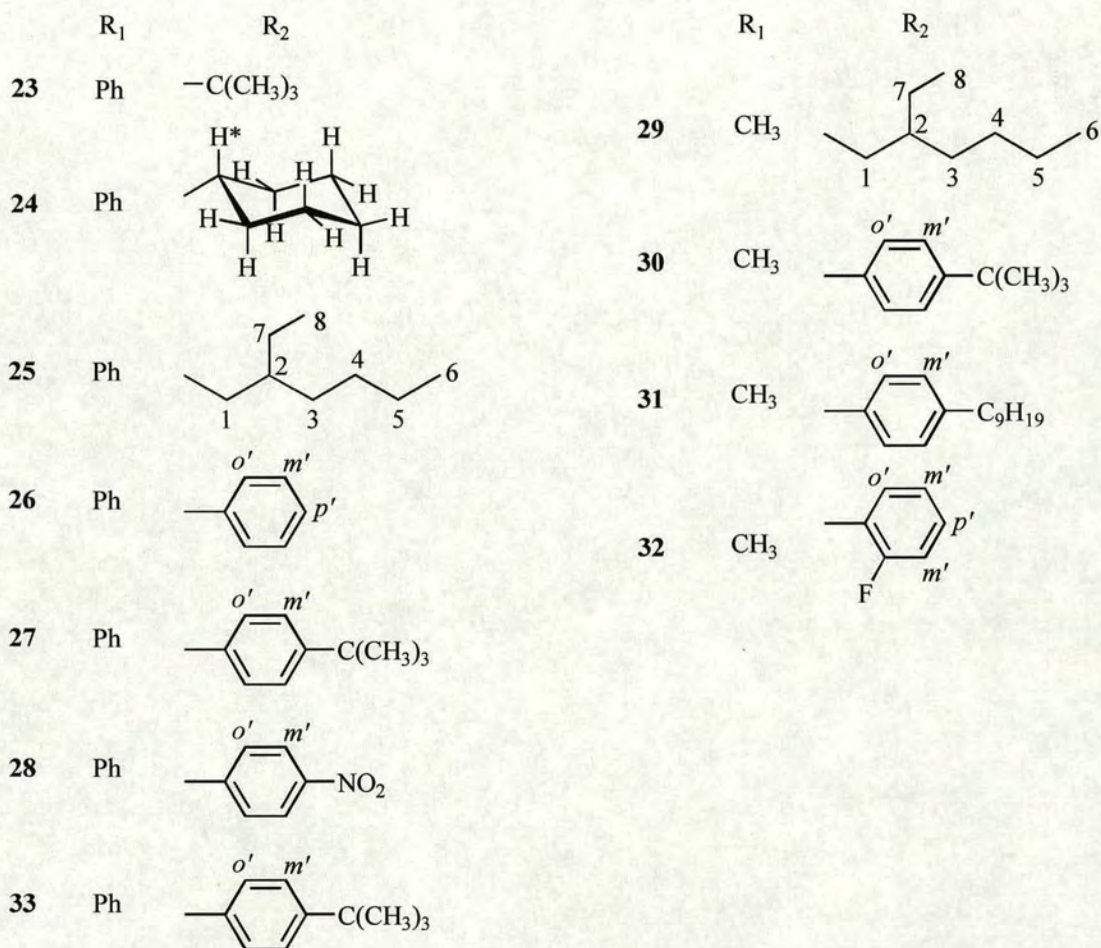
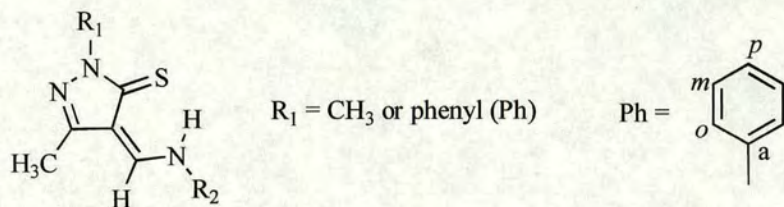


Figure 4.13. ^1H NMR proton labelling of the substituted pyrazol-5-thiones (**23-32**) where $X = \text{S}$ and the pyrazol-5-one (**33**) where $X = \text{O}$.

The ^{13}C NMR of a representative number of ligands (**27**, **29**, **30** and **33**) were recorded in CDCl_3 and assigned according to the labelling in Figure 4.14.

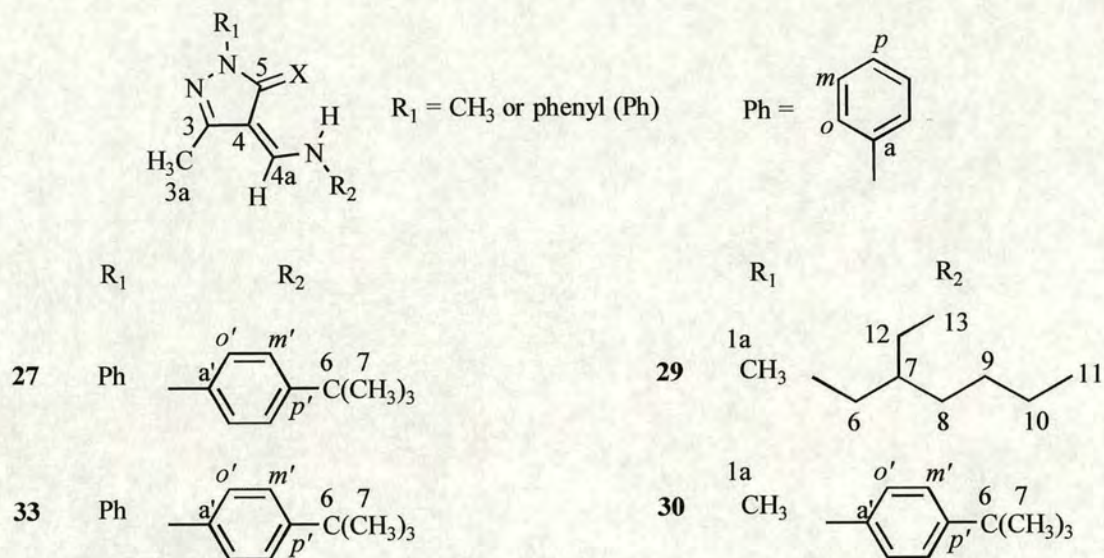


Figure 4.14. ^{13}C NMR labelling of the pyrazol-5-thiones (**27**, **29**, **30**) where $\text{X} = \text{S}$ and pyrazol-5-one (**33**) where $\text{X} = \text{O}$.

The complete assignment of the spectra for **27**, **29**, **30** and **33** has not been possible due to the complexity of the ligands and some overlap of signals, Table 4.2. The aromatic carbons in HL (**30**) have been assigned using estimated substituent values.⁴⁴ The signals for the C-3 and a'-aromatic carbons are indistinguishable, both having an identical chemical shift (150.3 ppm). Tentative assignments of the aromatic R_1 and R_2 substituents for HL (**27**) and (**33**) are based partly on the assignment for R_2 in HL (**30**). The *ortho* (*o*)- and *meta* (*m*)-aromatic carbons on the R_1 substituent are distinguishable in **27** and **33**. The smaller chemical shift has been assigned to the *o*-aromatic carbon due to the upfield shift (~9 ppm) of this signal when the sulfur at the C-5 position is replaced by oxygen which is expected to display greater shielding.

Ligand	Chemical shift (δ) / ppm														
	Pyrazole based					R ₁				R ₂					
	3	3a	4	4a	5	<i>o</i>	<i>m</i>	<i>p</i>	<i>a</i>	<i>o'</i>	<i>m'</i>	<i>p'</i>	<i>a'</i>	6	7
27	150.4 151.3	11.3	112.8	146.0	168.9	124.4	128.4	127.1	139.0	118.2	126.8	135.5	150.4 151.3	34.5	31.1
30	150.3	11.2	111.7	145.5	168.3	34.5 (C-1a)				118.0	126.8	135.4	150.3	34.5	31.1
33	147.9 148.9	12.6	102.5	142.8	165.5	116.8 118.8	128.6	124.2	138.7	116.8 118.6	126.7	135.8	147.9 148.9	34.4	31.1
Ligand	Pyrazole based					R ₁				R ₂					
	3	3a	4	4a	5	1a				6	7	8,9,10,12		11,13	
29	149.4	11.0	110.5	153.9	167.0	34.4				53.5	39.7	22.63-30.30		10.67 13.80	

Table 4.2. Assignment of the ¹³C NMR resonance's in CDCl₃ for the pyrazol-5-thiones (**27**, **29**, **30**) and the pyrazol-5-one (**33**).

4.2.2 Mass spectroscopy.

The EI spectra of the 1-substituted-3-methyl-2-pyrazolin-5-ones (19) and (20) and the 1-substituted-3-methyl-5-chloro-4-pyrazolecarboxaldehydes (21) and (22) are consistent with their respective expected structures. The EI spectra of the ligands (23-30, 32 and 33) contain a molecular ion peak in agreement with their respective molecular masses. Fragmentation is extensive and is dependent upon the substituents R_1 and R_2 . In general the decomposition pathway involves the complete or partial loss of R_2 and in some cases sulfur.

Identification of HL (31) using EIMS was unsuccessful due to the absence of the parent ion peak and a reliable fragmentation pattern. However the expected molecular ion was present in the positive FAB spectrum of the compound.

4.3 Preparation and characterisation of metal complexes.

The metal complexes of the 1-phenyl substituted pyrazol-5-thiones and pyrazol-5-ones with the general formula $[M(L)_2]$ (34-42) were prepared by an analogous method to the bis-pyridinethionato complexes, described in Section 3.3, by the addition of a hot methanol solution of the appropriate divalent metal acetate hydrate to a hot methanol solution containing the appropriate ligand (HL) using a metal:ligand ratio of 1:2, Figure 4.15.

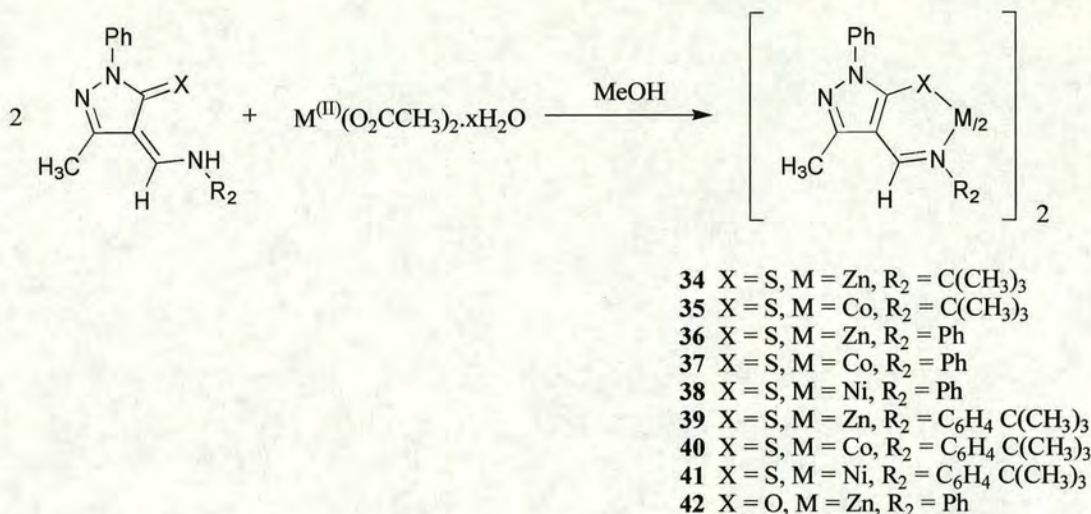


Figure 4.15. Synthesis of the metal complexes $[M(L)_2]$. When $M = Zn^{2+}$, Co^{2+} or Ni^{2+} . L = pyrazol-5-thiones (**23**, **26** and **27**) or pyrazol-5-one (**33**).

In general the expected 2:1 complexes are obtained under these conditions. An exception appears to be the copper complex of the thiopyrazolone (**27**) for which the elemental analysis (Section 4.11.2.2) of the product of this reaction does not support a stoichiometry based upon the formation of the $[M(L)_2]$ complex. It has been previously reported⁴⁵ that a copper(I) complex is easily prepared from the reaction of copper(II) acetate and related di-anionic tetradentate pyrazol-5-thiones in protic solvents, *i.e.* ethanol, to form a proposed $[Cu_4(L)_2]$ species. The product from ligand **27** is predominantly light green needles with a small percentage of deep red / brown needles suggesting a mixture which is predominantly a Cu(I) complex, $[Cu(\mathbf{27-H})]_n$ (**43**), containing a minor amount of the Cu(II) complex $[Cu(\mathbf{27-H})_2]$ (**43a**). The elemental analysis, ¹H NMR (Section 4.3.1) and the FABMS (Section 4.3.2) support this assumption.

4.3.1 NMR Spectroscopy.

The ^1H NMR spectra of the complexes $[\text{Zn}(\mathbf{23-H})_2]$ (**34**), $[\text{Zn}(\mathbf{26-H})_2]$ (**36**), $[\text{Zn}(\mathbf{27-H})_2]$ (**39**), $[\text{Zn}(\mathbf{33-H})_2]$ (**42**) and $[\text{Cu}(\mathbf{27-H})]_n$ (**43**) were recorded in CDCl_3 . The absence of the NH proton ($\sim 13\text{-}14$ ppm) is consistent with the deprotonation of the ligand upon complexation. Consequently the aldehydic proton (H-CN) appears as a singlet in comparison to the doublet formed by the coupling to the NH proton in the ligand spectra.

The spectrum of **43** is similar to that of HL (**27**) indicating the presence of the diamagnetic d^{10} Cu(I) ion. Minor broadening of the spectrum is observed which is associated with the small percentage of paramagnetic d^9 Cu(II) present in the sample.

4.3.2 Mass spectroscopy.

The positive FAB spectra of the complexes **34-42** show molecular ion peaks associated with $[\text{M}(\text{L})_2(\text{H})]^+$ which are in agreement with their elemental analyses (Section 4.11.2.2) based on the complexes having the molecular formula $[\text{M}(\text{L})_2]$.

In contrast to the tris-pyridinethionato cobalt(III) complex (**11**) (Chapter 3) the cobalt(II) acetate precursor is not oxidised but forms a stable pseudo-tetrahedral cobalt(II) complex in solution and in the solid state (Section 4.4). The stability of the d^7 tetrahedral complexes **35**, **37** and **40** can be attributed to:

1. The steric hindrance of the pyrazol-5-thiones disfavours the formation of a d^6 octahedral tris-pyrazol-5-thiolato cobalt(III) species.
2. The electronic contribution of the S_2N_2 donor set which possibly lowers the ligand field energy.

The fragmentation patterns of these complexes indicates the loss of a ligand (L) with fragmentation peaks associated with $[M(L)]^+$ and $[L]^+$ species.

As with the pyridinethionato complexes ion peaks greater than the parent ion peak are present in all the spectra, with the exception of **34** and **42**, and again are thought to arise as products of the FABMS technique. They have been tentatively assigned to three species; (i) $[M_2(L)_2]^+$ present in complexes **37**, **38**, **41**, (ii) $[M_2(L)_3]^+$ present in complexes **35-41**, (iii) $[M_2(L)_4]^+$ present in complex **37**.

The copper(I) complex, $[Cu(27-H)]_n$ (**43**), contains a small amount of the copper(II) complex, $[Cu(27-H)_2]$ (**43a**), see above. It shows high mass peaks associated with $[L]^+$, $[M(L)]^+$, $[M(L)_2]^+$, $[M_2(L)_2]^+$, and $[M_3(L)_2]^+$ species. It is unclear from the FAB spectrum of the molecular formula for the Cu(I) species although it is possible that it could be binuclear due to the presence of the $[M_2(L)_2]^+$ molecular ion.

4.4 Crystallographic characterisation.

The structures are represented in figures with atomic displacement ellipsoids generated by the XP⁴⁶ software, and the atoms labelled according to the system described in Section 3.4. The crystallographic data for the bidentate structures are summarised in Appendix IV.

4.4.1 Ligands.

From the ten mono-anionic bidentate pyrazol-5-thione ligands that were prepared (Scheme 4.1) four have been crystallographically characterised. They all comprise of a phenyl substituent attached to the pyrazole ring at the R₁ position together with a range of different substituents at the R₂ position, Table 4.3.

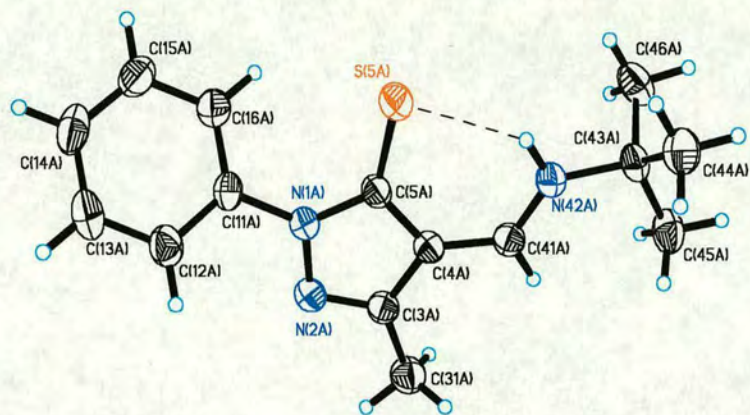
The CSD (September 1999) contains fourteen protonated bidentate mono-anionic ligands which are structurally related the enamine and hydrazone pyrazol-5-thiones and pyrazol-5-ones. Of the fourteen examples only one structure, 1-*i*-propyl-3-methyl-4-cyclohexylaldenamine-pyrazol-5-thione,⁴⁷ carrying the CSD code VUHGAG contains the enamine pyrazol-5-thione NS⁻ donor set, Table 4.3.

	HL	R₁	R₂
	23	Ph	<i>t</i> -butyl
	24	Ph	cyclohexyl
	27	Ph	4- <i>t</i> -butylphenyl
	28	Ph	4-nitrophenyl
	VUHGAG	<i>i</i> -propyl	cyclohexyl

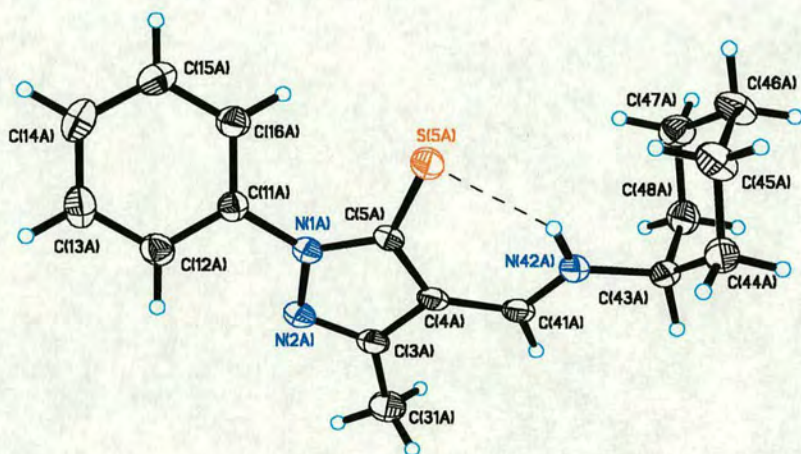
Table 4.3. Crystallographically characterised bidentate enamine pyrazol-5-thiones.

4.4.1.1 Comparison of 4-*t*-butyl, 4-cyclohexyl, 4-*t*-butylphenyl and 4-nitrophenylaldenamine-1-phenyl-3-methyl-pyrazol-5-thiones.

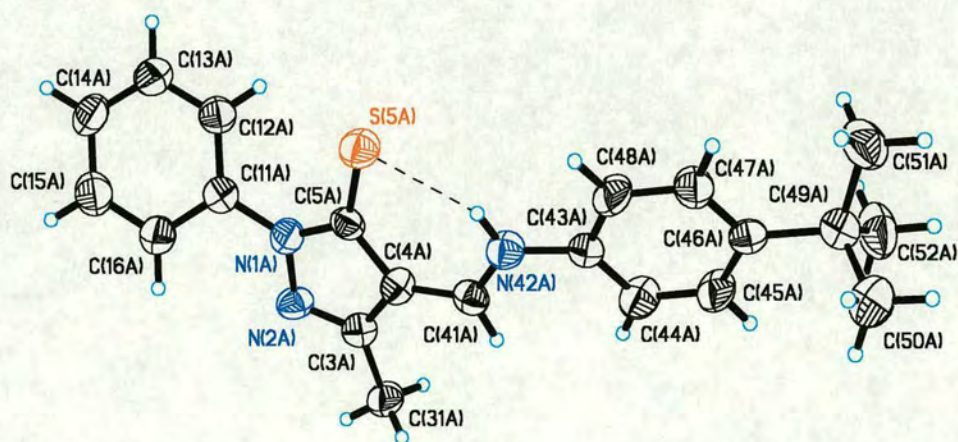
Crystals of HL (**23**) were obtained from hot ethanol as yellow blocks in the monoclinic system with space group P2₁/c (no.14), Figure 4.16(a). HL (**24**) and HL (**27**), Figure's 4.16(b) and (c) respectively, were obtained from hot methanol also as yellow blocks in the monoclinic system with space group P2₁/c (no.14). The asymmetric unit in each of the crystal structures consists of a single ligand.



(a)



(b)



(c)

Figure 4.16. The structures of (a) HL (23), (b) HL (24) and (c) HL (27) showing atomic displacement ellipsoids at the 50% probability level.

Orange plate crystals of HL (**28**).CHCl₃ were grown from hot ethylacetate / propan-2-ol in an orthorhombic crystal lattice with space group Pnma (no.62). The asymmetric unit consists of a single ligand and an associated molecule of chloroform in which Cl(1A) resides in the adjacent unit cell and is generated by the symmetry operation $x, \frac{1}{2}-y, z$, Figure 4.17. The phenyl group at the R₁ position in the ligand is disordered and the positions 50 % partially occupied. The chloroform has a weak, almost linear (170°), interaction with a methyl hydrogen on the pyrazole ring in an adjacent asymmetric unit (C(31A)⋯Cl(2S); 3.726(3) Å). A second chloroform molecule from an adjacent asymmetric unit forms a slightly stronger bifurcated hydrogen bond with the nitro group (C(1S)⋯O(49A); 3.168(9) Å and C(1S)⋯O(49B); 3.320(9) Å).

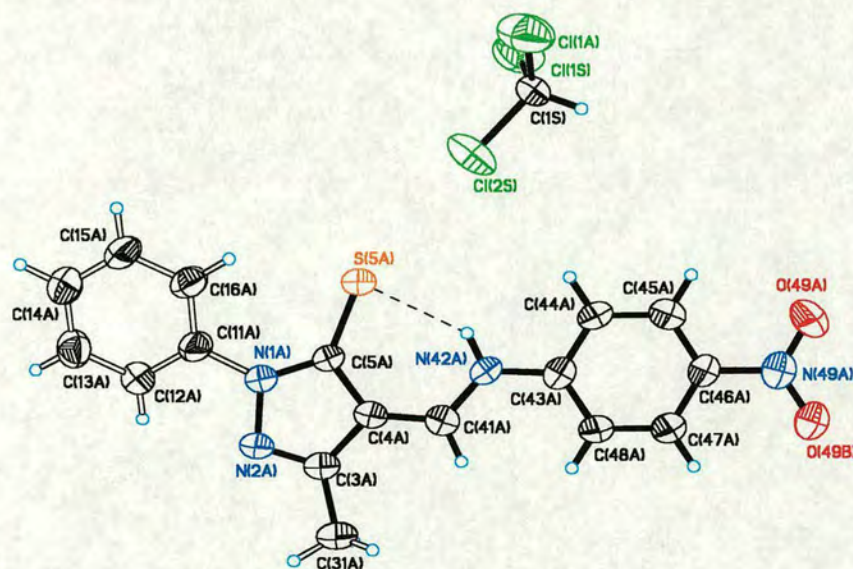


Figure 4.17. The structure of HL (**28**).CHCl₃ showing atomic displacement ellipsoids at the 50 % probability level and one of the disordered sites of the phenyl ring C(11A)-C(16A).

In the solid state these ligands exist in the enamine-thione tautomeric form with the acidic hydrogen located on the nitrogen of the chelate arm. The same tautomer is observed in solution by ^1H NMR spectroscopy (Section 4.2.1). The ligands adopt an *E* configuration around the enamine bond, C(41A)-N(42A), to form a 6-membered ring via a S \cdots H *intramolecular* hydrogen bond, Table 4.4. In comparison with the strong *intramolecular* O-H \cdots S hydrogen bond observed for the pyridinethione (**5**) (Section 3.4.1.1) here the pyrazol-5-thione N-H \cdots S *intramolecular* hydrogen bond is apparently weaker due to;

1. The lower electronegativity of nitrogen compared to oxygen.
2. The larger bite distance, N(42A) \cdots S(5A), attributed to the ring opening affect of the annealed 5-membered pyrazole ring.

The observed N \cdots S bite distances fall in the range 3.107(2)-3.043(7) Å (see Table 4.4). The variation, leading to the larger bite in **23**, is not associated with any significant difference in the summation of the bond lengths in the hydrogen bonded ring. However an increase in the bond angles (Table 4.6) around the ring correlates with the increase in bite distance.

The large volume occupied by the sulfur atom is associated with an S \cdots H interaction with one of the *ortho*-aromatic hydrogens, C(12A) or C(16A). This not only prevents the phenyl at the R₁ position from lying in the plane of the pyrazole ring but also hinders its rotation. The magnitude of this interaction can be related to the rotation of the phenyl group about the N(1)-C(11) bond to the pyrazole ring which can be evaluated using the torsion angles 1-4 shown in Table 4.5. As the rotation of the phenyl substituent increases from the plane of the pyrazole ring, HL (**28**) < HL (**27**) < HL (**23**) ~ HL (**24**), so the S \cdots H interaction decreases.

	D-H...A	D-H (Å)	H...A (Å)	D...A (Å)	D-H...A (°)
HL (23)	N(42A)-H(42A)...S(5A)	0.89(3)	2.36(3)	3.107(2)	141.8(19)
	C(16A)-H(16A)...S(5A)	0.940(3)	2.851(2)	3.312(2)	111.4(2)
	C(46A)-H(46A)...N(2A) ^(a)	0.969(10)	2.561(7)	3.462(3)	154.7(12)
HL (24)	N(42A)-H(42A)...S(5A)	0.91(2)	2.31(2)	3.0943(14)	144.6(17)
	C(16A)-H(16A)...S(5A)	0.940(2)	2.8693(17)	3.3138(17)	110.23(15)
HL (27)	N(42A)-H(42A)...S(5A)	0.870(9)	2.298(7)	3.043(7)	143.8(7)
	C(12A)-H(12A)...S(5A)	0.940(12)	2.675(9)	3.249(9)	120.0(7)
HL (28)	N(42A)-H(42A)...S(5A)	0.870(6)	2.324(2)	3.059(6)	142.2(3)
	C(16A)-H(16A)...S(5A)	0.9408	2.5264	3.209(10)	129.57
	C(1S)-H(1S)...O(49A) ^(b)	0.990(8)	2.482(6)	3.168(9)	126.2(5)
	C(1S)-H(1S)...O(49B) ^(b)	0.990(8)	2.330(5)	3.320(9)	178.9(5)
	C(31A)-H(31C)...Cl(2S) ^(c)	0.9703	2.7663	3.726(3)	170.00

Table 4.4. *Inter*- and *intramolecular* hydrogen bond interactions for HL (23), HL (24), HL (27) and HL (28).CHCl₃. Notations (a-c) represent *intermolecular* contacts with symmetry operations ^(a) -x, -y, 1-z, ^(b) x-1/2, 1/2-y, 1/2-z and ^(c) 2-x, y-1/2, 1-z.

	Torsion	HL (23)	HL (24)	HL (27)	HL (28)
1	C(5)-N(1)-C(11)-C(12)	141.6(2)	138.68(15)	32.0(12)	165.1(9) ^(a)
2	C(5)-N(1)-C(11)-C(16)	41.8(3)	43.5(2)	149.6(8)	14(2) ^(a)
3	N(2)-N(1)-C(11)-C(12)	40.4(3)	40.39(18)	148.8(7)	19.2(19) ^(a)
4	N(2)-N(1)-C(11)-C(16)	136.3(2)	137.44(14)	29.7(10)	161.2(12) ^(a)
5	C(4)-C(41)-N(42)-C(43)	174.4(2)	171.61(14)	172.3(7)	180.00(1)
6	C(41)-N(42)-C(43)-C(44)	-	-	6.8(12)	180.00(1)
7	C(41)-N(42)-C(43)-C(48)	-	-	175.3(7)	0.00(1)

Table 4.5. Selected torsion angles (°) for HL (23), HL (24), HL (27) and HL (28).CHCl₃. ^(a) Phenyl ring shows disordering.

The 5-membered pyrazole and 6-membered hydrogen bonded rings in each ligand lie in a plane with HL (23) displaying the maximum deviation from planarity (r.m.s. deviation from plane 0.033 Å, max. dev. S(5A) = 0.082 Å). There is a gradual increase in the planarity, HL (23) < HL (24) < HL (27) < HL (28), of these rings with HL (28) being planar (r.m.s <0.001 Å) and its planarity extended to incorporate the 4-nitrophenyl substituent. In contrast, the 4-*t*-butylphenyl substituent in HL (27) is rotated out of the least squares plane by approximately 6° (torsion angles 6 and 7, Table 4.5).

	HL (23)	HL (24)	HL (27)	HL (28)	VUHGAG
N(1A)-C(5A)	1.367(2)	1.365(2)	1.355(9)	1.353(9)	1.344(2)
N(1A)-N(2A)	1.392(2)	1.398(2)	1.422(7)	1.415(8)	1.391(3)
N(2A)-C(3A)	1.313(2)	1.307(2)	1.303(9)	1.302(9)	1.316(2)
N(1A)-C(11A)	1.427(2)	1.421(2)	1.407(8)	1.422(10)	1.457(3) ^(a)
C(3A)-C(4A)	1.422(3)	1.426(2)	1.418(10)	1.424(10)	1.416(3)
C(3A)-C(31A)	1.490(3)	1.493(2)	1.501(9)	1.498(10)	1.501(3)
C(4A)-C(41A)	1.402(3)	1.393(2)	1.384(10)	1.370(10)	1.396(2)
C(4A)-C(5A)	1.421(3)	1.426(2)	1.440(9)	1.435(10)	1.425(3)
C(41A)-N(42A)	1.298(3)	1.301(2)	1.313(8)	1.337(9)	1.306(3)
N(42A)-C(43A)	1.483(2)	1.471(2)	1.419(9)	1.397(9)	1.486(2)
C(5A)-S(5A)	1.697(2)	1.6992(15)	1.691(7)	1.699(7)	1.696(2)
S(5A)-C(5A)-C(4A)	129.07(15)	128.65(11)	127.5(6)	126.0(5)	129.7(2)
C(5A)-C(4A)-C(41A)	127.1(2)	127.36(14)	127.5(7)	129.0(7)	127.0(2)
C(4A)-C(41A)-N(42A)	124.4(2)	124.16(14)	122.8(7)	123.8(7)	123.5(2)

Table 4.6. Selected bond lengths (Å) and angles (°) in the HL (23), HL (24), HL (27), HL (28).CHCl₃ and 1-*i*-propyl-3-methyl-4-cyclohexylaldenamine-pyrazol-5-thione (VUHGAG). ^(a) R₁ substituent is *i*-propyl and not phenyl.

Within the observed enamine-thione tautomeric form a significant π -delocalisation is observed around the hydrogen bonded 6-membered ring which is facilitated by the planarity of the system, Table 4.6. The C(5A)-S(5A) bond lengths are intermediate between that of a thione (C=S; ~ 1.6 Å)⁴⁸ and that of the sum of the single bond covalent radii (C-SH; ~ 1.8 Å).⁴⁹ Likewise the enamine bond, C(41A)-N(42A) is shorter (~ 0.13 - 0.17 Å) than expected for a single C-N bond (~ 1.47 Å). Inspection of the other bond lengths indicates a degree of delocalisation over the whole of the molecule.

The electronic contribution of the R₂ substituent on the enamine nitrogen atom is linked to the planarity of the molecule and the degree of delocalisation. The observed variations in the bond lengths in Figure 4.18 correlate well with the electron withdrawing (e.w.) ability of the R₂ substituent, *t*-butyl in **23** \sim cyclohexyl in **24** $<$ 4-*t*-butylphenyl in **27** $<$ 4-nitrophenyl in **28**.⁵⁰

e.w. ability of R ₂	HL (28) > HL (27) > HL (24) \sim HL (23)
degree of planarity	HL (28) > HL (27) > HL (24) > HL (23)
C(41A)-N(42A)	HL (28) > HL (27) > HL (24) \sim HL (23)
C(4A)-C(41A)	HL (28) < HL (27) < HL (24) < HL (23)
C(4A)-C(5A)	HL (28) \sim HL (27) > HL (24) \sim HL (23)
C(5A)-S(5A)	HL (28) \sim HL (27) \sim HL (24) \sim HL (23)

Figure 4.18. Trends in a selection of bond lengths and in the planarity of the pyrazole and hydrogen bonded rings with respect to the electron withdrawing ability of the R₂ substituent. **23**; *t*-Bu, **24**; cyclo-C₆H₁₁, **27**; 4-*t*-BuPh and **28**; NO₂-Ph.

The 4-nitrophenyl group has the greatest electron withdrawing ability and consequently the enamine bond length in HL (**28**) is the longest and C(4)-C(41) is the shortest, indicating the delocalisation around the 6-membered ring shifts towards the enamine-thione canonical form in which the nitrogen atom is not charged, Figure 4.12. As expected the further away the R₂ substituent the lesser affect it has on the alternate lengthening and shortening of bond lengths. This is exemplified by the statistically similar C(5A)-S(5A) lengths regardless of the R₂ substituent.

Removal of electron density from the enamine nitrogen by the electron withdrawing 4-nitrophenyl and to a lesser extent 4-*t*-butylphenyl results in the deshielding of the NH proton, consequently altering the acidity of the ligand. The observed shift downfield of the proton correlates well with the observed lengthening of the enamine bond, Table 4.7. There is also a good agreement with the increasing values of the bite distance reducing the strength of the hydrogen bond, longer bonds showing smaller chemical shifts.

	HL (28)	HL (27)	HL (24)	HL (23)
δ_{NH} / ppm	14.84	14.81	13.16	13.06
C(41A)-N(42A) / (Å)	1.337(9)	1.313(8)	1.301(2)	1.298(3)
N(42)···S(5) / (Å)	3.059(6)	3.043(7)	3.0943(14)	3.107(2)

Table 4.7. The correlation between the C(41A)-N(42A) bond length (Å), bite distance (Å) and the chemical shift (ppm) of the NH resonance.

4.4.2 Metal complexes.

Seven neutral complexes of zinc, cobalt and nickel with bidentate pyrazol-5-thiolato units having different imino substituents have been crystallographically characterised. The literature contains thirteen related neutral complexes, predominantly containing nickel, and one positively charged iron(III) species comprising of two tridentate pyrazol-5-thiolato units with the donor set N_2S^+ , Table 4.8. The published structures date back as far as 1988 with three of the structures published during the course of this project.

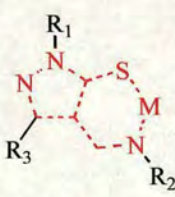
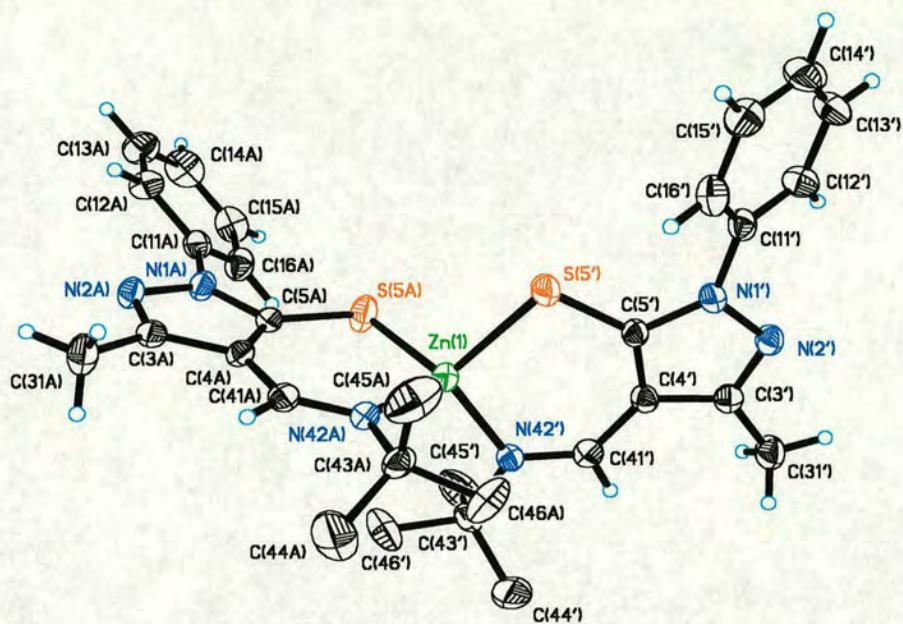
	[M(L) ₂]	R ₁	R ₂	R ₃	M
	34, 35	Ph	<i>t</i> -Bu	Me	Zn, Co
	36, 37, 38	Ph	Ph	Me	Zn, Co, Ni
	39, 40	Ph	4- <i>t</i> -BuPh	Me	Zn, Co
	(a)	<i>i</i> -Pr	cyclo-C ₆ H ₁₁	Me	Zn, Ni, Cd, Pd, Hg
	(b)	<i>i</i> -Pr	Me	Me	Ni
	(c)	<i>i</i> -Pr	<i>t</i> -Bu	Me	Ni
	(d)	<i>i</i> -Pr	Ph	Me	Ni
	(e)	Me	2,6-(Me)Ph	Ph	Zn, Ni
	(f)	Ph	Ph-ε ₆ -Cr(CO) ₃	Me	Ni
	(g)	Me	<i>i</i> -Pr	Me	Ni
	(h)	Ph	<i>i</i> -Pr	Me	Zn
(i)	Ph	quinoline	Me	Fe(III)	

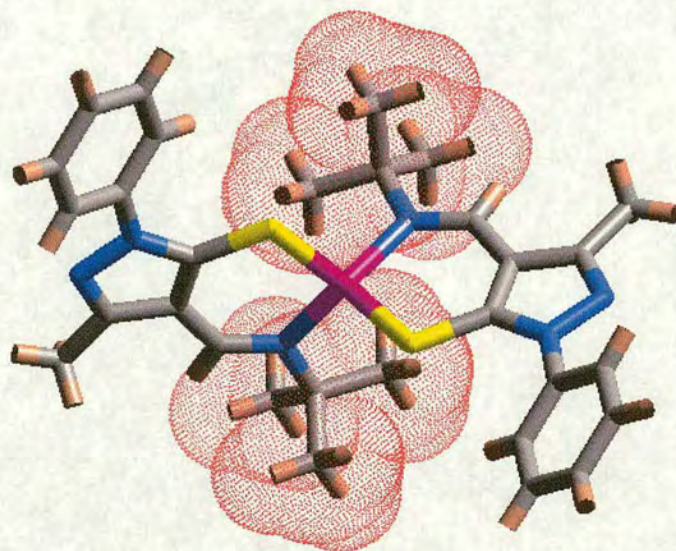
Table 4.8. The range of crystallographically characterised bis-chelating imino pyrazol-5-thiolato metal(II) complexes (34-48) presented in this thesis and those represented in the CSD. (a) Zn (GEXZOY),⁵¹ Ni (GEXZIS),⁵¹ Cd (GEXZUE),⁵¹ Pd (VISDEG),⁵² Hg (JIBVAR),⁵³ (b) KIZLUA,⁵⁴ (c) KIZMEL,⁵⁴ (d) KIZMAH,⁵⁴ (e) Zn (TIQLEK / TIQLIO),⁵⁵ Ni (YUDNUG),⁵⁶ (f) SAWMAE,⁵⁷ (g) VUTSUY,³⁵ (h) TIQLOU,⁵⁵ (i) NIMQUV.⁵⁸

The aim of this section is to compare geometrical and / or electronic influences of the ligand substituents on (1) the disposition of donor atoms in the chelate unit and (2) the disposition of the chelate units to each other and to relate these structures to the observed "strength" and selectivity of extraction (Section 4.5).

[Zn(23-H)₂] (34) and [Zn(26-H)₂] (36) and their respective isomorphous cobalt complexes, [Co(23-H)₂] (35) and [Co(26-H)₂] (37), were obtained as yellow and red plates in the orthorhombic crystal system, with space group Pbcn (no.60). The asymmetric units of [Zn(23-H)₂] (34) and [Co(23-H)₂] (35), Figure 4.19, and those of [Zn(26-H)₂] (36) and [Co(26-H)₂] (37), Figure 4.20, consist of one half of a [M(L)₂] unit which exhibits C₂ symmetry with a crystallographic two-fold axis bisecting the N(42A)-M(1)-N(42') and S(5A)-M(1)-S(5') angles. The bis-(1-phenyl-3-methyl-4-(4-*t*-butylphenylaldimino)-pyrazol-5-thiolato)zinc(II) (39) and cobalt(II) (40) complexes are also isomorphous, crystallising from methanol in the monoclinic system with space group P2₁/c. The two halves of the complex are not related crystallographically and the asymmetric unit contains a single [M(L)₂] unit, Figure 4.21.

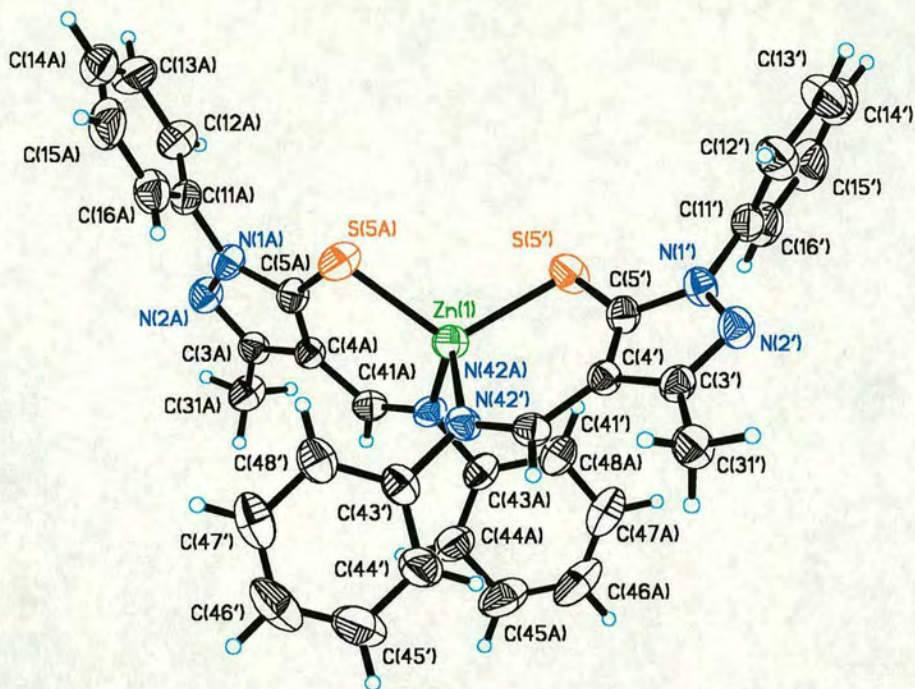


(a)

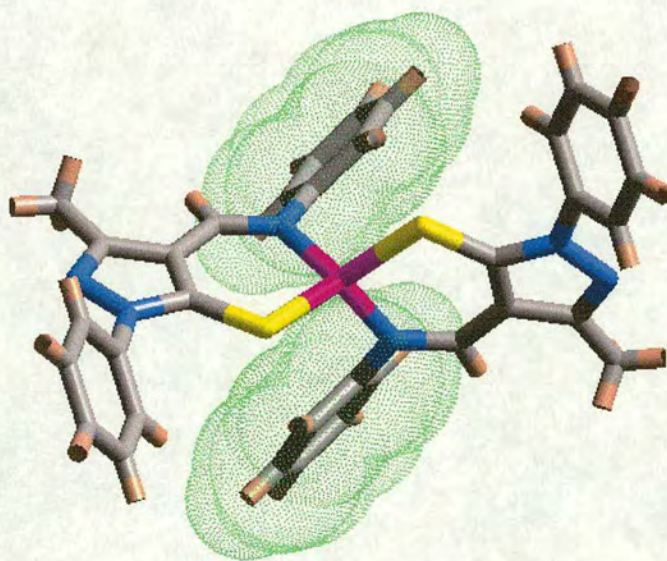


(b)

Figure 4.19. The structures of the Λ enantiomers of (a) $[\text{Zn}(\mathbf{23-H})_2]$ (**34**) showing atomic displacement ellipsoids at the 50 % probability level and the isostructural (b) $[\text{Co}(\mathbf{23-H})_2]$ (**35**) viewed along the C_2 axis and showing the van der Waal volume for the 4-*t*-butyl substituent. The bonds and atoms are represented as cylinders using Cerius.⁵⁹

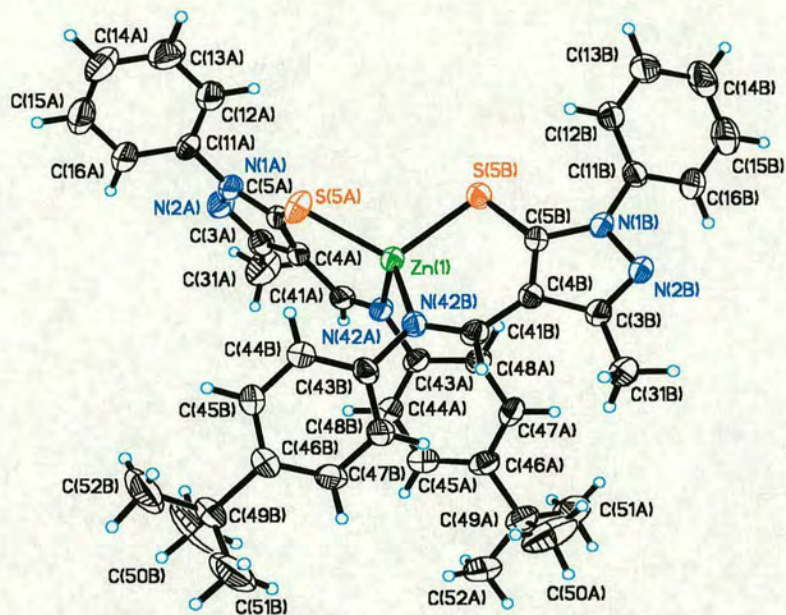


(a)

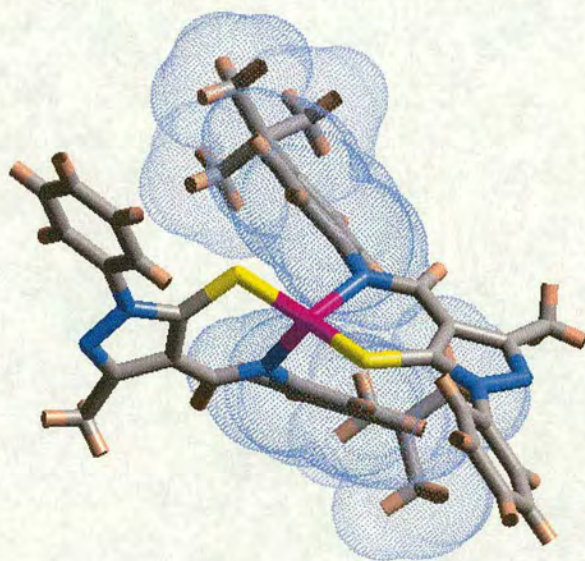


(b)

Figure 4.20. The structures of the Δ enantiomers of (a) $[\text{Zn}(\mathbf{26-H})_2]$ (**36**) showing atomic displacement ellipsoids at the 50 % probability level and the isostructural (b) $[\text{Co}(\mathbf{26-H})_2]$ (**37**) viewed along the C_2 axis and showing the van der Waals volume for the phenyl substituent.



(a)



(b)

Figure 4.21. The structures of (a) the Δ enantiomer of $[\text{Zn}(\mathbf{27-H})_2]$ (**39**) showing atomic displacement ellipsoids at the 50 % probability level and the isostructural (b) Λ enantiomer of $[\text{Co}(\mathbf{27-H})_2]$ (**40**) viewed along the pseudo- C_2 axis and showing the van der Waals volume for the 4-*t*-butylphenyl substituent.

[Ni(26-H)₂] (**38**) was obtained as red plates from methanol in the monoclinic crystal system, with space group C2/c (no.15). The asymmetric unit in the crystal structure consists of half the [Ni(26-H)₂] molecule, Figure 4.22. The second half of the molecule is related by C₂ rotational symmetry (1-x, y, ½-z) in which the two-fold axis bisects the N(42A)-Ni(1)-N(42') and S(5A)-Ni(1)-S(5') angles.

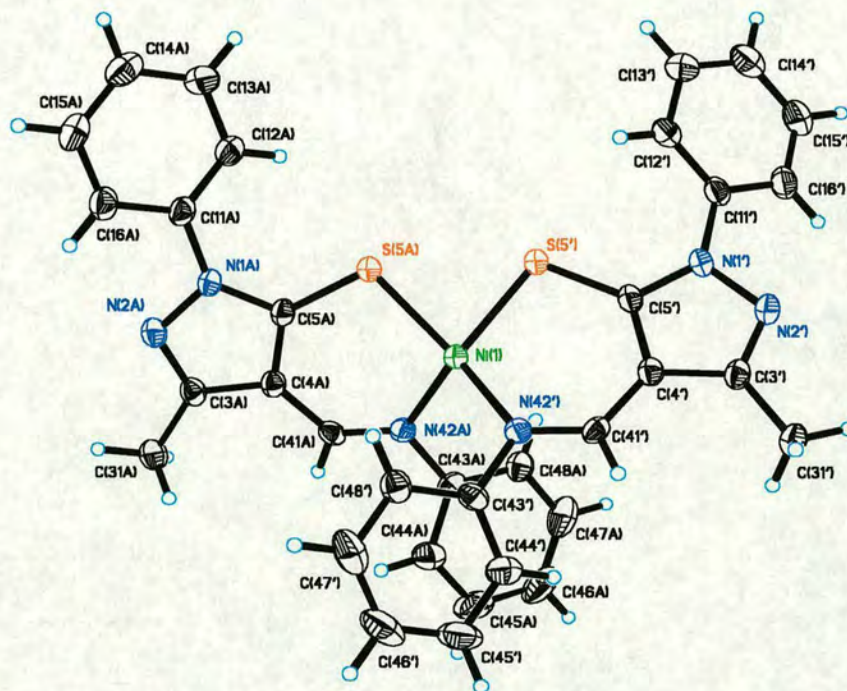


Figure 4.22. The structure of the Δ enantiomer of bis-(1-phenyl-3-methyl-4-(phenylaldimino)-pyrazol-5-thiolato) nickel(II) (**38**) showing atomic displacement ellipsoids at the 50 % probability level.

The geometry adopted with zinc and cobalt complexes approximates closely to tetrahedral. In general the zinc and cobalt complexes are distorted slightly towards a *cis* geometry, defined by the dihedral angle. In the few exceptions to this a distortion towards *trans* geometry is observed (see Section 4.4.2.1). A greater irregularity in

the geometries of the nickel complexes is observed. They are considerably more dependent on the ligand substituents and range between *trans*-planar to slightly *cis*-distorted tetrahedral.

The complexes **34-38** are chiral with both enantiomers (Λ and Δ) occurring in the unit cell and related by the crystallographic inversion centre. The Λ -form follows the movement of a left-handed propeller (anti-clockwise) when viewed along the C_2 axis (pseudo- C_2 axis for **39** and **40**) and for the Δ -form the movement is right-handed (clockwise). Three conceivable rearrangement mechanisms could lead to the $\Delta \rightleftharpoons \Lambda$ inversion at the metal centre:⁵³

1. An *intramolecular* diagonal twist without M-L bond breakage.
2. An *intramolecular* M-L bond breakage through an achiral tricoordinate intermediate.
3. An *intermolecular* ligand exchange.

Temperature dependent NMR spectroscopy in Ni(II), Zn(II), Cu(II) pyrazol-5-thione and pyrazol-5-one based systems^{35,45,51,53,55} suggests an *intramolecular* mechanism since the rate of inversion is independent of the solution concentration, with the diagonal twist mechanism favoured over the achiral intermediate, Figure 4.23.

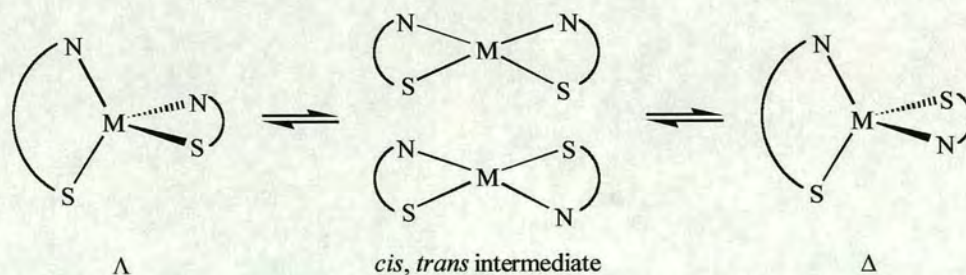


Figure 4.23. The *intramolecular* diagonal twist mechanism for the interconversion between ($\Delta \rightleftharpoons \Lambda$) enantiomers.

4.4.2.1 Structural effects of *t*-Bu, Ph and 4-*t*-BuPh imino substituents on the zinc(II) complexes.

The two most relevant parameters in determining tetrahedral geometry are (1) the disposition of the donor atoms, *i.e.* the bite distance and (2) the disposition of the chelate planes relative to each other, *i.e.* the dihedral angle. Both of these are affected by the metal-donor distance, planarity of the chelate ring and bond lengths and angles around the chelate which are in turn influenced within the series by the ligand substituents. By varying the imino substituent (R_2) at the C(4)-position on the pyrazole ring using groups which have different steric volumes and electronic characteristics (**34**; *t*-Bu, **36**; Ph and **39**; 4-*t*-BuPh), the geometry can be influenced. The three published structures used for comparison here show different groups not only at the imino (R_2) position but also at the R_1 and R_3 positions, Figure 4.24.

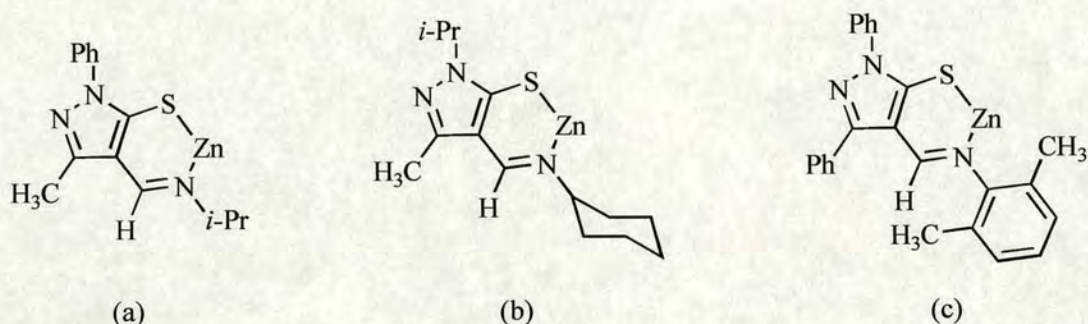


Figure 4.24. Structures of (a) TIQLOU, (b) GEXZOY, (c) TIQLEK / TIQLIO.

The two structures TIQLEK (triclinic) and TIQLIO (orthorhombic) are crystalline modifications of bis-(1,3-diphenyl-4-(2,6-dimethylphenylaldimino)-pyrazol-5-thiolato)zinc(II). In the case of TIQLIO the structure is of low resolution containing large standard deviations. Consequently it is not included here for the purpose of

comparison. TIQLOU and GEXZOY are similar in general structure and approximate closely to tetrahedral and will be compared with the structures reported here. In contrast the ligand units in TIQLEK contain an extremely bulky 2,6-dimethylphenyl group. Coupled with the replacement of the methyl on the pyrazole ring with a phenyl group, this complex suffers from excessive steric hindrance. As a result, the geometry is highly distorted from tetrahedral with the ligand units forming an umbrella arrangement around the central zinc atom.

	[Zn(23-H) ₂] (34) ^(a)		[Zn(26-H) ₂] (36) ^(a)		[Zn(27-H) ₂] (39)	
	L(A)	L(C)	L(A)	L(C)	L(A)	L(B)
N(1)-C(5)	1.370(5)	1.370(5)	1.357(4)	1.357(4)	1.356(3)	1.362(4)
N(1)-N(2)	1.385(4)	1.385(4)	1.397(3)	1.397(3)	1.389(3)	1.389(3)
N(2)-C(3)	1.304(5)	1.304(5)	1.311(4)	1.311(4)	1.322(4)	1.317(4)
N(1)-C(11)	1.426(5)	1.426(5)	1.422(4)	1.422(4)	1.427(4)	1.426(4)
C(3)-C(4)	1.431(5)	1.431(5)	1.428(4)	1.428(4)	1.420(4)	1.428(4)
C(3)-C(31)	1.491(5)	1.491(5)	1.494(4)	1.494(4)	1.489(5)	1.489(4)
C(4)-C(41)	1.423(5)	1.423(5)	1.418(4)	1.418(4)	1.415(4)	1.411(4)
C(4)-C(5)	1.394(5)	1.394(5)	1.396(4)	1.396(4)	1.410(4)	1.411(4)
C(41)-N(42)	1.294(5)	1.294(5)	1.298(4)	1.298(4)	1.294(4)	1.297(4)
N(42)-C(43)	1.507(5)	1.507(5)	1.434(4)	1.434(4)	1.429(4)	1.433(4)
C(5)-S(5)	1.721(4)	1.721(4)	1.723(3)	1.723(3)	1.718(3)	1.721(3)
S(5)-C(5)-C(4)	131.4(3)	131.4(3)	132.8(2)	132.8(2)	133.0(2)	131.5(2)
C(5)-C(4)-C(41)	132.0(3)	132.0(3)	130.8(3)	130.8(3)	129.8(3)	130.9(3)
C(4)-C(41)-N(42)	129.2(4)	129.2(4)	127.8(3)	127.8(3)	126.6(3)	127.8(3)
C(41)-N(42)-Zn(1)	121.4(3)	121.4(3)	123.5(2)	123.5(2)	123.8(2)	123.0(2)
C(5)-S(5)-Zn(1)	101.02(14)	101.02(14)	100.82(11)	100.82(11)	99.91(10)	100.72(10)

Table 4.9. Selected bond lengths (Å) and angles (°) in the chelate units of the complexes [Zn(23-H)₂] (34) and [Zn(26-H)₂] (36) and [Zn(27-H)₂] (39). ^(a) The two independent ligands are crystallographically related by the symmetry operation -x, y, 1/2-z.

The bond lengths observed in the chelate rings of the complexes are consistent with the electronic structure of the delocalised imino-thiolato tautomer, Table 4.9.

The Zn(II) cations in **34**, **36** and **39** lie at the centre of the N₂S₂ donor set which approximates closely to tetrahedral geometry, Figures 4.19(a), 4.20(a) and 4.21(a) respectively. The majority of bond lengths and angles around the periphery of the ligand units and chelate rings are similar in the three structures reported here and in the three related structures, published in the literature, Table 4.9. However some are different and can be related to the influence of the ligand substituents. These are described in greater detail below.

Upon complexation to zinc the C-S bond lengths in the ligands (**23**) and (**27**) increase by ~0.03 Å to 1.721 Å in **34** and to 1.718 Å and 1.721 Å in **39**. Alternate shortening (C(4)-C(5); ~0.01-0.02 Å) and lengthening (C(4)-C(41) ~0.02-0.03 Å) around the chelate ring is observed with the exception of C(41)-N(42) which remains similar to that seen for HL (**23**). However there is no significant difference between the imino (C=N) and thiol (C-S) bond lengths within this series of complexes. The greatest delocalisation of the chelate ring is observed for the complexes containing aromatic imino substituents, the maximum occurring in complex **39** such that C(4)-C(41) and C(4)-C(5) are almost identical, ranging from 1.410 Å to 1.415 Å. This can be attributed to the overlap and delocalisation of π -orbitals expected with the aromatic substituents even though the phenyl of the imino group is twisted out of the chelate plane, torsion angles 1 and 2, Table 4.10. The greater similarity, hence delocalisation, of C(4)-C(41) and C(4)-C(5) in **39** can be attributed to the smaller torsional rotation of the phenyl group.

	Torsion	[Zn(26-H) ₂] (36) ^(a)		[Zn(27-H) ₂] (39)	
		L(A)	L(*)	L(A)	L(B)
1	C(41)-N(42)-C(43)-C(44)	50.6(4)	50.6(4)	42.5(4)	139.6(4)
2	C(41)-N(42)-C(43)-C(48)	128.2(3)	128.2(3)	142.0(3)	43.6(5)

Table 4.10. Selected torsion angles in [Zn(26-H)₂] (36) and [Zn(27-H)₂] (39).

^(a) The two ligands are related by symmetry operation -x, y, ½-z.

Consequently the C(43)-N(42) bond is much shorter (0.06-0.07 Å) for the complexes containing aromatic imino substituents than for those with an aliphatic imino group, in which the bond length is close to 1.50 Å, Table 4.9.

The non-bonded donor atom distance N(42)⋯S(5) in the zinc complexes **34**, **36** and **39** necessarily increases (~ 0.3 Å), with respect to the free ligand, to accommodate the zinc ion. The observed increase in the bite distance, 3.380(3) Å to 3.448(4) Å correlates with the increase in Zn-S bond length, Table 4.11.

N(42)⋯S(5)	34 > 36 > GEXZOY ~ TIQLOU ≥ 39(B) ≥ 39(A)
Zn-S	34 > 36 ≥ 39(B) ≥ GEXZOY ≥ TIQLOU > 39(A)
N(42)-Zn(1)-S(5)	34 > 36 > 39(B) ≥ TIQLOU ≥ GEXZOY > 39(A)

As a consequence of this the chelate angle, N(42)-Zn(1)-S(5), in the *t*-butylimino substituted complex is greatest (105.03(9)°), and thereafter decreases following a similar trend, Figure 4.25. The chelate angles are close to that for ideal T_d geometry and are a great improvement compared with the 90° chelate angle observed for the pyridinethionato and pyridinonato complexes (Section 3.4). This can be attributed in

part to the inclusion of the annealed 5-membered pyrazole ring that serves to increase the separation between donor atoms.

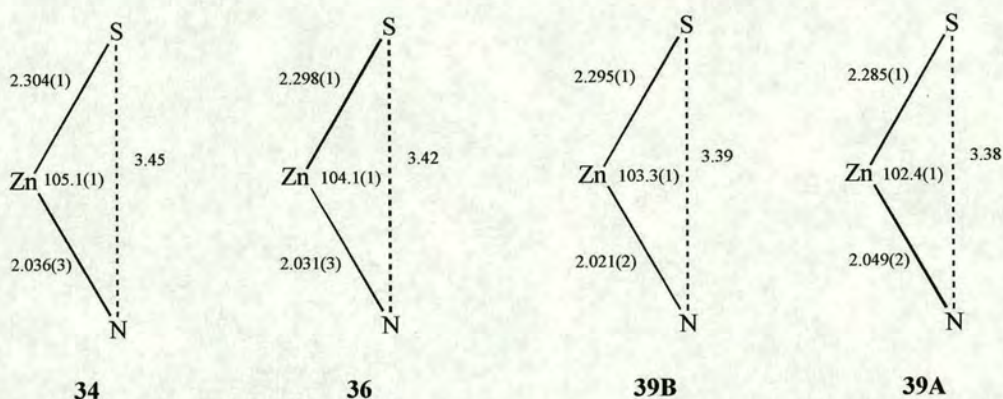


Figure 4.25. Illustration of the bite distance (Å) and chelate angle (°) varying proportionally with Zn-S bond length (Å).

The chelate rings in **34**, **36** are close to planar (r.m.s deviation from the plane 0.010 Å, max. dev. N(42) = 0.017 Å for **34** and 0.019 Å, max. dev. C(41) = 0.029 Å for **36**). In contrast the chelate rings in the 4-*t*-butylphenyl substituted complex **39** are distorted further from planarity, with the metal atom deviating out of the plane the furthest in chelate ring A (r.m.s deviation from the plane 0.113 Å, max. dev. Zn(1) = 0.174 Å). This may possibly be attributed to the necessary buckling of the ring due to the insufficiently large donor bite distance, Table 4.11. As expected the loss of planarity is mirrored by the decrease in summation of angles around the chelate ring ($\Sigma\theta_{\text{chelate}}$), both of which vary proportionally with bite distance.

Planarity	34 > 36 > 39(B) > 39(A)
$\Sigma\theta_{\text{chelate}}$	34 (720°) > 36 (719.8°) > 39(B) (717.2°) > 39(A) (714.6°)

	[Zn(23-H) ₂] (34)		[Zn(26-H) ₂] (36)		[Zn(27-H) ₂] (39)		TIQLOU	GEXZOY	TIQLEK (1)		TIQLEK (2)	
	L(A)	L(°)	L(A)	L(°)	L(A)	L(B)	L(A) / L(°)	L(A) / L(°)	L(A)	L(B)	L(A)	L(B)
Zn(1)-N(42)	2.036(3)	2.036(3)	2.031(3)	2.031(3)	2.049(3)	2.021(2)	2.039(3)	2.049(3)	2.052(4)	2.070(4)	2.073(4)	2.078(4)
Zn(1)-S(5)	2.3036(13)	2.3036(13)	2.2977(10)	2.2977(10)	2.2846(9)	2.2952(10)	2.293(1)	2.291(1)	2.280(1)	2.275(2)	2.285(1)	2.282(2)
C(5)-S(5)	1.721(4)	1.721(4)	1.723(3)	1.723(3)	1.718(3)	1.721(3)	1.719(4)	1.725(3)	1.733(5)	1.730(5)	1.739(4)	1.740(4)
C(41)-N(42)	1.294(5)	1.294(5)	1.298(4)	1.298(4)	1.294(4)	1.297(4)	1.306(5)	1.290(4)	1.296(5)	1.293(6)	1.298(6)	1.295(6)
N(42)-C(43)	1.507(5)	1.507(5)	1.434(4)	1.434(4)	1.429(4)	1.433(4)	1.484 ^(b)	1.479(5)	1.448 ^(b)	1.452 ^(b)	1.443 ^(b)	1.451 ^(b)
N(42)-Zn(1)-S(5)	105.03(9)	105.03(9)	104.07(8)	104.07(8)	102.36(7)	103.32(7)	103.20(9)	102.8(1)	101.8(1)	102.8(1)	99.8(1)	98.6(1)
N(42)···S(5)	3.448(4)	3.448(4)	3.416(3)	3.416(3)	3.380(3)	3.390(3)	3.398 ^(b)	3.397 ^(b)	3.365 ^(b)	3.398 ^(b)	3.338 ^(b)	3.308 ^(b)
N(42A)···N(42B)	3.480(5) ^(a)		3.143(3) ^(a)		3.131(4)		3.400 ^(b)	3.294 ^(b)	3.313 ^(b)		3.319 ^(b)	
S(5A)···S(5B)	3.7463(18) ^(a)		3.8210(15) ^(a)		3.7779(14)		3.590(2)	3.670 ^(b)	4.144(2)		4.241(2)	
θ	91.8		81.7		78.9		82.6	80.2	97.0		96.8	

Table 4.11. Metal donor bond lengths (Å), angles (°), chelate bite distances (Å) and dihedral angles (θ°) defined by the chelates in [Zn(23-H)₂] (34), [Zn(26-H)₂] (36), [Zn(27-H)₂] (39), TIQLOU, GEXZOY and TIQLEK. ^(a) The two ligands are related by the symmetry operation -x, y, ½-z. ^(b) Value measured using Cerius.⁵⁹ TIQLEK contains two molecules (1), (2) in the asymmetric unit.

The dihedral angles between the Zn,N,S chelate planes of the six structures vary between a minimum of 78.9° for **39** which is distorted towards a *cis* geometry and a maximum of 97.0° for TIQLEK (1) which is distorted towards a *trans* geometry, Table 4.11. This range of approximately 18° is a summation of the imposed steric volume of the imino substituent and the magnitude of the bite distance. A large bite implies the zinc atom sits closer to the ligand unit and therefore the two units must lie closer to each other. In such cases it is easily visualised that by increasing the dihedral angle, and thus exceeding 90° , the steric strain incurred by the close proximity of bulky ligand substituents can be partially elevated.

The steric volume of a substituent is expressed by the cone angle (θ_c) and can influence the chemical behaviour and bonding in a complex.⁶⁰ The value of the cone angle in a symmetric substituent is equal to the apex angle of a cylindrical conical surface centred a set distance from the substituent and just touching the van der Waals radii of the outer most atoms, Figure 4.26.

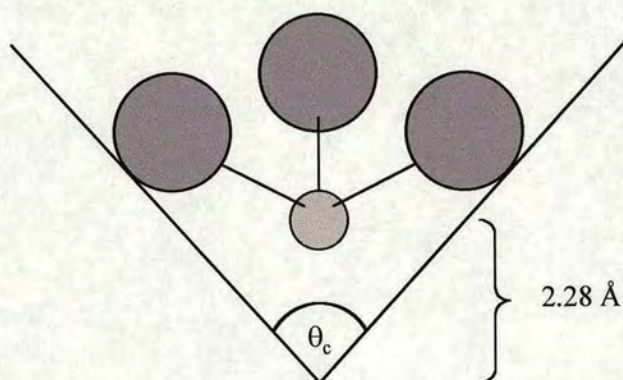


Figure 4.26. Determination of the cone angle, θ_c , for symmetrical PR_3 ligands.⁶⁰

When several rotational conformations of the R-groups are possible the one giving the minimum θ_c is used. Several cone angles, relevant for discussion here are listed in Table 4.12.

Phosphorus bound	$\theta_c / ^\circ$	Metal bound	$\theta_c / ^\circ$
P(Me) ₃	118	Me	90
P(Ph) ₃	143	Ph ^(a)	105
P(<i>i</i> -Pr) ₃	160	<i>i</i> -Pr	114
P(cyclohexyl) ₃	170	Cyclohexyl	n/a
P(<i>t</i> -Bu) ₃	182	<i>t</i> - Bu	126

Table 4.12. Cone angles for ligands bound to phosphorus (PR₃) and for ligands bound to a metal atom (based on a covalent metal radius of 1.32 Å). ^(a) The maximum and minimum angles are 130° and 80°. ⁶⁰

In general there is an increase in the dihedral angle which is similar to the gradual increase in cone angle:

$$\theta_c \quad \text{TIQLEK} > \mathbf{34} > \text{GEXZOY} > \text{TIQLOU} > \mathbf{36} \sim \mathbf{39}$$

$$\theta(\text{dihedral}) \quad \text{TIQLEK} > \mathbf{34} > \text{TIQLOU} > \mathbf{36} > \text{GEXZOY} > \mathbf{39}$$

The one exception to the decreasing trend is GEXZOY which can possibly be attributed to the inclusion a more bulky isopropyl group at the R₁ position, replacing the phenyl, and reducing the effect of the imino substituent.

The variation of the bond angles about the central metal is dependent on the steric volume of the imino group and the dihedral angle subtended, Table 4.13.

	[Zn(23-H) ₂] (34)		[Zn(26-H) ₂] (36)		[Zn(27-H) ₂] (39)	
	L(A)	L(‘)	L(A)	L(‘)	L(A)	L(B)
N(42)-Zn(1)-S(5)	105.03(9)	105.03(9)	104.07(8)	104.07(8)	102.36(7)	103.32(7)
N(42A)-Zn(1)-S(5B)	110.19(9) ^(a)		117.40(8) ^(a)		118.31(7)	
N(42B)-Zn(1)-S(5A)	110.19(9) ^(a)		117.40(8) ^(a)		121.65(7)	
N(42A)-Zn(1)-N(42B)	117.44(19) ^(a)		101.47(14) ^(a)		100.58(9)	
S(5A)-Zn(1)-S(5B)	108.81(7) ^(a)		112.49(6) ^(a)		111.15(4)	

Table 4.13. Donor-metal-donor angles (°) in [Zn(23-H)₂] (34), [Zn(26-H)₂] (36), [Zn(27-H)₂] (39). ^(a) The two ligands are related by the symmetry operation -x, y, ½-z.

The greatest and maximum deviation from the ideal 109.5° is observed for the N-Zn-N angle in **34**, which is attributed to the steric influence of the *t*-Bu group. Consequently the S(5A)-M(1)-S(5’) angle is smaller producing a S⋯S *intramolecular* distances for **34** of 3.7463(18) Å close to the sum of the van der Waals radii (3.6 Å).⁶¹ The slight distortion towards a *trans* geometry in **34**, with a dihedral angle of 91.8°, produces a non-bonded donor atom distance, N(42A)⋯N(42’) of 3.480(5) Å. In the phenyl and 4-*t*-butylphenyl substituted complexes, **36** and **39** respectively, the distribution of bond angles around the metal centre changes significantly, compared to those in **34**, such that the N(42A)-Zn(1)-S(5’) and N(42’)-Zn(1)-S(5A) angles between the two ligands deviate the greatest from the ideal 109.5°, Table 4.13. The less bulky phenyl containing imino groups cause a decrease in the N(42A)-Zn(1)-N(42’) angle and an increase in S(5A)-Zn(1)-

S(5') angle which are reflected by a decrease in the N(42A)···N(42') separation and an increase in the S(5A)···S(5') distance. In comparison, the S···S *intramolecular* distances in TIQLEK are significantly greater (~ 0.6 Å) than the sum of the van der Waals radii (Table 4.11) relating to the large *trans*-distorted dihedral angle (~97°).

4.4.2.2 Structural effects of *t*-Bu, Ph and 4-*t*-BuPh imino substituents on the cobalt(II) complexes.

The three cobalt structures **35**, **37** and **40** are isomorphous with their analogous zinc complexes **34**, **36** and **39** respectively, Figures 4.19(b), 4.20(b) and 4.21(b). The majority of bond lengths and angles in the chelate rings are also similar to those in the respective zinc complex, Table 4.14.

Only one crystallographically characterised cobalt complex of relevance here has been reported in the literature.⁶² This is a 5-coordinate [Co^{II}L].N-methylimidazole complex with the chelating tetradentate bis-(1-phenyl-3-methyl-pyrazol-5-thiolato)-4-phenylenedialdimino ligand unit, Figure 4.27.

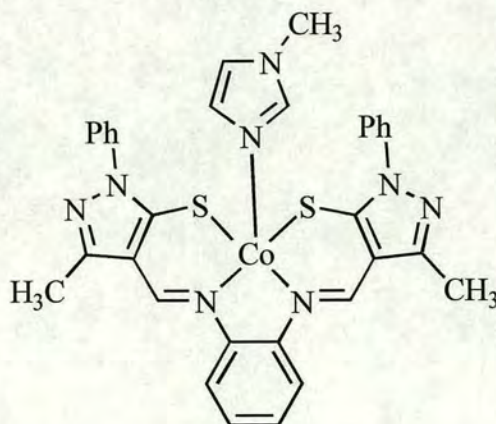


Figure 4.27. Bis-(1-phenyl-3-methyl-pyrazol-5-thiolato)-4-phenylenedialdimino cobalt(II) N-methylimidazole.

The structure consists of a 5-coordinated cobalt(II) centre bound to one tetradentate pyrazol-5-thiolato unit and one N-methylimidazole molecule in a distorted trigonal bipyramid. In this case the inflexible phenylene bridge prevents the formation of the more thermodynamically favourable 4-coordinate tetrahedral structure.

	[Co(23-H) ₂] (35) ^(a)		[Co(26-H) ₂] (37) ^(a)		[Co(27-H) ₂] (40)	
	L(A)	L(′)	L(A)	L(′)	L(A)	L(B)
N(1)-C(5)	1.363(9)	1.363(9)	1.358(6)	1.358(6)	1.357(4)	1.354(4)
N(1)-N(2)	1.397(10)	1.397(10)	1.386(5)	1.386(5)	1.385(4)	1.392(4)
N(2)-C(3)	1.313(9)	1.313(9)	1.320(6)	1.320(6)	1.317(4)	1.311(4)
N(1)-C(11)	1.419(10)	1.419(10)	1.425(6)	1.425(6)	1.427(4)	1.421(4)
C(3)-C(4)	1.416(9)	1.416(9)	1.416(6)	1.416(6)	1.414(5)	1.427(4)
C(3)-C(31)	1.491(9)	1.491(9)	1.485(7)	1.485(7)	1.498(5)	1.490(5)
C(4)-C(41)	1.432(9)	1.432(9)	1.414(7)	1.414(7)	1.414(5)	1.416(4)
C(4)-C(5)	1.407(10)	1.407(10)	1.404(6)	1.404(6)	1.409(5)	1.406(4)
C(41)-N(42)	1.287(8)	1.287(8)	1.301(6)	1.301(6)	1.298(4)	1.297(4)
N(42)-C(43)	1.512(9)	1.512(9)	1.446(6)	1.446(6)	1.427(4)	1.434(4)
C(5)-S(5)	1.718(8)	1.718(8)	1.712(5)	1.712(5)	1.711(3)	1.724(3)
S(5)-C(5)-C(4)	129.6(6)	129.6(6)	132.0(4)	132.0(4)	132.6(3)	130.2(3)
C(5)-C(4)-C(41)	131.5(7)	131.5(7)	130.0(4)	130.0(4)	129.0(3)	130.5(3)
C(4)-C(41)-N(42)	128.8(7)	128.8(7)	127.6(5)	127.6(5)	126.5(3)	127.1(3)
C(41)-N(42)-Co(1)	122.8(5)	122.8(5)	124.7(4)	124.7(4)	125.1(2)	123.8(2)
C(5)-S(5)-Co(1)	103.2(3)	103.2(3)	102.09(18)	102.09(18)	100.89(12)	101.67(12)

Table 4.14. Selected bond lengths (Å) and angles (°) in the chelate units of its complexes [Co(23-H)₂] (35), [Co(26-H)₂] (37) and [Co(27-H)₂] (40). ^(a) The two independent ligands are crystallographically related by the symmetry operation -x, y, ½-z.

The replacement of Zn(II) with Co(II) in complexes 35, 37 and 39 brings about only subtle changes in the disposition of the donor atoms around the central cobalt with

dihedral angles 90.5° , 81.5° and 78.5° respectively, approximately equal to those of the analogous zinc complexes. This is partly attributed to the similarity of the ionic radii⁶³ for tetrahedral Zn^{2+} (0.60 Å) and Co^{2+} (0.58 Å) cations and the imposed CFSE in those complexes containing cobalt. Tetrahedral high spin d^7 Co(II) has an associated CFSE which, conceivably, plays an important role in determining the solid state structures of its complexes with crystal-packing forces contributing slightly to the overall energy of the system. Ligand field considerations are not applicable to the zinc complexes and it is therefore plausible that the distortions observed in the solid state structures (Section 4.4.2.1) may be dominated by crystal-packing forces. However, the isomorphous structures seen for the analogous Zn(II) and Co(II) complexes may suggest that crystal-packing forces in the zinc complexes are minimal.

The arguments used in Section 4.4.2.1 are applicable in relation to the observed tetrahedrality of **35**, **37** and **40** and the effect of the imino substituent on the geometry. Similar trends, although less pronounced and occasionally crystallographically insignificant, are observed for the measured parameters in the cobalt complexes.

The metal-donor distances approximate to the difference in ionic radii. The Zn-S and Zn-N bonds (Table 4.11) are marginally longer than the Co-S and Co-N bond lengths (~ 0.01 Å and ~ 0.03 Å respectively), Table 4.15.

	[Co(23-H) ₂] (35)		[Co(26-H) ₂] (37)		[Co(27-H) ₂] (40)	
	L(A)	L(′)	L(A)	L(′)	L(A)	L(B)
Co(1)-N(42)	2.026(6)	2.026(6)	1.997(4)	1.997(4)	2.003(3)	1.994(3)
Co(1)-S(5)	2.276(3)	2.276(3)	2.2758(15)	2.2758(15)	2.2695(10)	2.2657(11)
N(42)-Co(1)-S(5)	103.97(18)	103.97(18)	103.49(13)	103.49(13)	102.15(8)	102.58(8)
N(42)⋯S(5)	3.392(7)	3.392(7)	3.359(4)	3.359(4)	3.328(3)	3.328(3)
N(42A)⋯N(42B)	3.512(9) ^(a)		3.163(6) ^(a)		3.133(4)	
S(5A)⋯S(5B)	3.634(4) ^(a)		3.713(2) ^(a)		3.6767(15)	
N(42A)-Co(1)-S(5B)	111.07(18) ^(a)		118.22(14) ^(a)		121.05(8)	
N(42B)-Co(1)-S(5A)	111.07(18) ^(a)		118.22(14) ^(a)		120.66(8)	
N(42A)-Co(1)-N(42B)	120.1(4) ^(a)		104.8(2) ^(a)		103.24(11)	
S(5A)-Co(1)-S(5B)	105.94(14) ^(a)		109.31(9) ^(a)		108.33(4)	
θ	90.5		81.5		78.5	

Table 4.15. Metal donor bond lengths (Å), angles (°), chelate bite distances (Å) and dihedral angles (θ°) defined by the chelates, together with the remaining bond angles at the metal in [Co(23-H)₂] (35), [Co(26-H)₂] (38) and [Co(27-H)₂] (40). ^(a) The two ligands are related by the symmetry operation -x, y, ½-z.

The bite distance expands less to accommodate the Co(II) than required for Zn(II) with the observed variation in the bite distance **35** > **37** > **40** following the same order for the ligand units as before. This correlates with the increase in chelate angle along these series, Table 4.15. The increase in the bite distance for each Zn(II) complex compared to its isomorphous Co(II) complex reflects the slight increase in size of the central metal. An increase of 0.285 Å is observed for HL (23) and HL (27) on complexation with cobalt whereas a larger increase on complexation with zinc of 0.341 Å for HL (23) and 0.337 Å for ligand A and 0.347 Å for ligand B of HL (27) is observed. In addition the chelate rings again approximate to planarity

with the greatest deviation occurring with the phenyl imino substituted complex **35** (r.m.s. deviation from the plane 0.012 Å, max. dev. S(5) = 0.018 Å). Similarly the chelate rings in the 4-*t*-butylphenyl substituted complex **40** are distorted from planarity, again with the metal atom deviating out of the plane the furthest (r.m.s deviation from the plane 0.106 Å, max. dev. Co(1) = 0.168 Å **40** ligand B). Overall the planarity is slightly more pronounced in the cobalt complexes which might possibly be attributed to the smaller cobalt ion having a radii more suited to the ideal bite distance produced by the ligand.

	Torsion	[Co(26-H) ₂] (37) ^(a)		[Co(27-H) ₂] (40)	
		L(A)	L(*)	L(A)	L(B)
1	C(41)-N(42)-C(43)-C(44)	49.9(7)	49.9(7)	42.8(5)	138.1(4)
2	C(41)-N(42)-C(43)-C(48)	126.7(5)	126.7(5)	142.3(4)	45.3(5)

Table 4.16. Selected torsion angles in [Co(26-H)₂] (**38**) and [Co(27-H)₂] (**40**).

^(a) The two ligands are related by symmetry operation -x, y, 1/2-z.

4.4.2.3 Bis-(1-phenyl-3-methyl-4-phenylaldimino-pyrazol-5-thiolato) nickel(II).

The nickel complexes of the bidentate enamine pyrazol-5-thione are most common in the CSD and comprise nearly half of the metal complexes of this ligand system, Table 4.8. The most structurally similar for comparison here is the [NiL₂] complex (KIZMAH)⁵⁴ where L is 1-*i*-propyl-3-methyl-4-phenylaldimino-pyrazol-5-thiolato. However the effect of the imino substituent (R₂) on the geometry of the nickel complexes can also be evaluated by comparing the structures of KIZMAH; R₂ = Ph,

KIZLUA; R₂ = Me, GEXZIS; R₂ = cyclohexyl(Cy) and KIZMAH; R₂ = *t*-Bu, Table 4.8.

The nickel complex **38** adopts a highly distorted *cis* square planar geometry with a dihedral angle of 32.5°, Table 4.17. The chelate angle, 97.46(7)°, is far from ideal for square planar geometry and is attributed to the large bite distance (N⋯S; 3.113(2) Å) provided by the presence of the 5-membered annealed pyrazole ring. However it remains smaller (~6-7°) than the chelate angles in the analogous Zn(II) and Co(II) complexes **36** and **37** respectively, which is expected due to the CFSE imposed square planar preference of the Ni(II) cation.

	[Ni(26-H) ₂] (38) ^(a)	
	L(A)	L(°)
Ni(1)-N(42)	1.941(2)	1.941(2)
Ni(1)-S(5)	2.1951(8)	2.1951(8)
N(42)-Ni(1)-S(5)	97.46(7)	97.46(7)
N⋯S	3.113(2)	3.113(2)
N(42)⋯N(42')	2.819(3)	
S(5)⋯S(5')	2.8840(10)	
N(42A)-Ni(1)-S(5')	155.05(7)	
N(42')-Ni(1)-S(5A)	155.05(7)	
N(42A)-Ni(1)-N(42')	93.16(13)	
S(5A)-Ni(1)-S(5')	82.13(4)	
θ	32.5	

Table 4.17. Metal donor bond lengths (Å), angles (°), chelate bite distances (Å) and dihedral angles (θ°) defined by the chelates, together with the remaining bond angles at the metal for in [Ni(26-H)₂] (**38**). ^(a) The two ligands are related by the symmetry operation 1-x, y, ½-z.

The phenyl that is attached to the pyrazole ring is twisted approximately 30° out of the plane (torsion angle's 1-4, Table 4.18). This is approximately 15-20° less than the rotation of the phenyl substituent observed for [Zn(**26-H**)₂] (**36**) and [Co(**26-H**)₂] (**37**) and possibly reflects the flattened nature of the nickel complex produced by the decrease in dihedral angle (~50°). However the rotation (torsion angle's 5 and 6) of the imino phenyl is similar to that observed in **36** and **37**.

	Torsion	[Ni(26-H) ₂] (38)	
		L(A)	L(°)
1	C(5)-N(1)-C(11)-C(12)	31.0(5)	31.0(5)
2	C(5)-N(1)-C(11)-C(16)	148.7(3)	148.7(3)
3	N(2)-N(1)-C(11)-C(12)	153.7(3)	153.7(3)
4	N(2)-N(1)-C(11)-C(16)	26.6(4)	26.6(4)
5	C(41)-N(42)-C(43)-C(44)	44.6(4)	44.6(4)
6	C(41)-N(42)-C(43)-C(48)	135.3(3)	135.3(3)

Table 4.18. Selected torsion angles in [Ni(**26-H**)₂] (**38**).

The chelate ring is twisted and deviates considerably from planarity (r.m.s. deviation from plane 0.142 Å, max. dev. S(5) = 0.212 Å). The deviation from the least squares plane is a result of the propensity of the nickel to impose a planar coordination geometry which is restricted by the steric influence of the phenyl R₂ substituent. As a consequence of the small dihedral angle (32.5°), the angles N(42A)-Ni(1)-N(42'); 93.16(13)° and S(5)-Ni(1)-S(5'); 82.13(4)°, Table 4.17, are significantly smaller than those in **36** and **37**, and relate more closely to that expected for square planar geometry. Of the two, the S(5)-Ni(1)-S(5') angle is the smallest reflecting the steric influence of the imino phenyl substituent, producing a S...S *intramolecular* distance

of 2.8840(10) Å, approximately 0.7 Å shorter than the sum of the van der Waal radii⁶¹ although ~0.8 Å greater than the sum of the covalent radii (2.04 Å).⁴⁹

By comparison the N₂S₂Ni coordination geometry in bis-(1-*i*-propyl-3-methyl-4-phenylaldimino-pyrazol-5-thiolato)nickel(II) complex, (KIZMAH)⁵⁴, approximates more closely to tetrahedral than square planar with a dihedral angle of 68.7° and a chelate angle of 100.2(1)°, Table 4.21. The C-C and C-N bond lengths around the chelate ring are similar to those in **38**, however an increase in the angles around the chelate ring, ~4.2°, (excluding N-Ni-S) provides a larger bite distance, Table 4.19.

	[Ni(26-H) ₂] (38)		KIZMAH
	L(A)	L(°)	L
N(1)-C(5)	1.364(3)	1.364(3)	1.344(6)
N(1)-N(2)	1.392(3)	1.392(3)	1.380(6)
N(2)-C(3)	1.311(3)	1.311(3)	1.311(5)
N(1)-C(11)	1.428(3)	1.428(3)	-
C(3)-C(4)	1.426(4)	1.426(4)	1.419(7)
C(3)-C(31)	1.491(4)	1.491(4)	-
C(4)-C(41)	1.410(4)	1.410(4)	1.412(5)
C(4)-C(5)	1.398(4)	1.398(4)	1.403(5)
C(41)-N(42)	1.298(3)	1.298(3)	1.300(6)
N(42)-C(43)	1.445(3)	1.445(3)	-
C(5)-S(5)	1.718(3)	1.718(3)	1.708(4)
S(5)-C(5)-C(4)	127.5(2)	127.5(2)	130.2(4)
C(5)-C(4)-C(41)	126.7(2)	126.7(2)	128.8(5)
C(4)-C(41)-N(42)	126.4(3)	126.4(3)	126.2(4)
C(41)-N(42)-Ni(1)	128.59(18)	128.59(18)	128.5(3)
C(5)-S(5)-Ni(1)	106.04(9)	106.04(9)	105.7(1)

Table 4.19. Selected bond lengths (Å) and angles (°) in the chelate units of the complexes [Ni(26-H)₂] (**38**) and KIZMAH.

The metal-donor distances reflect the nature of their respective coordination geometries, Table 4.20. The Zn-S and Zn-N bond lengths in the tetrahedral zinc complex **36** are longer (~ 0.10 Å and ~ 0.09 Å respectively) than the Ni-S and Ni-N bonds in **38**, similar to the difference between the tetrahedral zinc and square planar nickel ionic radii, 0.11 Å. A smaller difference in these bond lengths (M-S; ~ 0.07 Å and M-N; ~ 0.05 Å) between **36** and the nickel complex, KIZMAH, corresponds closely to the difference in ionic radii between tetrahedral zinc and tetrahedral nickel, 0.05 Å. Likewise the Ni-S and Ni-N bonds in **38** are approximately 0.03 Å and 0.04 Å shorter than in KIZMAH which is expected due to the greater tetrahedral character of the nickel cation in KIZMAH.

Complex	Metal	Ionic radii	M-S / Å	M-N / Å
36	Zn(II)	0.60 (T_d)	2.2977(10)	2.031(3)
37	Co(II)	0.58 (T_d)	2.2758(15)	1.997(4)
38	Ni(II)	0.49 (D_{4h})	2.1951(8)	1.941(2)
KIZMAH	Ni(II)	0.55 (T_d)	2.229(1)	1.984(3)

Table 4.20. The ionic radii⁶³ and metal-donor bond lengths (Å) in $[Zn(\mathbf{26-H})_2]$ (**36**), $[Co(\mathbf{26-H})_2]$ (**37**), $[Ni(\mathbf{26-H})_2]$ (**38**) and KIZMAH.

Comparison of four similar published structures (Table 4.21) highlights the influence of the imino substituent on the dihedral angle of the complex. The reported variations in the dihedral angles, KIZMEL(*t*-Bu) > GEXZIS(Cy) > KIZLUA(Me) > KIZMAH(Ph), correlates well with the increase in the steric size (Table 4.12) of the imino substituents, *t*-Bu > Cy > Ph > Me. The discrepancy in KIZMAH(Ph) displaying a smaller dihedral angle than KIZLUA(Me) can be partly explained by the

phenyl substituents ability to rotate providing a cone angle of 80° which is less than that for methyl (90°), Table 4.12. There is a slight increase in the Ni-S length and consequently in the chelate angle which mirrors the increase in steric volume of the imino substituent as discussed in Sections 4.4.2.1 and 4.4.2.2.

	KIZMAH	KIZLUA		GEXZIS		KIZMEL	
	L	Mol (1)	Mol (2)	L(A)	L(B)	L(A)	L(B)
Ni-S / Å	2.229(1)	2.237(2)	2.247(2)	2.242(1)	2.260(1)	2.253(1)	2.254(1)
Ni-N / Å	1.984(3)	1.957(7)	1.985(7)	1.967(4)	1.997(4)	1.984(4)	1.995(4)
S-Ni-N / °	100.2(1)	100.9(2)	101.8(2)	100.8(1)	100.4(1)	102.0(1)	102.2(1)
θ / °	68.7	81.9	82.4	85.4		96.3	
R ₂ group	Ph	Me		Cy		<i>t</i> -Bu	

Table 4.21. Selected metal-donor distances (Å), chelate angles (°) and dihedral angles (°) in KIZMAH, KIZLUA, GEXZIS and KIZMEL.

This increase in the steric volume of the imino substituent, which favours the formation of tetrahedral high spin complexes, has its limitations. The incorporation of bulky *ortho*-methyl substituents to the imino phenyl group (YUDNUG, Table 4.8) leads to the formation of a *trans*-planar N₂S₂ donor atom arrangement. It is suggested that the stabilisation of the low spin planar isomer may be explained by the requirements to minimise the steric interactions of the two 2,6-dimethylphenyl groups which is accompanied by a large twist away from the plane of the chelate ring (torsion angles ~70°).

	[Zn(33-H) ₂] (42)	
	L(A)	L(B)
Zn(1)-N(42)	1.996(2)	1.993(2)
Zn(1)-O(5)	1.9629(19)	1.947(2)
N(42)-Zn(1)-O(5)	98.91(8)	100.29(9)
N(42)···O(5)	3.008(3)	3.025(3)
N(42A)···N(42B)	3.338(3)	
O(5A)···O(5B)	3.168(3)	
N(42A)-Zn(1)-O(5B)	120.39(9)	
N(42B)-Zn(1)-O(5A)	116.26(9)	
N(42A)-Zn(1)-N(42B)	113.59(10)	
O(5A)-Zn(1)-O(5B)	108.23(8)	
θ	84.2	

Table 4.22. Metal donor bond lengths (Å), angles (°), chelate bite distances (Å) and dihedral angles (θ°) defined by the chelates, together with the remaining bond angles at the metal in [Zn(33-H)₂] (42).

As mentioned in Section 4.4.2.1 the ligands exhibit an imino-thiolato tautomeric character although there is extensive electron delocalisation around the chelate ring. Substitution of sulfur for oxygen appears to marginally increase the enamine-ketone character of the chelate ring. The C(5)-O(5) bond lengths in ligand A; 1.281(3) Å and ligand B; 1.298(3) Å are approximately 0.15 Å shorter than the sum of the covalent radii (~1.43 Å)⁴⁹ and exhibit a greater double bond character than the C-S bond length in **39**. The reduction in the imino character is also evident around the chelate ring with the C(4)-C(5) and C(41)-N(42) bonds lengths approximately 0.01-0.02 Å longer than those in **39**, exhibiting a greater single bond character whereas C(4)-C(41) is approximately 0.015 Å shorter and exhibits a greater double bond character, Figure 4.29.

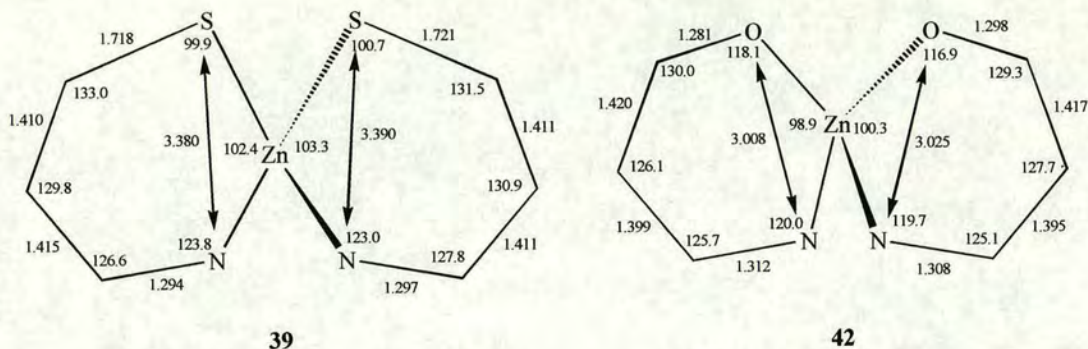


Figure 4.29. Comparison of the chelate ring geometries in $[\text{Zn}(\mathbf{27-H})_2]$ (**39**) and $[\text{Zn}(\mathbf{33-H})_2]$ (**42**).

The C(5)-O(5) bond lengths, Table 4.23, are approximately 0.34 Å shorter than the C(5)-S(5) in **39**, effectively reducing the N...O bite distance (3.008(3) Å in ligand A and 3.025(3) Å in ligand B) by ~0.37 Å in **42**. Generally the angles around the chelate ring, O(5) to N(42), decrease slightly with the exception of C(5)-O(5)-Zn(1) which increases by approximately 18°. However the limited bite restricts the chelate angles to 98.9° and 100.3° for ligand A and ligand B respectively in **42**. The shorter C(5)-O(5) bond results in a more symmetrical geometry around the central zinc in **42** than in **39** with Zn-O and Zn-N bonds comparable in length (~0.03-0.04 Å), Table 4.22. This is in contrast with the large difference in bond lengths between Zn-S and Zn-N (~0.25-0.27 Å). However Zn-N in **42** is shorter (0.03-0.05 Å) than Zn-N in **39** which can possibly be attributed to the greater enamine character of the longer C(41)-N(42) bond in the former.

	[Zn(33-H)₂] (42)	
	L(A)	L(B)
N(1)-C(5)	1.362(3)	1.352(4)
N(1)-N(2)	1.401(3)	1.407(3)
N(2)-C(3)	1.305(3)	1.303(4)
N(1)-C(11)	1.425(3)	1.422(4)
C(3)-C(4)	1.420(4)	1.422(4)
C(3)-C(31)	1.498(4)	1.496(4)
C(4)-C(41)	1.399(4)	1.395(4)
C(4)-C(5)	1.420(4)	1.417(4)
C(41)-N(42)	1.312(3)	1.308(3)
N(42)-C(43)	1.432(3)	1.430(4)
C(5)-O(5)	1.281(3)	1.298(3)
O(5)-C(5)-C(4)	130.0(3)	129.3(3)
C(5)-C(4)-C(41)	126.1(3)	127.7(3)
C(4)-C(41)-N(42)	125.7(3)	125.1(3)
C(41)-N(42)-Zn(1)	119.95(19)	119.7(2)
C(5)-O(5)-Zn(1)	118.08(17)	116.87(18)

Table 4.23. Selected bond lengths (Å) and angles (°) in the chelate units of the [Zn(33-H)₂] (42) complex.

4.4.2.5 Continuous symmetry measures.

The observed “tetrahedrality” of the complexes can be measured by continuous symmetry measures (CSM, described in Section 3.4). By generating 4-coordinate models the CSM can be evaluated to determine the consequence of changing the dihedral and chelate angles, Figure 4.30. Two models were generated in which the chelate angle was fixed at 90° (similar to those found in the bis-pyridinethionato complexes, Chapter 3) and 109.5° (ideal for tetrahedral geometry) and the dihedral angle between the two planes adjusted between 0° and 90°.

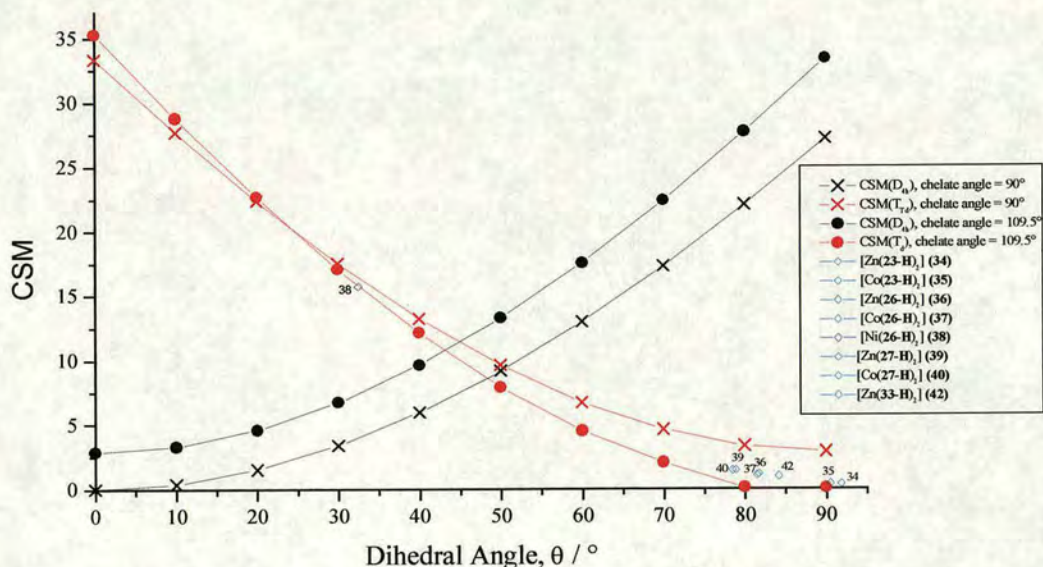


Figure 4.30. Ideal continuous symmetry measures (D_{4h} and T_d) of 4-coordinate donor atom arrays with fixed chelate angles of 90° and 109.5° and complexes **34-42**.

When the chelate angle is fixed at 90° in a square planar array the $CSM(D_{4h})$ is zero. As the dihedral angle increases so does the CSM to a maximum of ~ 27 where the two chelate planes are mutually orthogonal to each other. A similar increase in the $CSM(D_{4h})$ is attained for the model containing a fixed chelate angle of 109.5° although larger values are observed reflecting the inappropriately large chelate angle which is less suitable for planar geometries, and as expected the minimum CSM is greater than zero (~ 3) when the atoms lie in a plane. When the chelate angle is fixed at 109.5° and the dihedral angle is 90° the donor atom array describes a perfect tetrahedron with a $CSM(T_d)$ equal to zero. Similarly an offset from zero is incurred for the model with a fixed chelate angle of 90° , which is now unsuitable for tetrahedral geometries. However a crossover appears when the dihedral angle is reduced to 20° , after which the model with a fixed chelate angle of 109.5° becomes

less tetrahedral than the model with the 90° chelate angle with further decreases in the dihedral angle.

The models are based on Cartesian coordinates in which ideal chelate angles are preserved and the four metal-donor distances are equal. In the crystal structures described above for bis-pyrazol-5-thiolato (**34-40**) and bis-pyrazol-5-olato (**42**) complexes the metal-donor distances are unequal and the chelate angle is neither fixed or 109.5° but rather varies between 97.5 and 105°. However they do display values that coincide with those expected for the given dihedral angle, Figure 4.30. The graph indicates that a distortion from either planarity or a tetrahedron of 10-15° is mostly dependent on the chelate angle, *i.e.* the bite distance. Thereafter larger distortions become increasingly dominated by the dihedral angle. The zinc and cobalt complexes have tetrahedral CSM's which group around a value of 0-1.5, Table 4.24.

	CSM	
	T _d	D _{4h}
[Zn(23-H) ₂] (34)	0.33	30.77
[Zn(26-H) ₂] (36)	1.11	27.19
[Zn(27-H) ₂] (39)	1.42	25.23
[Zn(33-H) ₂] (42)	0.96	26.59
[Co(23-H) ₂] (35)	0.36	31.00
[Co(26-H) ₂] (37)	1.02	26.57
[Co(27-H) ₂] (40)	1.41	24.57
[Ni(26-H) ₂] (38)	15.69	4.77

Table 4.24. Continuous Symmetry Measures for pyrazol-5-thiolato and pyrazol-5-olato complexes.

Clearly it is difficult to differentiate between these relative values without questioning the precision but they do seem follow the general order relating to the increase in dihedral angle associated with the increase in steric volume of the imino substituent. Furthermore, replacement of sulfur in $[\text{Zn}(\mathbf{27-H})_2]$ (**39**) by oxygen, $[\text{Zn}(\mathbf{33-H})_2]$ (**42**), results in an increase in “tetrahedrality” which can be explained by the similarity of the M-O and M-N distances producing a more symmetrical geometry.

A question that arises from these observations is; in-light of the small decrease in “tetrahedrality” observed with a distortion of 10-15° from a tetrahedral geometry will the perceived loss in complex stability be as insignificant? Therefore will there be a stability advantage for an extractant capable of complexing with near perfect tetrahedral geometry as opposed to one that is not so perfect in order to gain maximum strength and selectivity during the solvent extraction process? The CSM only considers the geometrical aspect of the complex and does not take into consideration the electronic properties or CFSE. In the case of Zn(II), where there is no ligand-field considerations, this is reasonable and a geometry approximately tetrahedral will probably suffice. However for Co(II) and Ni(II), where the CFSE must be considered, distortions away from a tetrahedral geometry will effect the stability considerably more.

4.5 Solvent extraction of Zn(II), Co(II), Ni(II) and Cu(II) with 1-substituted-3-methyl-4-(alkylaldenamine)-pyrazol-5-thiones.

The aim of this section can be divided into two parts; firstly, to evaluate the selectivity and “strength” of a range of different substituted imino-pyrazol-5-thiones

as extraction candidates, and secondly, to relate the observed selectivity and extractant “strength” to: (1) the ligand acidity (pK_a), (2) ligand solubility and (3) the proposed stability of the extracted metal complex in relation to the degree of distortion away from a tetrahedral geometry.

Extraction of zinc(II), cobalt(II), nickel(II) and copper(II) using a number of imino-pyrazol-5-thiones from either a single metal or multi-metal sulfate solution (see Section 4.11.1 for procedure) into toluene or Orform SX-7 (a hydrocarbon solvent) was investigated as a function of pH. The data has been analysed graphically, in the form of “S-curves”, and in one instance numerically to determine the stoichiometry of the extracted species (Section 4.5.2).

4.5.1 Factors affecting the “S-curve” shape.

The shape of the “S-curve” is important in determining the composition of the extracted metal species (see Section 4.5.2). In the examples discussed below this shape can vary quite markedly. There are many factors that can influence the shape and consequently affect the observed $pH_{1/2}$. In an ideal situation the measured $pH_{1/2}$ reflects only the equilibrium between species in solution. However there are many factors which can affect this equilibrium which may include:

1. The formation of precipitates resulting from insufficient solubility of the extracted metal species (see section 4.5.1.1).
2. Competing metal hydrolysis at high pH (see Section 4.5.1.2).
3. Different distributions of the ligand and the extracted complexes between the aqueous and organic phases due to different solubilities.

4. The formation of different species in the organic phase, *e.g.* $ML_n.mHL$.
5. The degree of solvation of the metal cation, the ligand and the extracted complex which may affect the solubility and rate of extraction.
6. Entrainment of “crud” which may affect the phase disengagement and the time taken to filter each sample, resulting in an increase in the mass balance error (see Appendix VI).

4.5.1.1 Solubility determination of zinc(II) complexes.

The extractant and the extracted metal species must be sufficiently soluble to remain in solution over the pH range at which extraction occurs. A ligand concentration of 0.05 M is used in the extraction experiments (see Section 4.11.1), therefore when the organic phase is fully loaded (assuming a 1:2 metal/ligand complex ratio) the required solubility for the metal species is 0.025 M. If the solubility is less than this minimum value then precipitation of the metal species will occur resulting in an effective loss of metal from the system which will distort the true solution equilibrium, ultimately altering $pH_{1/2}$.

The solubility of the zinc complexes, in toluene, of the imino-pyrazol-5-thione ligands (**23-33**) and the azo-pyrazol-5-thione ligands (**48** and **49**) is shown in Table 4.25. The solubilities were determined in a two phase (toluene/water) system similar to that used in the solvent extraction experiments. The protocol that was followed involved the dissolution of a known amount of ligand in toluene at 70 °C. An aqueous solution of zinc acetate dihydrate in a 2-fold excess was added to this

followed by an equivalent amount of 1 M NaOH to ensure full deprotonation of the ligand. The mixture was then vigorously stirred at 70 °C for 1 hour then left to cool for three days. The toluene phase was then filtered to remove the zinc complex precipitate and the resulting solution analysed using ICP-OES to determine the zinc content and hence the maximum solubility of the zinc complex.

[M(L-H)₂]	R₁	R₂	Solubility / M
HL (23)	Ph	<i>t</i> -Bu	7.0 x 10 ⁻⁴
HL (24)	Ph	Cy	3.6 x 10 ⁻²
HL (25)	Ph	2-EtHex	1.6 x 10 ⁻¹
HL (26)	Ph	Ph	-
HL (27)	Ph	4- <i>t</i> -BuPh	3.9 x 10 ⁻²
HL (28)	Ph	4-NO ₂ Ph	4.3 x 10 ⁻⁴
HL (29)	Me	2-EtHex	4.0 x 10 ⁻¹
HL (30)	Me	4- <i>t</i> -BuPh	9.9 x 10 ⁻²
HL (31)	Me	4-nonylphenyl	2.0 x 10 ⁻¹
HL (32)	Me	<i>o</i> -fluorophenyl	1.7 x 10 ⁻¹
HL (48)	Ph	Ph	2.5 x 10 ⁻²
HL (49)	Ph	4- <i>t</i> -BuPh	2.2 x 10 ⁻²

Table 4.25. The solubility in toluene of the zinc(II) complexes of the imino-pyrazol-5-thione ligands (23-32) and the azo-pyrazol-5-thione ligands (48 and 49).

Most of the zinc(II) complexes have sufficient solubility to be used under the solvent extraction conditions with the exception of HL (23), HL (28). An additional exception is HL (32). Although its zinc complex solubility (1.7 x 10⁻¹ M in toluene) is sufficient for solvent extraction (0.025 M), the ligand itself did not meet the

solubility requirement of 0.05 M. In general when the phenyl group at R₁ is replaced with a methyl substituent the solubility is increased. The examples shown here, HL (25) → HL (29) and HL (27) → HL (30), both benefit from a 2 ½ fold increase in solubility. In addition to a methyl group at the R₁ position the solubility is, as expected, enhanced when the substituent at the R₂ position is an alkyl chain *i.e.* 2-ethylhexyl.

A common observation during solvent extraction experiments is that the zinc(II) complexes are generally slightly more soluble than the respective cobalt(II) complexes, which are in turn usually more soluble than those for nickel(II). In comparison the solubility of the extracted copper complexes is usually very low (Figure 4.31) resulting in copious precipitation.

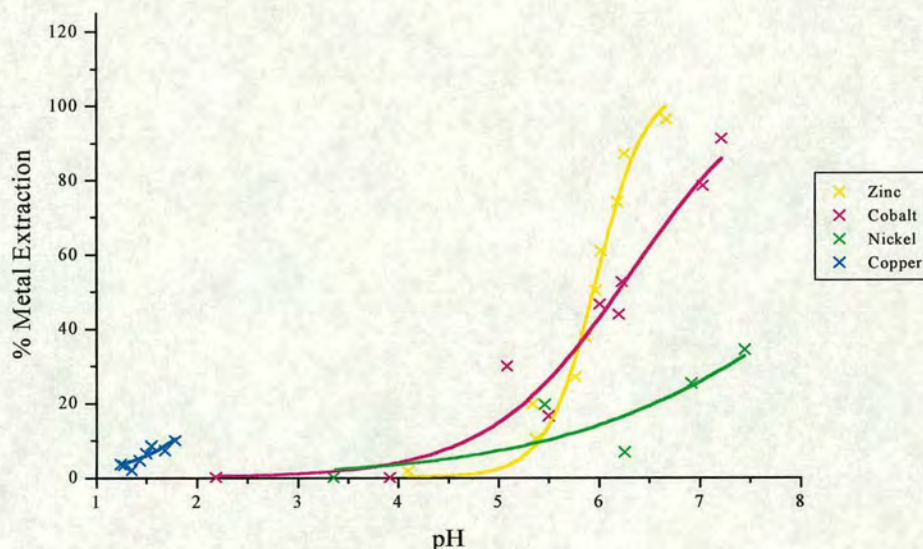


Figure 4.31. Single metal extraction of Zn(II), Co(II), Ni(II) and Cu(II) with 0.05 M 1-phenyl-3-methyl-4-cyclohexylaldenamine-pyrazol-5-thione (24) in toluene.

The implication of solubility on the shape of the “S-curve is evident from the extraction of Zn(II), Co(II) and Ni(II) using 1-phenyl-3-methyl-4-cyclohexylaldenamine-pyrazol-5-thione (**24**), Figure 4.31. The extraction of zinc produces the expected S-curve shape with the individual data points lying close to the calculated sigmoidal curve, generated using Origin.⁶⁴ However the calculated S-curves for the cobalt and nickel extractions are flattened with the data points more scattered. One possible explanation for this is the limiting solubility of the extracted species resulting in a poor mass balance (see Appendix VI) and the absence of a true solution equilibrium. Further examples of “flattened” S-curves are observed for the extraction of cobalt (Figure 4.38) and nickel (Figure 4.39) using 1-phenyl-3-methyl-4-(4-*t*-butylphenylaldenamine)-pyrazol-5-thione (**27**). An alternative explanation, or an additional factor, which may affect the shape of the extraction curve and promote its flattening is competing hydrolysis at high pH (see Section 4.5.1.2).

In other circumstances the extraction curve is much steeper (cobalt extraction by HL (**31**), Figure 4.32) which is attributed to the lack of extraction data points around key areas such as the two inflexions, *i.e.* in the initial and final 25 % loading of the organic phase.

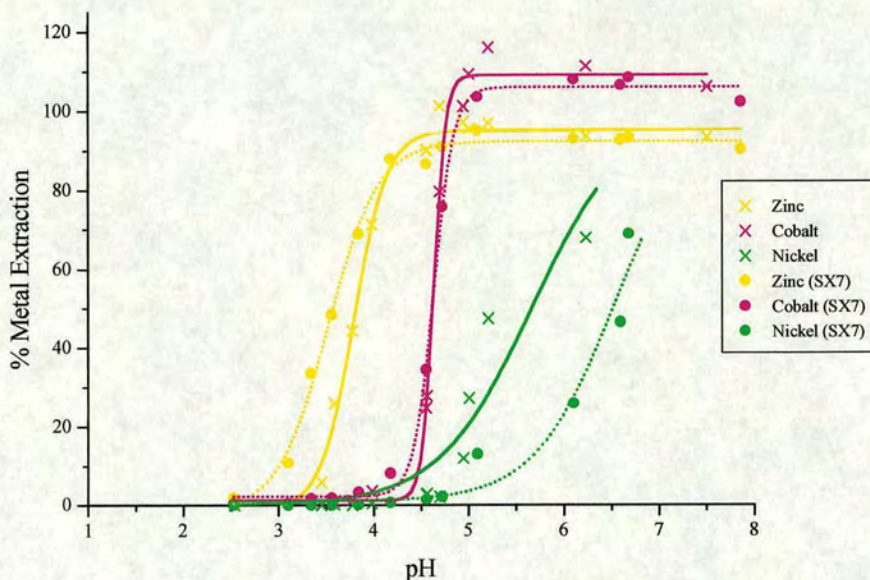
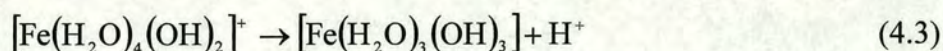
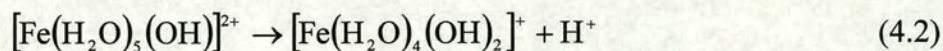
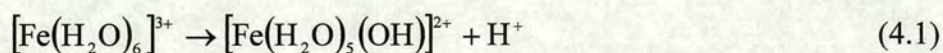


Figure 4.32. Multi-metal extraction of Zn(II), Co(II) and Ni(II) with 0.05 M 1,3-dimethyl-4-(4-nonylphenylaldenamine)-pyrazol-5-thione (**31**) in toluene and SX-7 at ambient temperature.

4.5.1.2 Metal hydrolysis at high pH.

Metal ions in aqueous solution are highly solvated by H₂O molecules. The loss of protons from bound water takes place readily producing an acidic solution and successively replaces each water molecule with a hydroxyl ion. For example iron(III) reacts until an uncharged species is formed (Equations 4.1 to 4.3).



This process is known as hydrolysis and when the metal ions become electrically neutral, the ionic forces keeping them apart are removed and precipitation occurs, Equation 4.4.



As the pH of the solution increases, for example in the loading of metal in the organic phase in solvent extraction, the equilibrium shifts to the right and can become a competing process. Metal hydroxides are produced at different pH's depending on the metal and its oxidation state. The pH at which some metal ions hydrolyse are shown in Table 4.26.

Metal	pH
Fe ³⁺	2.0
Cu ²⁺	5.3
Ni ²⁺	6.7
Co ²⁺	6.8
Zn ²⁺	7.0

Table 4.26. The pH at which hydroxide precipitation occurs from 0.02 M solutions.⁶⁵

The hydrolysis of iron(III) at ~ pH 2 implies that the extractant must be operate in the extraction circuit at a pH lower than 2 to prevent the detrimental precipitation of iron hydroxides.

A noticeable problem in the extractions performed in this study, mostly involving the extraction of nickel, is that some of the ligands operate at pH's where hydrolysis is a competing process.

For example, particularly weak extraction is observed with HL (**25**) and HL (**29**) which both contain the 2-ethylhexyl substituent at the imino R₂ position, Figures 4.33 and 4.34 respectively. For these two ligands, zinc(II) and copper(II) ions are fully extracted well below the pH at which hydrolysis occurs. However the pH range over which cobalt(II) and nickel(II) are extracted overlaps with the pH at which hydrolysis of the respective ions occurs and therefore the true solution extraction equilibrium must be affected.

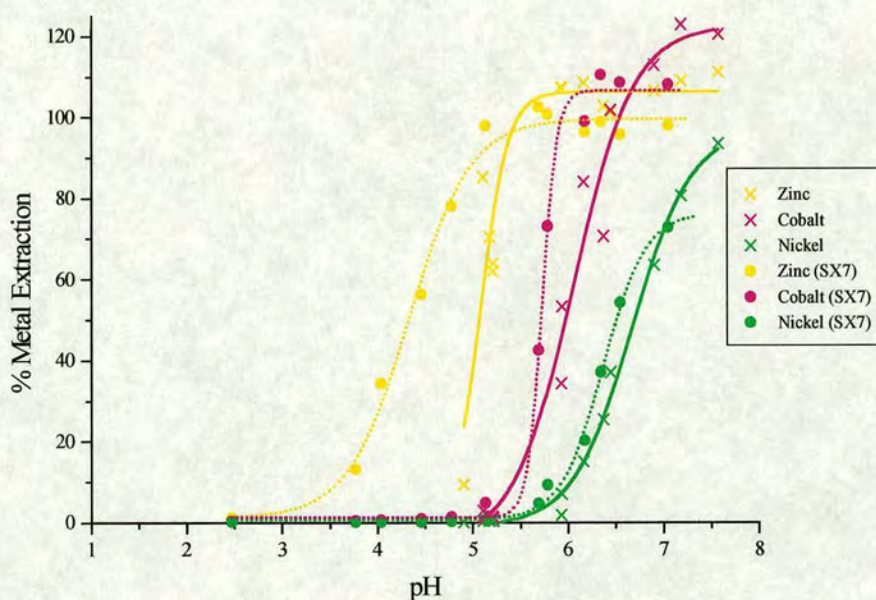


Figure 4.33. Multi-metal extraction of Zn(II), Co(II) and Ni(II) with 0.05 M 1-phenyl-3-methyl-4-(2-ethylhexylaldenamine)-pyrazol-5-thione (**25**) in toluene and SX-7 at ambient temperature.

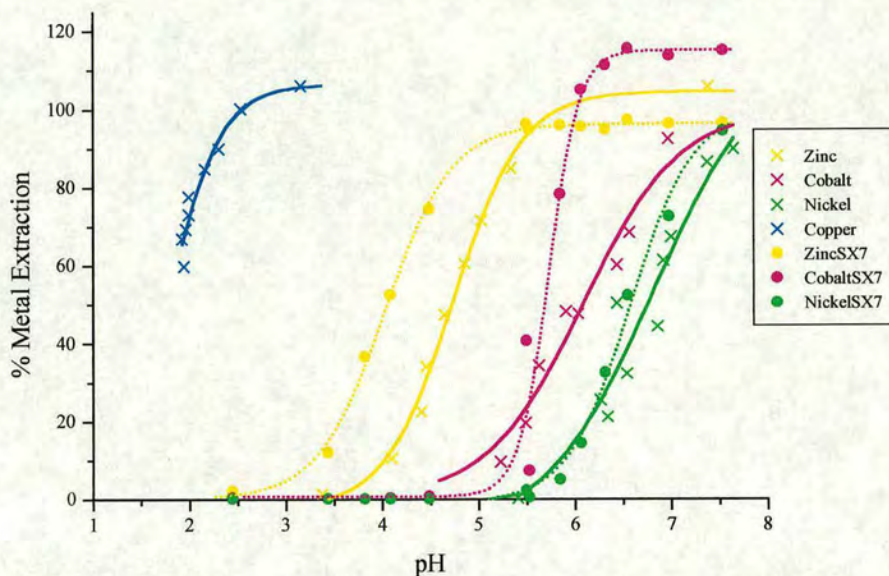


Figure 4.34. Multi-metal extraction of Zn(II), Co(II) and Ni(II) in SX-7 and single metal extraction of Zn(II), Co(II), Ni(II) and Cu(II) in toluene with 0.05 M 1,3-dimethyl-4-(2-ethylhexylaldenamine)-pyrazol-5-thione (**29**) at ambient temperature.

4.5.2 Stoichiometry of the extracted metal species.

The extraction of zinc(II), cobalt(II) and nickel(II) from a sulfate feed stream with 1,3-dimethyl-4-(4-*t*-butylphenylaldenamine)-pyrazol-5-thione (**30**) is shown in Figure 4.35.

The stoichiometric determination of the extracted metal species was performed using HL (**30**) due to the good solubility properties of the ligand and extracted metal species which provide smooth well shaped “S-curves” coupled with an acceptable mass balance (Appendix VI, Table 7.16).

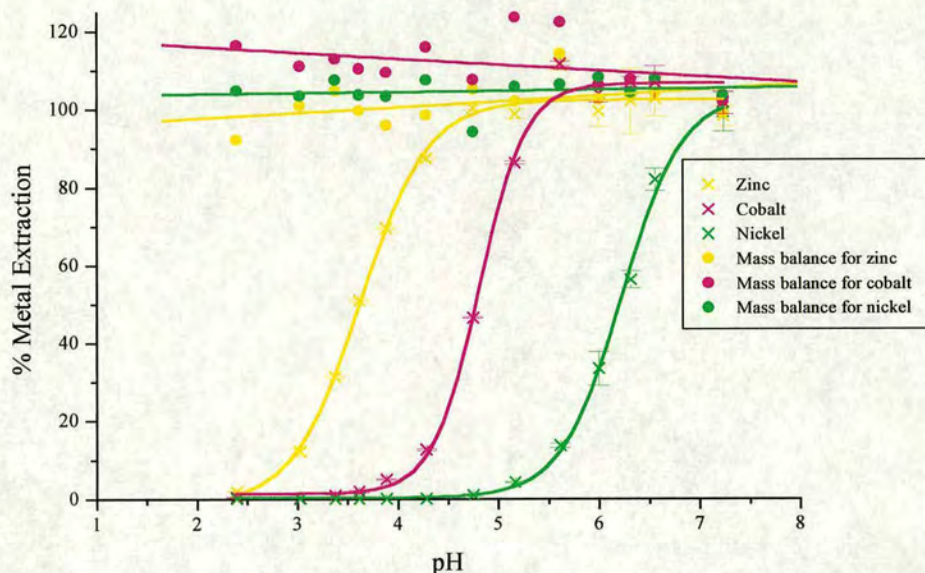
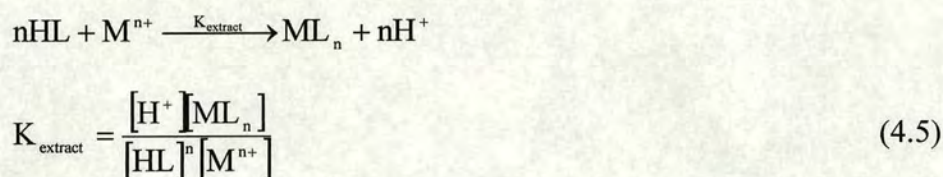


Figure 4.35. Multi-metal extraction of Zn(II), Co(II) and Ni(II) with 0.05 M 1,3-dimethyl-4-(4-*t*-butylphenylaldenamine)-pyrazol-5-thione (**30**) in toluene at ambient temperature.

The equilibrium constant, K_{extract} , involved in the formation of the extracted metal species by a mono-anionic bidentate ligand is expressed in Equation 4.5.



On reaching equilibrium the metal will be distributed between the aqueous and organic phases, depending on the pH. The transfer of metal ions from an aqueous to an organic phase is measured by the distribution coefficient, D , (Equation 4.6) where $[M]$ is the metal concentration.

$$D = \frac{[M]_{\text{org}}}{[M]_{\text{aq}}} = \frac{[ML_n]}{[M^{n+}]} \quad (4.6)$$

The distribution coefficient was calculated from the metal concentration in both the aqueous and organic phases after equilibrium was reached (Appendix VI, Table 7.16).

By combining equations 4.5 and 4.6 an expression relating the distribution coefficient and the extraction constant is obtained, Equation 4.7.

$$\log D = \log K_{\text{extract}} + n\text{pH} + n \log[\text{HL}] \quad (4.7)$$

In order to investigate the stoichiometry of the extracted metal species $\log D$ vs. pH was plotted. At 50 % extraction, *i.e.* when $\text{pH} = \text{pH}_{1/2}$, the distribution of metal between the aqueous and organic phases is theoretically equal and therefore $\log D = 0$ and equation 4.8 is valid.

$$\frac{-\log K_{\text{extract}}}{n} = \text{pH}_{1/2} + \log[\text{HL}]_{1/2} \quad (4.8)$$

Therefore the plot of $\log D$ vs. pH should give a straight line of slope n , where n is the number of protons liberated and indicates the number of deprotonated ligands associated with each metal ion.

The extraction of a stable metal complex into the organic phase requires the metal species to be charge neutral. Therefore the extraction of a divalent metal ion by a mono-anionic bidentate ligand, such as the imino-pyrazol-5-thiones, would require

two ligands, therefore the slope (n) of in the plot of $\log D$ vs. pH should equal 2. The composition of the extracted species was evaluated from the slope of the straight line, Figure 4.36.

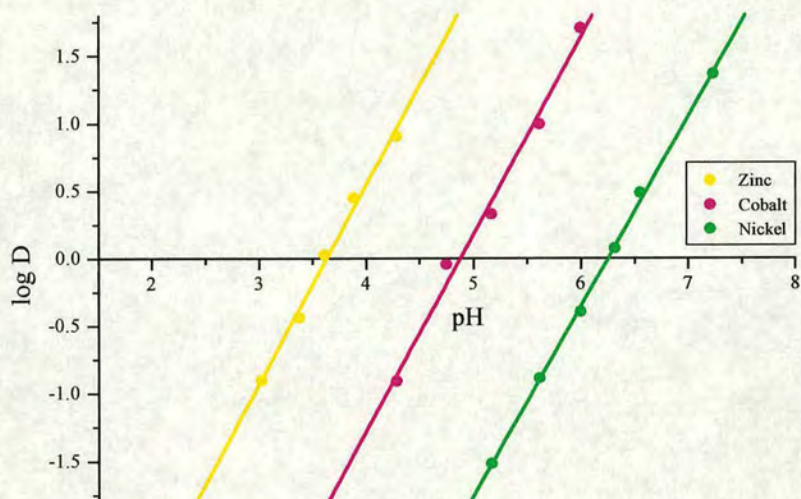


Figure 4.36. Plot of $\log D$ as a function of pH for the extraction of Zn(II), Co(II) and Ni(II) with HL (**30**) in toluene.

For the extraction of Zn(II), Co(II) and Ni(II) with HL (**30**) the slope of the extraction curves (Table 4.27) were found to be approximately 1.5. These results would seem to indicate that the extracted metal species is a 1:1.5 complex and would therefore carry a positive charge, *i.e.* $[ML_{1.5}]^{0.5+}$, making extraction in to the organic phase difficult. It is however more reasonable assume the errors associated with the measurement of the metal concentration in the aqueous and organic phases (see Appendix VI) account for the discrepancy from the expected 1:2 metal/ligand complex ratio and a charge neutral $[ML_2]$ complex is indeed extracted.

	Slope (n)	No. of points	Coefficient
Zn(II)	1.47	5	0.996
Co(II)	1.46	5	0.994
Ni(II)	1.40	6	0.999

Table 4.27. Results of the slope analysis for the determination of the extracted metal species by HL (30) in toluene at ambient temperature.

4.5.3 Effect of the ligand substituents on the extraction selectivity and “strength”.

The pH range over which Co^{2+} , Ni^{2+} , Zn^{2+} and in two cases Cu^{2+} ions are extracted into either toluene or Orform SX-7 was evaluated using a range of substituted imino-pyrazol-5-thiones. Solvent extraction follows the order $\text{Cu}^{2+} > \text{Zn}^{2+} > \text{Co}^{2+} > \text{Ni}^{2+}$ (Figures 4.31 to 4.35) irrespective of the ligand substitution and disagrees with the “normal” order of stability for complex formation defined by Irving and Williams (see Section 1.4.2.2). The structural influence of the imino-pyrazol-5-thiones and their propensity to adopt a tetrahedral coordination geometry with divalent metal ions in the solid state (see Section 4.4.2) is key to the determination of the observed selectivity order.

Table 4.28 shows the $\text{pH}_{1/2}$ values for the extraction of Co^{2+} , Cu^{2+} , Ni^{2+} and Zn^{2+} ions with different substituted imino-pyrazol-5-thiones. The extraction of Cu^{2+} ions was hindered by the extremely low solubility of the extracted species and the formation of precipitates. Consequently full extraction curves were not obtained and the $\text{pH}_{1/2}$ values quoted have been estimated by extrapolation. However the pH at which the extractions occurred were sufficiently lower than that of hydrolysis ($\text{pH} \sim 5.3$),

therefore they can be considered as a reasonable approximation to the true $\text{pH}_{1/2}$. However they do highlight the undesirable strong extraction of Cu^{2+} ions which is possibly favoured by the inclusion sulfur donor atoms.

Extractant	$\text{pH}_{1/2}$				Solvent
	Cu(II)	Zn(II)	Co(II)	Ni(II)	
HL (23)	-	$6.2 \pm 0.2^{(a)}$	-	-	Toluene
HL (24)	-	6.0 ± 0.1	6.3 ± 0.1	$8.4 \pm 0.9^{(b)}$	Toluene
HL (25)	-	5.1 ± 0.1	6.1 ± 0.1	6.7 ± 0.1	Toluene
	-	4.3 ± 0.1	5.7 ± 0.1	6.4 ± 0.1	SX-7
HL (27)	$1.7 \pm 0.2^{(a)(b)}$	4.2 ± 0.1	5.9 ± 0.2	6.7 ± 0.2	Toluene
HL(29)	$1.8 \pm 0.1^{(b)}$	4.7 ± 0.1	6.1 ± 0.1	6.8 ± 0.4	Toluene
	-	4.0 ± 0.1	5.7 ± 0.1	6.6 ± 0.1	SX-7
HL (30)	-	3.6 ± 0.1	4.8 ± 0.1	6.2 ± 0.1	Toluene
HL (31)	-	3.8 ± 0.1	4.6 ± 0.1	5.7 ± 0.2	Toluene
	-	3.5 ± 0.1	4.6 ± 0.1	6.5 ± 0.1	SX-7

Table 4.28. Measured $\text{pH}_{1/2}$ values for the extraction of Cu^{2+} , Co^{2+} , Ni^{2+} and Zn^{2+} ions. ^(a) Based on aqueous results. ^(b) Estimated using the curve fitting in origin.⁶⁴

The Co^{2+} , Ni^{2+} and Zn^{2+} ions are more weakly extracted at higher pH although the $\text{pH}_{1/2}$ at which this occurs can be highly dependent upon the substitution of the ligand. For example, the extraction of Zn^{2+} ions with the ligands listed in Table 4.28 is observed between pH's 2.5 and 7.0 with $\text{pH}_{1/2}$ measurements ranging between 3.5 and 6.2, Figure 4.37.

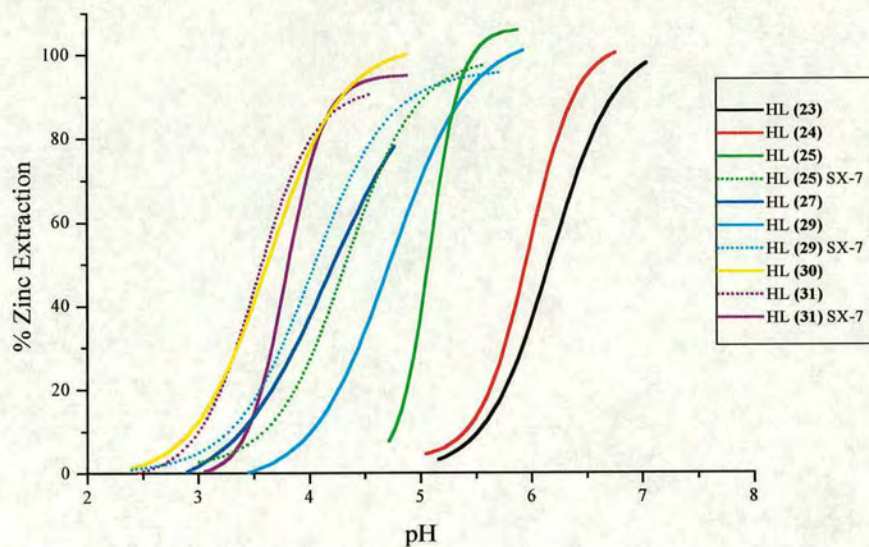


Figure 4.37. Comparison of the extraction of Zn(II) with imino-pyrazol-5-thiones (23-31) in either toluene or Orform SX-7.

Similarly the observed extraction range for Co^{2+} ions, albeit at an overall slightly higher pH range, gives rise to $\text{pH}_{1/2}$ values ranging between 4.6 and 6.3, Figure 4.38.

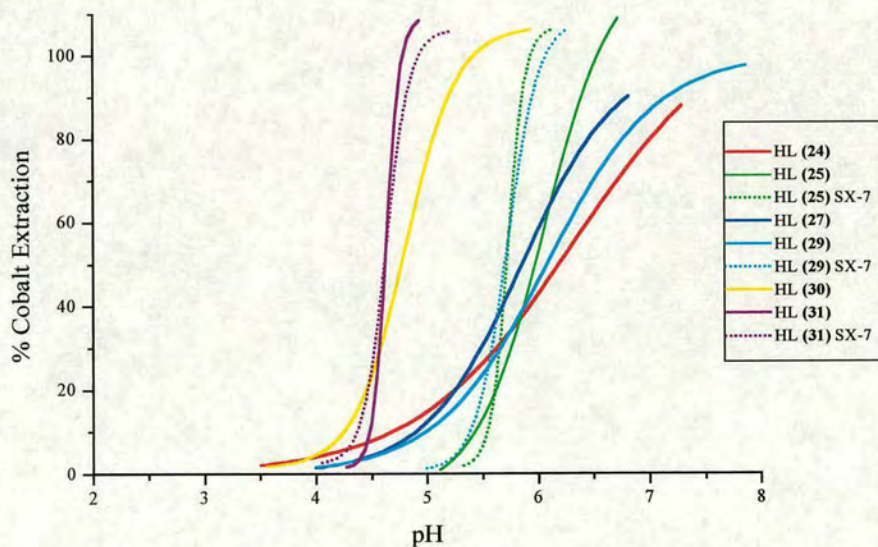


Figure 4.38. Comparison of the extraction of Co(II) with imino-pyrazol-5-thiones (23-31) in either toluene or Orform SX-7.

In contrast the extraction of Ni^{2+} ions, with the same range of ligands, occupies a much narrower pH band with the exceptions of HL (24) and HL (27) which exhibit flattened S-curves (see Section 4.5.1.1). In general similar $\text{pH}_{1/2}$ values were obtained for the extraction of nickel, which lie between pH 6.2 and 6.7. The one exception is with 1,3-dimethyl-4-(4-nonylphenylamine)-pyrazol-5-thione (31) which extracted nickel at a slightly lower $\text{pH}_{1/2}$ value of 5.7.

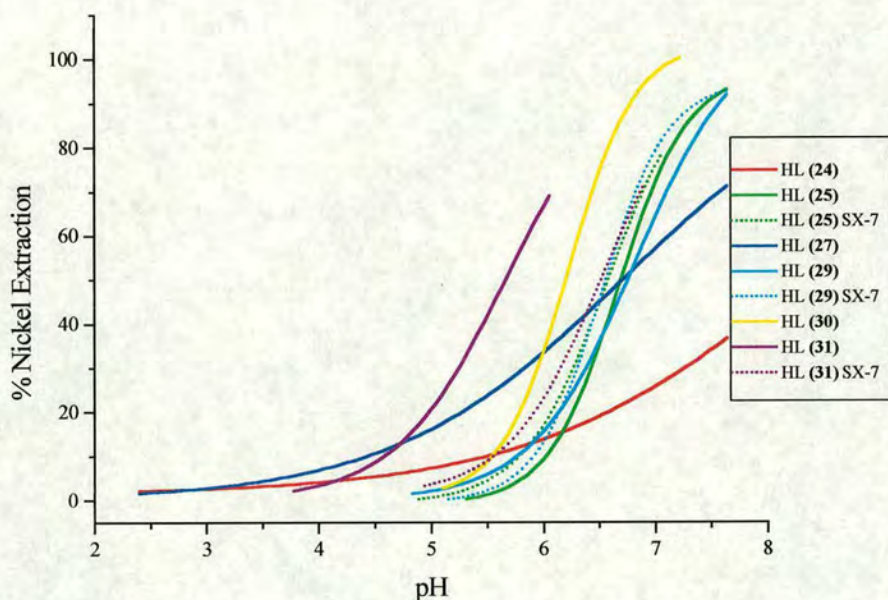


Figure 4.39. Comparison of the extraction of Ni(II) with imino-pyrazol-5-thiones (23-31) in either toluene or Orform SX-7.

The order of the extraction strength, for the range of ligands tested with each metal in toluene, follows approximately the same sequence, Figure 4.40. However care must be taken when distinguishing between significantly different $\text{pH}_{1/2}$ values in light of the large errors that can generate discrepancies in the mass balance (see Appendix VI) associated with limited solubility and hydroxide formation.

Zn ²⁺	30 ~ 31 > 29 > 27 > 25 > 24 ≥ 23
Co ²⁺	31 ~ 30 > 29 ≥ 27 ≥ 25 ≥ 24
Ni ²⁺	31 > 30 > 29 ~ 27 ~ 25 >> 24(estimated)

Figure 4.40. Trends in the extractant strength of several substituted imino-pyrazol-5-thiones.

The strength of extraction is related to the equilibrium constant, K_{extract} , defined by Equation 4.5 and is dependent on the nature of the substituents, which also contribute to the solubility and solvation of the ligand and the extracted metal compounds. In order to gain maximum extractant strength, *i.e.* a minimum extraction $\text{pH}_{1/2}$, a highly acidic ligand which forms very stable complexes would appear to be favourable. However since extraction is an equilibrium reaction between the complexation of the hydrogen ion (HL) and the metal ion (ML_2), strong ligand acidity will favour the stabilisation of the deprotonated anion producing a weak conjugate base (L^-) which may bring about a poor chelation ability.

The contribution towards the extraction “strength” provided by the ligands acidity, solubility and complex stability are rationalised below.

4.5.3.1 Extractant acidity.

The acid dissociation constants (K_a) of a selection of the imino-pyrazol-5-thiones were measured¹⁶⁶ by the titration of a 0.1 M tetrabutylammonium perchlorate (TBAP) in 95 % MeOH/H₂O containing the dissolved ligand against tetrabutylammonium hydroxide. In all cases precise measurements were unobtainable because the ligands

were too acidic to be measured with pK_a values lower than the measurable minimum of 2.

Alternatively the acidity of the substituted ligands relative to each other may be gauged by the comparison of the chemical shifts of the NH resonance in their respective ^1H NMR spectra (Table 4.1). The acidity of the ligands based on the resonance for the NH signal follows the order **27** > **30** ~ **31** > **23** > **24** > **25** > **29**. In general the inclusion of an electron withdrawing aromatic group at the R_2 position increases the acidity of the ligand. By inspection of Equation 4.5, K_{extract} and therefore the extractant “strength”, would also benefit from the inclusion of an aromatic ring. The “strength” of the extraction of Zn^{2+} , Co^{2+} and Ni^{2+} using these ligands does not follow the same order, Figure 4.40. However, the general, those ligands that do possess a phenyl group at the R_2 position, *i.e.* **27**, **30** and **31**, are stronger ligands and operate at a lower pH range. For example, extraction of Zn^{2+} ions using imino-alkyl substituted pyrazol-5-thiones (**23**, **24** and **25**) occurs at $\text{pH}_{1/2}$ 6.2, 6.0 and 5.1, respectively, whereas the extraction with imino-aromatic pyrazol-5-thiones (**27**, **30** and **31**) occurs at significantly lower $\text{pH}_{1/2}$, 4.2, 3.6 and 3.8 respectively, Table 4.28. The one exception is 1,3-dimethyl-4-(2-ethylhexylaldenamine)-pyrazol-5-thione (**29**) which operates at $\text{pH}_{1/2}$ 4.7, which may be attributed to its high solubility characteristics (see Section 4.5.1.1). A similar, but less pronounced, difference is also observed for the extraction of Co^{2+} ions (Table 4.28) with the imino-alkyl substituted ligands (**24**, **25** and **29**) operating at $\text{pH}_{1/2}$ 6.1-6.3 while the imino-aromatic pyrazol-5-thiones **27**, **30** and **31** operate at $\text{pH}_{1/2}$ 5.9, 4.8 and 4.6 respectively.

By increasing the acidity of the ligand it might be expected that the increase in extraction “strength”, *i.e.* the decrease in $\text{pH}_{1/2}$, would be the same for each metal. However this does not appear to hold true. For example the difference in $\text{pH}_{1/2}$ between the 2-ethylhexyl substituted ligand (25) and 4-*t*-butylphenyl substituted ligand (27) is greater for the extraction of Zn^{2+} ions than for Co^{2+} ions with the extraction of Ni^{2+} ions showing little difference, Table 4.29.

Extractants	$\Delta\text{pH}_{1/2}$			Solvent
	Zn(II)	Co(II)	Ni(II)	
25 – 27	-0.9	-0.2	~0	Toluene
29 – 30	-1.1	-1.3	-0.6	Toluene
29 – 31	-0.9	-1.5	-1.1	Toluene
	-0.5	-1.1	-0.1	SX-7

Figure 4.29. The difference in $\text{pH}_{1/2}$ between ligands for the extraction of Zn(II), Co(II) and Ni(II).

There does not appear to be a simple association between the increase in acidity of the ligand and the relative change in $\text{pH}_{1/2}$ for each metal. Changing the substituents not only alters the acidity but invariably affects the solvation energies of the ligands and complexes which in turn can affect the stability of the metal complex.

4.5.3.2 Extractant solubility.

A commercial extractant requires a minimum solubility of 0.1 M in a kerosene-derived diluent. In general the extractants discussed here do not meet this requirement with the exceptions of the 1,3-dimethyl (25) and 1-phenyl-3-methyl (29)

4-(2-ethylhexylaldenamine)-pyrazol-5-thiones and the 1,3-dimethyl-4-(4-nonyl phenylaldenamine)-pyrazol-5-thione (**31**), Table 4.25.

The solubility of the ligand and the extracted metal species is not only a determining factor in the shape of the extraction curve (See Section 4.5.1.1) but must also be taken into consideration when maximising the extractant “strength”.

Substitution of the phenyl group, attached directly to the pyrazole ring, in **25** and **27** by a methyl group as in **29** and **30** leads to a decrease in the observed $\text{pH}_{1/2}$ for Zn^{2+} ion extraction in toluene of 0.4 and 0.6 pH units respectively, Table 4.28. A similar decrease of 0.3 pH units is observed between ligands **25** and **29** in Orform SX-7. A decrease 1.1 and 0.5 pH units is also observed for Co^{2+} and Ni^{2+} extraction respectively when the phenyl group in HL (**27**) is replaced with methyl group in HL (**30**). In contrast there is no observable gain in “strength”, within experimental error, for the extraction of Co^{2+} or Ni^{2+} ions by replacing the phenyl group in HL (**25**) with a methyl group in HL (**29**) in either toluene or Orform SX-7.

These increases in extraction “strength” are in part associated with the increase in the lipophilicity, with the thermodynamic stability of the metal complex benefiting from an increase in the solubility and solvation energies of the metal species.

The organic solvent also has an effect on the pH at which a metal ion is extracted. Ligands (**25**, **29** and **31**) possessed sufficient solubility in Orform SX-7 for extraction of Zn^{2+} , Co^{2+} and Ni^{2+} to be assessed. As expected the extractants operated at a slightly lower pH when the more lipophilic Orform SX-7 was used as the diluent compared with toluene, Table 4.28. For the extraction of Zn^{2+} ions, the $\text{pH}_{1/2}$ was decreased by 0.8, 0.7 and 0.3 pH units for **25**, **29** and **31** respectively. The depression of the $\text{pH}_{1/2}$ was less so for Co^{2+} ion extraction with a decrease of 0.4 pH

units for **25** and **29** while there was no measurable difference for HL (**31**). In contrast Ni²⁺ ion extraction did not appear to benefit greatly from the use of Orform SX-7. In the case of extraction with HL (**31**) an increase of 0.8 pH units was measured compared to that with toluene. This might be attributed to the lower solubility and poor solvation of the extracted nickel complexes due to their large distortion from a tetrahedral geometry, see Section 4.4.2.3.

4.5.3.3 Coordination geometry and stability of metal complexes.

The tetrahedral coordination geometry that is imposed by the pyrazol-5-thiones on divalent metal(II) ions is crucial to the order in which metals are selectively extracted (see Section 4.5.3). However, it is of interest to determine whether the tetrahedrality of the extracted complex contributes significantly to its stability, and therefore can be utilised to optimise the pH_{1/2}.

The structural investigation in the solid state (see Sections 4.4.2.1 and 4.4.2.2) showed that the imino-*t*-butyl substituted zinc(II) (**34**) and cobalt(II) (**35**) complexes displayed dihedral and chelate angles closest to those for pure a tetrahedral coordination geometry of 90° and 109.5° respectively due to the large steric volume of the *t*-butyl group. Likewise the steric volume of the imino substituent also determined the coordination geometry and their distortion away from planarity of the nickel(II) complexes (see Section 4.4.2.3). Care must be taken when relating the solid state geometry to that in solution due to factors such as crystal packing and fluxional behaviour which could influence the geometry adopted. An additional complication, due to the different requirements for crystallisation and solvent extraction, is that only one of the ligands represented as a metal complex in the solid

state has been tested under solvent extraction conditions, *i.e.* 1-phenyl-3-methyl-4-(4-*t*-butylphenylaldenamine)-pyrazol-5-thione (27).

However, in general, bulky substituents such as *t*-butyl and branched alkyl chains, *e.g.* 2-ethylhexyl, should provide the steric volume most likely to impose a coordination geometry closest to that of a pure tetrahedron. On this basis, if the degree of "tetrahedrality" was a dominant factor in the stability of the extracted metal species then it would be expected that extraction at lower a pH would occur with ligands incorporating bulky imino groups, *e.g.* HL (23), HL (24), HL (25) and HL (29).

For Zn^{2+} ion extraction, where there is no CSFE, this effect is expected to be minimal. Indeed there seems no discernible advantage for the incorporation of bulky alkyl groups with respect to lowering the $pH_{1/2}$. The exception to this is for the 2-ethylhexyl group, which possibly increases the stability of the metal complex due much improved solubility. However, d^7 cobalt(II) complexes will lose CSFE as they distort further away from a tetrahedral geometry. Likewise, nickel(II) complexes will lose CSFE as they tend away from a planar geometry. The results for the solvent extraction of Co^{2+} and Ni^{2+} ions do not indicate any contribution to the "strength" of extraction due to the incorporation of bulky tetrahedral promoting groups.

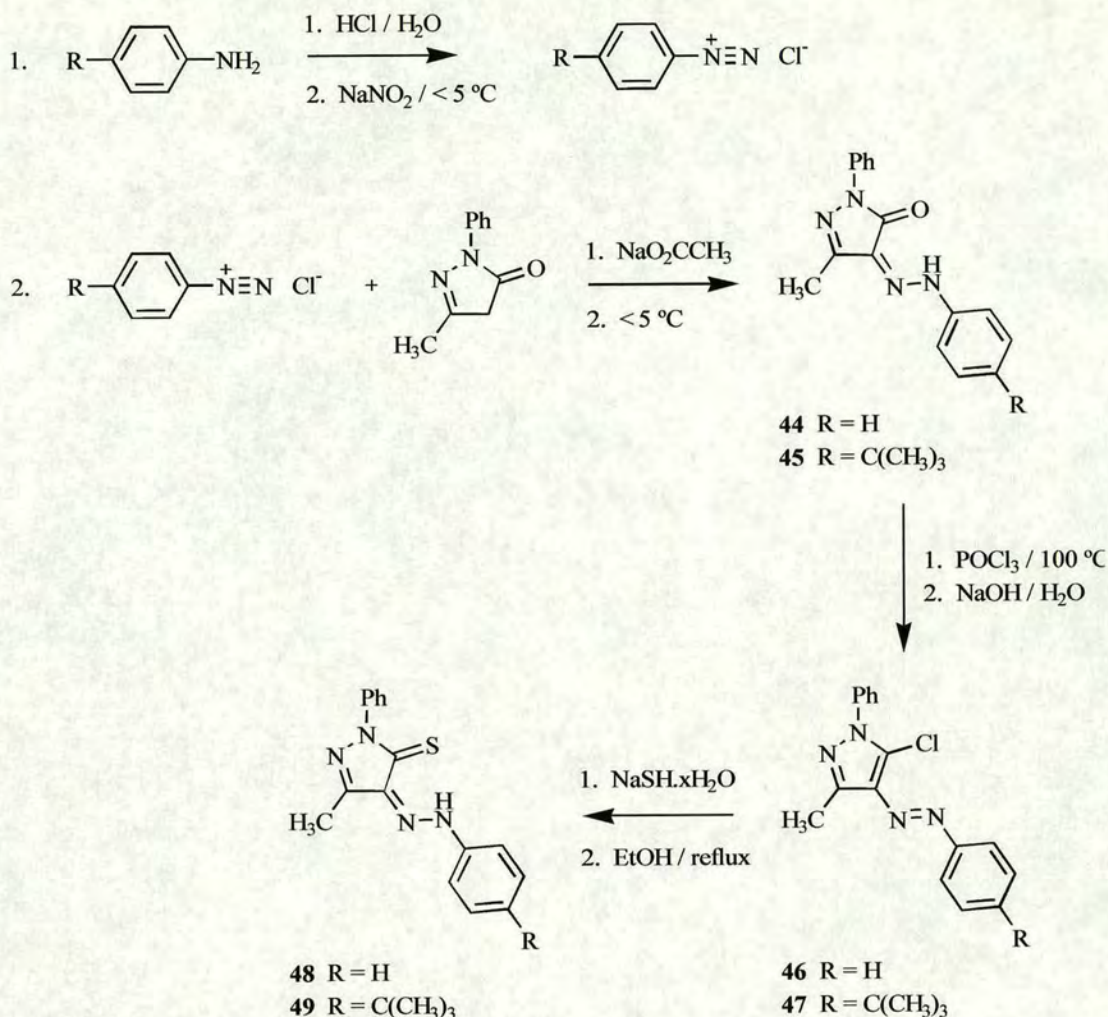
4.6 Preparation and characterisation of hydrazone-pyrazol-5-thiones.

The formation of the hydrazone-pyrazol-5-thiones (**48**) and (**49**) is *via* a 3-step synthetic pathway similar to that used in the preparation of the enamine pyrazol-5-thiones, Scheme 4.2. Although not optimised, the overall yield of the reaction scheme is reasonable at ~40 % for **48** and ~45 % for **49**.

The first step is the coupling between the commercially available 2-pyrazolin-5-one and the aromatic diazonium chloride. The diazonium salt is generated under standard conditions^{67,68} by the treatment of the primary aromatic amine, dissolved in dilute HCl, with sodium nitrite. The temperature was kept below 5 °C to minimise the decomposition of the diazonium chloride. The hydrazone-pyrazol-5-ones were obtained by the coupling between 2-pyrazolin-5-one and the corresponding diazonium salt in mildly alkaline conditions using sodium acetate³ in good yields, ~85 % (**44**) and ~70 % (**45**), although not optimised.

The 1-phenyl-3-methyl-5-chloro-4-phenylazo-pyrazoles (**46**) and (**47**) were prepared in good yield (~70 % and ~80 % respectively) by heating a 1:2 ratio of the corresponding hydrazone-pyrazol-5-one with POCl₃ at 100 °C.⁶ The excess acid was neutralised with aqueous NaOH.

The final step in the formation of the 1-phenyl-3-methyl-4-phenylhydrazone-pyrazol-5-thiones (**48**) and (**49**) involves the nucleophilic substitution of the chlorine at the C-4 position using sodium hydrogen sulfide as previously described in Section 4.2 with corresponding yields of ~65 % and ~85 % respectively.



Scheme 4.2. Synthetic procedure for 1-phenyl-3-methyl-4-phenylhydrazono-pyrazol-5-thiones.

4.6.1 NMR spectroscopy.

Full experimental characterisation is given in Section 4.11.2.3. The ¹H NMR of the hydrazono-pyrazol-5-ones (**44**, **45**) and the hydrazono-pyrazol-5-thiones (**48**, **49**) and the synthetic 5-chloro-pyrazole intermediates (**46**, **47**) were recorded in CDCl₃.

The ligands **44**, **45**, **48** and **49** exhibit azo-hydrazono tautomerism similar to the keto-enol tautomerism described in Section 4.2.1. This type of compound has traditionally been classed as an azo-compound on account of its similarity to the azo-

benzene compounds which contain the N=N group, Figure 4.41(a). More recent crystallographic^{69,70} and ¹⁵N NMR studies⁷¹ have shown that the presence of the pyrazol-5-one(thione) ring favours the hydrazone-ketone(thione) tautomer, Figure 4.41(b).

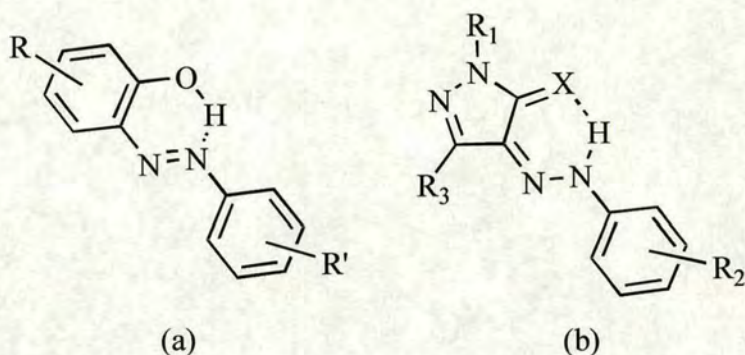


Figure 4.41. The favoured tautomeric forms of (a) *ortho*-hydroxy-azo-benzene and (b) hydrazone-pyrazol-5-one(thione) where X = O(S).

The appearance of sharp singlets for the NH resonance in the ¹H NMR at ~13.6 ppm for the pyrazol-5-ones (**44**, **45**) and ~17.1 ppm for the pyrazol-5-thiones (**48**, **49**) confirms the hydrazone tautomeric form in solution and suggests strong hydrogen bonding. A downfield shift for the hydrazone proton of ~3.5 ppm is observed, as expected, when the oxygen at the C-5 position is replaced with the less shielding sulfur atom. This downfield shift is comparable in size to the shift seen in the enamine-thione system (~3.6 ppm) for the replacement of oxygen with sulfur. The NH proton in hydrazone derivatives is further shifted downfield (~2.3 ppm) compared to the analogous enamine pyrazol-5-one(thione) due to the incorporation of the second nitrogen which again further decreases the shielding of the NH proton.

4.6.2 Mass spectroscopy.

The EI spectra of the 1-phenyl-3-methyl-arylhydrazono-pyrazol-5-ones (**44**, **45**) and pyrazol-5-thiones (**48**, **49**) and their 5-chloro-4-arylo-pyrazole intermediates (**46**, **47**) are consistent with their respective structures and contain molecular ion peaks in agreement with their respective molecular masses.

The elemental analysis of **48** and **49** are inconsistent with their expected molecular formulae. However due to their positive analysis by ^1H NMR and EIMS and the correct elemental analysis for the $[\text{Zn}(\mathbf{48-H})_2]$ (**50**) and $[\text{Co}(\mathbf{48-H})_2]$ (**51**) it is reasoned that this discrepancy was due to low sample purity.

4.7 Preparation and characterisation of metal complexes.

The metal complexes, $[\text{Zn}(\mathbf{48-H})_2]$ (**50**) and $[\text{Co}(\mathbf{48-H})_2]$ (**51**), were prepared (Figure 4.42) by the addition of a hot methanol solution of 1-phenyl-3-methyl-4-phenylhydrazono-pyrazol-5-thione (**48**) to a methanol solution of zinc(II) or cobalt(II) acetate using a ligand / metal ratio of 2:1, as described in Section 4.3.

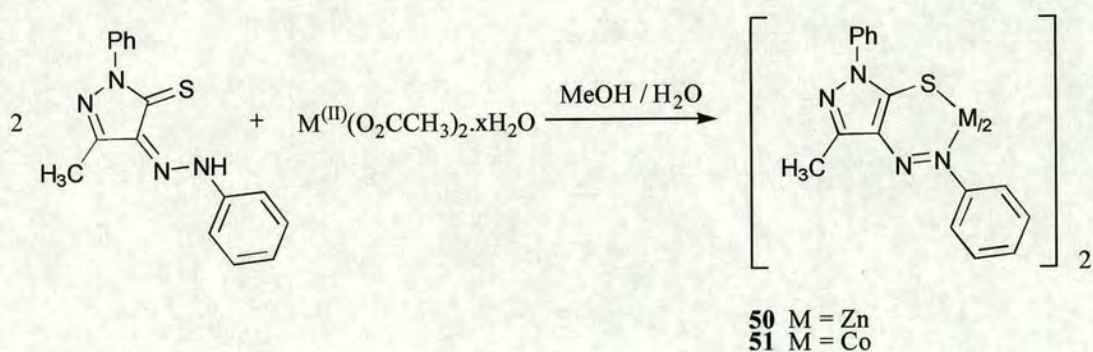


Figure 4.42. Synthesis of the complexes $[\text{Zn}(\mathbf{48-H})_2]$ (**50**) and $[\text{Co}(\mathbf{48-H})_2]$ (**51**).

4.7.1 NMR spectroscopy.

Full experimental characterisation is given in Section 4.11.2.4. The ^1H NMR of $[\text{Zn}(\mathbf{48-H})_2]$ (**50**) was recorded in CDCl_3 . The spectrum is similar to imino-pyrazol-5-thiolato zinc(II) spectra (Section 4.3.1) with the absence of the NH proton resonance (~ 17 ppm). The replacement of the imino carbon with the azo nitrogen results in the absence of the aldehydic (H-CN) signal representative of the imino complexes.

4.7.2 Mass spectroscopy.

The positive FAB spectra of complexes **50** and **51** show the molecular ion peaks associated with $[\text{M}(\text{L})_2(\text{H})]^+$ which is in agreement with the structure. However because of the weak intensity of the signals any fragmentation patterns are lost in background noise.

4.8 Crystallographic characterisation.

The crystallographic data are summarised in Appendix IV.

4.8.1 Bis-(1-phenyl-3-methyl-4-phenylazo-pyrazol-5-thiolato) zinc(II).

Orange plate-like crystals of $[\text{Zn}(\mathbf{48-H})_2]$ (**50**) were grown from ethanol / methanol (1:1) in the triclinic crystal system with space group $\text{P}\bar{1}$ (no.2). The asymmetric unit contains a single $[\text{Zn}(\mathbf{48-H})_2]$ molecule, Figure 4.43. The complex is chiral with both enantiomers (Λ and Δ) occurring in the unit cell and related by the crystallographic inversion centre.

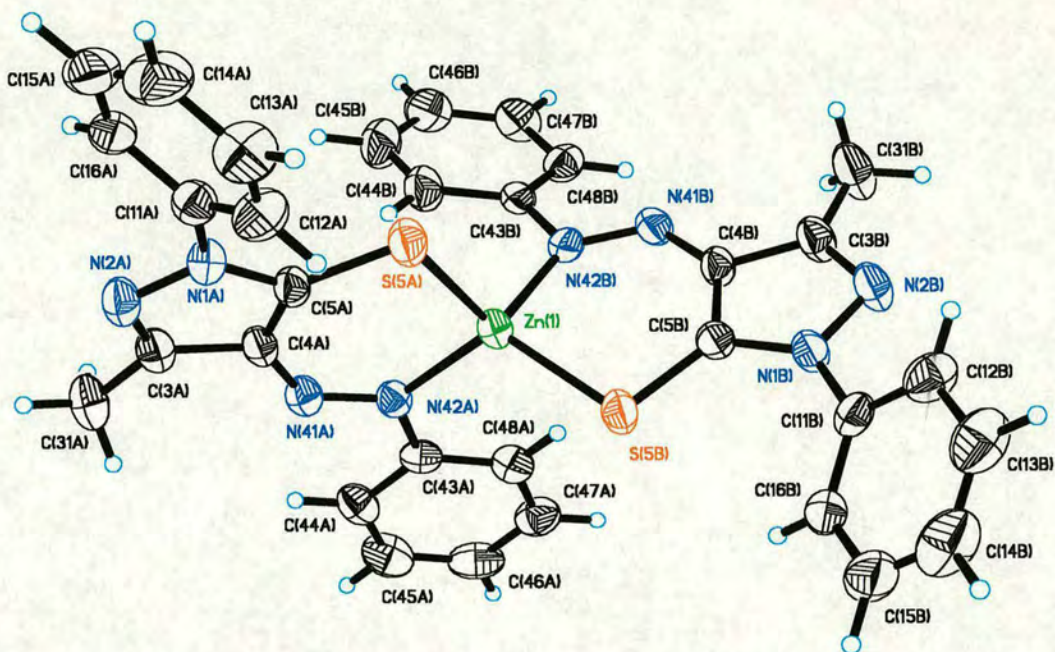


Figure 4.43. The structure of bis-(1-phenyl-3-methyl-4-phenylazo-pyrazol-5-thiolato) zinc(II) (**50**) showing atomic displacement ellipsoids at the 50 % probability level.

The zinc(II) azo-pyrazol-5-thiolato complex (**50**) is structurally very similar the zinc(II) imino-pyrazol-5-thiolato complexes described in Section 4.4. Most relevant for comparison here is $[\text{Zn}(\mathbf{26-H})_2]$ (**36**) in which the imino C(41) is replaced with the azo N(41) atom with the rest of the complex identical.

	[Zn(48-H) ₂] (50)	
	L(A)	L(B)
N(1)-C(5)	1.354(5)	1.357(5)
N(1)-N(2)	1.396(5)	1.400(5)
N(2)-C(3)	1.300(6)	1.304(6)
N(1)-C(11)	1.429(6)	1.418(6)
C(3)-C(4)	1.439(6)	1.430(6)
C(3)-C(31)	1.490(6)	1.489(6)
C(4)-N(41)	1.351(5)	1.353(5)
C(4)-C(5)	1.426(6)	1.418(6)
N(41)-N(42)	1.288(5)	1.286(5)
N(42)-C(43)	1.437(5)	1.436(5)
C(5)-S(5)	1.711(4)	1.722(4)
S(5)-C(5)-C(4)	132.0(3)	131.8(3)
C(5)-C(4)-C(41)	135.0(4)	135.4(4)
C(4)-N(41)-N(42)	122.5(4)	122.4(4)
N(41)-N(42)-Zn(1)	126.7(3)	126.2(3)
C(5)-S(5)-Zn(1)	99.36(16)	98.59(17)

Table 4.30. Selected bond lengths (Å) and angles (°) in the chelate units of the [Zn(48-H)₂] (50) complex.

The bond lengths and angles around the chelate ring are affected by the inclusion of the hetero atom. C(4)-N(41); 1.351(5) Å in ligand A and 1.353(5) Å in ligand B (Table 4.30) are approximately 0.07 Å shorter than C(4)-C(41) in **36** (Table 4.9) which correlates well with the decrease in covalent radii (~0.07 Å).⁴⁹ A small increase (0.02-0.03 Å) in the length of C(4)-C(5) is observed which might possibly be attributed to a slight decrease in electron density at these atoms, therefore reducing the bond strength, due to the greater electronegativity of N(41). The C(5)-S(5) bond is unaffected by the distant N(41) hetero atom and is similar to that in **36**.

The N(41)-N(42) distance, 1.288(5) Å in ligand A and 1.286(5) Å in ligand B, shows a greater double bond character with its length closer to that for a purely double bond ($d(\text{N}=\text{N}) = 1.240$ Å and $d(\text{N}-\text{N}) = 1.401$ Å).^{72,73} However it is only marginally shorter than C(41)-N(42), 1.298(4) Å possibly related to a rearrangement in the electron delocalisation in the azo-thiolato tautomer.

An analysis of the angles in the chelate ring shows a significant change in the distribution compared with **36**, Figure 4.44. However on summation these angles, 719.5° in ligand A and 717.4° in ligand B, are only marginally smaller than that for **39**; 719.8°. This is reflected in a slight decrease in planarity of the chelate rings (r.m.s deviation from the plane 0.043 Å, max. dev. O(5A) = 0.076 Å for ligand A and 0.051 Å, max. dev. Zn(1) = 0.081 Å for ligand B).

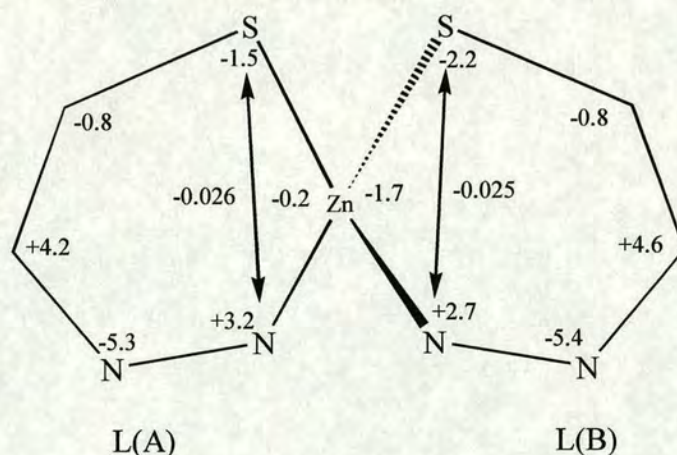


Figure 4.44. The difference in angles (°) and bite distance (Å) in the chelating ring of $[\text{Zn}(\mathbf{33}\text{-H})_2]$ (**50**) compared with $[\text{Zn}(\mathbf{26}\text{-H})_2]$ (**39**).

The shorter C(4)-N(41) bond subtends a bite distance, N(42)⋯S(5); 3.390(5) Å in ligand A and 3.391(4) Å in ligand B, that is significantly shorter than the bite

distance in **36**; 3.416(3) Å. As a consequence the Zn(1)-S(5) bond is reduced in length by approximately 0.03 Å, Table 4.31.

	[Zn(48-H)₂] (50)	
	L(A)	L(B)
Zn(1)-N(42)	2.032(4)	2.039(4)
Zn(1)-S(5)	2.2699(17)	2.2694(18)
N(42)-Zn(1)-S(5)	103.90(11)	102.99(11)
N...S	3.390(5)	3.391(4)
N(42A)...N(42B)	3.359(6)	
S(5A)...S(5B)	3.737(3)	
N(42A)-Zn(1)-S(5B)	118.22(11)	
N(42B)-Zn(1)-S(5A)	110.50(11)	
N(42A)-Zn(1)-N(42B)	111.21(14)	
S(5A)-Zn(1)-S(5B)	110.09(7)	
θ	87.5	

Table 4.31. Metal donor bond lengths (Å), angles (°), chelate bite distances (Å) and dihedral angles (θ°) defined by the chelates, together with the remaining bond angles at the metal in [Zn(**48-H**)₂] (**50**).

The dihedral angle for **50** is close to that for tetrahedral geometry with an angle of 87.5° between the two N-Zn-S chelate planes, ~6° greater than in **36**. This can be partly explained by an effective increase in steric volume of the phenyl imino substituents. The phenyl groups are closer to the plane of the pyrazole and chelate rings with the torsion angles at the N(42)-C(43) bond (torsions 1 and 2, Table 4.32) approximately 42° in ligand A and B, which are more planar than in **36** (~50° out of the plane). As expected this is accompanied by a redistribution of the angles around the central zinc and an increase in the N...N separation of 0.216 Å.

	Torsion	[Zn(48-H) ₂] (50)	
		L(A)	L(B)
1	N(41)-N(42)-C(43)-C(44)	139.8	138.1
2	N(41)-N(42)-C(43)-C(48)	42.2	42.7

Table 4.32. Selected torsion angles in [Zn(48-H)₂] (50).

4.9 Solvent extraction of Zn(II), Co(II) and Ni(II) with 1-phenyl-3-methyl-4-phenylhydrazono-pyrazol-5-thiones.

Solvent extraction using the azo-pyrazol-5-thiones (48 and 49) follows the same order (Zn > Co > Ni) as that observed for extraction with the imino-pyrazol-5-thione derivatives, Figure 4.45. In contrast the extraction of metal ions into benzene from an acidic chloride feed⁶ using 1,3-dimethyl-4-phenylhydrazone-pyrazol-5-thione shows a reversal in the selectivity of Co²⁺ and Ni²⁺ with pH_{1/2} values of ~6.3 and ~4.7 respectively.

The acidity of the hydrazono-pyrazol-5-thiones, 48 and 49, compared to their imino-pyrazol-5-thione counterparts, 26 and 27 respectively, are increased due to the incorporation of the electron withdrawing hydrazono nitrogen atom. This is indicated by an increase in the chemical shift for the NH signal in the respective ¹H NMR spectra by approximately 2.3 ppm. Therefore a decrease in the pH at which Zn²⁺, Co²⁺ and Ni²⁺ are extracted would be expected using the hydrazono derivatives. Although there were severe solubility problems in some cases (see Figure 4.45) making the estimation of some pH_{1/2} values difficult (see Table 4.33) it is clear that the extraction of these metal(II) ions do not benefit from the inclusion of the hydrazono nitrogen atom.

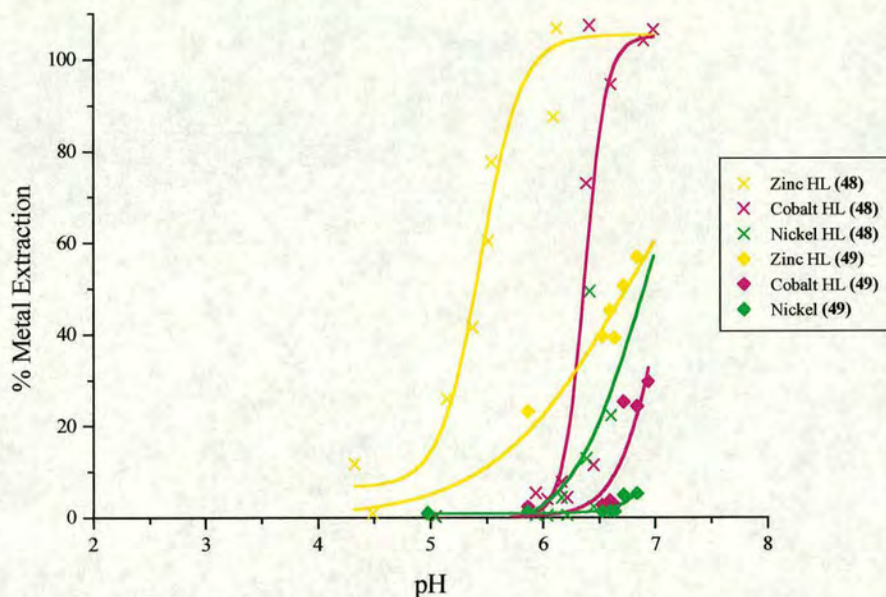


Figure 4.45. Multi-metal extraction of Zn(II), Co(II) and Ni(II) in toluene with 0.05 M 1-phenyl-3-methyl-4-phenylhydrazono-pyrazol-5-thione (**48**) and 0.05 M 1-phenyl-3-methyl-4-(4-*t*-butyl-phenylhydrazono)-pyrazol-5-thione (**49**) at ambient temperature.

For example the extraction of Zn^{2+} , Co^{2+} and Ni^{2+} ions in toluene with 1-phenyl-3-methyl-4-(4-*t*-butylphenylaldenamine)-pyrazol-5-thione (**27**) occurs at $pH_{1/2}$ 4.2, 5.9 and 6.2 respectively, Table 4.28, whereas with 1-phenyl-3-methyl-4-phenylhydrazono-pyrazol-5-thione (**48**) the $pH_{1/2}$ value for Zn^{2+} and Co^{2+} extractions are increased by 1.3 and 0.5 pH units respectively, with no change observed between for the extraction of Ni^{2+} ions. A further increase was estimated for the extraction using 1-phenyl-3-methyl-4-(4-*t*-butylphenylhydrazono)-pyrazol-5-thione (**49**) although large errors are associated with the estimations due to the poor solubility of the extracted species.

Extractant	pH _½			Solvent
	Zn(II)	Co(II)	Ni(II)	
HL (48)	5.5 ± 0.1	6.4 ± 0.1	6.9 ± 0.4 ^(a)	Toluene
HL (49)	6.7 ± 0.1 ^(a)	7.1 ± 0.1 ^(a)	7.3 ± 0.9 ^(a)	Toluene

Table 4.33. Measured pH_½ values for the extraction of Co²⁺, Ni²⁺ and Zn²⁺ ions. ^(a) Estimated using the curve fitting in origin.⁶⁴

There is very little difference structurally between [Zn(26-H)₂] (36) (Section 4.4.2.1) and [Zn(48-H)₂] (50) (Section 4.8.1) in the solid state which would warrant such a large increase in the pH_½. However the presence of the azo-nitrogen possibly stabilises the deprotonated ligand producing a weak conjugate base (L⁻), therefore decreasing its chelation ability.

4.10 Conclusions.

Crystallographic and ¹H NMR studies have been used to demonstrate that the protonated bidentate pyrazol-5-thione ligands (23-32) and the azo-derivatives (48, 49) represented in this chapter exist as the enamine-thione and hydrazone-thione tautomers, respectively, in the solid state and in solution. However, upon complexation to 1st row transition metals (Cu²⁺, Co²⁺, Ni²⁺ and Zn²⁺) the electronic configuration around the chelate ring is more in line with the imino-thiol tautomer.

The geometrical constraints imposed by these ligands on complexation to zinc(II) and cobalt(II) ions favour the formation of slightly distorted tetrahedral coordination geometries. In the case of nickel(II), where a tetrahedral geometry is disfavoured, a compromise between planarity and “tetrahedrality” results, although when suitably bulky substituents are present a highly distorted tetrahedral configuration ensues.

The bite ($N\cdots S$) of the pyrazol-5-thiones reported here is larger than that found for the pyridinethiones(ones), see Chapter 3, which can be attributed to the ring opening effect of the 5-membered pyrazole ring which is attached to the 6-membered chelate ring. As a consequence they subtend to chelate angles that range between 102° and 105° for the zinc(II) (**34**, **36**, **39**) and cobalt(II) (**35**, **37**, **40**) complexes, and are therefore more suited for the formation of tetrahedral complexes. A small degree of flexibility in the chelate ring allows the ligand in complexes containing smaller metal ions, *e.g.* nickel(II) (**38**), to subtend to a chelate angle (97.5°) intermediate between that ideal for planar and octahedral complexes and that for tetrahedral complexes. However it is assumed, with confidence, that these ligands are insufficiently flexible to allow the formation of chelate angles which are significantly smaller than 97° , *i.e.* close to 90° . Coupled with the inclusion of sterically hindering imino substituents and the NS^- donor set, the formation of a stable neutral octahedral iron(III) complex is thought unlikely.

Solvent extraction, using several of the enamine-pyrazol-5-thiones and 1-phenyl-3-methyl-4-phenylhydrazone-pyrazol-5-thione, followed the selectivity order $Cu(II) > Zn(II) > Co(II) > Ni(II)$. The order correlates with the propensity of the metal to adopt a stable tetrahedral configuration rather than following the Irving-Williams stability order for divalent metal ions. The ligand substituents greatly affect the $pH_{1/2}$ at which each metal is extracted. In general, the “strength” of the extractant is maximised by the incorporation of an imino-aromatic group, thereby increasing the acidity of the ligand. However a decrease in “strength” is observed when the ligand becomes too acidic due to an associated decrease in the stability of the extracted complex, as in the case of the hydrazone-pyrazol-5-thiones. There was no clear

evidence that the degree of “tetrahedrality” contributed significantly to the “strength” of extraction although it is fundamental to the selectivity order. It has also been demonstrated that a favourable increase in “strength” and solubility may be gained by using suitably lipophilic substituents, such as 2-ethylhexyl, and replacing the phenyl attached directly to the pyrazole ring with a methyl group. Therefore a balance between acidity and lipophilicity, *i.e.* aromatic and long chain aliphatic groups, provides the most beneficial ligand substitution for maximising the extractants “strength”, which was observed in the case of 1,3-dimethyl-4-(4-nonylphenylaldenamine)-pyrazol-5-thione (31).

4.11 Experimental.

4.11.1 Solvent Extraction.

Preliminary solvent extraction experiments were carried out on systems containing a single metal using zinc, nickel, copper and cobalt sulfate. After initial investigation into the pH range required to give complete extraction into the organic phase, experiments were performed on multi-metal systems containing zinc, cobalt and nickel sulfate. Standard solutions of the metal sulfates salts (0.085 M) were prepared in de-ionised water. A standard solution of the extractant (0.05 M) was prepared in toluene for the single metal system or in either toluene or Orform SX7 for the multi-metal system (see below). The experimental solutions were taken from these as required.

4.11.1.1 Single metal extraction.

The aqueous metal feed (1.25 cm³, 0.11 mmol) was placed into a 15 cm³ glass jar and set to stir. To this solution the extractant containing organic phase (5 cm³, 0.25 mmol) was added such that a suspension of organic droplets in a continuous aqueous phase was attained. The pH of the system was adjusted with a calculated amount of NaOH (~ 1 M), so as to provide deprotonation of only a fraction of the extractant, then distilled water added to make the total aqueous volume 5 cm³ such that the ratio of extractant to metal sulfate is 2.3:1. Note, the concentration of the metal sulfate is decreased to 0.027 mmol after the addition of the acid or base and distilled water. The next sample is prepared in a similar manner followed by an increase in the volume of NaOH used, to further increase the pH of the system and the percentage extraction, again distilled water was added to provide a total aqueous volume of 5 cm³. Sufficient samples were prepared such that a total of between 10 and 15 points on the extraction curve were obtained, Table 4.34. In some extractant cases addition of H₂SO₄ (~1 M) was necessary as partial extraction occurred without the addition of base. The sample bottles were sealed and stirred vigorously over night to allow the system to reach equilibrium.

Extractant / cm ³	Metal / cm ³	NaOH / cm ³	Water / cm ³	Total / cm ³
5	1.25	0	3.75	10
5	1.25	0.024	3.726	10
5	1.25	0.050	3.700	10
5	1.25	0.074	3.676	10
5	1.25	0.100	3.650	10
5	1.25	0.124	3.626	10
5	1.25	0.150	3.600	10
5	1.25	0.174	3.576	10
5	1.25	0.200	3.550	10
5	1.25	0.224	3.526	10

Table 4.34. Typical volumes of reactants used to make the samples for single metal extraction.

After stirring, the two phases were allowed to disengage. The organic and aqueous phases were separated by filtration using phase separation paper, the organic phase passed through while the aqueous was retained. The aqueous phase was then removed and passed through filter paper. It was then separated into two portions, one half was used to measure the pH of the sample at equilibrium while the other half was used for metal analysis.

The aqueous and the organic phases were analysed, using an Inductively Coupled Plasma-Optical Emission Spectrometer (ICP-OES), for the metal content in each. The organic samples were diluted using Stoddard reagent, a relatively non-volatile solvent with a high vapour pressure necessary for ICP-OES operation, and the aqueous samples in distilled water. The dilutions were performed (10 or 100-fold) such that the samples had a metal content between 0 and 30 ppm, the range over which the spectrometer had been calibrated.

4.11.1.2 Multi-metal extraction.

The multi-metal extraction experiments were carried out on a slightly larger scale by an analogous method to that for the single metal extraction. In this case the aqueous metal feed (3.0 cm³, 0.26 mmol) and the organic phase (12 cm³, 0.60 mmol) were added together as before in a 30 cm³ glass jar. The total concentration of metal in the aqueous feed was divided equally between zinc, cobalt and nickel. The volume of the aqueous phase in each sample was adjusted to 12 cm³ by the addition of acid or base and then distilled water, such that the molar ratio of the extractant to metal sulfate was 2.3:1, as shown in Table 4.35. Note, the concentration of the metal feed was reduced to 0.064 mmol.

Extractant / cm ³	Metal / cm ³	NaOH / cm ³	Water / cm ³	Total / cm ³
12	3.0	0	9.00	24
12	3.0	0.08	8.92	24
12	3.0	0.16	8.84	24
12	3.0	0.24	8.76	24
12	3.0	0.32	8.68	24
12	3.0	0.40	8.60	24
12	3.0	0.48	8.52	24
12	3.0	0.56	8.44	24
12	3.0	0.64	8.36	24
12	3.0	0.72	8.28	24
12	3.0	0.80	8.20	24
12	3.0	0.88	8.12	24
12	3.0	0.96	8.04	24

Table 4.35. Typical volumes of reactants used to make the samples for multi metal solvent extraction.

The aqueous and the organic phases were analysed, using an Atomic Absorption Spectrometer (AAS). The aqueous samples were diluted as before whereas the organic samples were diluted using Orform SX7, an 80 % aliphatic and 20 % aromatic containing hydrocarbon solvent.

4.11.2 Synthesis.

4.11.2.1 Pyrazol-5-thione and pyrazol-5-one ligands.

1,3-Dimethyl-2-pyrazolin-5-one (19).

A solution of methyl hydrazine (5.770 g, 125 mmol) in methanol (120 cm³) was cooled to < 0 °C using a salt-ice bath. Ethylacetoacetate (14.777 g, 114 mmol) was added dropwise, with stirring, to the cooled methanol solution at such a rate that the temperature did not exceed 0 °C. The mixture was stirred at 0 °C for 4 h, heated at reflux for 24 h, and then allowed to cool. The solvent was removed by rotary evaporation to yield a cream solid (11.87 g, 92.7 %) which was recrystallised from cyclohexane / toluene. M.P. (decomp.) 130 °C (Lit. 117 °C²²); (Found: C, 53.60; H, 7.17; N, 24.85; EIMS *m/z* 112. C₅H₈N₂O requires C, 53.56; H, 7.19; N, 24.98 %; *M* 112); ¹H NMR (CDCl₃, 200 MHz) δ: 2.07 (s, 3H, CH₃), 3.16 (s, 2H, CH₂), 3.25 (s, 3H, N-CH₃). IR (cm⁻¹, KBr disk) ν: 2927(m), 2448(m), 1785(m), 1546(s), 1394(s), 1271(s), 1186(m), 1035(s), 975(m), 832(m), 742(s), 684(m).

1-*t*-Butyl-3-methyl-2-pyrazolin-5-one (20).

Ethylacetoacetate (32.59 g, 0.250 mol) was added dropwise to a solution of *t*-butyl hydrazine hydrochloride (34.26 g, 0.275 mol) and triethylamine (60 cm³) in methanol (250 cm³) cooled to 0 °C using a salt-ice bath, such that the temperature did not exceed 0 °C. The mixture was stirred at 0 °C for 4 h and then heated at reflux for 65 h. The solvent was removed by rotary evaporation and the residue partitioned between dichloromethane and water. The organic layer was washed twice with water, once with dilute HCl then finally again with water. The organic layer was dried over MgSO₄ and the dichloromethane removed to leave a solid which was taken up in petroleum ether (40-60) to yield a pale yellow solid isolated by filtration (22.58 g, 53.2 %). Recrystallisation from cyclohexane yielded a white solid (22.17 g, 52.3 %). M.P. 124-126 °C (Lit. 120 °C⁷⁴); (Found: C, 62.40; H, 9.41; N, 18.23; EIMS *m/z* 155. C₈H₁₄N₂O requires C, 62.31; H, 9.15; N, 18.17 %; *M* 154); ¹H NMR (CDCl₃, 300 MHz) δ: 1.5 (s, 9H, C(CH₃)₃), 2.05 (s, 3H, CH₃), 3.15 (s, 2H, CH₂). IR (cm⁻¹, KBr disk) ν: 2988(m), 2600(s), 1870(m), 1594(s), 1509(s), 1458(m), 1400(s), 1368(m), 1226(m), 1156(m), 1018(m), 837(m), 789(m), 782(m), 746(m), 654(m).

1-Phenyl-3-methyl-5-chloro-4-pyrazolecarboxaldehyde (21).

A 3-necked round bottom flask equipped with a reflux condenser, mechanical stirrer and a CaCl₂ guard tube was charged with 1-phenyl-3-methyl-2-pyrazolin-5-one (5.012 g, 29 mmol) and N,N-dimethylformamide (DMF) (4.5 cm³, 58 mmol). Phosphorus oxychloride (POCl₃) (5.4 cm³, 58 mmol) was then slowly added dropwise at ambient temperature *via* a dropping funnel. On completion of the

addition of POCl₃ the mixture was heated at 100 °C for 3 h then cooled in a salt-ice bath (< 0 °C) and neutralised with a sodium acetate solution (11.998 g, 146 mmol) in water (200 cm³). The precipitate that formed was stirred for a further 2 h at 0 °C then isolated by filtration to give an orange solid (4.02 g, 62.8 %) which was recrystallised from EtOH / H₂O (1:1) (2.246 g, 29.0 %). A portion of this was further purified by dry-flash chromatography, using ethyl acetate / hexane (1:1), a white solid was obtained. M.P. 147-148 °C (Lit. 148 °C³¹); (Found: C, 59.16; H, 4.09; N, 12.68; EIMS *m/z* 219 (100 %). C₁₁H₉ClN₂O · 0.125H₂O requires C, 59.27; H, 4.18; N, 12.57 %; *M* 221); ¹H NMR (CDCl₃, 200 MHz) δ: 2.54 (s, 3H, CH₃), 7.45-7.56 (m, 5H, Ph), 9.97 (s, 1H, HC=O). IR (cm⁻¹, KBr disk) ν: 3064(w), 1677(s), 1599(m), 1528(m), 1506(m), 1477(m), 1464(m), 1438(m), 1376(m), 1005(w), 778(m), 764(s), 697(m).

1,3-Dimethyl-5-chloro-4-pyrazolecarboxaldehyde (22).

A mixture of 1,3-dimethyl-2-pyrazolin-5-one (5.017 g, 45 mmol) and DMF (7 cm³, 90 mmol) was mechanically stirred in a 3-necked round bottom flask fitted with a CaCl₂ guard tube to which POCl₃ (8.4 cm³, 90 mmol) was continuously added dropwise at ambient temperature. The mixture was then heated at 100 °C for 2 h then cooled to 0 °C in a salt-ice bath then neutralised with a solution of sodium acetate (18.51 g, 226 mmol) in water (250 cm³) and finally stirred for a further 2 h. The resulting precipitate was isolated by filtration to yield a beige solid (3.72 g, 52.1 %). A portion of this was further purified by dry-flash chromatography, using ethyl acetate / hexane (80:20), a white solid was obtained. M.P. 80-81 °C (Lit. 78-79° C³⁰); (Found: C, 45.36; H, 4.37; N, 17.43; EIMS *m/z* 157 (100 %).

$C_6H_7ClN_2O$ requires C, 45.44; H, 4.45; N, 17.66 %; M 159); 1H NMR (d_6 -DMSO, 200 MHz) δ : 2.33 (s, 3H, CH_3), 3.77 (s, 3H, N- CH_3), 9.76 (s, 1H, HC=O). IR (cm^{-1} , KBr disk) ν : 2948(m), 2811(m), 2729(m), 1684(s), 1522(s), 1471(s), 1412(s), 1377(s), 1222(m), 1110(m), 1048(m), 1021(m), 994(m), 852(w), 771(s).

1-Phenyl-3-methyl-4-(*t*-butylaldenamine)-pyrazol-5-thione (23).

A suspension of 1-phenyl-3-methyl-5-chloro-4-pyrazolecarboxaldehyde (4.001 g, 18 mmol) in ethanol (75 cm^3) was prepared to which NaSH. xH_2O (2.015 g, 36 mmol) and *t*-butylamine (1.335 g, 18 mmol) were added. The mixture was heated at reflux for 24 h then allowed to cool. The solvent was removed by rotary evaporation and the resultant solid partitioned between water and CH_2Cl_2 . The organic phase was washed 3 times with water (100 cm^3), twice using 0.1 M HCl (100 cm^3) and finally again using water. The dichloromethane layer was dried using $MgSO_4$, filtered and the filtrate reduced to leave a brown oil which was recrystallised from ethanol to give yellow, X-ray crystallographic grade, crystals (1.36 g, 27.6 %). M.P. 147-148.5 °C; (Found: C, 65.92; H, 7.04; N, 15.35; EIMS m/z 273. $C_{15}H_{19}N_3S$ requires C, 65.90; H, 7.00; N, 15.37 %; M 273); 1H NMR ($CDCl_3$, 200 MHz) δ : 1.50 (s, 9H, $C(CH_3)_3$), 2.31 (s, 3H, CH_3), 7.25-7.48 (m, 3H, (*m*, *p*)Ph), 7.83-7.91 (m, 3H, (*o*)Ph, H-CN), 13.43 (br s, 1H, NH). IR (cm^{-1} , KBr disk) ν : 2976(m), 1654(s), 1595(m), 1531(m), 1498(m), 1371(m), 1332(m), 1245(m), 1204(w), 989(m), 842(w), 758(m), 689(m), 668(m).

The 1-phenyl-3-methyl-4-(alkylaldenamine)-pyrazol-5-thiones (**24-28**) were prepared from 1-phenyl-3-methyl-5-chloro-4-pyrazolecarboxaldehyde (**21**) and the appropriate amine according to the method described above for **23**.

1-Phenyl-3-methyl-4-cyclohexylaldenamine-pyrazol-5-thione. (24).

The brown solid that remained after the reduction of the filtrate was recrystallised from methanol to give yellow / brown, X-ray crystallographic grade, crystals (3.888 g, 72.4 %). M.P. 142.5-143 °C; (Found: C, 68.28; H, 7.13; N, 13.82; EIMS m/z 299. $C_{17}H_{20}N_3S$ requires C, 68.42; H, 6.75; N, 14.08 %; M 298); 1H NMR ($CDCl_3$, 200 MHz) δ : 1.24-2.07 (m, 10H, cyclo- CH_2), 2.29 (s, 3H, CH_3), 3.42-3.53 (m, 1H, cyclo- CH^*), 7.24-7.48 (m, 3H, (*m, p*)Ph), 7.82-7.91 (m, 3H, (*o*)Ph, H-CN), 13.16 (br s, 1H, NH). IR (cm^{-1} , KBr disk) ν : 3046(w), 2989(w), 2928(m), 2856(m), 1641(s), 1596(m), 1530(s), 1451(m), 1423(m), 1370(s), 1346(s), 1299(m), 1269(m), 1237(m), 1140(m), 1080(w), 1053(w), 1021(w), 925(m), 826(m), 768(m), 711(m), 696(m), 672(m), 638(w).

1-Phenyl-3-methyl-4-(2-ethylhexylaldenamine)-pyrazol-5-thione (25).

The red / brown oil remaining after the reduction of the filtrate was further purified by dry-flash column chromatography using ethyl acetate / hexane (1:1) yielding a viscous red oil (9.63 g, 81.2 %), (Found: C, 69.54; H, 8.29; N, 12.57; EIMS m/z 329. $C_{19}H_{27}N_3S$ requires C, 69.26; H, 8.26; N, 12.75 %; M 329); 1H NMR ($CDCl_3$, 200 MHz) δ : 0.75 (m, 6H, $2CH_3(2EtHex-6,8)$), 1.22-1.71 (m, 8H, $4CH_2(2EtHex-3,4,5,7)$), 2.29 (s, 3H, CH_3), 2.56 (s, 1H, $CH(2EtHex-2)$), 3.48 (t, $^3J_{HH}$ 5.9 Hz, 2H, $CH_2(2EtHex-1)$), 7.22-7.48 (m, 3H, (*m, p*)Ph), 7.76 (d, $^3J_{HH}$ 13.7 Hz, 1H, H-CN),

7.85-7.99 (m, 2H, (*o*)Ph), 13.06 (br s, 1H, NH). IR (cm⁻¹, KBr disk) ν : 3060(w), 2958(m), 2926(m), 2858(m), 1651(s), 1594(m), 1530(m), 1498(m), 1425(m), 1348(m), 1236(m), 1153(m), 993(m), 826(w), 760(m), 691(m), 670(m).

1-Phenyl-3-methyl-4-(phenylaldenamine)-pyrazol-5-thione (26).

The brown solid that remained after the reduction of the filtrate was recrystallised from methanol to give yellow / brown crystals (1 g, 25 %). M.P. 157.5-159 °C; (Found: C, 67.88; H, 5.01; N, 13.94; EIMS *m/z* 293. C₁₇H₁₅N₃S 0.5H₂O requires C, 67.52; H, 5.33; N, 13.90 %; *M* 293); ¹H NMR (CDCl₃, 200 MHz) δ : 2.37 (s, 3H, CH₃), 7.26-7.51 (m, 8H, (*m*, *p*)Ph, (*o'*, *m'*, *p'*)Ph), 7.89-7.95 (m, 2H, (*o*)Ph), 8.23 (d, ³*J*_{HH} 13.2 Hz, 1H, H-CN), 14.84 (d, ³*J*_{HH} 13.4 Hz, 1H, NH). IR (cm⁻¹, KBr disk) ν : 3049(m), 1648(m), 1588(m), 1527(m), 1494(m), 1481(m), 1433(m), 1322(s), 1246(m), 1152(m), 998(m), 771(m), 756(m), 689(m), 670(m).

1-Phenyl-3-methyl-4-(4-*t*-butylphenylaldenamine)-pyrazol-5-thione (27).

The brown solid that remained after the reduction of the filtrate was recrystallised from methanol to give yellow, X-ray crystallographic grade, crystals (7.65 g, 60.8 %). M.P. 155-159 °C; (Found: C, 71.73; H, 6.78; N, 11.95; EIMS *m/z* 349. C₂₁H₂₃N₃S 0.125H₂O requires C, 71.17; H, 6.62; N, 11.95 %; *M* 349); ¹H NMR (CDCl₃, 200 MHz) δ : 1.33 (s, 9H, C(CH₃)₃), 2.37 (s, 3H, CH₃), 7.12-7.50 (m, 7H, (*m*, *p*)Ph, (*o'*, *m'*)Ph), 7.88-7.97 (m, 2H, (*o*)Ph), 8.21 (d, ³*J*_{HH} 13.3 Hz, 1H, H-CN), 14.81 (d, ³*J*_{HH} 13.6 Hz, 1H, NH). ¹³C NMR (CDCl₃, 250 MHz) δ : 11.26 (CH₃, C-3a), 31.10 (CH₃, C-7), 34.54 (CH₃, C-6), 112.80 (q, C-4), 118.23 (CH, *o'*-arom.), 124.41 (CH, *o*-arom.), 126.82 (CH, *m*-, *m'*-arom.), 127.12 (CH, *p*-arom), 128.41

(CH, *m*-, *m'*-arom.), 135.48 (CH, *p'*-arom.), 138.97 (CH, *a*-arom.), 145.99 (CH, C-4a), 150.40 (q, C-3, *a'*-arom.), 151.25 (q, C-3, *a'*-arom.), 168.85 (q, C-5). IR (cm⁻¹, KBr disk) ν : 2954(m), 1649(s), 1479(m), 1365(m), 1320(m), 1308(s), 1265(w), 1238(w), 1048(w), 958(w), 836(w), 764(m), 691(w).

1-Phenyl-3-methyl-4-(4-nitrophenylaldenamine)-pyrazol-5-thione.(chloroform) (28).

The red solid that remained after the reduction of the filtrate was recrystallised using ethyl acetate / propan-2-ol (1:1) to give orange, X-ray crystallographic grade, plate crystals (1.63 g, 13.4 %). M.P. 205-207 °C; (Found: C, 59.90; H, 4.38; N, 16.22; EIMS *m/z* 337 (100 %). C₁₇H₁₄N₄O₂S 0.125H₂O requires C, 59.94; H, 4.22; N, 16.44 %; *M* 338); ¹H NMR (CDCl₃, 200 MHz) δ : 2.39 (s, 3H, CH₃), 7.24-7.52 (m, 5H, (*m*, *p*)Ph, (*o'*)Ph), 7.86-7.93 (m, 2H, (*o*)Ph), 8.23 (d, ³*J*_{HH} 12.7 Hz, 1H, H-CN), 8.27-8.36 (m, 2H, (*m'*)Ph), 14.99 (d, ³*J*_{HH} 12.9 Hz, 1H, NH). IR (cm⁻¹, KBr disk) ν : 3090(w), 1654(s), 1590(m), 1550(m), 1522(m), 1490(w), 1329(m), 1312(s), 1223(w), 1142(m), 1110(w), 1045(w), 953(w), 845(m), 765(m), 671(w).

The 1,3-dimethyl-4-(alkylaldenamine)-pyrazol-5-thiones (**29-32**) were prepared from 1,3-dimethyl-5-chloro-4-pyrazolecarboxaldehyde (**22**) and the appropriate amine according to the method described above for **23**.

1,3-Dimethyl-4-(2-ethylhexylaldenamine)-pyrazol-5-thione (29).

The yellow / brown waxy solid remaining after the reduction of the filtrate was further purified by dry-flash column chromatography using ethyl acetate / hexane

(70:30) to give a yellow waxy solid (5.23 g, 85.0 %). M.P. 48-50 °C; (Found: C, 62.97; H, 9.31; N, 15.80; EIMS m/z 267. $C_{14}H_{25}N_3S$ requires C, 62.88; H, 9.42; N, 15.71 %; M 267); 1H NMR ($CDCl_3$, 200 MHz) δ : 0.92 (m, 6H, $2CH_3(2EtHex-6,8)$), 1.23-1.56 (m, 9H, $4CH_2(2EtHex-3,4,5,7)$, $CH(2EtHex-2)$), 2.21 (s, 3H, CH_3), 3.45 (t, $^3J_{HH}$ 5.9 Hz, 2H, $CH_2(2EtHex-1)$), 3.71 (s, 3H, N- CH_3), 7.66 (d, $^3J_{HH}$ 13.8 Hz, 1H, H-CN), 12.65 (br s, 1H, NH). ^{13}C NMR ($CDCl_3$, 250 MHz) δ : 10.67 (CH_3 , C-10 / C-13), 11.01 (CH_3 , C-3a), 13.80 (CH_3 , C-10 / C-13), 22.63 (CH_2 , C-8 / C-9, C-10, C-12), 23.71 (CH_2 , C-8 / C-9, C-10, C-12), 28.48 (CH_2 , C-8 / C-9, C-10, C-12), 30.30 (CH_2 , C-8 / C-9, C-10, C-12), 34.43 (CH_3 , C-1a), 39.70 (CH, C-7), 53.50 (CH_2 , C-6), 110.45 (CH, C-4), 149.40 (CH, C-3), 166.95 (q, C-5). IR (cm^{-1} , KBr disk) ν : 2959(m), 2926(m), 2871(m), 1656(s), 1522(m), 1466(m), 1360(m), 1273(w), 1231(w), 1169(w), 1090(w), 1006(w), 982(w), 815(w), 641(m).

1,3-Dimethyl-4-(4-*t*-butylphenylaldenamine)-pyrazol-5-thione (30).

The orange solid that remained after the reduction of the filtrate (3.21 g, 69.8 %) was recrystallised from methanol to give orange crystals (2.89 g, 62.8 %). M.P. 177-179 °C; (Found: C, 65.43; H, 7.21; N, 14.30; EIMS m/z 287. $C_{16}H_{21}N_3S \cdot 0.25H_2O$ requires C, 65.83; H, 7.42; N, 14.39 %; M 287); 1H NMR ($CDCl_3$, 200 MHz) δ : 1.32 (m, 9H, $C(CH_3)_3$), 2.30 (s, 3H, CH_3), 3.74 (s, 3H, N- CH_3), 7.24-7.48 ('ab' q, $^3J_{HH}$ 8.8 Hz, 4H, (*o'*, *m'*)Ph), 8.12 (d, $^3J_{HH}$ 13.4 Hz, 1H, H-CN), 14.42 (d, $^3J_{HH}$ 13.4 Hz, 1H, NH). ^{13}C NMR ($CDCl_3$, 250 MHz) δ : 11.24 (CH_3 , C-3a), 31.10 (CH_3 , C-7), 34.53 (CH_3 , C-6), 34.60 (CH_3 , C-1a), 111.69 (q, C-4), 118.02 (CH, *o'*-arom.), 126.80 (CH, *m'*-arom.), 135.37 (CH, *p'*-arom.), 145.51 (CH, C-4a), 150.25 (q, C-3, *a'*-arom.), 168.26 (q, C-5). IR (cm^{-1} , KBr disk) ν : 2965(m), 1667(s),

1520(m), 1483(m), 1328(s), 1263(m), 1170(w), 1089(m), 1012(m), 950(w), 829(m), 800(m), 684(w), 629(w).

1,3-Dimethyl-4-(4-nonylphenylaldenamine)-pyrazol-5-thione (31).

The brown oil (21.88 g, 97.1 %) remaining after the reduction of the filtrate was further purified by dry-flash column chromatography, using ethyl acetate / hexane (1:1), yielding a yellow / brown oily solid. M.P. 70-80 °C; (Found: C, 70.60; H, 9.06; N, 10.96; FABMS m/z 357. $C_{21}H_{31}N_3S$ 0.15Hexane requires C, 71.00; H, 9.21; N, 11.34 %; M 358); 1H NMR ($CDCl_3$, 200 MHz) δ : 0.78-1.60 (m, 17H, nonyl), 2.28 (s, 3H, CH_3), 2.60 (m, 2H, N- CH_2 (nonyl)), 3.72 (s, 3H, N- CH_3), 7.22-7.31 (m, 4H, (o' , m')Ph), 8.12 (d, $^3J_{HH}$ 13.4 Hz, 1H, H-CN), 14.40 (d, $^3J_{HH}$ 13.3 Hz, 1H, NH). IR (cm^{-1} , KBr disk) ν : 2954(m), 1647(s), 1587(w), 1519(m), 1484(m), 1364(w), 1313(s), 1160(w), 1086(w), 1022(w), 829(w), 635(w).

1,3-Dimethyl-4-(2-fluorophenylaldenamine)-pyrazol-5-thione (32).

The red solid that remained after the reduction of the filtrate was recrystallised from toluene to give red crystals (5.72 g, 39.6 %). M.P. 202-204 °C; (Found: C, 57.46; H, 4.89; N, 16.88; EIMS m/z 249. $C_{12}H_{12}FN_3S$ requires C, 57.81; H, 4.85; N, 16.86 %; M 249); 1H NMR ($CDCl_3$, 200 MHz) δ : 2.29 (s, 3H, CH_3), 3.71 (s, 3H, N- CH_3), 7.17-7.46 (m, 4H, Ph), 8.19 (d, $^3J_{HH}$ 13.1 Hz, 1H, H-CN), 14.35 (d, $^3J_{HH}$ 12.1 Hz, 1H, NH). IR (cm^{-1} , KBr disk) ν : 3080(w), 2935(w), 1657(s), 1517(m), 1466(m), 1439(m), 1380(w), 1330(s), 1274(m), 1245(w), 1106(w), 1013(w), 951(w), 794(m), 751(m), 637(m).

1-Phenyl-3-methyl-4-(4-*t*-butylphenylaldenamine)-pyrazol-5-one (33).

A suspension of 1-phenyl-3-methyl-5-chloro-4-pyrazolecarboxaldehyde (4.011 g, 18 mmol) in dry ethanol (75 cm³) was prepared to which KOH.xH₂O (2.155 g, 38 mmol) and 4-*t*-butylaniline (2.701 g, 18 mmol) were added and the mixture heated at reflux for 17 h then left to cool. The KCl produced was filtered from the solution then the solvent removed from the filtrate by rotary evaporation resulting in a cream solid that was partitioned between water and dichloromethane. The organic phase was washed 3 times with water (100 cm³), twice using 0.1 M HCl (100 cm³) and finally again using water. The dichloromethane was dried using MgSO₄, filtered and the filtrate reduced to leave a brown oil which was recrystallised from propan-2-ol to give yellow / orange crystals which were isolated by filtration (0.584 g, 9.7 %). M.P. 162-164 °C; (Found: C, 73.76; H, 6.78; N, 12.08; EIMS *m/z* 333. C₂₁H₂₃N₃O 0.5H₂O requires C, 73.66; H, 6.78; N, 12.27 %; *M* 333); ¹H NMR (CDCl₃, 200 MHz) δ: 1.32 (s, 9H, C(CH₃)₃), 2.30 (s, 3H, CH₃), 7.10-7.46 (m, 7H, (*m*, *p*)Ph, (*o*', *m*')Ph), 7.89 (s, 1H, H-CN), 7.93-8.02 (m, 2H, (*o*)Ph), 11.26 (br s, 1H, NH). ¹³C NMR (CDCl₃, 250 MHz) δ: 12.55 (CH₃, C-3a), 31.14 (CH₃, C-7), 34.41 (CH₃, C-6), 102.52 (q, C-4), 116.80 (CH, *o*-, *o*'-arom.), 118.84 (CH, *o*-, *o*'-arom.), 124.24 (CH, *p*-arom.), 126.74 (CH, *m*-, *m*'-arom.), 128.63 (CH, *m*-, *m*'-arom.), 135.83 (CH, *p*'-arom.), 138.75 (CH, *a*-arom.), 142.82 (CH, C-4a), 147.86 (q, C-3, *a*'-arom.), 148.94 (q, C-3, *a*'-arom.), 165.47 (q, C-5). IR (cm⁻¹, KBr disk) ν: 3050(w), 2964(m), 1670(s), 1627(m), 1500(m), 1486(m), 1407(m), 1356(m), 1299(m), 1287(m), 1264(m), 1158(w), 1101(m), 1006(m), 954(m), 820(m), 790(m), 759(m), 691(m).

4.11.2.2 Complexes of pyrazol-5-thiones and pyrazol-5-ones.

Bis(1-phenyl-3-methyl-4-*t*-butylaldimino-pyrazol-5-thiolato)zinc(II) (34).

A hot solution of zinc acetate dihydrate (0.086 g, 0.39 mmol) in methanol (3 cm³) was added to a solution of HL (**23**) (0.216 g, 0.79 mmol) in hot methanol (10 cm³). The mixture was heated at reflux for 15 min then left to stand and cool. The precipitate was isolated by filtration and the crude product (0.184 g, 76.3 %) recrystallised from methanol to yield yellow, X-ray crystallographic grade, plate crystals. M.P. 307-311 °C; (Found: C, 58.95; H, 5.95; N, 13.96; FABMS *m/z* 611. C₃₀H₃₆N₆S₂Zn requires C, 59.05; H, 5.95; N, 13.77 %; *M* 610); ¹H NMR (CDCl₃, 200 MHz) δ: 1.42 (s, 9H, C(CH₃)₃), 2.34 (s, 3H, CH₃), 7.26-7.90 (m, 10H, 2(*o*, *m*, *p*)Ph), 8.31 (s, 2H, 2H-CN). IR (cm⁻¹, KBr disk) υ: 3045(w), 2984(m), 2921(w), 1604(s), 1519(m), 1499(m), 1443(m), 1417(m), 1373(s), 1189(m), 1015(m), 1003(m), 935(m), 761(s), 692(m), 673(m).

Bis(1-phenyl-3-methyl-4-*t*-butylaldimino-pyrazol-5-thiolato)cobalt(II) (35).

A hot solution of cobalt acetate tetrahydrate (0.097 g, 0.39 mmol) in methanol (3 cm³) was added to a solution of HL (**23**) (0.212 g, 0.78 mmol) in hot methanol (10 cm³). The mixture was heated at reflux for 15 min then left to stand and cool. The precipitate was isolated by filtration and the crude product (0.159 g, 67.5 %) recrystallised from methanol to yield dark red, X-ray crystallographic grade, plate crystals. M.P. 315 °C; (Found: C, 59.52; H, 5.93; N, 13.86; FABMS *m/z* 603. C₃₀H₃₆N₆S₂Co requires C, 59.69; H, 6.01; N, 13.92 %; *M* 604). IR (cm⁻¹, KBr disk)

ν : 3050(w), 2964(m), 1587(s), 1519(m), 1499(m), 1415(m), 1373(s), 1189(m), 1004(m), 760(m), 692(m), 672(m).

Bis(1-phenyl-3-methyl-4-phenylaldimino-pyrazol-5-thiolato)zinc(II) (36).

A hot solution of zinc acetate dihydrate (0.039 g, 0.175 mmol) in methanol (2 cm³) was added to a solution of HL (**26**) (0.103 g, 0.35 mmol) in hot methanol (25 cm³). The mixture was heated at reflux for 15 min then left to stand and cool. The precipitate was isolated by filtration and recrystallised from methanol to yield pale yellow, X-ray crystallographic grade, plate crystals (0.086 g, 75.9 %). M.P. 241-245 °C; (Found: C, 62.57; H, 4.42; N, 12.74; FABMS m/z 650. C₃₄H₂₈N₆S₂Zn requires C, 62.81; H, 4.34; N, 12.93 %; M 650); ¹H NMR (CDCl₃, 200 MHz) δ : 2.30 (m, 6H, 2CH₃), 6.98-7.75 (m, 20H, 2(*o*, *m*, *p*)Ph, 2(*o'*, *m'*)Ph), 8.09 (s, 2H, 2H-CN). IR (cm⁻¹, KBr disk) ν : 3050(w), 2930(w), 1607(m), 1580(s), 1520(m), 1499(m), 1442(m), 1360(m), 1259(w), 1214(m), 1080(w), 1000(m), 765(m), 693(m).

Bis(1-phenyl-3-methyl-4-phenylaldimino-pyrazol-5-thiolato)cobalt(II) (37).

A hot solution of cobalt acetate tetrahydrate (0.046 g, 0.18 mmol) in methanol (2 cm³) was added to a solution of HL (**26**) (0.104 g, 0.35 mmol) in hot methanol (25 cm³). The mixture was heated at reflux for 15 min then left to stand and cool. The precipitate was isolated by filtration and recrystallised from methanol to yield red, X-ray grade, plate crystals (0.103 g, 90.5 %). M.P. 252-255 °C; (Found: C, 63.21; H, 4.35; N, 13.06; FABMS m/z 644. C₃₄H₂₈CoN₆S₂ requires C, 63.44; H, 4.38; N, 13.06 %; M 644). IR (cm⁻¹, KBr disk) ν : 3040(w), 2950(w), 1575(s),

1519(m), 1498(m), 1484(m), 1441(m), 1412(m), 1358(m), 1258(m), 1211(m), 996(m), 764(m), 715(m), 692(m), 674(m).

Bis(1-phenyl-3-methyl-4-phenylaldimino-pyrazol-5-thiolato)nickel(II) (38).

A hot solution of nickel acetate tetrahydrate (0.046 g, 0.18 mmol) in methanol (2 cm³) was added to a solution of HL (**26**) (0.102 g, 0.35 mmol) in hot methanol (25 cm³). The mixture was heated at reflux for 15 min then left to stand and cool. The precipitate was isolated by filtration and recrystallised from methanol to yield red, X-ray crystallographic grade, plate crystals (0.086 g, 77.0 %). M.P. 232 °C; (Found: C, 62.68; H, 4.40; N, 12.88; FABMS *m/z* 644. C₃₄H₂₈NiN₆S₂ 0.125H₂O requires C, 62.59; H, 4.48; N, 12.88 %; *M* 643). IR (cm⁻¹, KBr disk) ν : 3046(w), 1596(m), 1575(s), 1522(s), 1500(s), 1486(s), 1444(m), 1413(m), 1351(s), 1250(m), 1202(m), 1000(m), 755(m), 718(m), 692(m), 671(m).

Bis(1-phenyl-3-methyl-4-(4-*t*-butylphenylaldimino)-pyrazol-5-thiolato)zinc(II) (39).

A hot solution of zinc acetate dihydrate (0.044 g, 0.20 mmol) in methanol (2 cm³) was added to a solution of HL (**27**) (0.141 g, 0.40 mmol) in hot methanol (20 cm³). The mixture was heated at reflux for 15 min then left to stand and cool. The precipitate was isolated by filtration and the crude product (0.111 g, 72.3 %) recrystallised from methanol to yield yellow, X-ray crystallographic grade crystals. M.P. 272-275 °C; (Found: C, 64.53; H, 5.63; N, 10.75; FABMS *m/z* 760. C₄₂H₄₄N₆S₂Zn 0.5H₂O, 0.5MeOH requires C, 64.83; H, 6.02; N, 10.67 %; *M* 762); ¹H NMR (CDCl₃, 200 MHz) δ : 1.30 (s, 18H, 2C(CH₃)₃), 2.30 (s, 6H, 2CH₃), 6.88-

7.24 ('ab' q, $^3J_{HH}$ 8.7 Hz, 8H, 2(*o'*, *m'*),Ph), 7.31-7.75 (m, 10H, 2(*o*, *m*, *p*)Ph), 8.11 (s, 2H, 2H-CN). IR (cm⁻¹, KBr disk) ν : 3050(w), 2961(m), 1612(m), 1587(s), 1506(s), 1445(m), 1409(m), 1358(s), 1219(w), 1017(m), 1000(m), 835(m), 763(m), 692(m), 680(m).

Bis(1-phenyl-3-methyl-4-(4-*t*-butylphenylaldimino)-pyrazol-5-thiolato)cobalt(II) (40).

A hot solution of cobalt acetate tetrahydrate (0.052 g, 0.21 mmol) in water (2 cm³) was added to a solution of HL (27) (0.143 g, 0.41 mmol) in hot methanol (20 cm³). The mixture was heated at reflux for 15 min then left to stand and cool. The precipitate was isolated by filtration and the crude product (0.096 g, 61.0 %) recrystallised from methanol to yield dark red, X-ray crystallographic grade crystals. M.P. 290 °C; (Found: C, 66.80; H, 5.90; N, 11.06; FABMS *m/z* 757. C₄₂H₄₄CoN₆S₂ requires C, 66.74; H, 5.87; N, 11.12 %; *M* 756). IR (cm⁻¹, KBr disk) ν : 3050(w), 2962(m), 1579(s), 1500(s), 1444(m), 1408(m), 1353(m), 1268(w), 1217(w), 1017(m), 1001(m), 836(m), 762(m), 692(m), 680(m).

Bis(1-phenyl-3-methyl-4-(4-*t*-butylphenylaldimino)pyrazol-5-thiolato)nickel(II) (41).

A hot solution of nickel acetate tetrahydrate (0.054 g, 0.22 mmol) in water (2 cm³) was added to a solution of HL (27) (0.151 g, 0.43 mmol) in hot methanol (20 cm³). The mixture was heated at reflux for 15 min then left to stand and cool. The precipitate was isolated by filtration and recrystallised, using a Soxhlet Extractor, from methanol / acetone to yield a red solid (0.112 g, 68.1 %). M.P. 260 °C; (Found:

C, 66.64; H, 5.81; N, 11.05; FABMS m/z 755. $C_{42}H_{44}NiN_6S_2$ requires C, 66.76; H, 5.87; N, 11.12 %; M 756). IR (cm^{-1} , KBr disk) ν : 3050(w), 2955(m), 1585(s), 1500(s), 1448(m), 1417(m), 1366(s), 1214(m), 1020(m), 837(m), 758(m), 694(m).

Bis(1-phenyl-3-methyl-4-(4-*t*-butylphenylaldimino)-pyrazol-5-ato)zinc(II) (42).

A hot solution of zinc acetate dihydrate (0.035 g, 0.16 mmol) in methanol (5 cm^3) was added to a solution of HL (**33**) (0.106 g, 0.32 mmol) in hot methanol (10 cm^3). The mixture was heated at reflux for 15 min then left to cool. The precipitate was isolated by filtration (0.085 g, 75.1 %) and recrystallised from acetonitrile to give colourless, X-ray crystallographic grade crystals (0.042 g, 37.2 %). M.P. 253 °C; (Found: C, 69.03; H, 6.13; N, 11.50; FABMS m/z 730. $C_{42}H_{44}N_6O_2Zn$ requires C, 69.08; H, 6.07; N, 11.51 %; M 730); 1H NMR ($CDCl_3$, 200 MHz) δ : 1.27 (s, 18H, $2C(CH_3)_3$), 2.35 (s, 6H, $2CH_3$), 6.96-7.41 (m, 14H, $2(m, p)Ph$, $2(o', m')Ph$), 7.92-7.97 (m, 4H, $2(o)Ph$), 8.27 (s, 2H, $2H-CN$). IR (cm^{-1} , KBr disk) ν : 3032(w), 2959(m), 2902(m), 2865(w), 1616(s), 1584(s), 1564(s), 1526(s), 1499(s), 1456(m), 1401(m), 1370(m), 1337(s), 1235(m), 1188(w), 1072(m), 1059(m), 1029(m), 1007(m), 981(m), 839(m), 757(m), 690(m), 608(m).

Bis(1-phenyl-3-methyl-4-(4-*t*-butylphenylaldimino)-pyrazol-5-thiolato)bis-copper(I) (43)

A hot solution of copper acetate monohydrate (0.041 g, 0.21 mmol) in water (2 cm^3) was added to a solution of HL (**27**) (0.141 g, 0.40 mmol) in hot methanol (20 cm^3). The mixture was heated at reflux for 15 min then left to stand and cool. The precipitate was isolated by filtration and the crude product (0.091 g, 58.6 %)

recrystallised from methanol to yield pale green needles containing a small amount of deep red / brown needles. M.P. 252 °C; (Found: C, 60.27; H, 5.39; N, 10.14; FABMS m/z 822. $C_{21}H_{22}CuN_3S\frac{1}{4}H_2O$ requires C, 60.55; H, 5.44; N, 10.09 %; M 823); 1H NMR ($CDCl_3$, 200 MHz) δ : 1.30 (s, 18H, $2C(CH_3)_3$), 2.33 (s, 6H, $2CH_3$), 6.52-7.11 ('ab' q, $^3J_{HH}$ 8.5 Hz, 8H, $2(o', m')$ Ph), 7.26-7.34 (m, 10H, $2(o, m, p)$ Ph), 8.00 (s, 2H, 2H-CN). IR (cm^{-1} , KBr disk) ν : 3050(w), 2961(m), 1585(s), 1501(s), 1446(m), 1411(m), 1366(m), 1269(w), 1217(w), 1002(m), 836(m), 761(m), 691(m).

4.11.2.3 Hydrazono-pyrazol-5-thiones ligands.

1-Phenyl-3-methyl-4-phenylhydrazono-pyrazol-5-one (44).

The phenyl diazonium chloride was prepared by the dropwise addition of a 2M solution of sodium nitrite (11.5 cm^3) to a solution of aniline (4.66 g, 23 mmol) in concentrated HCl (4.6 cm^3) and water (125 cm^3) at such a rate that the temperature did not exceed 5 °C.

A suspension of 1-phenyl-3-methyl-pyrazolin-5-one (4.051 g, 23 mmol) in a mixture of acetone (60 cm^3) and water (50 cm^3) was cooled to 0-5 °C using a salt-ice bath. The phenyl diazonium chloride, previously prepared, was added dropwise to this suspension at such a rate that the temperature did not exceed 5 °C. Sodium acetate (11.51 g, 140 mmol) was then added and the mixture stirred for 2 h. The resulting precipitate was isolated by filtration to yield orange crystals then recrystallised from propan-2-ol / water (5.40 g, 85.8 %). M.P. 158-159 °C (Lit. 155 °C⁷); (Found: C, 68.67; H, 4.85; N, 19.78; EIMS m/z 278. $C_{16}H_{14}N_4O$ requires C, 69.05; H, 5.07; N, 20.13 %; M 278); 1H NMR ($CDCl_3$, 200 MHz) δ : 2.36 (s, 3H, CH_3), 7.15-7.47 (m,

8H, 2Ph), 7.91-7.97 (m, 2H, 2Ph), 13.57 (s, 1H, NH). IR (cm⁻¹, KBr disk) ν : 1658(m), 1592(m), 1552(s), 1500(s), 1490(s), 1480(s), 1367(m), 1344(s), 1258(s), 1155(m), 1073(m), 1047(m), 1004(m), 912(m), 752(m), 690(m), 672(m).

1-Phenyl-3-methyl-4-(4-*t*-butylphenylhydrazono)-pyrazol-5-one (45).

The phenyl diazonium chloride was prepared by the dropwise addition of a 2M solution of sodium nitrite (15.5 cm³) to a solution of 4-*t*-butylaniline (10.004 g, 67 mmol) in conc. HCl (6.2 cm³) and water (200 cm³) at such a rate that the temperature did not exceed 5 °C.

A suspension of 1-phenyl-3-methyl-pyrazolin-5-one (5.834 g, 33 mmol) in a mixture of acetone (70 cm³) and water (70 cm³) was cooled to 0-5 °C using a salt-ice bath. The phenyl diazonium chloride was added dropwise to this suspension at such a rate that the temperature did not exceed 5 °C. Sodium acetate (15.38 g, 187 mmol) was added and then the mixture was stirred for 2 h. The resulting precipitate was isolated by filtration to yield orange crystals and then recrystallised from ethanol (7.44 g, 67.4 %). M.P. 133-135 °C; (Found: C, 71.75; H, 6.65; N, 16.60; EIMS *m/z* 334. C₂₀H₂₂N₄O requires C, 71.83; H, 6.63; N, 16.75 %; *M* 334); ¹H NMR (CDCl₃, 200 MHz) δ : 1.33 (s, 9H, 3CH₃), 2.36 (s, 3H, CH₃), 7.15-7.47 (m, 7H, 2Ph), 7.91-7.97 (m, 2H, 2Ph), 13.62 (s, 1H, NH). IR (cm⁻¹, KBr disk) ν : 3066(w), 2965(m), 2866(w), 1654(m), 1591(m), 1552(s), 1500(s), 1486(m), 1370(m), 1341(m), 1277(s), 1182(m), 1160(m), 1110(m), 1049(m), 1004(m), 914(w), 827(m), 758(m), 690(m).

1-Phenyl-3-methyl-5-chloro-4-phenylazo-pyrazole (46).

A mixture of 1-phenyl-3-methyl-4-phenylhydrazono-pyrazol-5-one (4.016 g, 14.4 mmol) and POCl₃ (3.350 g, 22 mmol) was heated to 100 °C for 3 h. Ice water was then added and the mixture neutralised with aqueous NaOH to pH 7 then extracted into chloroform. The organic layer was washed twice with water then dried over MgSO₄ and filtered. The chloroform was removed by rotary evaporation and the resulting yellow / brown solid was recrystallised from toluene / 60-80 petroleum ether (1:3) to give yellow needles (3.02 g, 70.4 %). M.P. 114.5-115 °C (Lit. 109-110 °C⁶); (Found: C, 64.70; H, 4.31; N, 18.60; EIMS *m/z* 296. C₁₆H₁₃ClN₄ requires C, 64.54; H, 4.74; N, 18.82 %; *M* 297); ¹H NMR (CDCl₃, 200 MHz) δ: 2.59 (s, 3H, CH₃), 7.29-7.65 (m, 8H, 2Ph), 7.82-7.90 (m, 2H, 2Ph). IR (cm⁻¹, KBr disk) ν: 3050(w), 2960(w), 2920(w), 1594(m), 1534(s), 1502(m), 1452(m), 1421(s), 1382(m), 1370(m), 756(m), 688(m).

1-Phenyl-3-methyl-5-chloro-4-(4-*t*-butylphenylazo)-pyrazole (47).

A mixture of 1-phenyl-3-methyl-4-(4-*t*-phenylhydrazono)-pyrazol-5-one (7.049 g, 21 mmol) and POCl₃ (4.834 g, 31.5 mmol) was heated to 100 °C for 3 h. Ice water was then added and the mixture neutralised with aqueous NaOH to pH 7 then extracted into chloroform. The organic layer was washed twice with water then dried over MgSO₄ and filtered. The chloroform was removed by rotary evaporation and the resulting yellow / brown solid was recrystallised from propan-2-ol to give yellow needles (5.96 g, 80.4 %). M.P. 96-98 °C; (Found: C, 67.91; H, 5.95; N, 15.81; EIMS *m/z* 352. C₂₀H₂₁ClN₄ requires C, 68.08; H, 6.00; N, 15.88 %; *M* 353); ¹H NMR (CDCl₃, 200 MHz) δ: 1.36 (s, 9H, 3CH₃), 2.58 (s, 3H, CH₃), 7.40-

7.83 (m, 9H, 2Ph). IR (cm⁻¹, KBr disk) ν : 3059(w), 2961(m), 1601(m), 1533(s), 1504(s), 1472(m), 1448(m), 1414(s), 1383(m), 1267(m), 1105(m), 1010(m), 1000(m), 901(m), 844(m), 766(m), 690(m), 672(m), 642(m), 621(m).

1-Phenyl-3-methyl-4-phenylhydrazono-pyrazol-5-thione (48).

1-Phenyl-3-methyl-5-chloro-4-phenylazo-pyrazole (11.06 g, 37 mmol) and NaSH.xH₂O (4.179 g, 74 mmol) was heated at reflux for 2 h in ethanol / water (1:1) (200 cm³). The reaction was cooled to ambient temperature and acidified with dilute HCl to pH ~2 and then extracted into chloroform. The chloroform was washed with water (3 x 50 cm³) and dried using MgSO₄ then filtered. The chloroform was removed from the filtrate by rotary evaporation to yielding red oil which was recrystallised from methanol to give deep red crystals (7.17 g, 65.8 %). M.P. 101-103 °C (Lit. 100-101 °C⁶); (EIMS *m/z* 294, *M* 294); ¹H NMR (CDCl₃, 200 MHz) δ : 2.42 (s, 3H, CH₃), 7.24-7.62 (m, 8H, 2Ph), 7.87-7.94 (m, 2H, 2Ph), 17.09 (s, 1H, NH). IR (cm⁻¹, KBr disk) ν : 1654(m), 1592(m), 1552(s), 1490(s), 1479(s), 1362(s), 1343(m), 1260(m), 1230(m), 1142(m), 1073(m), 1014(m), 901(w), 754(s), 683(m), 665(m).

1-Phenyl-3-methyl-4-(4-*t*-butylphenylhydrazono)-pyrazol-5-thione (49).

1-Phenyl-3-methyl-5-chloro-4-(4-*t*-butylphenylazo)-pyrazole (5.042 g, 14 mmol) and NaSH.xH₂O (1.598 g, 28 mmol) was heated at reflux for 4 h in ethanol / water (1:1) (100 cm³). The reaction was cooled to ambient temperature and acidified with dilute HCl to pH ~2 and extracted into chloroform. The chloroform was washed with water (3 x 50 cm³) and dried using MgSO₄ then filtered. The chloroform was removed

from the filtrate by rotary evaporation to give a dark red oil. The red oil was dissolved in ethanol and precipitated with water to yield a red solid (4.18 g, 85.2 %). M.P. 84-86 °C; (EIMS m/z 350, M 350); ^1H NMR (CDCl_3 , 200 MHz) δ : 1.37 (s, 9H, 3CH₃), 2.33 (s, 3H, CH₃), 7.26-7.93 (m, 9H, 2Ph), 17.14 (s, 1H, NH). IR (cm^{-1} , KBr disk) ν : 3049(w), 2962(s), 2903(m), 2867(m), 1598(m), 1543(m), 1518(m), 1499(s), 1467(m), 1442(m), 1396(s), 1366(s), 1268(m), 1234(m), 1147(m), 1106(m), 1011(m), 907(w), 844(m), 760(m), 691(m), 671(m).

4.11.2.4 Complexes of hyrazono-pyrazol-5-thiones.

Bis(1-phenyl-3-methyl-4-phenylazo-pyrazol-5-thiolato)zinc(II) (50).

A hot solution of zinc acetate dihydrate (0.116 g, 0.53 mmol) in water (2.5 cm³) was added to a solution of HL (48) (0.313 g, 1.1 mmol) in hot methanol (30 cm³). The mixture was heated at reflux for 15 min then left to stand and cool. The precipitate was filtered and the crude product (0.314 g, 90.9 %) recrystallised with a Soxhlet Extractor using ethanol / methanol (1:1) to yield orange, X-ray crystallographic grade plate crystals (0.206 g, 59.6 %). M.P. 225-227 °C (Lit. 225-227 °C⁶); (Found: C, 57.58; H, 4.20; N, 16.19; FABMS m/z 653. $\text{C}_{32}\text{H}_{26}\text{N}_8\text{S}_2\text{Zn}\cdot\text{CH}_3\text{OH}$ requires C, 57.93; H, 4.42; N, 16.38 %; M 652); ^1H NMR (CDCl_3 , 200 MHz) δ : 2.50 (s, 6H, 2CH₃), 7.22-7.74 (m, 20H, 4Ph). IR (cm^{-1} , KBr disk) ν : 1591(w), 1534(w), 1409(s), 1390(s), 1254(m), 1199(m), 1159(m), 1050(m), 762(m), 686(m), 670(m).

Bis(1-phenyl-3-methyl-4-phenylazo-pyrazol-5-thiolato)cobalt(II) (51).

A hot solution of cobalt acetate tetrahydrate (0.134 g, 0.54 mmol) in water (2.5 cm³) was added to a solution of HL (48) (0.315 g, 1.1 mmol) in hot methanol (30 cm³). The mixture was heated at reflux for 15 min then left to stand and cool. The precipitate was filtered and the crude product (0.292 g, 84.4 %) recrystallised with a Soxhlet Extractor using ethanol to yield deep red crystals (0.278 g, 80.3 %). M.P. 237 °C (Lit. 228-230 °C⁶); (Found: C, 58.51; H, 4.01; N, 16.95; FABMS *m/z* 645. C₃₂H₂₆CoN₈S₂ 0.75CH₃OH requires C, 58.74; H, 4.36; N, 16.73 %; *M* 646). IR (cm⁻¹, KBr disk) ν : 1591(m), 1534(w), 1409(s), 1387(s), 1252(m), 1194(m), 1160(m), 1051(m), 762(m), 686(m), 670(m).

4.12 References.

1. L. Knorr, *Ber. Chemie*, 1883, 2597.
2. R.H. Wiley, P. Wiley, *Heterocyclic Compounds*, ed. A. Weissberger, John Wiley and Sons Inc., NY, 1964, vol.20, pt.2, ch.1-5, pp143-157.
3. A.R. Katritzky, B. Rachwal, S. Rachwal, D. Macomber, T.P. Smith, *J. Heterocycl. Chem.*, 1993, **30**, 135.
4. J.L. Huppatz, *Aust. J. Chem.*, 1983, **36**, 135.
5. G. Hinsche, E. Uhlemann, K. Gloe, P. M[ü]hl, *Z. Chem.*, 1989, **29**, 182.
6. T. Tanaka, K. Tanaka, *Chem. Pharm. Bull.*, 1981, **29**, 445.
7. F.A. Snavely, W.C. Fernelius, B.P. Block, *J. Am. Chem. Soc.*, 1957, **79**, 1028.
8. F.A. Snavely, B.D. Kreckler, C.G. Clark, *J. Am. Chem. Soc.*, 1959, **81**, 2337.
9. F.A. Snavely, B.D. Kreckler, *J. Am. Chem. Soc.*, 1959, **81**, 4199.
10. S. Umetani, M. Matsui, *Bull. Chem. Soc. Jpn.*, 1983, **56**, 3426.
11. S. Miyazaki, H. Mukai, S. Umetani, S. Kihara, M. Matsui, *Inorg. Chem.*, 1989, **28**, 3014.
12. W. Mickler, A. Reich, E. Uhlemann, *Separation Science and Technology*, 1998, **33**, 425.
13. S. Umetani, M. Matsui, J. Toei, T. Shigematsu, *Anal. Chim. Acta.*, 1980, **113**, 315.
14. W. Mickler, A. Reich, E. Uhlemann, *Separation Science and Technology*, 1995, **30**, 2585.
15. S. Umetani, Y. Kawsae, Q.T.H. Le, M. Matsui, *Inorg. Chim. Acta.*, 1998, **267**, 201.

16. W. Mickler, A. Reich, E. Uhlemann, ISEC '96, Melbourne, Australia, pp.415-420.
17. B.S. Jensen, *Acta. Chem. Scanda.*, 1959, **13**, 1890.
18. J.P. Brunette, M. Taheri, G. Goetz-Grandmont, M.J.F. Leroy, *Polyhedron*, 1982, **1**, 457.
19. J.P. Brunette, M. Lakkis, G. Goetz-Grandmont, M.J.F. Leroy, *Polyhedron*, 1982, **1**, 461.
20. R.H. Wiley, P. Wiley, *Heterocyclic Compounds*, ed. A. Weissberger, John Wiley and Sons Inc., NY, 1964, vol.20, pt.1, ch.2, pp13-19.
21. R.H. Wiley, P. Wiley, *Heterocyclic Compounds*, ed. A. Weissberger, John Wiley and Sons Inc., NY, 1964, vol.20, pp161-206.
22. S. Viebel, K. Eggerson, S.C. Linholt, *Acta. Chem. Scanda.*, 1954, **8**, 768.
23. J. DeRuiter, D.A. Carter, W.S. Arledge, P.J. Sullivan, *J. Heterocyclic. Chem.*, 1987, **24**, 149.
24. L.F. Tietze, T. Brumby, M. Pretor, G. Remberg, *J. Org. Chem.*, 1988, **53**, 810.
25. L.H. Briggs, E.F. Orgias, *J. Chem. Soc. Sect. C*, 1970, 1885.
26. D. Villeman, B. Labiad, *Synthetic Communications*, 1990, **20**, 3213.
27. J.D. Wilson, T.D. Fulmer, L.P. Dasher, C.F. Beam, *J. Heterocyclic Chem.*, 1980, **17**, 389.
28. P.R. Giles, C.M. Marson, *Tetrahedron Letters*, 1990, **31**, 5227.
29. J. Becher, P.H. Olesen, N.A. Knudsen, H. Toftlund, *Sulfur Lett.*, 1986, **4**, 175.
30. B.A. Porai-Koshits, I.Y. Kvitko, E. A. Shutkova, *Khim.-Farm. Zh.*, 1970, **4**, 19.
31. R.A. Pawar, A.A. Patil, *Ind. J. Chem.*, 1994, **33**, 156.

32. S. Alunni, P. Linda, G. Marino, S. Santini, G. Savelli, *J. Chem. Soc. Perkin II*, 1972, **2**, 2070.
33. G. Jugie, J.A.S. Smith, G.J. Martin, *J. Chem. Soc. Perkin II*, 1975, **2**, 925.
34. J. Becher, P.L. Jogensen, K. Pluta, N. J. Krake, B. Falt-Hansen, *J. Org. Chem.*, 1992, **57**, 2127.
35. A. la Cour, B. Adhikhari, H. Toftlund, *Inorg. Chim. Acta.*, 1992, **202**, 145.
36. B.S. Jensen, *Acta. Chem. Scanda.*, 1959, **13**, 1668.
37. L. Hennig, G. Mann, *Z. Chem.*, 1988, **28**, 364.
38. J.L. Hughey IV, T.G. Fawcett, S.M. Rudich, R.A. Lalancette, J.A. Polenga, H.J. Schugar, *J. Am. Chem. Soc.*, 1979, **101**, 2617.
39. J. Becher, H. Toftlund, P.H. Olesen, *J. Chem. Soc., Chem. Commun.*, 1983, 740.
40. L. Hennig, R. Kirme, O. Hammerich, S. Larsen, H. Frydendahl, H. Toftlund, J. Becher, *Inorg. Chim. Acta.*, 1995, **234**, 67.
41. O.P. Anderson, J. Becher, H. Frydendahl, L.F. Taylor, H. Toftlund, *J. Chem. Soc., Chem. Commun.*, 1986, 699.
42. J. Becher, H. Toftlund, P.H. Olesen, H. Nissen, *Inorg. Chim. Acta.*, 1985, **103**, 167.
43. A.R. Katrinkzy, F.W. Maine, *Tetrahedron*, 1964, 299.
44. D.H. Williams, I. Fleming, *Spectroscopic Methods in Organic Chemistry*, McGraw-Hill, Avon, 5th Ed., 1995, ch.3, pp.63-169.
45. A. la Cour, M. Findeisen, A. Hazell, R. Hazell, G. Zdobinsky, *J. Chem. Soc., Dalton Trans.*, 1997, 121.
46. G.M. Sheldrick, SHELXL-97, University of Göttingen, Germany, 1997.

47. T.G. Takhirov, O.A. D'yachenko, D.B. Tagiev, A.L. Nivorozhkin, L.E. Nivorozhkin, V.I. Minki, *Koord. Khim.*, 1991, **17**, 817.
48. A.G. Orpen, L.Brammer, F.H. Allen, O. Kennard, D.G. Watson, R. Taylor, *J. Chem. Soc., Perkin II*, 1987, **S1**.
49. D.D. Ebbing, *General Chemistry*, ed. M.S. Wrighton, Houghton Mifflin, Boston, 5th edn., 1996, ch.9, pp343-386.
50. J. March, *Advanced Organic Chemistry: Reactions, Mechanisms and Structures*, Wiley-Interscience, NY, 4th edn., 1992, ch.1, pp.3-25.
51. T.G. Takhirov, O.A. D'yachenko, D.B. Tagiev, A.L. Nivorozhkin, L.E. Nivorozhkin, V.I. Minkin, *Koord. Khim.*, 1988, **14**, 131.
52. A.S. Antsishkina, M.A. Porai-Koshits, A.L. Nivorozhkin, I.S. Vasilchenko, L.E. Nivorozhkin, A.D. Garnovsky, *Inorg. Chim. Acta.*, 1991, **180**, 151.
53. A.L. Nivorozhkin, E.V. Sukholenko, L.E. Nivorozhkin, N.I. Borisenko, V.I. Minkin, Y.K. Grishin, O.A. D'yachenko, T.G. Takhirov, D.B. Tagiev, *Polyhedron*, 1989, **8**, 569.
54. A.L. Nivorozhkin, L.E. Nivorozhkin, V.I. Minkin, T.G. Takhirov, O.A. D'yachenko, *Polyhedron*, 1991, **10**, 179.
55. O.P. Anderson, A. la Cour, M. Findeisen, L. Hennig, O. Simonsen, L.F. Taylor, H. Toftlund, *J. Chem. Soc., Dalton Trans.*, 1997, 111.
56. H. Toftlund, A.L. Nivorozhkin, A. la Cour, B. Adhikary, K. Murray, G.D. Fallon, L.E. Nivorozhkin, *Inorg. Chim. Acta.*, 1995, **228**, 237.
57. A.I. Uraev, A.L. Nivorozhkin, A.S. Frenkel, A.S. Antsishkina, M.A. Porai-Koshits, L.E. Nivorozhkin, G.K.I Magomedov, A.D. Garnovsky, *J. Organomet. Chem.*, 1989, **368**, 303.

58. A.L. Nivorozhkin, A.I. Uraev, G.I. Bondarenko, A.S. Antsishkina, V. Kurbatov, A.D. Garnovskii, C.I. Turta, N.D. Brashoveanu, *J. Chem. Soc., Chem. Commun.*, 1997, 1711.
59. Graphical display was obtained from Cerius² molecular modelling system under licence from Molecular Simulations Inc., San Diego, CA.
60. C. Tolman, *Chem. Rev.*, 1977, **77**, 313.
61. A. Bondi, *J. Phys. Chem.*, 1964, **68**, 441.
62. A.L. Nivorozhkin, H. Toftlund, M. Nielsen, *J. Chem. Soc., Dalton Trans.*, 1994, 361.
63. R.D. Shannon, *Acta. Crystallogr.*, 1976, **A32**, 751.
64. Microcal Origin 5.0 software, Inc.
65. F. Habashi, *A Textbook Of Hydrometallurgy*, ed. F. Habashi, Métallurgie Extractive Québec, 1993, ch.24, pp.563-602.
66. Work carried out by Dr. D.J. White and Prof. L. Lindoy at Sydney University, Australia with funding provided by the EPSRC.
67. J. March, *Advanced Organic Chemistry: Reactions, Mechanisms and Structures*, Wiley-Interscience, NY, 4th edn. 1992, ch.12, pp.635-637.
68. R.N. Bulter, *Chem. Rev.*, 1975, **75**, 241.
69. A. Whitaker, *Acta. Crystallogr.*, 1988, **C44**, 1578.
70. A. Whitaker, *Acta. Crystallogr.*, 1988, **C44**, 1767.
71. J.A. Connor, R.J. Kennedy, H.M. Dawes, M.B. Hursthouse, N.P.C. Walker, *J. Chem. Soc. Perkin Trans. II*, 1990, 203.
72. L. Pauling, *J. Am. Chem. Soc.*, 1947, **69**, 542.
73. V. Bertolasi, P. Gilli, V. Ferretti, G. Gilli, *Acta. Crystallogr.*, 1994, **B50**, 617.

74. J. Buchi, R. Ursprung, G. Lauener, *Helv. Chim. Acta.*, 1949, **32**, 984.

Chapter 5

Tetradentate Thiopyrazolone

Chemistry

5.1 Introduction.

This chapter describes the synthesis, characterisation and solid state structures of several tetradentate ligands based on two bidentate pyrazol-5-thione units (Chapter 4) bridged by various diimino substituents and some of their complexes with Ni(II) and Zn(II). The solubility (Section 5.3) of these ligands was severely reduced in comparison to the equivalent bidentate ligands and it was not possible to assess their strength as extractants.

In Chapter 4 it was shown that bidentate imino pyrazol-5-thiones are weak extractants and show selectivity towards zinc(II) over cobalt(II) and nickel(II). A minimum $\text{pH}_{1/2}$ value of 3.6 for zinc was observed with the extraction strength dominated by the electronic nature of the imino substituent and hence the acidity of the ligand. However to prevent the precipitation of iron(III) hydroxides a successful extractant must be capable of extracting zinc at a $\text{pH} < 2.5$, in practice this will require a $\text{pH}_{1/2} < 2$. A further increase in the acidity, to increase the extractant strength may have the detrimental effect of decreasing the basicity of the deprotonated ligand lowering the stability of the metal complex. This chapter explores an alternative approach using tetradentate di-anionic ligands, which due to the chelate effect (Section 2.2.3) should show increased metal complex stability and therefore lower $\text{pH}_{1/2}$ values.

In addition, if tetradentate ligands are prepared which are predisposed to a tetrahedral coordination geometry they should show both high strength and maintained or improved selectivity of Zn(II) over Co(II) and Ni(II).

5.2 Preparation and characterisation of pyrazol-5-thiones.

The bis-(1-phenyl-3-methyl-pyrazol-5-thione)-4-alkyldialdenamines (**52-55**) and the bis-(1,3-dimethyl-pyrazol-5-thione)-4-alkyldialdenamines (**56-58**) were prepared using the synthetic strategy, described in Section 4.2, based upon 1-phenyl-3-methyl- and 1,3-dimethyl-5-chloro-4-pyrazolecarboxaldehydes, (**21**) and (**22**) respectively, Figure 5.1. The procedure is modified slightly by using a 1:2:4 ratio of amine / chloroaldehyde / sodium hydrogen sulfide instead of 1:1:2 to take into account the double imine condensation linking the two pyrazole units. The yield, although not fully optimised, is approximately 50 % for the range of tetradentate compounds presented here for this step in the synthetic procedure and is much lower than those obtained for the bidentate compounds (Section 4.11.2.1).

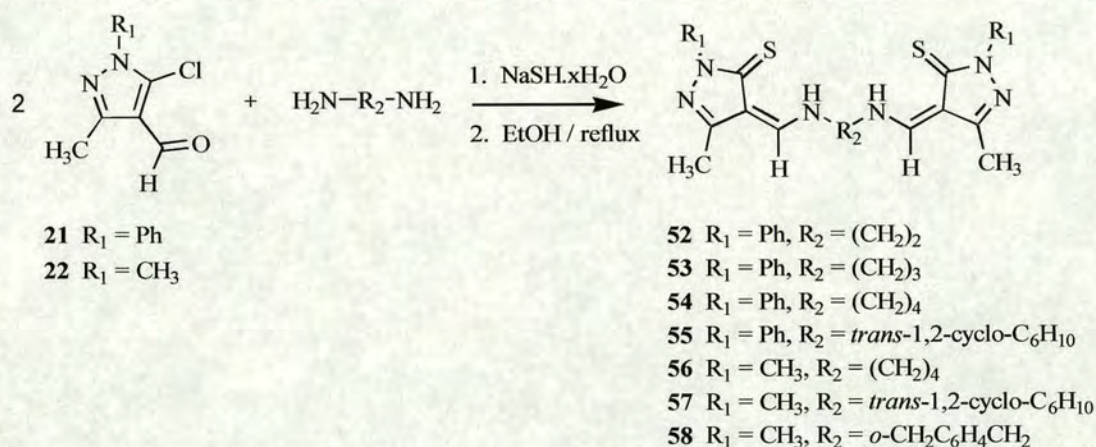


Figure 5.1. The “one-pot” nucleophilic substitution and diimine condensation for the preparation of bis-(1-substituted-3-methyl-5-pyrazol-5-thione)-4-alkyldialdenamines (**52-58**).

The diamines used were obtained commercially with the exception of *o*-xylene-diamine (**60**) which was prepared from the commercially available precursor

dibromo-*o*-xylene following the procedure for the Gabriel synthesis¹ of primary amines, Figure 5.2.

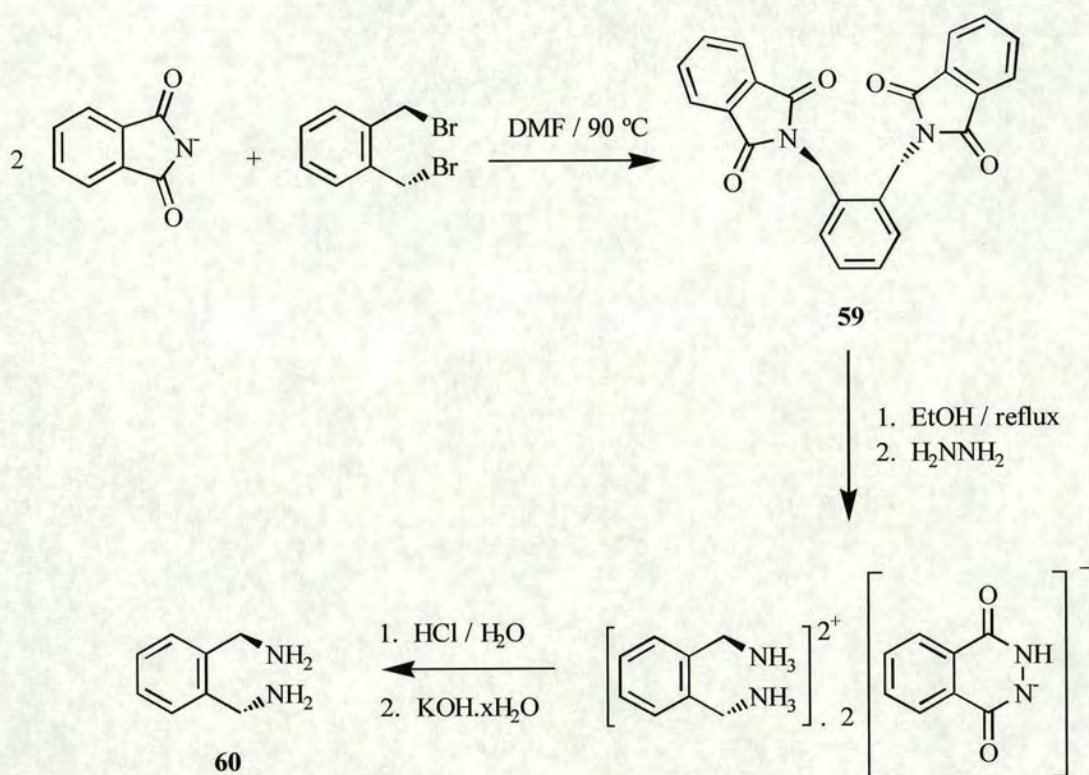


Figure 5.2. Gabriel synthesis of *o*-xylene-diamine (60).

A 1.5 fold excess of potassium phthalimide was used in the reaction with dibromo-*o*-xylene to produce N,N-(*o*-methylenexylene)-diphthalimide (59) in the first stage of the synthesis. Yields are generally high for primary alkyl halides with the exception of those which are sterically hindered. The obtained yield of 75 % suggests that even though two transformations are occurring in close proximity the system is not highly sterically hindered.

The N,N-(*o*-methylenexylene)-diphthalimide was converted to the corresponding diamine by hydrazinolysis in the second stage in approximately 75 % yield. The

intermediate diamine salt of phthalhydrazide formed was isolated then redissolved in water and acidified to pH 2 using dilute HCl, precipitating the phthalhydrazide and leaving the diamine dihydrochloride in solution. Treatment of the dihydrochloride salt with a dilute KOH afforded the free base. Although not optimised, the overall yield for the synthesis of *o*-xylene-diamine is ~55 %.

5.2.1 NMR spectroscopy.

Full experimental characterisation is given in Section 5.6.1. The ^1H NMR spectra of the ligands (**52-58**) were recorded in CDCl_3 . As with the bidentate pyrazol-5-thiones (Section 4.6.1) the tetradentate analogues exist in the enamine-thione tautomer with the NH resonance occurring in the range 12.69 ppm to 13.16 ppm. The complete assignment of the spectra for **55** and **57** has not been possible due to the overlap of the methylene signals for the cyclohexyl substituent. In those spectra containing a phenyl group attached directly to the pyrazole ring **52-55** the doublet associated with the aldehydic proton (H-CN) is hidden in the aromatic region. In those spectra where the phenyl ring is absent (**56-58**) the doublet appears at ~7.5 ppm with a coupling constant ($^3J_{\text{HH}} \sim 13.5$ Hz) similar in magnitude to the bidentate analogues.

The methylene signal for the spectra containing the xylyl group (**58**) is shifted downfield to 4.79 ppm due to the presence of the aromatic phenyl. It appears as a doublet ($^2J_{\text{HH}} \sim 5.5$ Hz), attributed to the geminal splitting of the two protons due to their hindered rotation and magnetic inequivalence.

The ^1H NMR of the N,N-(*o*-methylene-xylene)-diphthalimide (**59**) was recorded in CDCl_3 . In contrast to **58** a singlet is observed for the methylene protons (5.21 ppm) indicating the free rotation of the phthalimide group. The hydrazinolysis and

acidification the dipthalimide (**59**) was confirmed by the positive identification of the precipitated phthalhydrazide² by-product, recorded in d_6 -DMSO, and the agreement with literature³ of the ^1H NMR and ^{13}C NMR of *o*-xylene-diamine dihydrochloride, recorded in D_2O .

5.2.2 Mass spectroscopy.

The EI spectra of bis-(1-phenyl-3-methyl-pyrazol-5-thione)-4-*trans*-1,2-cyclohexyldialdenamine (**55**) contains the parent ion ($m/z = 514$, 100 %) consistent with the expected structure. The fragmentation pattern suggests decomposition of the compound *via* the cleavage of the carbon-nitrogen bond adjacent to the cyclohexyl ring. Identification of the remaining ligands (H_2L) using the electron impact technique was unsuccessful with the absence of the parent ion peaks or a representative fragmentation pattern. However the molecular ions for ligands **52-54**, **57** and **58** are present in the positive FAB spectra.

Positive FABMS was also used to characterise the *o*-xylene-diamine dihydrochloride, which showed ion peaks for the of loss one ($m/z = 174$) and two ($m/z = 137$) chlorine anions associated with *o*-xylene-diamine monochloride and *o*-xylene-diamine cation ions respectively.

5.3 Preparation and characterisation of metal complexes.

The metal complexes of the bis-(1-substituted-3-methyl-pyrazol-5-thione)-4-alkyldialdenamines (**55-58**) with the general formula $[\text{M}(\text{L})]$ (**61-66**) were prepared by the addition of the appropriate metal(II) acetate to the ligand (H_2L) as described in Section 3.3 using a metal:ligand ratio of 1:1, Figure 5.3.

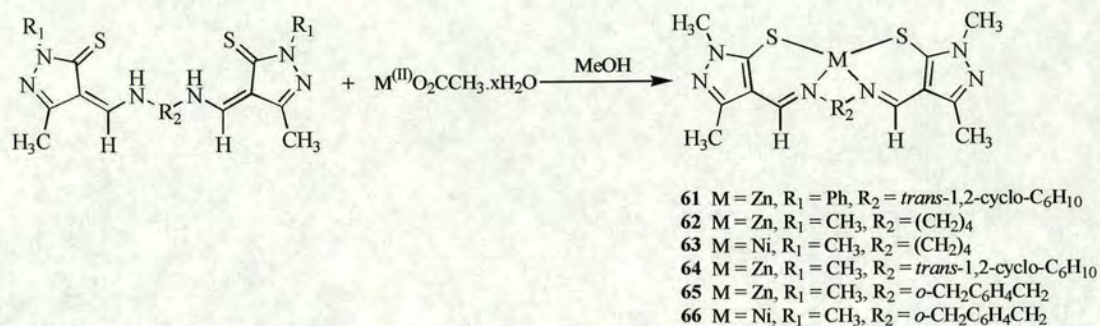


Figure 5.3. Synthesis of the bis-(pyrazol-5-thiolato)-4-alkyldialdimino metal complexes.

Immediate precipitation of the zinc complexes **61** and **64** occurred on the addition of the zinc(II) acetate solution to the ligands containing the 1,2-*trans*-cyclohexyl bridging diimine group. This reflects the low solubility measured for these complexes, Table 5.1. The more soluble complexes, **62** and **65**, showed immediate decolourisation of the ligands on addition of zinc(II) acetate, however on cooling an insoluble precipitate formed.

Complex	Solubility / M
[Zn(55-2H)] (61)	4.3 x 10 ⁻⁴
[Zn(56-2H)] (62)	5.7 x 10 ⁻³
[Zn(57-2H)] (64)	1.6 x 10 ⁻⁵
[Zn(58-2H)] (65)	3.7 x 10 ⁻²

Table 5.1. Solubility of the zinc complexes **61**, **62**, **64** and **65** in toluene.

To assess the extractive capabilities in the solvent extraction system the ligand and metal complex are required to have a minimum solubility of 0.05 M in toluene. Clearly the tetradentate ligands, described here, and to an even greater extent their

zinc complexes do not meet this requirement. Extensive precipitation was expected and observed in preliminary solvent extraction experiments such that the extraction equilibrium could not be measured.

5.3.1 NMR spectroscopy.

Full experimental characterisation is detailed in Section 5.6.2. The ^1H NMR spectrum of $[\text{Zn}(\mathbf{58-2H})]$ (**65**) was recorded in CDCl_3 whereas the spectra for $[\text{Zn}(\mathbf{55-2H})]$ (**61**), $[\text{Zn}(\mathbf{56-2H})]$ (**62**) and $[\text{Zn}(\mathbf{57-2H})]$ (**64**) were obtained in d_6 -DMSO due to their insolubility in chloroform. The absence of the NH resonance (~ 13 ppm) and the appearance of a singlet associated with the aldehydic proton (~ 8.3 ppm) is consistent with the double deprotonation of the ligand and confirms its complexation to zinc.

The methylene protons in the spectrum of **65** appear as an “ab” quartet (4.39-5.34 ppm, $^2J_{HH}$ 14.3 Hz), attributed to the magnetic inequivalence of the two protons with the inclusion of a chiral centre. The large difference in chemical shift between the two mutually coupled protons is an indication of their quite different environments, Zn(1)-H(43a) is ~ 2.9 Å whereas Zn(1)-H(43b) is ~ 3.7 Å, and is possibly augmented by a hindered rotation, (see Figure 5.6). In contrast the chemical shift of the benzylic protons in $[\text{Co}(\mathbf{5-H})_2]$ (**11**) are more similar, possibly because of less rotational hindrance (Section 3.3.1, Figure 3.7).

5.3.2 Mass spectroscopy.

The positive FAB spectra of $[\text{Zn}(\mathbf{55-2H})]$ (**61**), $[\text{Zn}(\mathbf{56-2H})]$ (**62**), $[\text{Ni}(\mathbf{56-2H})]$ (**63**), $[\text{Zn}(\mathbf{57-2H})]$ (**64**), $[\text{Zn}(\mathbf{58-2H})]$ (**65**) and $[\text{Ni}(\mathbf{58-2H})]$ (**66**) show molecular ion peaks

associated with $[M(L)(H)]^+$ which are expected for the tetradentate pyrazol-5-thiolato complexes with the generalised molecular formula $[M(L)]$. In contrast with the bis-bidentate-imino-pyrazol-5-thiolato complexes (Section 4.3.2) there is an absence of any recognisable fragmentation patterns or ion peaks greater than the parent ion signal. This may be attributed partly to the weak intensity of the ion signals, compared to the background noise, and partly to an increase in the stability of the tetradentate pyrazol-5-thiolato complexes.

5.4 Crystallographic characterisation.

The structural figures were generated using XP software⁴ showing atomic displacement ellipsoids and with the atoms labelled according to the system described in Section 3.4. The crystallographic data for the tetradentate structures are summarised in Appendix V.

5.4.1 Ligands.

5.4.1.1 Comparison of *trans*-1,2-cyclohexyl and *n*-butyl bridging groups.

H_2L (**55**). $\frac{1}{8}H_2O$ crystallises as yellow blocks in a triclinic crystal system with the space group $P\bar{1}$ (no.2). The asymmetric unit contains two essentially identical ligands, one of which is associated with a 25 % partially occupied water molecule. A single molecule from the asymmetric unit is shown in Figure 5.4(a). H_2L (**56**) crystallises in a monoclinic crystal system with the space group $P2_1/c$. The asymmetric unit contains one half of the ligand which exhibits C_2 symmetry with the crystallographic two-fold axis bisecting the butyl bridge at a point equidistant

Selected bond lengths and angles for H₂L (**55**). $\frac{1}{8}$ H₂O and H₂L (**56**) are listed in Table 5.2. The geometry of the two pyrazole units in both ligands show no significant differences due to the influence of the backbones as compared to the bidentate pyrazol-5-thione ligands (Section 4.4.1.1) and, as expected, exist as the enamine-thione tautomer as in the bidentate analogues.

	H ₂ L (55). $\frac{1}{8}$ H ₂ O		H ₂ L (56)	
	Part(A)	Part(B)	Part(A)	Part(*)
N(1)-C(5)	1.367(5)	1.359(5)	1.346(2)	1.346(2)
N(1)-N(2)	1.398(4)	1.394(5)	1.385(2)	1.385(2)
N(2)-C(3)	1.301(5)	1.317(6)	1.311(2)	1.311(2)
N(1)-C(11)	1.426(5)	1.417(6)	1.450(2)	1.450(2)
C(3)-C(4)	1.428(5)	1.425(6)	1.422(3)	1.422(3)
C(3)-C(31)	1.493(5)	1.490(6)	1.491(3)	1.491(3)
C(4)-C(41)	1.380(5)	1.375(6)	1.389(3)	1.389(3)
C(4)-C(5)	1.423(5)	1.429(5)	1.428(3)	1.428(3)
C(41)-N(42)	1.306(5)	1.310(5)	1.289(3)	1.289(3)
N(42)-C(43)	1.460(5)	1.446(5)	1.470(3)	1.470(3)
C(43A)-C(43B)	1.535(6)		-	
C(43)-C(44)	-	-	1.499(3)	1.499(3)
C(44A)-C(44A')	-		1.519(4) ^(a)	
C(5)-S(5)	1.693(4)	1.682(4)	1.692(2)	1.692(2)
S(5)-C(5)-C(4)	127.9(3)	128.2(3)	130.10(15)	130.10(15)
C(5)-C(4)-C(41)	127.6(4)	127.9(4)	127.35(18)	127.35(18)
C(4)-C(41)-N(42)	124.2(4)	125.0(4)	125.2(2)	125.2(2)

Table 5.2. Selected bond lengths (Å) and angles (°) in H₂L (**55**). $\frac{1}{8}$ H₂O and H₂L (**56**). ^(a) Crystallographically related by rotational symmetry(-x-1, 2-y, -z).

An *E*-configuration is adopted around the enamine bonds, C(41)-N(42), forming two 6-membered rings *via* S \cdots H-N *intramolecular* hydrogen bonding. The observed

N(42)⋯S(5) bite distances range from 3.067(5) Å in **55** (part A) to 3.151(2) Å in **56**, (see Table 5.3), the magnitudes of which correlate closely with the increase in bond angles around the ring (see Table 5.2) and follows the trend seen for the analogous bidentate ligands, see Section 4.4.1.1. An additional, weaker, *intramolecular* hydrogen bond in **55** is seen between the *ortho*-aromatic hydrogen, C(12A), and the pyrazol-5-thione sulfur as well as a very weak *intermolecular* interaction, C(43B)-H(43B)⋯S(5B), between stacked independent ligands. The 6-membered hydrogen bonded rings are almost planar in all cases with H₂L (**55**), part A, displaying the maximum deviation from the calculated least squares plane (r.m.s deviation from plane 0.031 Å, max. dev. N(42A) = 0.052 Å).

	D-H⋯A	D-H (Å)	H⋯A (Å)	D⋯A (Å)	D-H⋯A (°)
H ₂ L (55)	N(42A)-H(42A)⋯S(5A)	0.8701	2.3415	3.067(5)	141.03
	N(42B)-H(42B)⋯S(5B)	0.8702	2.3842	3.101(5)	139.94
	C(12A)-H(12A)⋯S(5A)	0.9386	2.8706	3.318(5)	110.50
	C(43B)-H(43B)⋯S(5B) ^(a)	0.9891	2.8340	3.799(5)	165.26
H ₂ L (56)	N(42)-H(42)⋯S(5)	0.8596	2.4437	3.151(2)	139.94

Table 5.3. *Inter*- and *intramolecular* hydrogen bond interactions for H₂L (**55**). $\frac{1}{8}$ H₂O and H₂L (**56**). ^(a) *Intermolecular* contact is generated by the symmetry operation -x, 1-y, 1-z.

With the inclusion of a bridging group a degree of control over the disposition of the N₂S₂ donor set is possible, whereas in the bidentate analogues there is no control over the orientation of donor atoms in two independent ligands.

The flexible n-butyl bridge in H₂L (**56**) adopts an extended configuration around the C(44A)-C(44A') bond resulting in the two pyrazole rings in the ligand having a minimally strained skew conformation. On complexation it must therefore undergo a conformational rearrangement to a more strained geometry. In contrast the less flexible 1,2-*trans*-cyclohexyl bridge adopts a chair conformation with a torsion angle at the C(43A)-C(43B) bond close to 60°, (torsion 1, Table 5.4). The pyrazole arms are further rotated (torsion angles 2 and 3) such that the hydrogen bonded rings nearly face in opposing directions. The nitrogen atoms are held in a *trans* position with a non-contact *intramolecular* N(42A)⋯N(42B) distance of 2.876(6) Å overcoming some electrostatic repulsion energy.

	Torsion	H ₂ L (55)
1	N(42A)-C(43A)-C(43B)-N(42B)	58.8(4)
2	C(41A)-N(42A)-C(43A)-C(43B)	119.4(4)
3	C(41B)-N(42B)-C(43B)-C(43A)	106.1(5)

Table 5.4. Selected torsion angles (°) in H₂L (**55**). ½ H₂O.

One literature structure available for comparison is the ethylenediamine bridged bis-(1-phenyl-3-methyl-pyrazol-5-thione)-4-ethylenedibenzylamine ligand,⁵ Figure 5.5. It has a structure similar to H₂L (**56**) also adopting a skew geometry with a bite distance of 3.018(3) Å.

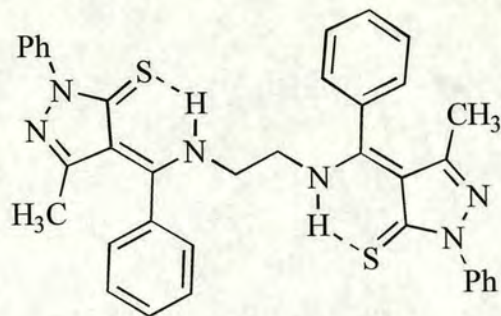


Figure 5.5. Bis-(1-phenyl-3-methyl-pyrazol-5-thione)-4-ethylenedibenzylamine.

As well as the two 6-membered chelate rings that will form on complexation, there will also be an additional chelate ring associated with the bridging group. The size of this ring will be of importance and will impose a constraint and a preferred geometry on the complex. H_2L (**55**), $\frac{1}{8}\text{H}_2\text{O}$ and the published ligand (Figure 5.5), will generate an additional 5-membered chelate, whereas H_2L (**56**) will generate a 7-membered ring. Considering the results from Chapter 3 involving the pyridinethione-based ligands, a 5-membered chelate ring will provide an insufficiently large $\text{N}\cdots\text{N}$ separation, promoting a nitrogen-metal-nitrogen angle close to 90° and therefore favour a planar geometry. The flexible ethylene bridged ligand is therefore most likely to impose planar geometry. Although the *trans*-1,2-cyclohexyl bridge also offers a 5-membered chelate ring the imposed 60° torsion angle, $\text{N}(42\text{A})\text{-C}(43\text{A})\text{-C}(43\text{B})\text{-N}(42\text{B})$, will offset the nitrogen atoms disfavouring a stable planar complex. Although the longer butyl bridge will give a 7-membered chelate ring and a greater $\text{N}\cdots\text{N}$ distance the high flexibility of the linker may reduce this effect.

5.4.2 Complexes.

One zinc(II) (**65**) and two nickel(II) (**63** and **66**) mononuclear complexes of the type [M(L)] have been crystallographically characterised where L is a tetradentate imino-pyrazol-5-thiolato derivative, see Table 5.5. A survey of the literature shows there are fifteen such complexes consisting of similar tetradentate pyrazol-5-thiolato ligand units reported. They are all mononuclear complexes containing either Ni(II) or Cu(II), Table 5.5.

	Ref	[M(L)]	R ₁	R ₂	R ₃	R ₄	M
	-	63	Me	(CH ₂) ₄	Me	H	Ni
	-	65, 66	Me	<i>o</i> -xylyl	Me	H	Ni, Zn
	5	ZEFJUF	Ph	biph	Me	Ph	Cu
	6	DOCYEZ	Ph	biph	Me	H	Cu
	7	ZEVJUF	Ph	biph	Ph	Ph	Cu
	5	JOQYET	Ph	(CH ₂) ₂	Me	Ph	Cu
	5	n/a	Ph	(CH ₂) ₃	Me	Ph	Cu
	5	n/a	Ph	1,2-Ph	Me	Ph	Cu
	5	n/a	Ph	2,3-naphthyl	Me	Ph	Cu
	8	JIGWOL	<i>i</i> -Pr	(CH ₂) ₂	Me	H	Ni
	9	NEKFEO	Me	(CH ₂) ₃	Me	H	Ni
	9	NEKFIS	Ph	(CH ₂) ₃	Me	H	Ni
	8	JIGWUR	<i>i</i> -Pr	(CH ₂) ₄	Me	H	Ni
	10	NILDOB	Me	(CH ₂) ₄	Me	H	Ni
	11	REQSAH	Me	(CH ₂) ₄	Ph	H	Ni
12	ZAZJUF	Me	dmbiph	Me	H	Ni	
12	ZAZKEQ	Ph	biph	Me	H	Ni	

Table 5.5. The range of crystallographically characterised tetradentate metal(II) complexes (**63**, **65** and **66**) presented in this thesis and those reported in the literature. Note, biph = 2,2'-biphenyl and dmbiph = 2,2'-(6,6'-dimethyl)biphenyl.

The examples of copper coordination have been studied with respect to the biomimetic modelling of tetrahedral copper sites in metalloenzymes, whereas the nickel complexes follow on from the bidentate pyrazol-5-thione temperature dependent NMR studies on spin-equilibrium in pseudo-tetrahedral complexes, briefly mentioned in Section 4.4.2.

5.4.2.1 (Bis-(1,3-dimethyl-pyrazol-5-thiolato)-4-*o*-xylyldialdimino)zinc(II).

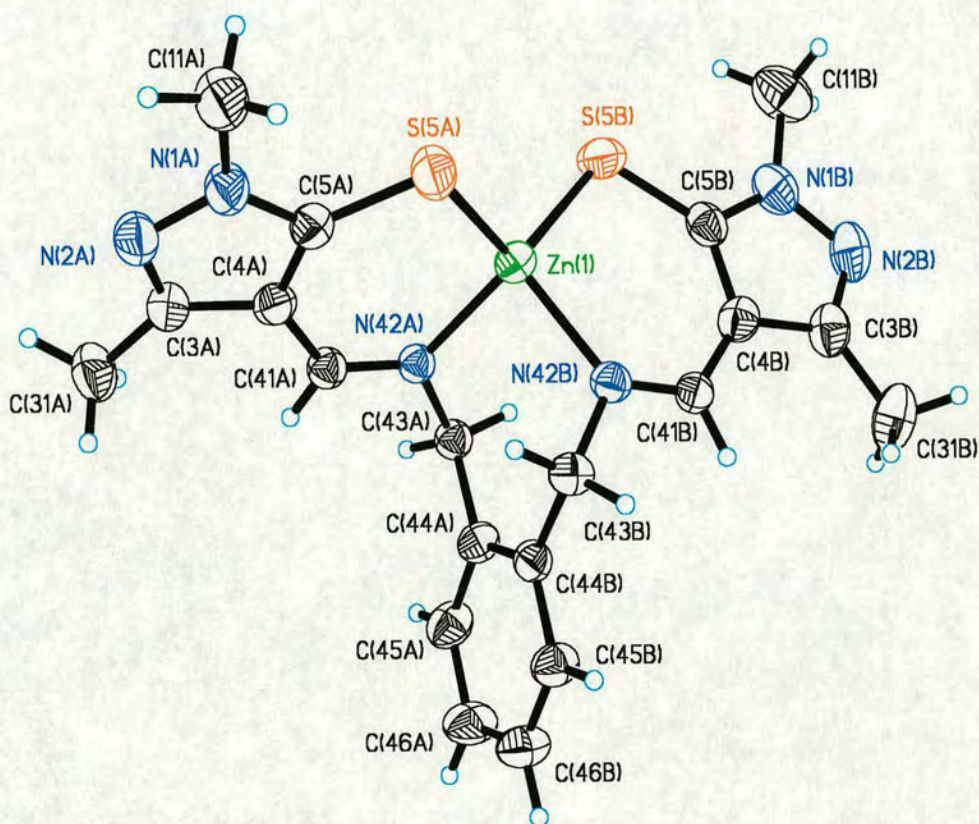


Figure 5.6. The structure of bis-(1,3-dimethyl-pyrazol-5-thiolato)-4-*o*-xylyldialdimino zinc(II) (**65**) showing atomic displacement ellipsoids at the 50 % probability level.

Colourless crystals of [Zn(**58-2H**)] (**65**) were grown from toluene in the triclinic crystal system with space group $P\bar{1}$ (no.2). The asymmetric unit contains a single [Zn(**58-2H**)] molecule, Figure 5.6.

Selected bond lengths and angles are listed in Table 5.7. The geometry of the pyrazole units shows no significant changes due to the influence of the bridging group compared with the bis-bidentate zinc(II) pyrazol-5-thiolato complexes **34**, **36** and **39** (described in Section 4.4.2.1). The two pyrazole chelate rings are almost planar and deviate only slightly from the calculated least squares plane, the greatest distortion from planarity observed for part A (r.m.s deviation from planarity 0.047 Å, max. dev. Zn(1) = 0.074 Å). In accordance with the bis-bidentate zinc complexes, this slight puckering of the chelate rings may be attributed to an insufficiently large N(42)⋯S(5) bite distance, 3.384(4) Å in part A and 3.361(4) Å in part B, (Table 5.6) which is at the lower end of the range observed in Section 4.4.2.1.

The N₂S₂ donor atoms adopt a pseudo-tetrahedral coordination geometry around the central zinc(II) ion with a dihedral angle between the chelate planes of 72.5°, Table 5.6. The *o*-xylyl phenyl group is twisted out of the N(42A)-Zn(1)-N(42B) plane by 37.5° with the two methylene carbons lying slightly out of the plane of the phenyl ring, C(43A)-C(44A)-C(44B)-C(43B) is 3.3(6)°. The inflexible *o*-xylyl backbone constrains the N(42A)⋯N(42B) distance, 2.835(5) Å, and the N(42A)-Zn(1)-N(42B) angle, 89.45(13)°, to values which are more appropriate for planar geometries. They are significantly smaller (0.30-0.65 Å and 11.1-28.0° respectively) than the range observed for the bis-bidentate zinc(II) complexes (Tables 4.11 and 4.13). However, because of the twist of the methylene carbons in the *o*-xylyl backbone, the nitrogen donors do not lie in the ZnS₂ plane.

	[Zn(58-2H)] (65)	
	Part(A)	Part(B)
Zn(1)-N(42)	2.014(4)	2.014(3)
Zn(1)-S(5)	2.2798(13)	2.2988(14)
N(42)-Zn(1)-S(5)	103.83(10)	102.19(10)
N...S	3.384(4)	3.361(4)
N(42A)...N(42B)	2.835(5)	
S(5A)...S(5B)	3.8469(19)	
N(42A)-Zn(1)-S(5B)	123.58(11)	
N(42B)-Zn(1)-S(5A)	122.49(10)	
N(42A)-Zn(1)-N(42B)	89.45(13)	
S(5A)-Zn(1)-S(5B)	114.32(5)	
θ	72.5	

Table 5.6. Metal donor bond lengths (Å), angles (°), chelate bite distances (Å) and dihedral angles (θ°) defined by the chelates, together with the remaining bond angles at the metal in [Zn(58-2H)] (65).

In contrast the S(5A)...S(5B) distance, 3.8469(19) Å, and the S(5A)-Zn(1)-S(5B) angle, 114.32(5)°, in **65** are only slightly larger (0.02-0.07 Å and 1.8-5.5° respectively) than those observed for **34**, **36** and **39**. This finding indicates that the ZnS₂ fragment remains nearly unchanged and the geometrical changes forcing the system from a tetrahedral arrangement of donor atoms results mainly from the different positions of the nitrogen donors relative to the zinc ion. Interestingly a similar pseudo-tetrahedral geometry with a dihedral angle of 75.3° has been reported where the *o*-xylyl backbone is replaced with 2,2'-(6,6'-dimethyl)biphenyl.¹²

[Zn(58-2H)] (65)		
	Part(A)	Part(B)
N(1)-C(5)	1.344(5)	1.344(6)
N(1)-N(2)	1.379(5)	1.376(6)
N(2)-C(3)	1.310(6)	1.310(7)
N(1)-C(11)	1.456(6)	1.463(7)
C(3)-C(4)	1.421(6)	1.428(6)
C(3)-C(31)	1.497(6)	1.481(7)
C(4)-C(41)	1.422(6)	1.405(6)
C(4)-C(5)	1.406(6)	1.406(6)
C(41)-N(42)	1.282(5)	1.293(5)
N(42)-C(43)	1.474(5)	1.471(5)
C(5)-S(5)	1.735(5)	1.728(4)
C(43)-C(44)	1.522(6)	1.515(5)
C(44A)-C(44B)	1.402(6)	
S(5)-C(5)-C(4)	133.6(3)	133.0(3)
C(5)-C(4)-C(41)	129.8(4)	130.2(4)
C(4)-C(41)-N(42)	126.2(4)	126.0(4)
M(1)-S(5)-C(5)	100.02(15)	101.25(16)
M(1)-N(42)C(41)	125.7(3)	127.0(3)

Table 5.7. Selected bond lengths (Å) and angles (°) the chelate arms of [Zn(58-2H)] (65).

5.4.2.2 n-Butyl and o-xyllyl bridged nickel(II) complexes.

Olive plates of [Ni(56-2H)].CH₃NO₂ (63) were grown from nitromethane in an orthorhombic crystal system with space group P2₁2₁2₁ (no.19). The asymmetric unit consists of two essentially identical molecules (one of which is shown in Figure 5.7) related by an inversion centre and two methanol molecules.

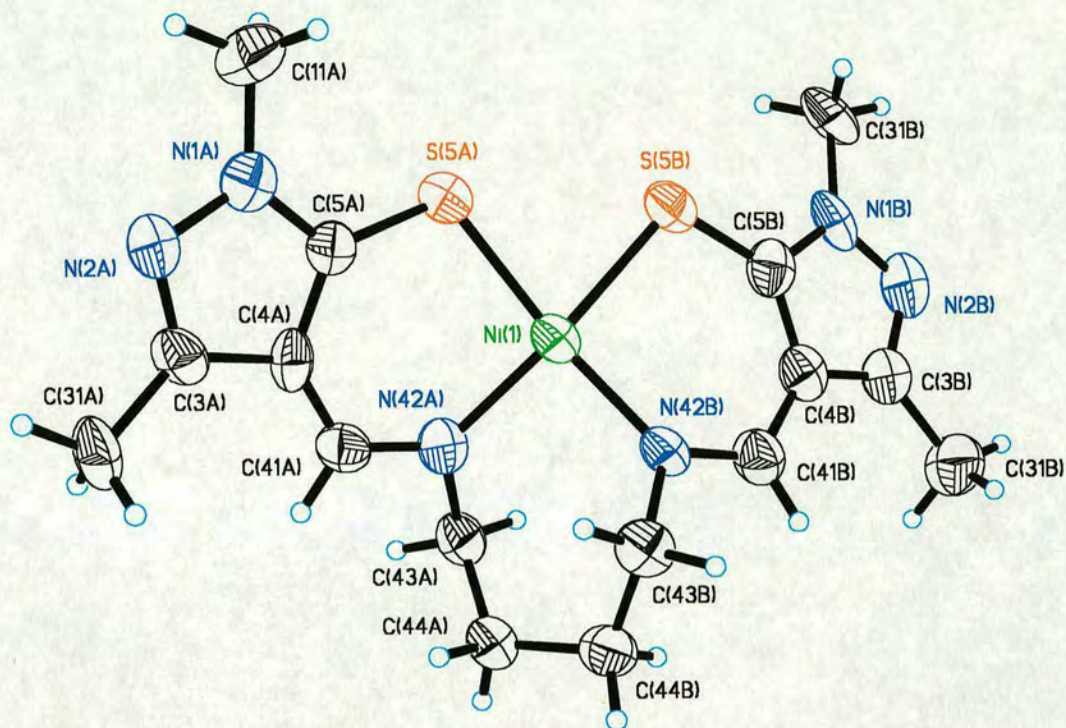


Figure 5.7. The structure of bis-(1,3-dimethyl-pyrazol-5-thiolato)-4-butylaldimino nickel(II) (**63**) showing atomic displacement ellipsoids at the 50 % probability level.

Although the structure of this complex has been previously reported in the literature, NILDOB,¹⁰ the published structure has high standard deviations in some bond lengths and angles and therefore we redetermined it. Unfortunately the structure reported here is twinned (this possibly accounts for the poor quality of NILDOB) although the refinement produced smaller standard deviations on bond lengths and angles, which are listed in Table 5.8.

	[Ni(56-2H)] (63)		[Ni(58-2H)] (66)	
	Part(A)	Part(B)	Part(A)	Part(A')
N(1)-C(5)	1.348(17)	1.341(17)	1.356(8)	1.356(8)
N(1)-N(2)	1.383(17)	1.375(16)	1.381(8)	1.381(8)
N(2)-C(3)	1.324(18)	1.329(19)	1.317(9)	1.317(9)
N(1)-C(11)	1.449(19)	1.446(18)	1.457(9)	1.457(9)
C(3)-C(4)	1.449(18)	1.391(19)	1.423(9)	1.423(9)
C(3)-C(31)	1.447(19)	1.51(2)	1.508(10)	1.508(10)
C(4)-C(41)	1.379(18)	1.466(19)	1.401(9)	1.401(9)
C(4)-C(5)	1.398(19)	1.400(19)	1.411(9)	1.411(9)
C(41)-N(42)	1.303(16)	1.295(16)	1.302(7)	1.302(7)
N(42)-C(43)	1.529(16)	1.487(16)	1.482(8)	1.482(8)
C(5)-S(5)	1.719(14)	1.722(14)	1.707(7)	1.707(7)
C(43)-C(44)	1.526(18)	1.542(18)	1.515(9)	1.515(9)
C(44A)-C(44A')	1.508(19)		1.413(15) ^(a)	
S(5)-C(5)-C(4)	128.5(10)	128.7(11)	130.4(5)	130.4(5)
C(5)-C(4)-C(41)	125.6(12)	123.9(12)	124.8(6)	124.8(6)
C(4)-C(41)-N(42)	125.2(13)	124.6(13)	124.7(6)	124.7(6)
Ni(1)-S(5)-C(5)	103.3(4)	104.7(5)	103.1(2)	103.1(2)
Ni(1)-N(42)-C(41)	129.6(9)	130.5(9)	130.5(5)	130.5(5)

Table 5.8. Selected bond lengths (Å) and angles (°) the chelate units of [Ni(**56-2H**)].CH₃NO₂ (**63**) and [Ni(**58-2H**)].MeOH (**66**). ^(a) C(44A) and C(44A') are related by the symmetry operation $x, 3/2-y, 1/2-z$.

The structure remains poorly resolved and it is difficult to make statistically reliable comparisons. However it is still possible to discuss the general geometry of the coordination sphere around the nickel centre with respect to the affect of the bridging butyl group.

On complexation H₂L (**56**) changes from its skew conformation, Figure 5.4(b), to a gauche arrangement of donor atoms. The nickel(II) centre is surrounded by a

flattened tetrahedron comprising of the N₂S₂ donor set with a dihedral angle between the N(42A)-Ni(1)-S(5A) and N(42B)-Ni(1)-S(5B) planes of 15.4° in **63** and 7.9° in NILDOB, Table 5.9. The observed difference between the two can be attributed to the inability of the flexible butyl bridge to impose a constrained geometry and therefore slightly different conformations are adopted in the solid state, possibly resulting from different recrystallisation conditions.

	[Ni(56-2H)] (63)		NILDOB		[Ni(58-2H)] (66)	
	Part(A)	Part(B)	Part(A)	Part(B)	Part(A)	Part(A')
Ni(1)-N(42)	1.910(10)	1.917(10)	2.001(8)	1.867(9)	1.916(5)	1.916(5)
Ni(1)-S(5)	2.185(4)	2.196(4)	2.195(4)	2.188(4)	2.1937(19)	2.1937(19)
N(42)-Ni(1)-S(5)	96.0(3)	96.0(3)	92.9(3)	94.4(3)	97.64(16)	97.64(16)
N...S	3.049(9)	3.062(7)	-	-	3.099(6)	3.099(6)
N(42A)...N(42B)	2.708(3)		-		2.662(7) ^(a)	
S(5A)...S(5B)	2.820(1)		2.850(5)		2.945(2) ^(a)	
N(42A)-Ni(1)-S(5B)	168.0(3)		172.7(3)		158.9(2) ^(a)	
N(42B)-Ni(1)-S(5A)	167.0(3)		171.4(3)		158.9(2) ^(a)	
N(42A)-Ni(1)-N(42B)	90.1(4)		92.1(4)		88.0(3) ^(a)	
S(5A)-Ni(1)-S(5B)	80.14(14)		81.1(1)		84.34(10) ^(a)	
θ	15.4		7.9		28.0	

Table 5.9. Metal donor bond lengths (Å), angles (°), chelate bite distances (Å) and dihedral angles (θ°) defined by the chelates, together with the remaining bond angles at the metal in [Ni(**56-2H**)].CH₃NO₂ (**63**), NILDOB and [Ni(**58-2H**)].MeOH (**66**).

^(a) The part (A') atoms in these cases are related to the part (A) atoms by the symmetry operation x, 3/2-y, 1/2-z.

The N(42A)-Ni(1)-N(42B) angle, 90.1(4)°, in **63** is smaller (~2.8°) than in the bidentate [Ni(**26-H**)₂] (**38**) complex as a result of a flatter geometry, Table 5.9. This

matched with a similar decrease (~ 0.11 Å) in the *intramolecular* N \cdots N distance and also with a smaller decrease (~ 0.06 Å) in the S \cdots S distance, ~ 0.8 Å smaller than the sum of the van der Waals radii (3.6 Å)¹³. This underlies the fact that although the butyl bridge forms a 7-membered chelate ring on complexation it imposes a minimal constraint on the geometry due to its flexibility.

Red plates of [Ni(**58-2H**)]·MeOH (**66**) were grown from methanol in the orthorhombic crystal system with space group Pnna (no.52). The asymmetric unit consists of half of a [Ni(**58-2H**)] complex. The second half of the molecule is related by C_2 rotational symmetry ($x, 3/2-y, 1/2-z$) in which the two-fold axis bisects the bridging group, C(44A)-C(44A') and C(46A)-C(46A'), and the metal is positioned along the axis, Figure 5.8. The asymmetric unit also contains a molecule of methanol which is 50 % occupied.

The ligand adopts a more highly distorted *cis*-planar geometry around the metal centre with a dihedral angle of 28° between the N(42)-Ni-S(5) planes, Figure 5.8. Even though complexes **63** and **66** both feature 7-membered bridging chelate rings, complex **63** with a bridging butyl unit shows a distinctly smaller ($\sim 12.6^\circ$) dihedral angle. This can be attributed to the different ligand flexibilities resulting from a hindered rotation around the C(44A)-C(44A') bond in **66**. The inclusion of the aromatic phenyl in the *o*-xylyl bridge not only reduces the flexibility but also reduces the C(44A)-C(44A') bond length, 1.413(15) Å in **66**, which is shorter (~ 0.09 Å) than the respective bond length in the fully saturated butyl bridge in complex **63** (1.508(19) Å), Table 5.8. Consequently the N \cdots N distance in **66**, 2.662(7) Å, is approximately 0.05 Å shorter than in **63**, 2.708(3) Å, Table 5.9. This is also reflected in the smaller N-Ni-N angle.

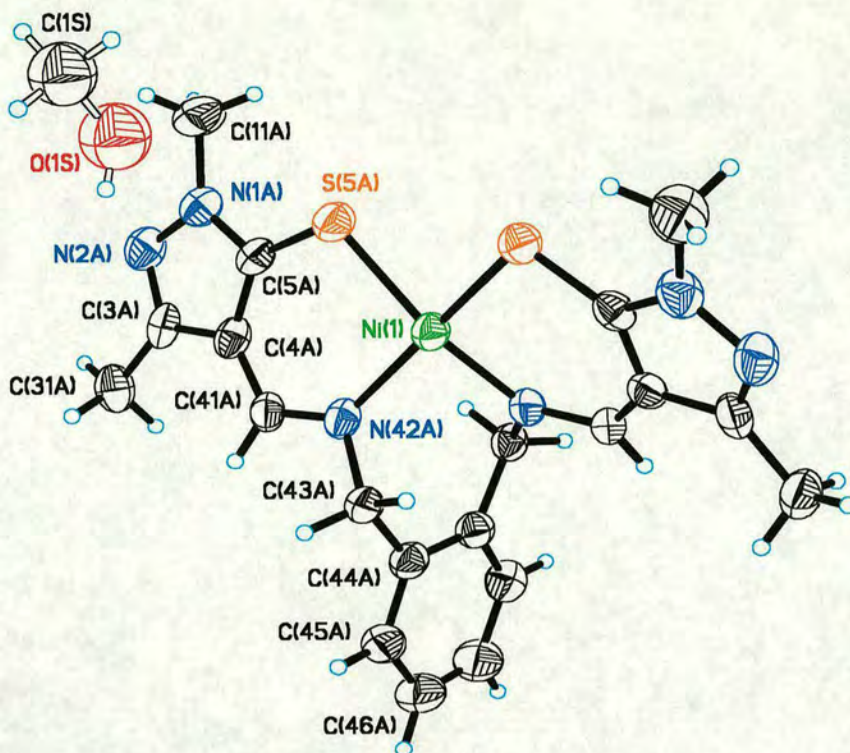


Figure 5.8. The structure of bis-(1,3-dimethyl-pyrazol-5-thiolato)-4-*o*-xylyldialdimino nickel(II) (**66**) showing atomic displacement ellipsoids at the 50 % probability level.

The geometry of the coordination sphere is intermediate between that of the more planar nickel complex, **63** (Figure 5.7), and the more distorted bis-bidentate complex **38**, Figure 4.22. In all three cases the Ni(1)-S(5) bond lengths are similar. However the Ni(1)-N(42) distance in **38** (Table 4.17) is significantly longer, ~ 0.03 Å, than in **66** (Table 5.9), which is similar to the distance in **63**. In contrast the bite distance (N \cdots S; 3.099(6) Å) and chelate angle (N(42)-Ni(1)-S(5); 97.64(16) $^\circ$) in **66** closely approximate to those observed for **38**, while those seen in **63** are significantly smaller which is expected for less distorted geometry. In accordance with the bis-bidentate nickel complex (**38**) the two chelate rings, fused to the pyrazole, are considerably

distorted from the calculated least squares plane (r.m.s deviation from plane 0.160 Å, max. dev. Ni(1) = 0.237 Å). This results from the opposing propensity of the nickel to adopt a planar coordination and the restrictions imposed by the inflexible bridging group.

5.4.2.2 Comparison of nickel complexes.

Comparison of **63** and **66** with the other tetradentate pyrazol-5-thiolato based structures reported in the literature reveals that the dihedral angles between the N(42)-Ni(1)-S(5) planes are generally in the range 0-36°, Table 5.10. The ligands involved in these literature structures are defined in Table 5.5.

Angles near the lower end of this range, representing a smaller distortion from planarity, are found in the complexes containing shorter alkyl chain bridges. As expected JIGWOL, with only two carbon atoms in the bridge, has the most planar coordination sphere producing a dihedral angle of 5.7°. The small ethylene group produces a nitrogen-nitrogen distance (2.589 Å) which is more suited to planar coordination. As the number of carbon atoms increases in the alkyl bridge, *i.e.* to $n = 3$ as in NEKFEO and NEKFIS (where n is the number of carbons in the bridge), the distance between the nitrogen donors increases and they subtend a slightly larger N-Ni-N angle. This results in a slight increase in the distortion from planarity, with the dihedral angle ranging between 6.9° and 10.2°. In the examples where a butyl backbone is included, a range of dihedral angles are observed (7.9-18.3°). The reason for this, which is also seen for the complexes containing the propyl backbone, is unclear. It is possibly due to the fact that the alkyl bridge is flexible and can tolerate a ring strain which covers a range of conformations and therefore crystal

packing in the solid state has an influence. However in the case for JIGWUR, where $R_1 = i\text{-Pr}$, the increase in steric bulk compared to the methyl substituent possibly contributes to the larger dihedral angle (18.3°), Table 5.10.

Code	Bridge	S-Ni-S	S...S	N-Ni-N	N...N	θ	CSM (T_d)	Ref
JIGWOL	(CH ₂) ₂	79.9 ^(b)	2.806 ^(b)	85.48	2.589 ^(b)	5.7	30.33	8
NEKFEO	(CH ₂) ₃	80.83(3)	2.851(1)	88.55(9)	2.702(3)	6.9	30.02	9
NEKFIS ^(a)	(CH ₂) ₃	81.3(4)	2.88(1)	92(1)	2.70(4)	7.2	29.30	9
NEKFIS ^(a)	(CH ₂) ₃	81.4(4)	2.88(1)	88(1)	2.70(3)	10.2		9
NILDOB	(CH ₂) ₄	81.1(1)	2.850(5)	92.1(4)	n/a	7.9	n/a	10
REQSAH	(CH ₂) ₄	81.40(3)	2.858(1)	89.89(9)	2.7328	12.7	26.10	11
63	(CH ₂) ₄	80.14(14)	2.820(1)	90.1(4)	2.708(3)	15.4	24.60	-
JIGWUR	(CH ₂) ₄	80.7 ^(b)	2.841 ^(b)	90.6 ^(b)	2.743 ^(b)	18.3	23.00	8
66	<i>o</i> -xylyl	84.34(10)	2.945(2)	88.0(3)	2.835(5)	28.0	17.87	-
ZAZKEQ	biph	81.4(1)	2.850(1)	93.5(1)	n/a	35.7	n/a	12
ZAZJUF	dmbiph	117.6(1)	3.834(2)	96.4(1)	2.928*	77.4	2.42	12

Table 5.10. Selected bond lengths (Å) and angles ($^\circ$) for NiN₂S₂ complexes incorporating the tetradentate bis-(pyrazol-5-thiolato) unit. ^(a) Two molecules in the asymmetric unit. ^(b) Calculated using CERIU.S.¹⁴

The incorporation of the less flexible *o*-xylyl backbone further increases the dihedral angle (28.0°) and consequently increases the N...N distance. However a decrease is observed for the N-Ni-N angle as a consequence of the shorter C(44A)-C(44A') due to the inclusion of the phenyl ring.

The use of a biphenyl backbone for the control of the geometry in coordination complexes was first reported by Lions.¹⁵ When a 2,2'-biphenyl bridge is present, *i.e.* ZAZKEQ, the dihedral angle increases to 35.7° since the biphenyl necessarily twists

to reduce the strain between its two phenyl rings, (torsion between the phenyl planes when viewed along the C-C bond joining the two rings is 49.5°).¹² The incorporation of methyl groups at the 6 and 6' positions, *i.e.* ZAZJUF, further increases the torsional twist between the two phenyl planes to 66.8° resulting in a pseudo tetrahedral coordination geometry around the nickel centre with a dihedral angle¹² of 77.4° .

A gradual decrease is observed for the tetrahedral continuous symmetry measures, which correlates well with the increase in the distortion from a planar structure to a pseudo-tetrahedral conformation, as the backbone imposes a greater restriction on the geometry. Interestingly, the nickel(II) complex, ZAZJUF,¹² has a larger dihedral angle ($\sim 5^\circ$) than [Zn(**58-2H**)] (**65**) and consequently a smaller CSM(T_d) value, (CSM(T_d) for **65** is 2.91) and therefore it could be said exhibits a more tetrahedral geometry.

5.5 Conclusions.

This chapter has endeavoured to assess the effect of some bridging backbones in the tetradentate imino-pyrazol-5-thiolato complexes. The structural data indicates a strong influence of the diamine bridging unit on disposition of the nitrogen donor atoms resulting in tetrahedral distortions of the nickel complexes. In agreement with the bis-bidentate complexes (Chapter 4) a larger angle between the two nitrogen donors (ideally N-Ni-N would approach 109.5°) increases the tendency to form a pseudo-tetrahedral coordination sphere and attain a dihedral angle closest to 90° . The N-Ni-N angle is influenced by both the steric demands of the corresponding bridge connecting the two donors and its conformational flexibility. The backbones

which resulted in 5 and 6-membered bridging chelate rings do not provide a sufficient distance between the nitrogen donors necessary for distortions away from planarity. Whereas the larger 7-membered rings discussed, butyl, *o*-xylyl, biph and dmbiph, allow a more suitable N...N distance. Perhaps the most essential feature is the incorporation of rigidity into the backbone coupled with a twist to prevent the nitrogen donors from lying in the metal-sulfur plane. It is reported that the necessary twist resulting in pseudo-tetrahedral geometry can most effectively be introduced to date by using a 2,2'-(6,6'-dimethyl)-biphenyl backbone in the ligand.¹² However some success was achieved here with the *o*-xylyl backbone producing a large distortion of the nickel complex from planarity while retaining a pseudo-tetrahedral geometry on complexation of zinc.

5.6 Experimental.

5.6.1 Pyrazol-5-thiones.

Bis-(1-phenyl-3-methyl-pyrazol-5-thione)-4-ethyldialdenamine (52)

A suspension of 1-phenyl-3-methyl-4-pyrazolecarboxaldehyde (**21**) (2.91 g, 13 mmol) in dry ethanol (60 cm³) was prepared to which NaSH.xH₂O (1.52 g, 27 mmol) and 1,3-diaminopropane (0.40 g, 6.6 mmol) were added. The mixture was heated at reflux for 24 h and then the solvent was removed by rotary evaporation. The resulting solid was dissolved in dichloromethane (300 cm³) then washed with water (5 x 100 cm³) and finally 0.1 M HCl (1 x 100 cm³). The dichloromethane layer was dried with MgSO₄ and then filtered. The solvent was removed to yield a

brown oil (6.41 g, 75.0 %). Which was recrystallised from toluene / acetonitrile (2:1) and washed with 60-80 petroleum ether to give a yellow solid. The solid was passed through a dry-flash column using chloroform / methanol (95:5) to yield a yellow solid (0.714 g, 11.9 %). M.P. (decomp) 264 °C (Lit. 279-280 °C¹⁶); (Found: C, 61.47; H, 5.27; N, 17.76; FABMS m/z 461. $C_{24}H_{24}N_6S_2 \cdot 0.5H_2O$ requires C, 61.38; H, 5.37; N, 17.90 %; M 461); ¹H NMR (CDCl₃, 200 MHz) δ : 2.14 (s, 6H, 2CH₃), 4.11 (d, ³ J_{HH} 7.2 Hz, 4H, 2CH₂(1, 2)), 7.25-7.88 (m, 12H, 2(*o*, *m*, *p*)Ph, 2H-CN), 13.1 (m, 2H, 2NH). IR (cm⁻¹, KBr disk) ν : 1648(s), 1597(m), 1529(m), 1498(m), 1440(w), 1360(s), 1222(m), 994(m), 806(w), 758(w), 688(w), 672(w).

Bis-(1-phenyl-3-methyl-pyrazol-5-thione)-4-propyldialdenamine. (53)

The brown oil (6.41 g, 75.0 %) that remained after the reduction of the filtrate was passed through a dry-flash column using chloroform / ethanol (95:5) and recrystallised from toluene / acetonitrile (2:1) to yield a yellow crystalline solid (4.71 g, 55.1 %). M.P. 188-191 °C (Lit. 279-280 °C¹⁶); (Found: C, 63.51; H, 5.62; N, 17.94; FABMS m/z 475. $C_{25}H_{26}N_6S_2$ requires C, 63.26; H, 5.52; N, 17.71 %; M 475); ¹H NMR (CDCl₃, 200 MHz) δ : 2.25 (m, 8H, CH₂(2), 2CH₃), 3.77 (q, ³ J_{HH} 12.6, 6.3 Hz, 4H, 2CH₂(1, 3)), 7.25-7.45 & 7.83-7.98 (m, 12H, 2(*o*, *m*, *p*)Ph, 2H-CN), 13.18 (m, 2H, 2NH). IR (cm⁻¹, KBr disk) ν : 3071(w), 2924(w), 1649(s), 1592(m), 1540(m), 1490(m), 1448(m), 1354(s), 1276(m), 1226(m), 1134(m), 989(m), 819(m), 755(m), 686(m), 669(m).

Bis-(1-phenyl-3-methyl-pyrazol-5-thione)-4-butyldialdenamine. (54)

The yellow / brown solid (7.65 g, 87.0 %) that remained after the reduction of the filtrate was passed through a dry-flash column using chloroform / acetonitrile (70:30) and recrystallised from cyclohexane to yield a yellow solid (4.49 g, 51.0 %). M.P. 235-237 °C; (Found: C, 61.75; H, 5.69; N, 16.67; FABMS m/z 489. $C_{26}H_{28}N_6S_2 \cdot H_2O$ requires C, 61.63; H, 5.97; N, 16.59 %; M 488); 1H NMR ($CDCl_3$, 200 MHz) δ : 1.98 (m, 4H, $2CH_2(2, 3)$), 2.27 (s, 6H, $2CH_3$), 3.65 (d, $^3J_{HH}$ 5.7 Hz, 4H, $2CH_2(1, 4)$), 7.24-7.49 & 7.80-7.90 (m, 12H, $2(o, m, p)Ph$, 2H-CN), 13.16 (m, 2H, 2NH). IR (cm^{-1} , KBr disk) ν : 2940(w), 1651(s), 1596(m), 1519(m), 1498(m), 1420(m), 1351(m), 1338(m), 1245(w), 999(w), 813(w), 764(w), 695(w), 671(w).

Bis-(1-phenyl-3-methyl-pyrazol-5-thione)-4-*trans*-1,2-cyclohexyldialdenamine.

$\frac{1}{8}$ water. (55)

The brown oil that remained after the reduction of the filtrate was recrystallised from propan-2-ol to give X-ray crystallographic grade yellow crystals (1.189 g, 54.6 %). M.P. 237-238 °C; (Found: C, 64.79; H, 6.03; N, 16.05; EIMS m/z 514 (100 %). $C_{28}H_{30}N_6S_2$ requires C, 65.06; H, 5.90; N, 16.26 %; M 514); 1H NMR ($CDCl_3$, 200 MHz) δ : 1.55 (s, 8H, cyclo- CH_2), 2.06 (s, 6H, $2CH_3$), 3.35 (m, 2H, cyclo- CH^*), 7.24-7.85 (m, 12H, $2(o, m, p)Ph$, 2H-CN), 12.97 (m, 2H, 2NH). IR (cm^{-1} , KBr disk) ν : 2950(m), 2850(m), 1652(s), 1593(m), 1528(m), 1498(m), 1424(w), 1378(m), 1341(m), 1240(m), 1146(w), 989(w), 762(w), 692(w), 670(w).

Bis-(1,3-dimethyl-pyrazol-5-thione)-4-butyldialdenamine. (56)

The yellow solid that remained after the reduction of the filtrate was recrystallised from methanol to give X-ray crystallographic grade yellow crystals (1.83 g, 52.8 %). M.P. 234 °C; (Found: C, 51.87; H, 6.56; N, 22.63; FABMS m/z 365. $C_{16}H_{24}N_6S_2$ 0.4MeOH requires C, 52.20; H, 6.64; N, 22.27 %; M 364); 1H NMR ($CDCl_3$, 200 MHz) δ : 1.92 (t, $^3J_{HH}$ 2.9 Hz, 4H, $2CH_2(2, 3)$), 2.20 (s, 6H, $2CH_3$), 3.61 (d, $^3J_{HH}$ 6.0 Hz, 4H, $2CH_2(1, 4)$), 3.69 (s, 6H, $2N-CH_3$), 7.75 (d, $^3J_{HH}$ 13.6 Hz, 2H, $2H-CN$), 12.69 (m, 2H, $2NH$). IR (cm^{-1} , KBr disk) ν : 2931(m), 1649(s), 1517(m), 1420(m), 1356(m), 1296(m), 1272(w), 1199(m), 1168(m), 1091(w), 980(m), 802(m), 642(m).

Bis-(1,3-dimethyl-pyrazol-5-thione)-4-*trans*-1,2-cyclohexyldialdenamine. (57)

The yellow / brown solid that remained after the reduction of the filtrate was passed through a dry-flash column using chloroform / methanol (90:10) and recrystallised from 40 % ethanol to yield yellow crystals that were isolated by filtration (0.95 g, 53.3 %). M.P. 248 °C; (Found: C, 55.17; H, 6.56; N, 21.12; FABMS m/z 391. $C_{18}H_{26}N_6S_2$ requires C, 55.36; H, 6.71; N, 21.52 %; M 390); 1H NMR ($CDCl_3$, 200 MHz) δ : 1.41-1.74 (m, 6H, cyclo- CH_2), 2.00 (s, 6H, $2CH_3$), 2.34 (m, 2H, cyclo- CH_2), 3.30 (m, 2H, cyclo- CH^*), 3.64 (s, 6H, $2N-CH_3$), 7.67 (d, $^3J_{HH}$ 13.4 Hz, 2H, $2H-CN$), 12.63 (m, 2H, $2NH$). IR (cm^{-1} , KBr disk) ν : 2932(m), 1647(s), 1524(m), 1443(w), 1388(m), 1337(w), 1310(w), 1148(w), 861(w), 640(w).

Bis-(1,3-dimethyl-pyrazol-5-thione)-4-*o*-xylyldialdenamine. (58)

The yellow / brown solid that remained after the reduction of the filtrate was recrystallised from nitromethane to give a yellow fibrous solid (1.88 g, 53.6 %).

M.P. (decomp.) 190 °C; (Found: C, 57.37; H, 5.91; N, 19.87; FABMS m/z 413. $C_{20}H_{24}N_6S_2 \cdot 0.25 H_2O$ requires C, 57.60; H, 5.92; N, 20.15 %; M 412); 1H NMR ($CDCl_3$, 200 MHz) δ : 2.15 (s, 6H, 2CH₃), 3.66 (s, 6H, 2N-CH₃), 4.79 (d, $^2J_{HH}$ 5.5 Hz, 2H, CH₂(1,2)), 7.44 (s, 4H, Ph), 7.75 (d, $^3J_{HH}$ 13.4 Hz, 2H, 2H-CN), 12.97 (m, 2H, 2NH). IR (cm^{-1} , KBr disk) ν : 2916(w), 1659(s), 1516(m), 1441(m), 1363(m), 1220(w), 1167(w), 1101(w), 808(w), 748(w), 636(w).

N,N-(*o*-methylene-xylene)-diphthalimide. (59)

Potassium phthalimide (11.10 g, 60 mmol) was added to a suspension of α,α -dibromo-*o*-xylene (5.286 g, 20 mmol) in DMF (75 cm³). The mixture was heated at 90 °C for 17 h. The DMF was removed by rotary evaporation and the remaining white solid partitioned between dichloromethane (500 cm³) and water (500 cm³) and the bi-phasic solution filtered. The organic phase was washed with water (3 x 100 cm³) then dried using MgSO₄ and then filtered. The dichloromethane was removed by rotary evaporation leaving a white solid (7.13 g, 89.9 %) which was recrystallised from nitromethane to give a fibrous white solid (5.829 g, 73.5 %). M.P. 264-265 °C; (Found: C, 72.56; H, 4.16; N, 6.93; FABMS m/z 397. $C_{24}H_{16}N_2O_4$ requires C, 72.72; H, 4.07; N, 7.07 %; M 396); 1H NMR ($CDCl_3$, 200 MHz) δ : 5.21 (s, 4H, 2CH₂), 7.18-7.43 (m, 4H, Ph), 7.68-7.88 (m, 8H, C₆H₄(CO)₂N). IR (cm^{-1} , KBr disk) ν : 3031(w), 1767(m), 1716(s), 1703(s), 1612(m), 1396(s), 1349(m), 1328(m), 1110(m), 963(m), 934(m), 786(w), 762(m), 724(m), 717(m), 637(w).

***o*-Xylene-diamine. (60)**

N,N-(*o*-methylene-xylene)-diphthalimide (1.997 g, 5.0 mmol) was suspended in ethanol (200 cm³) and heated to reflux. Hydrazine monohydrate (1.027 g, 21 mmol) was added dropwise. The suspension slowly dissolved over a 3 h period and with further heating (15 h) a white solid precipitated. The solvent was removed by rotary evaporation and the resulting white solid was dissolved in water (500 cm³) and then filtered. The solution was acidified (pH 2) with dilute HCl and the resulting precipitate removed by filtration. The water was removed from the filtrate to yield a white solid, *o*-xylene-diamine dihydrochloride (0.89 g, 83.5 %). M.P. >330 °C; (Found: C, 44.43; H, 6.78; N, 13.08; FABMS *m/z* 174. C₈H₁₄Cl₂N₂ 0.5H₂O requires C, 44.05; H, 6.93; N, 12.84 %; *M* 209); ¹H NMR³ (D₂O, 200 MHz) δ: 4.32 (s, 4H, 2CH₂), 7.52 (s, 4H, Ph). ¹³C NMR³ (D₂O, 250 MHz) δ: 36.96 (CH₂), 127.60 (CH), 128.72 (C-q). IR (cm⁻¹, KBr disk) ν: 3446(m), 3145(m), 3007(br. s), 2902(s), 1602(m), 1587(m), 1490(m), 1374(m), 1222(m), 1082(w), 951(w), 772(m), 765(m). The *o*-xylene-diamine dihydrochloride (0.794 g, 3.8 mmol) was suspended in methanol (50 cm³) containing KOH.xH₂O (0.499 g, 8.9 mmol) and stirred at ambient temperature for ½ h. The solvent was removed by rotary evaporation. The residue was taken dissolved in diethylether then filtered. The diethylether was removed to yield a pale brown liquid (0.462 g, 89.3 %); ¹H NMR (CDCl₃, 200 MHz) δ: 1.66 (s, 4H, 2NH₂), 3.87 (s, 4H, 2CH₂), 7.17-7.30 (m, 4H, Ph).

5.6.2 Complexes of pyrazol-5-thiones.

(Bis-(1-phenyl-3-methyl-pyrazol-5-thiolato)-4-*trans*-1,2-cyclohexyldialdimino) zinc(II). (61)

A solution of zinc acetate dihydrate (0.113 g, 0.52 mmol) in hot methanol (2.5 cm³) was added to a solution of H₂L (55) (0.304 g, 0.59 mmol) in hot methanol (20 cm³) and propan-2-ol (30 cm³). The precipitate which formed instantly and was isolated by filtration to give a pale yellow insoluble solid (0.299 g, >95 %). M.P. (decomp.) 270 °C; (Found: C, 57.40; H, 5.28; N, 14.26; FABMS *m/z* 577. C₂₈H₂₈N₆S₂Zn 0.5H₂O requires C, 57.28; H, 4.98; N, 14.31 %; *M* 578); ¹H NMR (CDCl₃, 200 MHz) δ: 1.17 (m, 8H, cyclo-CH₂), 2.08 (m, 2H, cyclo-CH*), 2.34(s, 6H, CH₃), 7.12-7.56 (m, 12H, 2(*o*, *m*, *p*)Ph, 2H-CN). IR (cm⁻¹, KBr disk) ν: 3049(w), 2926(m), 2857(m), 1643(m), 1594(s), 1515(s), 1499(m), 1445(m), 1385(m), 1244(w), 1142(m), 1086(m), 1000(m), 763(m), 692(m), 674(m).

(Bis-(1,3-dimethyl-pyrazol-5-thiolato)-4-butyldialdimino)zinc(II). (62)

A hot solution of zinc acetate dihydrate (0.348 g, 1.6 mmol) in methanol (10 cm³) was added to a solution of H₂L (56) (0.577 g, 1.6 mmol) in hot methanol (70 cm³). A precipitate formed instantly and was isolated by filtration to give a pale yellow insoluble solid (0.617 g, 91.3 %). M.P. 300 °C; (Found: C, 44.39; H, 5.21; N, 19.06; FABMS *m/z* 429. C₁₆H₂₂N₆S₂Zn 0.5H₂O requires C, 43.99; H, 5.31; N, 19.23 %; *M* 428); ¹H NMR (d₆-DMSO, 200 MHz) δ: 1.55 (br s, 2H, CH₂(2 / 3)), 2.08 (br s, 2H, CH₂(2 / 3)), 2.21 (s, 6H, 2CH₃), 3.60 (s, 6H, N-CH₃), 3.66 (s, 4H, 2CH₂(1, 3)), 8.43 (s, 2H, H-CN). IR (cm⁻¹, KBr disk) ν: 2992(m), 2860(m), 1612(s), 1509(s),

1444(s), 1410(m), 1384(s), 1311(m), 1282(m), 1185(m), 1089(m), 986(m), 939(m), 924(m), 714(w), 700(m), 644(m).

(Bis-(1,3-dimethyl-pyrazol-5-thiolato)-4-butyldialdimino)nickel(II)

(nitromethane) (63)

A hot solution of nickel acetate tetrahydrate (0.154 g, 0.62 mmol) in methanol (10 cm³) was added to a solution of H₂L (56) (0.224 g, 0.62 mmol) in hot methanol (60 cm³). The mixture was heated at reflux for 15 min then solution was reduced in volume by rotary evaporation and left to cool. The precipitate was isolated by filtration (0.213 g, 82.2 %), then recrystallised from propan-2-ol to yield green crystals (0.1476 g, 57.1 %). X-ray crystallographic grade crystals were grown from hot nitromethane. M.P. 250-252 °C; (Found: C, 45.30; H, 4.90; N, 19.44; FABMS *m/z* 421. C₁₆H₂₂NiN₆S₂ 0.1 H₂O requires C, 45.43; H, 5.29; N, 19.87 %; *M* 421). IR (cm⁻¹, KBr disk) ν : 2976(w), 2931(m), 2882(w), 1597(s), 1508(m), 1466(m), 1442(m), 1411(m), 1376(m), 1340(m), 1102(w), 1000(m), 725(w), 640(m).

(Bis-(1,3-dimethyl-pyrazol-5-thiolato)-4-*trans*-1,2-cyclohexyldialdimino)zinc(II).

(64)

A hot solution of zinc acetate dihydrate (0.201 g, 0.91 mmol) in methanol (5 cm³) was added to a solution of H₂L (57) (0.356 g, 0.91 mmol) in hot methanol (30 cm³). A precipitate formed instantly and was isolated by filtration to give a pale yellow insoluble solid (0.314 g, 75.8 %). M.P. (decomp.) 300 °C; (Found: C, 46.29; H, 5.79; N, 17.94; FABMS *m/z* 455. C₁₈H₂₄N₆S₂Zn 0.5H₂O requires C, 46.70; H, 5.44; N, 18.15 %; *M* 454); ¹H NMR (CDCl₃, 200 MHz) δ : 1.36 (m, 4H, cyclo-CH₂),

1.89 (s, 2H, cyclo-CH₂), 2.17 (s, 6H, 2CH₃), 2.45 (m, 2H, cyclo-CH₂), 3.16 (s, 2H, cyclo-CH*), 3.58 (s, 6H, 2N-CH₃), 8.28 (s, 2H, H-CN). IR (cm⁻¹, KBr disk) ν : 2931(m), 2858(w), 1642(m), 1598(s), 1509(s), 1447(m), 1391(m), 1189(m), 1143(m), 1091(m), 987(w), 972(w), 652(m).

(Bis-(1,3-dimethyl-pyrazol-5-thiolato)-4-*o*-xylyldialdimino)zinc(II). (65)

A hot solution of zinc acetate dihydrate (0.080 g, 0.36 mmol) in methanol (5 cm³) was added to a solution of H₂L (58) (0.149 g, 0.36 mmol) in hot methanol (50 cm³). The solution was heated at reflux for 15 min then left too cool. The methanol was removed by rotary evaporation and the resulting pale yellow solid recrystallised using toluene / cyclohexane to give a colourless solid (0.054 g, 30.3 %). X-ray crystallographic grade crystals were grown from hot toluene. M.P. (decomp.) 230 °C; (Found: C, 50.13; H, 4.81; N, 17.05; FABMS *m/z* 475. C₂₀H₂₂N₆S₂Zn 0.3H₂O requires C, 49.91; H, 4.73; N, 17.45 %; *M* 476); ¹H NMR (CDCl₃, 200 MHz) δ : 2.22 (s, 6H, 2CH₃), 3.75 (s, 6H, 2NCH₃), 4.39-5.34 ('ab' q, ²*J*_{HH} 14.3 Hz, 4H, 2CH₂), 7.25 (s, 4H, Ph), 8.23 (s, 2H, H-CN). IR (cm⁻¹, KBr disk) ν : 2920(w), 1613(s), 1510(m), 1444(m), 1409(w), 1370(m), 1190(w), 989(w), 931(w), 750(w), 649(w).

(Bis-(1,3-dimethyl-pyrazol-5-thiolato)-4-*o*-xylyldialdimino)nickel(II).(methanol) (66)

A hot solution of nickel acetate tetrahydrate (0.107 g, 0.43 mmol) in methanol (5 cm³) was added to a solution of H₂L (58) (0.174 g, 0.42 mmol) in hot methanol (50 cm³). The solution was heated at reflux for 15 min then left too cool. The

precipitate was isolated by filtration to yield red / brown crystals (0.131 g, 66.5 %) and then recrystallised using propan-2-ol (0.072 g, 39.1 %). X-ray crystallographic grade crystals were grown from hot methanol. M.P. 310 °C; (Found: C, 51.09; H, 4.60; N, 17.74; FABMS m/z 470. $C_{20}H_{22}NiN_6S_2$ requires C, 51.19; H, 4.30; N, 17.91 %; M 469). IR (cm^{-1} , KBr disk) ν : ~3000(w), ~2950(w), 2923(w), 1610(s), 1509(m), 1450(m), 1408(m), 1366(m), 1095(w), 858(w), 756(m), 649(m).

5.7 References.

1. M.S. Gibson, R.W. Bradshaw, *Angew. Chem. Internat. Edit.*, 1968, **7**, 919.
2. C.J. Pouchet, J. Behnke, *The Aldrich Library ¹³C and ¹H FT NMR Spectra*, Aldrich Chemical Company Inc., 1st edn., 1993, vol.3, p1416(A).
3. G. Lunn, *J. Org. Chem.*, 1987, **52**, 1043.
4. G.M. Sheldrick, SHELXL-97, University of Göttingen, Germany, 1997.
5. S. Knoblauch, R. Benedix, M. Ecke, T. Gelbrich, J. Sieler, F. Somoza, H. Hennig, *Eur. J. Inorg. Chem.*, 1999, 1393.
6. O.P. Anderson, J. Becher, H. Frydendahl, L.F. Taylor, H. Toftlund, *J. Chem. Soc., Chem. Commun.*, 1986, 699.
7. L. Hennig, R. Kirmse, O. Hammerich, S. Larsen, H. Frydendahl, H. Toftlund, J. Becher, *Inorg. Chim. Acta.*, 1995, **234**, 67.
8. A.L. Nivorozhkin, *Izv. Akad. Nauk SSSR Ser. Khim.*, 1990, 327.
9. B. Adihikari, O.P. Anderson, A. la Cour, R. Hazell, S.M. Millar, C.E. Olsen, H. Toftlund, *J. Chem. Soc., Dalton Trans.*, 1997, 4539.
10. A. la Cour, M. Findiesen, K. Hansen, R. Hazell, L. Hennig, C.E. Olsen, L. Pedersen, O. Simonsen, *J. Chem. Soc., Dalton Trans.*, 1997, 2045.
11. A. la Cour, M. Findeisen, A. Hazell, R. Hazell, G. Zdobinsky, *J. Chem. Soc., Dalton Trans.*, 1997, 121.
12. H. Frydendahl, H. Toftlund, J. Becher, J.C. Dutton, K.S. Murray, L.F. Taylor, O.P. Anderson, E.R.T. Tiekink, *Inorg. Chem.*, 1995, **34**, 4467.
13. A. Bondi, *J. Phys. Chem.*, 1964, **68**, 441.
14. Cerius² molecular modelling system under licence from Molecular Simulations Inc., San Diego, CA.

15. F. Lions, K.V. Martin, *J. Am. Chem. Soc.*, 1957, **73**, 1273.
16. A.L. Nivorozhkin, H. Toftlund, M. Neilsen, *J. Chem. Soc. Dalton Trans.*, 1994, 361.

Chapter 6

Conclusions and Further Work

The main objective of the work presented in this thesis was to identify alternative and highly selective complexing agents, which could be used for the recovery of zinc from a highly acidic sulfate feedstream, as replacements for the proposed dithiophosphoramidate (L2083). A key requirement for such a reagent would be its ability to operate at a pH lower than 2 and show very high selectivity for zinc(II) over iron(III). A secondary aim of the project was to identify weaker zinc extractants which would operate in a circuit, in which iron(III) has previously been removed by precipitation. Such a reagent is seen as a potential replacement for di(2-ethylhexyl)phosphoric acid (D2EHPA).

From a review of the coordination chemistry of zinc it emerged that ligands which favour a tetrahedral geometry and provide a $S_2N_2^{2-}$ donor set should give very stable zinc(II) complexes and possibly discriminate against other transition metals, primarily iron(III). A complementary experimental investigation, using a series of 3-substituted-pyridin-2-ones to define the influence of donor atom types on complex stability, was largely inconclusive due to the difficulty in preparing a coherent set of ligands. However, it did indicate that ligands containing a 5-membered chelate ring to which a 6-membered aromatic ring is fused preferentially lead to the formation of octahedral or planar coordination geometries and are therefore unlikely to show selectivity for zinc(II) over other divalent transition metal cations.

Both 1-substituted-3-methyl-4-alkylaldenamine-pyrazol-5-thiones and the 1-substituted-3-methyl-4-arylhydrazone-pyrazol-5-thiones have been shown to fulfil some of the essential solvent extractant requirements, *e.g.* ease of synthesis and good solubility characteristics, when appropriately large solubilising groups are present. Analysis of the ligands, by 1H NMR, demonstrated that they exist as enamine-thione

tautomers in solution and a crystallographic survey of a number of these ligands confirmed that this tautomer exists in the solid state. Complexation to divalent 1st row transition metals (including zinc) leads to an electronic arrangement around the chelate ring approximating more closely to the imino-thiol tautomer. Structure determination also shows that steric volume the imino substituent can have a significant effect on the coordination geometry adopted by the metal complex. In general an increase in the steric volume leads to a geometry closer to that of a tetrahedron.

It was proposed that the selectivity and “strength” of extraction would depend upon the extractant’s ability to complex in a tetrahedral fashion. This was found to be partly true and the selectivity order for the enamine- and hydrazone-pyrazol-5-thiones, $\text{Cu}^{2+} > \text{Zn}^{2+} > \text{Co}^{2+} > \text{Ni}^{2+}$, does not follow the Irving-Williams stability series for divalent metals but instead closely correlates with the propensity of the metal ions to adopt tetrahedral geometries. However, the steric volume of the imino substituent did not have any perceived influence on the extractant’s “strength”, which was predominantly dependent on three factors; (1) the ligand’s acidity, (2) the ligand’s solubility and (3) the lipophilicity of the diluent.

As the enamine-pyrazol-5-thiones were observed to be stronger extractants than the hydrazone derivatives the bulk of the work carried out was based on them. To date no bidentate enamine-pyrazol-5-thione candidates have matched the “strength” of L2083. They would however operate at a medium pH and are strong enough to recover zinc from operations where the pH has previously been increased to remove iron(III) as oxyhydroxides and hydroxides. The enamine-pyrazol-5-thiones have been shown to extract and strip copper(II) in the right pH range for an acidic leach

circuit and are suitable candidates for the replacement of the commercial phenolic oxime copper(II) extractant (P50 oxime). In this respect their performance is better than that of the dithiophosphoramides (L2083) which provide a S_4^{2-} donor set. Extraction is accompanied by reduction to copper(I) which cannot be stripped, effectively poisoning the extractant. The enamine-pyrazol-5-thiones provide the copper with a $S_2N_2^{2-}$ donor set and no reduction to copper(I) is observed. Furthermore, the interesting “anti” Irving-Williams selectivity for cobalt(II) over nickel(II) highlights their potential in solvent extraction operations to enable the separation of cobalt from nickel.

This work has also established the potential for extending the bidentate-enamine-pyrazol-5-thiones to tetradentate analogues by uniting two ligand units *via* a bridging group that predisposes the $N_2S_2^{2-}$ donor set to a geometry close to that required for tetrahedral complexation. Further work in this area requires an increase in the ligands solubility to permit solvent extraction testing in a hope to further increase the stability of the extracted zinc(II) complex and hence increase the extractant “strength”, perhaps to a $pH < 2$ which would allow extraction to proceed in the presence of iron(III).

Appendix

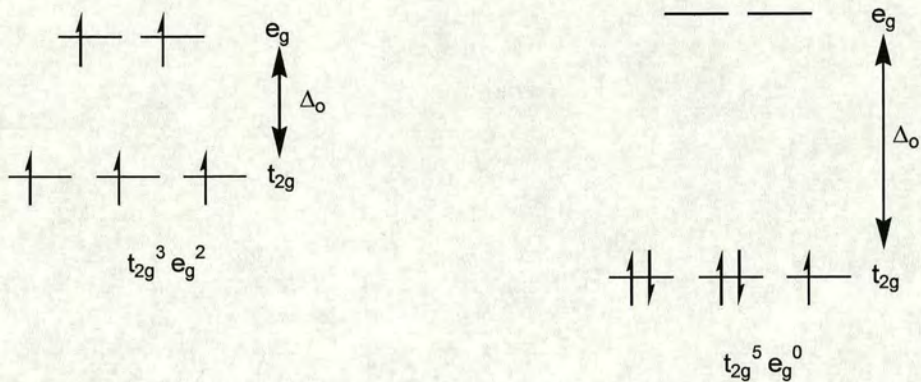
Appendix I.

Magnetic Susceptibility of [Fe(5-H)₃] (12).

The solid state magnetic susceptibility of [Fe(5-H)₃] (12) was measured using a Johnson-Matthey Magnetic Susceptibility balance using the Gouy method. The sample was prepared by grinding the complex with a mortar and pestle and packing it into a pre-weighed fused silica tube and magnetic susceptibility then measured. The diamagnetic correction for the ligand was made by measuring the magnetic susceptibility of N-benzyl-3-hydroxy-2(1H)-pyridinethione (5) and subtracting its contribution from that of the iron complex. The theoretical number of unpaired electrons, *i.e.* the magnetic moment (μ_{so}), was calculated using Equation 7.1, where S is the number of unpaired electrons.

$$\mu_{so} = 2\sqrt{S(S+1)} \quad (7.1)$$

Octahedral d⁵ iron(III) can be either high spin (HS) with 5 unpaired electrons or low spin (LS) with 1 unpaired electron. Low spin configurations are favoured by the spin pairing energy being less than Δ_o and are stabilised by π -acceptor ligands, *e.g.* [Fe(CN)₆]³⁻, whereas high spin compounds favour π -donor ligands, *e.g.* [Fe(O₂H)₆]³⁺, Figure 7.1 shows the two cases.



$$\mu_{\text{eff}} = 2\sqrt{S(S+1)}$$

$$\mu_{\text{eff}} = 2\sqrt{5/2(5/2+1)}$$

$$\mu_{\text{eff}} = 5.92$$

(a)

$$\mu_{\text{eff}} = 2\sqrt{S(S+1)}$$

$$\mu_{\text{eff}} = 2\sqrt{1/2(1/2+1)}$$

$$\mu_{\text{eff}} = 1.73$$

(b)

Figure 7.1. (a) High spin iron(III) and (b) low spin iron(III).

The effective magnetic moment (μ_{eff}) for $[\text{Fe}(\mathbf{5-H})_2]$ (12) was calculated using equations (7.2), (7.3) and (7.4).

$$\chi_g = \frac{c.L.(R - R_o)}{10^9.m} \quad (7.2)$$

$$\chi_m = \chi_g.Mwt \quad (7.3)$$

$$\mu_{\text{eff}} = 2.821\sqrt{\chi_m.T} \quad (7.4)$$

where

χ_g = magnetic susceptibility.

χ_m = molar magnetic susceptibility.

c = balance constant (1.38).

l = length of sample (cm).

R = magnetic susceptibility of sample and tube.

R_0 = magnetic susceptibility of empty tube.

m = mass of sample (g).

T = temperature (K).

The molar magnetic susceptibility (χ_m) for [Fe(**5-H**)₃] (**12**) and the diamagnetic correction for the HL (**5**) are shown below:

[Fe(5-H) ₃] (12)	HL (5)
$\chi_g = \frac{1.38 \times 1.35 \times (776 - (-22))}{1 \times 10^9 \times 0.0648}$	$\chi_g = \frac{1.38 \times 1.5 \times (228 - (-22))}{1 \times 10^9 \times 0.1062}$
$\chi_g = 2.294 \times 10^{-5}$	$\chi_g = 4.873 \times 10^{-6}$
$\chi_m = 2.294 \times 10^{-5} \times 704.68$	$\chi_m = 4.873 \times 10^{-6} \times 217.3$
$\chi_m = 1.617 \times 10^{-2}$	$\chi_m = 1.056 \times 10^{-3}$

The effective magnetic moment is:

$$\mu_{\text{eff}} = 2.821 \sqrt{(1.617 \times 10^{-2} \times 292.5) - 3(1.056 \times 10^{-3} \times 286)}$$
$$\mu_{\text{eff}} = 5.51$$

Appendix II.

Chemicals and instrumentation.

All chemicals used were reagent grade, unless otherwise specified, and used as received from Aldrich, Fisher-Acros or Avocado. The *p*-nonyl aniline was obtained from Avecia as a mixture of straight and branched isomers and used without purification. Ethanol and methanol were dried over 4 Å molecular sieves before use in the synthetic procedures.

¹H NMR (except compound **20**) and ¹³C NMR spectra were obtained using a Bruker AC200 spectrometer and a Bruker AC250 spectrometer respectively at ambient temperature, as (CD₃)₂SO, CDCl₃ or D₂O solutions referenced to residual solvent protons. The ¹H NMR spectrum of **20** was obtained, at Avecia, on a Bruker DPX300 and calibrated using TMS.

Electron impact (EI) mass spectrometry was carried out on a Finnigan MAT 4600 quadrupole spectrometer or a Kratos MS50TC. Fast atom bombardment (FAB) mass spectrometry was carried out using a Kratos MS50TC, in a NOBA or thioglycerol matrix. Electrospray mass spectrometry was carried out using a Thermoquest LCQ Spectrometer.

Elemental analysis was obtained using a Perkin Elmer 2400 CHN Elemental Analyser. Melting points were determined using a Gallenkamp melting point apparatus and are uncorrected.

The electronic spectra were measured on an ATI UNICAM UV/vis Spectrometer UV2 with 1 cm path length quartz cuvettes, using reagent grade chloroform as the solvent.

The infra-red spectra of the compounds were obtained by the preparation of KBr disks using a Perkin Elmer Paragon 1000 FT-IR Spectrometer.

The magnetic susceptibility measurement of $[\text{Fe}(\mathbf{5-H})_3]$ (**12**) was performed on a Johnson-Matthey Magnetic Susceptibility balance using a fused silica sample tube.

Solvent extraction analysis was carried out using a Thermo Jarrell Ash Iris ICP-OES Spectrometer. The pH measurements of the aqueous phase of the solvent extractions were made using an Orion[®] pH meter (model 410A) fitted with a BDH Gelplas epoxy body, sealed reference, combination glass electrode.

Appendix III.

Crystallographic data for N-benzyl-3-hydroxy-2(1H)-pyridinethione and N-benzyl-3-hydroxy-2(1H)-pyridinone and their metal complexes.

In all cases data were collected at 220 K on a Stoe Stadi-4 diffractometer equipped with an Oxford Cryosystems low temperature device by Dr. Simon Parsons of the University of Edinburgh, using Cu-K α radiation for complexes **5** and **10** and Mo-K α radiation for **7**, **8**, **9**, **11** and **16**. Reflections were scanned in omega-theta mode (ω - θ), with on-line profile fitting for **8**, **9** and **11**.¹ The structures were solved by direct methods (SHELXTL)² or (SIR92)³ and completed by iterative cycles of least-squares refinement against F^2 and difference Fourier maps (SHELXTL). The hydrogen atoms were refined geometrically, those incorporated in the OH group for compounds **5** and **7** being first located in a difference synthesis, and modelled with isotropic displacement parameters. In all cases all non-hydrogen atoms were modelled with anisotropic displacement parameters, the final refinement statistics presented are in Tables 7.1 to 7.3.

	HL (5)	HL (7)
Formula	C ₁₂ H ₁₁ NOS	C ₁₂ H ₁₁ NO ₂
RMM	217.28	201.22
Crystal system	Monoclinic	Monoclinic
Space group	P2 ₁ /n	P2 ₁ /c
a / Å	7.2847(11)	8.9024(17)
b / Å	9.740(3)	12.638(3)
c / Å	15.231(2)	8.951(2)
α / °	90	90
β / °	94.386(13)	91.544(14)
γ / °	90	90
U / Å ³	1077.5(4)	1006.7(4)
Crystal size / mm	0.58 × 0.08 × 0.08	0.51 × 0.39 × 0.27
D _c / g cm ⁻³	1.339	1.328
Z	4	4
μ / cm ⁻¹	24.25	0.91
Transmission factors	-	-
θ Limits / °	5-60	3-25
Reflections measured	3228	3558
No. of unique data	3225	1778
R _{int}	0.0000	0.0145
No. data with I > 2 σ (I)	2163	1353
No. variables	138	138
R	0.0609	0.0369
wR(F ²)	0.1688	0.0987
$\Delta\rho_{\max}, \Delta\rho_{\min}$ / eÅ ⁻³	0.282, -0.369	0.157, -0.158

Table 7.1. Crystallographic refinement data for N-benzyl-3-hydroxy-2(1H)-pyridinethione (5) and N-benzyl-3-hydroxy-2(1H)-pyridinone (7).

	[Zn(5-H) ₂] (8)	[Cu(5-H) ₂] (9)	[Ni(5-H) ₂].MeOH (10)
Formula	C ₂₄ H ₂₀ N ₂ O ₂ S ₂ Zn	C ₂₄ H ₂₀ CuN ₂ O ₂ S ₂	C ₂₅ H ₂₄ N ₂ NiO ₃ S ₂
RMM	497.91	496.08	523.29
Crystal system	Monoclinic	Monoclinic	Triclinic
Space group	P2 ₁ /c	P2 ₁ /c	P-1
a / Å	10.009(2)	10.5703(18)	7.504(10)
b / Å	13.668(3)	7.4791(12)	11.042(18)
c / Å	16.543(4)	14.205(3)	14.853(16)
α / °	90	90	108.35(13)
β / °	101.489(19)	102.833(16)	93.06(6)
γ / °	90	90	96.52(6)
U / Å ³	2217.7(9)	1094.9(3)	1155(3)
Crystal size / mm	0.58 × 0.50 × 0.39	0.43 × 0.39 × 0.08	0.32 × 0.19 × 0.12
D _c / g cm ⁻³	1.491	1.505	1.504
Z	4	2	2
μ / cm ⁻¹	13.2	12.12	31.54
Transmission factors	0.451-0.512 ^(a)	0.657-0.962 ^(a)	0.486-0.735 ^(a)
θ Limits / °	2-25	2-25	3-60
Reflections measured	3968	2637	5844
No. of unique data	3910	1885	3396
R _{int}	0.0670	0.0324	0.0344
No. data with I > 2σ(I)	3385	1580	2289
No. variables	281	143	301
R	0.0326	0.0370	0.0430
wR(F ²)	0.0863	0.0883	0.1004
Δρ _{max} , Δρ _{min} / eÅ ⁻³	0.465, -0.353	0.313, -0.487	0.360, -0.397

Table 7.2. Crystallographic refinement data for complexes [Zn(5-H)₃] (8), [Cu(5-H)₂] (9) and [Ni(5-H)₂].MeOH (10). ^(a) Absorption corrections based on ψ-scans.

	[Co(5-H) ₃].2MeOH (11)	[Cu(7-H) ₂].2EtOH (16)	[Zn ₃ (7-H) ₄ (OAc)] _n (17)
Formula	C ₃₈ H ₃₈ CoN ₃ O ₅ S ₃	C ₂₈ H ₃₂ CuN ₂ O ₆	C ₃₂ H ₃₂ N ₂ O ₁₂ Zn ₃
RMM	771.82	556.10	832.71
Crystal system	Triclinic	Monoclinic	Triclinic
Space group	P-1	P2 ₁ /n	P-1
a / Å	10.104(5)	15.606(8)	8.614(4)
b / Å	13.372(6)	9.844(5)	10.905(5)
c / Å	15.191(7)	18.263(8)	10.911(5)
α / °	71.78(3)	90	102.41(2)
β / °	72.15(2)	108.57(4)	108.13(2)
γ / °	69.20(2)	90	111.69(2)
U / Å ³	1778(2)	2660(2)	839.5(7)
Crystal size / mm	0.54 × 0.19 × 0.08	0.58 × 0.35 × 0.19	0.60 × 0.39 × 0.35
D _c / g cm ⁻³	1.442	1.389	1.647
Z	2	4	1
μ / cm ⁻¹	7.07	8.66	30.69
Transmission factors	-	0.739-0.852 ^(b)	0.485-0.768 ^(a)
θ Limits / °	2-25	2.5-22.5	5-70
Reflections measured	6799	3459	2928
No. of unique data	6126	3459	2924
R _{int}	0.1068	0.0000	0.0083
No. data with I > 2σ(I)	4361	2381	2771
No. variables	465	336	224
R	0.0516	0.0505	0.0429
wR(F ²)	0.1050	0.1161	0.0447
Δρ _{max} , Δρ _{min} / eÅ ⁻³	0.371, -0.333	0.409, -0.324	1.031, -0.719

Table 7.3. Crystallographic refinement data for complexes [Co(5-H)₃].2MeOH (11), [Cu(7-H)₂].2EtOH (16) and [Zn₃(7-H)₄(OAc)]_n (17). Absorption corrections based on ^(a) ψ-scans, ^(b) numerically optimised.

Appendix IV.

Crystallographic data for bidentate pyrazol-5-thiones.

Data were collected as described in Appendix III in all cases, with the exception of **42** which was collected at 150 K on a Nonius KappaCCD diffractometer equipped with an Oxford Cryosystems low temperature device by Dr. Simon Coles at the EPSRC National Crystallography Service, University of Southampton. A Cu-K α radiation source was used for the complexes **24**, **27**, **28**, **34**, **36** and **38** and Mo-K α radiation for **23**, **35**, **39**, **37**, **42**, **40** and **47**. Reflections were scanned in omega-theta mode (ω - θ) except for **43** which was scanned in omega-phi mode (ω - ϕ), with on-line profile fitting for **39**, **40** and **47**.¹ The structures were solved by Patterson synthesis (DIRDIF)⁴ except for **27**, **28** and **38** which were solved by direct methods (SHELXTL)² and completed by iterative cycles of least-squares refinement against F^2 and difference Fourier maps (SHELXTL). The hydrogen atoms were refined geometrically, those incorporated in NH or CH₃ groups being first located in a difference synthesis, and modelled with isotropic displacement parameters. In all cases all non-hydrogen atoms were modelled with anisotropic displacement parameters, the final refinement statistics are presented in Tables 7.4 to 7.9.

	HL (23)	HL (24)
Formula	C ₁₅ H ₁₉ N ₃ S	C ₁₇ H ₂₁ N ₃ S
RMM	273.39	299.43
Crystal system	Monoclinic	Monoclinic
Space group	P2 ₁ /c	P2 ₁ /c
a / Å	12.672(2)	10.6595(8)
b / Å	10.277(2)	10.5940(6)
c / Å	12.488(2)	14.0002(8)
$\alpha / ^\circ$	90	90
$\beta / ^\circ$	115.981(12)	92.867(6)
$\gamma / ^\circ$	90	90
U / Å ³	1462.0(4)	1579.0(2)
Crystal size / mm	0.39 × 0.35 × 0.31	0.35 × 0.31 × 0.23
D _c / g cm ⁻³	1.242	1.260
Z	4	4
μ / cm ⁻¹	2.12	17.81
Transmission factors	-	0.281-0.649 ^(a)
θ Limits / °	3-25	4-70
Reflections measured	3755	12724
No. of unique data	2577	2906
R _{int}	0.0339	0.0477
No. data with I > 2 σ (I)	1947	2585
No. variables	181	196
R	0.0397	0.0341
wR(F ²)	0.0965	0.0875
$\Delta\rho_{\max}, \Delta\rho_{\min} / \text{e}\text{\AA}^{-3}$	0.217, -0.189	0.256, -0.182

Table 7.4. Crystallographic refinement data for HL (23) and HL (24).

	HL (27)	HL (28).CHCl ₃
Formula	C ₂₁ H ₂₃ N ₃ S	C ₁₈ H ₁₅ Cl ₃ N ₄ O ₂ S
RMM	349.48	457.75
Crystal system	Monoclinic	Orthorhombic
Space group	P2 ₁ /c	Pnma
a / Å	7.204(4)	11.465(2)
b / Å	20.962(8)	7.0016(15)
c / Å	12.334(10)	25.499(5)
α / °	90	90
β / °	92.72(6)	90
γ / °	90	90
U / Å ³	1861(2)	2046.9(7)
Crystal size / mm	0.47 × 0.16 × 0.12	0.62 × 0.23 × 0.04
D _c / g cm ⁻³	1.248	1.485
Z	4	4
μ / cm ⁻¹	15.89	52.02
Transmission factors	-	0.273-0.968 ^(a)
θ Limits / °	4-60	3-70
Reflections measured	2695	3280
No. of unique data	2691	2018
R _{int}	0.0000	0.0867
No. data with I > 2σ(I)	1191	1213
No. variables	227	186
R	0.0877	0.0806
wR(F ²)	0.2400	0.2106
Δρ _{max} , Δρ _{min} / eÅ ⁻³	0.357, -0.289	0.360, -0.441

Table 7.5. Crystallographic refinement data for HL (27) and HL (28).CHCl₃.

^(a) Absorption corrections based on ψ-scans.

	[Zn(23-H) ₂] (34)	[Co(23-H) ₂] (35)
Formula	C ₃₀ H ₃₆ N ₆ S ₂ Zn	C ₃₀ H ₃₆ CoN ₆ S ₂
RMM	610.14	603.70
Crystal system	Orthorhombic	Orthorhombic
Space group	Pbcn	Pbcn
a / Å	11.838(3)	11.867(5)
b / Å	11.450(2)	11.410(3)
c / Å	21.974(3)	21.962(6)
$\alpha / ^\circ$	90	90
$\beta / ^\circ$	90	90
$\gamma / ^\circ$	90	90
U / Å ³	2978.5(11)	2973.7(16)
Crystal size / mm	0.23 × 0.12 × 0.04	0.52 × 0.52 × 0.04
D _c / g cm ⁻³	1.361	1.348
Z	4	4
μ / cm ⁻¹	26.84	7.48
Transmission factors	0.639-0.879 ^(b)	0.835-0.992 ^(b)
θ Limits / °	4-70	2.5-25
Reflections measured	5000	2973
No. of unique data	2532	2629
R _{int}	0.0568	0.0800
No. data with I > 2 σ (I)	1504	1030
No. variables	178	177
R	0.0496	0.0819
wR(F ²)	0.0973	0.1618
$\Delta\rho_{\max}, \Delta\rho_{\min}$ / eÅ ⁻³	0.318, -0.451	0.439, -0.453

Table 7.6. Crystallographic refinement parameters for [Zn(23-H)₂] (34) and [Co(23-H)₂] (35). ^(b) Numerically optimised.

	[Zn(26-H) ₂] (36)	[Co(26-H) ₂] (37)	[Ni(26-H) ₂] (38)
Formula	C ₃₄ H ₂₈ N ₆ S ₂ Zn	C ₃₄ H ₂₈ CoN ₆ S ₂	C ₃₄ H ₂₈ N ₆ NiS ₂
RMM	650.11	643.67	643.45
Crystal system	Orthorhombic	Orthorhombic	Monoclinic
Space group	Pbcn	Pbcn	C2/c
a / Å	10.1153(14)	10.1299(10)	21.0686(19)
b / Å	12.8699(18)	12.8515(12)	9.7935(9)
c / Å	24.2049(19)	24.132(3)	14.8154(14)
α / °	90	90	90
β / °	90	90	109.255(6)
γ / °	90	90	90
U / Å ³	3151.1(7)	3141.6(6)	2885.9(5)
Crystal size / mm	0.51 × 0.27 × 0.08	0.97 × 0.54 × 0.08	0.40 × 0.18 × 0.08
D _c / g cm ⁻³	1.370	1.361	1.481
Z	4	4	4
μ / cm ⁻¹	25.82	7.13	26.08
Transmission factors	0.408-0.842 ^(b)	0.770-0.986 ^(b)	0.379-0.788 ^(a)
θ Limits / °	4-70	2.5-25	4-70
Reflections measured	2660	3102	2486
No. of unique data	2518	2770	2475
R _{int}	0.0147	0.0689	0.0143
No. data with I > 2σ(I)	1787	1583	1914
No. variables	196	196	197
R	0.0401	0.0603	0.0395
wR(F ²)	0.0996	0.1493	0.0942
Δρ _{max} , Δρ _{min} / eÅ ⁻³	0.236, -0.252	0.414, -0.366	0.248, -0.318

Table 7.7. Crystallographic refinement parameters for [Zn(26-H)₂] (36), [Co(26-H)₂] (37) and [Ni(26-H)₂] (38). Absorption corrections based on ^(a) ψ-scans, ^(b) numerically optimised.

	[Zn(27-H) ₂] (39)	[Co(27-H) ₂] (40)
Formula	C ₄₂ H ₄₄ N ₆ S ₂ Zn	C ₄₂ H ₄₄ CoN ₆ S ₂
RMM	762.32	755.88
Crystal system	Monoclinic	Monoclinic
Space group	P2 ₁ /c	P2 ₁ /c
A / Å	12.1093(12)	12.121(2)
b / Å	27.954(6)	27.944(5)
c / Å	12.6411(13)	12.636(2)
α / °	90	90
β / °	113.448(7)	113.633(9)
γ / °	90	90
U / Å ³	3925.7(11)	3921.1(10)
Crystal size / mm	0.54 × 0.39 × 0.39	0.51 × 0.27 × 0.19
D _c / g cm ⁻³	1.290	1.280
Z	4	4
μ / cm ⁻¹	7.70	5.82
Transmission factors	0.643-0.693 ^(a)	0.632-0.668 ^(a)
θ Limits / °	3-25	3-25
Reflections measured	9637	9060
No. of unique data	6868	6865
R _{int}	0.0200	0.0299
No. data with I > 2 σ (I)	5284	4893
No. variables	469	468
R	0.0427	0.0509
wR(F ²)	0.0965	0.1132
$\Delta\rho_{\max}, \Delta\rho_{\min}$ / eÅ ⁻³	0.407, -0.294	0.481, -0.248

Table 7.8. Crystallographic refinement data for [Zn(27-H)₂] (39) and [Co(27-H)₂] (40). Absorption corrections based on ^(a) ψ -scans.

	[Zn(33-H) ₂] (42)	[Zn(48-H) ₂] (50)
Formula	C ₄₂ H ₄₄ N ₆ O ₂ Zn	C ₃₂ H ₂₆ N ₈ S ₂ Zn
RMM	730.20	652.10
Crystal system	Triclinic	Triclinic
Space group	P-1	P-1
a / Å	10.8423(9)	9.920(5)
b / Å	12.5272(9)	12.550(6)
c / Å	14.0804(7)	13.215(6)
α / °	98.321(4)	68.92(3)
β / °	95.147(4)	88.45(4)
γ / °	100.652	80.60(3)
U / Å ³	1846.3(2)	1513.7(13)
Crystal size / mm	0.10 × 0.10 × 0.05	0.47 × 0.27 × 0.04
D _c / g cm ⁻³	1.313	1.431
Z	2	2
μ / cm ⁻¹	7.10	9.86
Transmission factors	0.873-0.967 ^(c)	0.766-0.954 ^(b)
θ Limits / °	4-25	3-25
Reflections measured	39360	5456
No. of unique data	6480	5366
R _{int}	0.1200	0.2681
No. data with I > 2σ(I)	4270	3651
No. variables	462	390
R	0.0478	0.0547
wR(F ²)	0.1031	0.1163
Δρ _{max} , Δρ _{min} / eÅ ⁻³	0.417, -0.342	0.519, -0.361

Table 7.9. Crystallographic refinement data for [Zn(33-H)₂] (42), and [Zn(48-H)₂] (50). Absorption corrections ^(b) numerically optimised, ^(c) Sortav^{5,6} (absorption correction software package).

Appendix V.

Crystallographic data for tetradentate pyrazol-5-thiones.

In all cases data were collected as described in Appendix III (H₂L (**56**) was collected at 293 K) by Dr. Simon Parsons and Mr. Andrew Parkin of the University of Edinburgh, using Cu-K α radiation for all the complexes. Reflections were scanned in omega-theta mode (ω - θ), with on-line profile fitting for H₂L (**55**).¹ The structures were solved by direct methods (SHELXTL)² except for **65** which was solved using the Patterson synthesis (DIRDIF),⁴ and completed by iterative cycles of least-squares refinement against F^2 and difference Fourier maps (SHELXTL). The hydrogen atoms were refined geometrically, except for those located on the nitrogen atoms in **55** and **66** which were refined by difference synthesis, and modelled with isotropic displacement parameters. In all cases all non-hydrogen atoms were modelled with anisotropic displacement parameters, the final refinement statistics are presented in Tables 7.10 and 7.11.

	H₂L (55). 1/8 H₂O	H₂L (56)
Formula	C ₂₈ H _{30.25} N ₆ O _{0.125} S ₂	C ₁₆ H ₂₄ N ₆ S ₂
RMM	516.95	364.53
Crystal system	Triclinic	Monoclinic
Space group	P-1	P2 ₁ /c
a / Å	11.503(9)	5.1665(3)
b / Å	13.686(10)	6.2297(3)
c / Å	19.666(15)	29.2936(11)
α / °	76.69(4)	90
β / °	87.45(5)	93.256(4)
γ / °	65.24(4)	90
U / Å ³	2731(4)	941.31(8)
Crystal size / mm	0.35 × 0.19 × 0.16	0.43 × 0.23 × 0.08
D _c / g cm ⁻¹	1.257	1.286
Z	4	2
μ / cm ⁻¹	19.85	26.41
Transmission factors	-	0.561-0.807 ^(b)
θ Limits / °	4-70	3-70
Reflections measured	9801	4319
No. of unique data	9578	1665
R _{int}	0.1164	0.0196
No. data with I > 2σ(I)	4270	1372
No. variables	658	112
R	0.0626	0.0367
wR(F ²)	0.1653	0.1045
Δρ _{max} , Δρ _{min} / eÅ ⁻³	0.236, -0.246	0.218, -0.158

Table 7.10. Crystallographic refinement data for H₂L (55). 1/8 H₂O and H₂L (56).

^(b) Absorption corrections are numerically optimised.

	[Ni(56-2H)].CH ₃ NO ₂ (63)	[Zn(58-2H)] (65)	[Ni(58-2H)].MeOH (66)
Formula	C ₁₇ H ₂₅ N ₇ NiO ₂ S ₂	C ₂₀ H ₂₂ N ₆ S ₂ Zn	C ₂₁ H ₂₆ N ₆ NiOS ₂
RMM	482.27	475.93	501.31
Crystal system	Orthorhombic	Triclinic	Orthorhombic
Space group	P2(1)2(1)2(1)	P-1	Pnna
a / Å	12.0735(17)	7.5508(10)	19.940(6)
b / Å	13.9530(13)	8.3374(16)	15.323(5)
c / Å	25.755(4)	17.276(3)	7.332(2)
α / °	90	85.652(12)	90
β / °	90	83.300(8)	90
γ / °	90	89.486(10)	90
U / Å ³	4338.8(10)	1077.0(3)	2240.1(12)
Crystal size / mm	0.86 × 0.66 × 0.23	0.64 × 0.27 × 0.18	0.23 × 0.19 × 0.08
D _c / g cm ⁻³	1.477	1.468	1.486
Z	8	2	4
μ / cm ⁻¹	33.31	35.43	32.05
Transmission factors	0.08720-0.36460 ^(d)	0.233-0.577 ^(b)	0.254-0.360 ^(a)
θ Limits / °	3-60	5-70	4-70
Reflections measured	3679	3193	2388
No. of unique data	3354	2654	1924
R _{int}	0.0105	0.0198	0.0883
No. data with I > 2σ(I)	3073	2381	1100
No. variables	500	267	143
R	0.0814	0.0421	0.0851
wR(F ²)	0.2504	0.1396	0.2474
Δρ _{max} , Δρ _{min} / eÅ ⁻³	1.514, -1.376	0.359, -0.318	0.982, -0.887

Table 7.11. Crystallographic refinement data for [Ni(56-2H)].CH₃NO₂ (63), [Zn(58-2H)] (65) and [Ni(58-2H)].MeOH (66). Absorption corrections are ^(a) based on ψ-scans, ^(b) numerically optimised, ^(d) face-indexed.

Appendix VI.

Solvent extraction data.

The experimental technique employed here (Section 4.11.1) for the quantitative analysis of the extractive capabilities of a number of ligands incorporates a certain degree of experimental error. Although there are always errors associated with instrument accuracy, *e.g.* calibration and measurement of pH, these are assumed to contribute only slightly and are therefore not treated rigorously. It is thought that the significant contribution to the accuracy of the result is dependent on factors such as the solubility of the extracted complex and the formation of metal hydroxides at high pH. Both of these result in the precipitation of metal species and result in other equilibrium processes being present which may distort the true pH range over which a metal is extracted.

One way of monitoring the validity of the extraction is by measuring the amount of metal present in solution for both the organic and aqueous phases, after the equilibrium has been reached. By summing the metal present in both phases a mass balance for each sample is obtained, Tables 7.12 to 7.26. The error associated with the amount of metal present for each sample (Error $\pm x$ %) has been calculated based on the three times the standard deviation of the sample reading. It has been calculated to demonstrate the unavoidably large error propagated by the necessary dilution of samples for analysis, although it has not been used in calculating the error associated with the $\text{pH}_{1/2}$ values quoted in this thesis (Sections 4.5 and 4.9). The error on the $\text{pH}_{1/2}$ is taken from the sigmoidal curve fitted to the data points, representing the percentage metal found in the organic phase at a given pH, using Origin 5.0 software.⁷

It has been estimated that errors, which are mainly associated with the high dilutions involved in the sample analysis, totalling $\pm 5-10\%$ of the theoretical 100 % mass balance are acceptable⁸ when there are no other competing equilibrium resulting from high pH or low solubility. Where there are obvious deficiencies in the mass balance, which are thought to arise from precipitation ($> 5-10\%$, shown in red in Table's 7.12 to 7.26), they have been omitted from the graphical results.

These discrepancies fall into two categories, (1) mass balances greater than 100 %, and (2) mass balances less than 100 %. Two scenarios are observed for mass balances totalling more than 100 %. Firstly, in some cases the total metal present progressively increases with pH, *e.g.* zinc extraction using HL (24) in Table 7.19. This may possibly be caused due to the limited solubility of the associated zinc complex ($\sim 0.04\text{ M}$ in toluene, see Section 4.5.1.1) or the hydrolysis of zinc at higher pH (see Section 4.5.1.2) resulting in the formation of precipitates. A small amount of precipitation increases the time taken to filter the organic and aqueous (Section 4.11.1) and therefore allows more time for the evaporation of solvent, resulting in the concentration of metal in both phases. As expected, the increase of metal present is mostly attributed to the evaporation of toluene in the organic phase due to its higher volatility. Secondly, the mass balance in the case for some cobalt extractions is constantly greater than 100 %, *e.g.* extraction using HL (29) Table 7.14 and 7.15 using toluene and Orform SX-7 respectively. This may be attributed to a discrepancy in the concentration of the cobalt standards, used in the calibration of the AAS, possibly resulting from the use of old standards.

It is thought that when the total metal present falls below the accepted 5-10 % error margin, it is due to the low solubility (Figure 7.2), *e.g.* zinc extraction using HL (27),

Table 7.20. This usually occurs when the metal loading is high, *i.e.* near full extraction. However, at high pH there is also the possibility of competing hydrolysis of the metal complex resulting in the effective removal of metal from the system, *e.g.* nickel extraction.

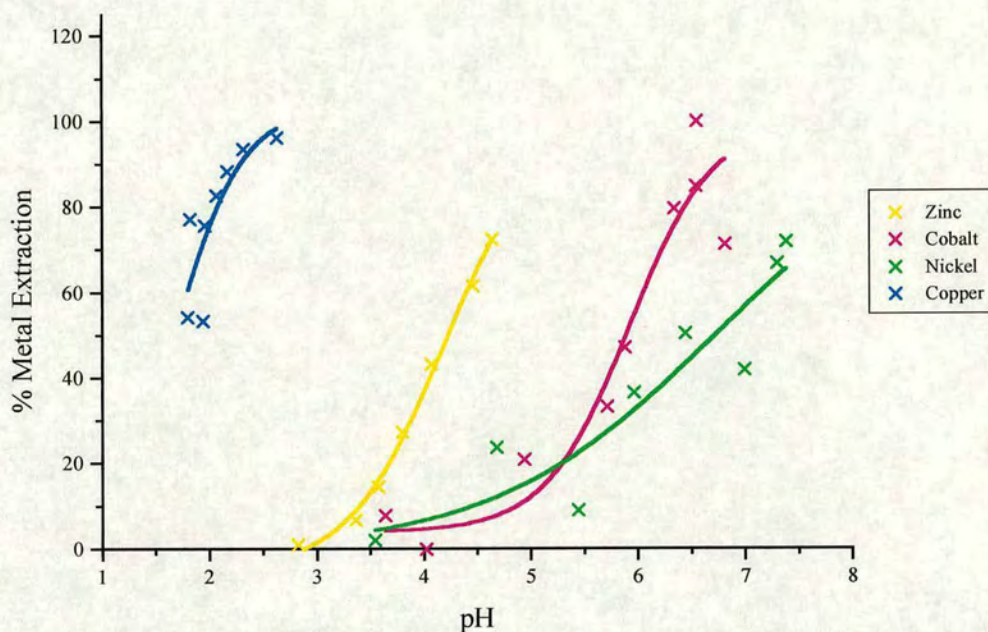


Figure 7.2. Single metal extraction of Zn(II), Co(II), Ni(II) and Cu(II) with 0.05 M 1-phenyl-3-methyl-4-(4-*t*-butylphenylaldenamine)-pyrazol-5-thione (**27**) in toluene at ambient temperature. Copper and cobalt results are based on aqueous measurements.

pH	Organic (%)	Error (\pm %)	Aqueous (%)	Error (\pm %)	Mass Balance
Zinc					
4.91	9.2	0.5	89.8	5.5	99.0
5.22	63.9	0.3	38.6	2.9	102.5
5.21	62.0	0.3	34.8	1.1	96.8
5.18	70.4	0.5	28.4	1.3	98.8
5.11	85.1	0.3	20.5	1.9	105.6
5.93	107.3	0.8	0.0	0.3	107.3
5.94	107.1	0.6	0.0	0.6	107.1
6.17	108.4	0.5	0.0	0.6	108.4
6.38	102.6	1.0	0.0	0.3	102.6
6.45	101.1	5.8	0.0	0.5	101.1
6.91	106.3	10.4	0.0	0.6	106.3
7.19	108.9	6.5	0.0	0.3	108.9
7.58	111.0	11.7	0.0	0.1	111.0
Cobalt					
4.91	0.0	0.1	106.5	4.9	106.5
5.22	1.0	0.6	102.3	5.2	103.3
5.21	1.5	0.5	97.8	2.3	99.3
5.18	1.6	0.9	101.3	4.1	102.9
5.11	2.8	5.0	105.9	1.6	108.7
5.93	34.2	0.6	78.2	4.0	112.4
5.94	53.2	0.1	65.0	2.0	118.2
6.17	83.9	0.1	34.1	0.7	118.0
6.38	70.5	0.3	21.0	0.7	91.5
6.45	101.7	1.4	15.1	2.2	116.8
6.91	112.7	1.4	7.0	2.0	119.7
7.19	122.8	2.2	3.0	0.9	125.8
7.58	120.4	2.9	0.6	0.3	121.0
Nickel					
4.91	0.0	0.3	97.4	10.6	97.4
5.22	0.4	0.6	98.3	6.1	98.7
5.21	0.4	0.9	105.5	5.6	105.9
5.18	0.4	0.9	98.0	7.4	98.4
5.11	0.4	3.2	101.7	8.1	102.1
5.93	1.8	1.5	98.4	7.0	100.2
5.94	6.9	0.2	95.1	5.4	102.0
6.17	14.9	0.2	84.4	9.0	99.3
6.38	25.2	0.3	72.7	3.2	97.9
6.45	37.0	2.2	55.3	3.1	92.4
6.91	63.5	2.9	32.3	1.1	95.7
7.19	80.5	2.2	19.4	1.4	100.0
7.58	93.3	5.8	2.4	0.4	95.7

Table 7.12. Multi-metal extraction data for Zn(II), Co(II) and Ni(II) using 0.05 M 1-phenyl-3-methyl-4-[2-ethylhexylaldenamine]-pyrazol-5-thione (**25**) in toluene.

pH	Organic (%)	Error (\pm %)	Aqueous (%)	Error (\pm %)	Mass Balance
Zinc					
2.48	1.0	0.2	106.2	16.4	107.2
3.77	13.1	1.1	82.4	2.6	95.5
4.04	34.3	0.1	64.5	5.0	98.8
4.47	56.2	0.5	42.4	2.4	98.6
4.78	78.0	0.8	23.2	1.3	101.2
5.14	97.8	0.6	4.9	0.5	102.8
5.70	102.2	1.9	1.2	0.6	103.4
5.79	100.6	0.8	0.9	0.5	101.6
6.18	96.1	0.3	0.6	1.5	96.7
6.35	98.7	3.9	0.4	0.2	99.1
6.55	95.5	3.9	0.2	0.2	95.7
7.06	97.8	8.4	0.1	0.2	97.9
8.05	82.9	6.5	0.2	0.2	83.1
10.74	78.0	3.9	0.0	0.1	78.0
Cobalt					
2.48	0.2	0.1	109.7	5.4	110.0
3.77	0.3	0.1	115.0	3.8	115.3
4.04	0.5	0.1	109.2	5.0	109.7
4.47	0.8	0.1	110.0	2.9	110.7
4.78	1.3	0.1	111.2	2.0	112.5
5.14	4.7	0.1	110.7	2.0	115.3
5.70	42.4	0.6	76.6	4.1	119.0
5.79	72.9	0.2	43.5	2.7	116.4
6.18	98.8	0.1	17.0	1.1	115.8
6.35	110.3	2.9	8.1	0.5	118.4
6.55	108.4	2.9	4.8	0.6	113.2
7.06	107.9	1.4	2.9	0.4	110.8
8.05	75.8	2.2	0.2	0.2	75.9
10.74	50.4	0.7	0.2	0.3	50.5
Nickel					
2.48	0.0	0.2	101.1	5.2	101.1
3.77	0.0	0.1	96.5	5.8	96.5
4.04	0.0	0.1	99.4	11.9	99.4
4.47	0.1	0.1	90.4	3.1	90.5
4.78	0.2	0.4	93.3	9.9	93.5
5.14	0.6	0.1	90.1	3.6	90.8
5.70	4.6	0.2	88.8	9.2	93.3
5.79	9.1	0.4	87.4	7.9	96.5
6.18	20.1	0.4	75.5	7.4	95.6
6.35	37.0	2.2	62.1	4.1	99.2
6.55	54.1	3.6	42.5	3.5	96.6
7.06	72.6	2.9	18.4	1.7	91.0
8.05	58.9	1.4	0.7	0.3	59.6
10.74	32.9	2.9	0.1	0.2	33.1

Table 7.13. Multi-metal extraction data for Zn(II), Co(II) and Ni(II) using 0.05 M 1-phenyl-3-methyl-4-[2-ethylhexylaldenamine]-pyrazol-5-thione (**25**) in Orform-SX7.

pH	Organic (%)	Error (\pm %)	Aqueous (%)	Error (\pm %)	Mass Balance
Zinc					
2.53	0.2	0.1	104.5	21.7	104.7
3.86	8.1	0.5	89.8	9.1	97.9
4.18	25.3	1.9	71.2	8.4	96.4
4.35	44.9	2.6	48.4	3.6	93.3
4.42	63.3	1.9	30.0	4.4	93.3
4.64	85.1	4.5	4.9	1.3	90.0
4.78	93.3	3.2	3.1	0.8	96.4
4.81	94.0	3.9	2.4	0.8	96.4
5.14	94.4	3.9	2.4	0.6	96.8
5.25	94.8	4.5	2.6	0.8	97.4
7.24	97.8	5.2	2.9	0.1	100.7
6.85	94.8	7.8	3.4	0.3	98.2
7.64	97.4	3.2	3.6	0.2	101.0
10.39	92.2	3.2	3.7	0.1	95.9
Cobalt					
2.53	0.0	0.1	115.0	3.6	115.0
3.86	0.3	0.1	112.8	4.3	113.1
4.18	0.0	0.1	110.9	4.1	110.9
4.35	0.3	0.1	114.3	1.6	114.6
4.42	0.0	0.1	113.3	1.3	113.4
4.64	2.3	0.1	113.7	3.8	116.0
4.78	40.2	0.6	77.1	2.7	117.3
4.81	76.7	1.4	38.3	3.6	115.0
5.14	99.8	1.4	14.6	1.3	114.4
5.25	108.4	2.2	6.6	1.1	115.0
7.24	108.9	3.6	0.6	0.3	109.5
6.85	109.8	1.4	0.8	0.2	110.6
7.64	104.1	1.4	0.4	0.1	104.5
10.39	71.5	1.4	0.7	0.4	72.1
Nickel					
2.53	0.0	0.1	105.0	5.4	105.0
3.86	0.0	0.1	105.0	3.6	105.0
4.18	0.0	0.1	103.2	2.9	103.2
4.35	0.0	0.1	99.3	7.2	99.3
4.42	0.0	0.1	102.6	2.7	102.6
4.64	0.1	0.1	102.6	4.7	102.7
4.78	2.1	0.1	99.6	6.1	101.6
4.81	7.0	0.3	90.6	4.5	97.5
5.14	18.7	0.4	85.1	5.0	103.8
5.25	32.9	1.4	67.6	3.2	100.5
7.24	87.7	1.4	2.9	0.3	90.6
6.85	73.1	2.2	18.7	1.3	91.8
7.64	84.9	2.2	0.8	0.4	85.7
10.39	54.1	1.4	0.5	0.7	54.6

Table 7.14. Multi-metal extraction data for Zn(II), Co(II) and Ni(II) using 0.05 M 1,3-dimethyl-4-[2-ethylhexylaldenamine]-pyrazol-5-thione (**29**) in toluene.

pH	Organic (%)	Error (\pm x %)	Aqueous (%)	Error (\pm x %)	Mass Balance
Zinc					
2.45	2.1	0.1	97.8	14.3	99.9
3.44	12.0	0.2	87.0	5.8	99.0
3.82	36.5	1.1	65.8	4.9	102.3
4.09	52.5	0.3	42.0	3.7	94.5
4.49	74.5	0.8	21.7	2.8	96.2
5.53	94.8	0.9	0.8	0.6	95.6
5.50	96.3	0.4	0.6	0.8	97.0
5.85	95.9	0.5	0.3	0.6	96.2
6.07	95.5	0.3	0.2	0.5	95.6
6.32	94.8	2.6	0.2	0.8	95.0
6.55	97.2	5.2	0.1	0.4	97.3
6.98	96.3	3.2	0.3	0.4	96.6
7.54	96.5	5.2	0.2	0.2	96.7
8.48	81.6	1.9	0.2	0.0	81.9
Cobalt					
2.45	0.2	0.1	113.3	2.3	113.5
3.44	0.0	0.1	112.4	3.1	112.4
3.82	0.1	0.1	111.8	2.0	111.9
4.09	0.3	0.1	113.2	2.9	113.5
4.49	0.7	0.1	110.6	2.9	111.2
5.53	7.3	0.2	119.3	2.0	126.6
5.50	40.6	0.6	75.3	1.8	115.8
5.85	78.2	0.1	38.0	1.8	116.2
6.07	105.0	0.1	10.5	0.7	115.5
6.32	111.3	0.7	3.9	1.6	115.2
6.55	115.6	2.2	1.3	0.5	116.9
6.98	113.7	2.2	1.4	0.2	115.1
7.54	115.1	2.2	0.1	0.2	115.3
8.48	101.2	0.7	0.2	0.1	101.4
Nickel					
2.45	0.0	0.2	103.5	3.2	103.5
3.44	0.0	0.1	97.2	7.8	97.2
3.82	0.0	0.1	98.7	5.4	98.7
4.09	0.0	0.1	99.0	2.2	99.0
4.49	0.0	0.1	98.7	9.6	98.7
5.53	0.4	0.1	95.9	2.7	96.3
5.50	2.2	0.1	98.4	3.6	100.6
5.85	5.0	0.1	90.2	2.9	95.2
6.07	14.3	0.2	84.4	5.9	98.7
6.32	32.5	1.4	65.3	1.8	97.8
6.55	52.2	2.2	44.5	1.7	96.7
6.98	72.6	1.4	22.1	0.9	94.7
7.54	94.5	2.9	1.8	0.5	96.2
8.48	81.0	2.9	0.6	0.2	81.6

Table 7.15. Multi-metal extraction data for Zn(II), Co(II) and Ni(II) using 0.05 M 1,3-dimethyl-4-[2-ethylhexylaldenamine]-pyrazol-5-thione (**29**) in Orform-SX7.

pH	Organic (%)	Error (\pm x %)	Aqueous (%)	Error (\pm x %)	Mass Balance
Zinc					
2.40	1.8	0.1	90.4	5.3	92.2
3.03	12.1	0.8	88.9	7.0	101.0
3.38	31.3	0.3	73.4	9.1	104.8
3.62	51.0	0.4	48.9	2.4	99.8
3.89	69.5	0.3	26.4	1.9	96.0
4.29	87.5	0.5	11.1	0.6	98.6
4.75	100.4	0.6	4.8	2.4	105.2
5.17	98.9	1.1	3.1	0.2	102.1
5.62	111.4	1.5	2.9	0.5	114.3
6.00	99.6	3.9	3.1	1.0	102.6
6.32	102.2	8.4	1.2	0.3	103.3
6.56	102.8	4.5	1.4	0.3	104.2
7.24	98.3	2.6	0.7	0.1	98.9
9.54	98.1	7.8	0.7	0.2	98.7
Cobalt					
2.40	0.3	0.1	116.1	2.2	116.4
3.03	0.1	0.2	110.9	2.9	111.1
3.38	0.9	0.2	112.1	2.9	113.0
3.62	1.9	0.3	108.5	4.1	110.4
3.89	5.0	0.2	104.4	5.0	109.5
4.29	12.7	0.3	103.4	4.7	116.0
4.75	46.5	0.2	61.2	2.2	107.7
5.17	86.3	0.4	37.3	0.5	123.6
5.62	111.8	0.5	10.7	0.4	122.4
6.00	104.1	2.2	2.3	0.4	106.3
6.32	107.0	1.4	0.7	0.4	107.7
6.56	107.0	4.3	0.7	0.9	107.6
7.24	101.7	2.9	0.3	0.3	101.9
9.54	92.6	2.2	0.0	0.3	92.6
Nickel					
2.40	0.0	0.1	104.8	5.9	104.8
3.03	0.0	0.2	103.5	6.5	103.5
3.38	0.0	0.2	107.6	5.2	107.6
3.62	0.0	0.1	103.7	6.5	103.7
3.89	0.0	0.2	103.4	1.8	103.4
4.29	0.0	0.3	107.6	5.6	107.6
4.75	1.0	0.3	93.3	6.7	94.3
5.17	4.2	0.1	101.7	7.2	105.9
5.62	13.6	0.6	92.8	4.5	106.5
6.00	33.4	4.3	74.8	2.5	108.2
6.32	56.3	2.2	48.1	1.5	104.4
6.56	82.0	2.9	25.9	1.7	107.9
7.24	99.3	5.0	4.4	0.3	103.6
9.54	95.2	3.6	0.7	0.2	95.9

Table 7.16. Multi-metal extraction data for Zn(II), Co(II) and Ni(II) using 0.05 M 1,3-dimethyl-4-[4-*t*-butylphenylaldenamine]-pyrazol-5-thione (**30**) in toluene.

pH	Organic (%)	Error (\pm x %)	Aqueous (%)	Error (\pm x %)	Mass Balance
Zinc					
2.54	0.5	0.1	97.3	8.9	97.8
3.46	5.8	0.3	92.3	7.3	98.1
3.59	25.9	0.6	69.8	6.2	95.7
3.78	44.3	1.9	55.0	2.4	99.3
3.99	71.3	5.8	36.0	1.9	107.3
4.56	90.1	6.5	5.0	0.6	95.0
4.57	90.3	6.5	5.0	1.1	95.2
4.70	101.3	13.0	5.2	0.8	106.5
4.95	97.2	5.2	4.4	0.6	101.6
5.01	95.5	6.5	4.4	0.6	99.8
5.21	97.0	6.5	4.4	0.3	101.3
6.24	93.5	5.2	4.5	0.4	98.0
7.51	93.3	5.2	4.4	0.2	97.7
Cobalt					
2.54	0.0	0.1	107.6	2.2	107.6
3.46	0.1	0.1	114.0	4.1	114.2
3.59	1.0	0.1	109.5	1.6	110.5
3.78	1.2	0.1	110.2	4.7	111.4
3.99	3.6	0.1	106.8	3.1	110.4
4.56	24.7	0.4	89.0	2.3	113.6
4.57	27.7	0.3	90.6	2.3	118.4
4.70	79.6	4.3	37.4	1.4	117.0
4.95	101.2	4.3	8.4	1.1	109.6
5.01	109.4	2.9	2.8	0.7	112.1
5.21	116.1	3.6	1.2	0.2	117.3
6.24	111.3	1.4	0.9	0.2	112.2
7.51	106.0	2.2	0.8	0.3	106.8
Nickel					
2.54	0.0	0.1	101.0	4.1	101.0
3.46	0.0	0.1	101.3	6.7	101.3
3.59	0.1	0.1	100.2	1.6	100.3
3.78	0.0	0.1	95.4	9.4	95.4
3.99	0.3	0.2	99.8	3.2	100.2
4.56	2.7	0.1	98.2	7.6	100.9
4.57	3.0	0.2	101.6	4.7	104.6
4.70	2.1	0.3	102.7	2.5	104.8
4.95	11.8	0.5	94.9	4.5	106.7
5.01	27.2	0.7	74.1	2.0	101.3
5.21	47.4	2.2	53.5	2.2	100.8
6.24	67.8	2.9	27.3	1.2	95.1
7.51	78.6	1.4	5.7	0.6	84.3

Table 7.17. Multi-metal extraction data for Zn(II), Co(II) and Ni(II) using 0.05 M 1,3-dimethyl-4-[4-nonylphenylaldenamine]-pyrazol-5-thione (**31**) in toluene.

pH	Organic (%)	Error (\pm x %)	Aqueous (%)	Error (\pm x %)	Mass Balance
Zinc					
2.53	1.68	0.06	93.0	8.6	94.7
3.11	10.73	0.32	83.6	7.6	94.4
3.35	33.48	0.19	64.3	3.1	97.7
3.56	48.38	0.13	48.3	1.6	96.7
3.85	68.90	0.13	32.2	2.8	101.1
4.18	87.90	0.52	17.1	0.5	105.0
4.56	86.61	0.45	6.3	0.5	93.0
4.73	90.93	0.65	5.3	0.5	96.3
5.10	95.03	0.58	4.6	0.6	99.7
6.11	92.87	7.13	4.5	0.6	97.4
6.60	92.66	3.89	4.6	0.3	97.3
6.69	93.09	4.54	4.6	0.1	97.7
7.87	90.28	5.18	4.6	0.1	94.9
10.80	53.13	1.30	4.7	0.3	57.8
Cobalt					
2.53	0.14	0.07	116.4	2.7	116.6
3.11	0.29	0.22	112.8	3.6	113.1
3.35	1.58	0.07	113.7	0.9	115.3
3.56	1.68	0.00	113.5	1.4	115.2
3.85	3.21	0.14	107.8	1.6	111.0
4.18	8.06	0.14	107.6	2.0	115.6
4.56	34.48	0.50	75.4	1.8	109.9
4.73	75.78	0.29	40.6	2.2	116.4
5.10	103.60	0.29	7.0	0.5	110.6
6.11	107.91	2.16	2.7	0.4	110.6
6.60	106.47	2.16	1.6	0.7	108.1
6.69	108.39	1.44	1.0	0.4	109.4
7.87	102.16	1.44	0.7	0.6	102.9
10.80	47.48	1.44	0.8	0.4	48.2
Nickel					
2.53	0.00	0.14	99.1	3.6	99.1
3.11	0.00	0.22	96.6	2.5	96.6
3.35	0.00	0.29	97.1	2.3	97.1
3.56	0.00	0.22	97.2	2.2	97.2
3.85	0.10	0.14	95.5	4.0	95.6
4.18	0.58	0.22	96.4	5.2	97.0
4.56	1.37	0.14	98.1	6.1	99.5
4.73	2.07	0.14	97.3	5.8	99.4
5.10	12.88	0.14	87.4	5.6	100.3
6.11	25.72	2.16	68.0	2.0	93.8
6.60	46.39	1.44	48.8	2.2	95.2
6.69	68.75	1.44	24.8	0.4	93.6
7.87	76.92	2.16	5.5	0.6	82.4
10.80	31.73	1.44	0.8	0.5	32.6

Table 7.18. Multi-metal extraction data for Zn(II), Co(II) and Ni(II) using 0.05 M 1,3-dimethyl-4-[4-nonylphenylaldenamine]-pyrazol-5-thione (**31**) in Orform-SX7.

pH	Organic (%)	Error (\pm x %)	Aqueous (%)	Error (\pm x %)	Mass Balance
Zinc					
4.10	1.7	0.0	98.3	2.2	100.0
5.37	12.0	0.8	89.6	2.9	101.6
5.34	24.4	1.4	80.2	2.4	104.6
5.77	36.8	2.1	72.9	3.5	109.6
5.87	50.1	3.1	62.3	2.5	112.4
5.97	67.0	4.2	49.8	1.8	116.8
6.02	78.2	4.7	39.1	1.4	117.3
6.19	92.1	4.8	26.0	1.5	118.1
6.26	108.9	5.4	13.0	0.6	121.9
6.67	122.5	7.0	3.7	0.2	126.2
Cobalt					
2.19			103.9	5.4	
3.92			102.7	3.5	
5.09			70.0	2.9	
5.50			83.4	2.6	
6.01			53.4	2.6	
6.20			56.2	2.9	
6.23			47.5	2.2	
7.04			21.6	1.8	
7.22			8.9	0.8	
9.24			0.0	0.0	
Nickel					
3.36	0.0	0.1	110.3	2.1	110.3
6.26	6.8	1.3	95.9	1.1	102.7
5.46	19.6	2.3	88.7	3.3	108.3
6.92	25.3	2.5	68.2	3.1	93.6
7.45	34.4	3.4	59.3	3.3	93.7
7.5	26.1	2.4	41.1	3.2	67.2
7.76	41.5	5.9	30.5	1.7	71.9
6.86	40.5	4.3	20.1	1.9	60.6
Copper					
1.25			96.4	4.0	
1.28			96.7	4.1	
1.36			98.0	4.0	
1.44			95.4	3.5	
1.50			93.6	3.4	
1.55			91.5	3.3	
1.69			92.7	3.0	
1.79			90.0	3.0	
1.55			91.5	3.3	
1.96			79.3	2.7	
2.15			71.9	1.6	
2.37			63.2	1.3	

Table 7.19. Single metal extraction data for Zn(II), Co(II), Ni(II) and Cu(II) using 0.05 M 1-phenyl-3-methyl-4-cyclohexylaldenamine-pyrazol-5-thione (**24**) in toluene. Aqueous data only for Co(II) and Cu(II).

pH	Organic (%)	Error (\pm x %)	Aqueous (%)	Error (\pm x %)	Mass Balance
Zinc					
2.82	1.0	0.1	113.0	9.4	114.0
3.36	6.8	0.5	100.9	8.8	107.8
3.57	14.5	0.9	88.3	7.2	102.7
3.80	27.4	1.4	75.4	7.0	102.8
4.07	43.2	1.7	61.2	5.1	104.4
4.46	61.6	2.1	50.9	4.6	112.5
4.64	72.5	1.6	35.6	4.1	108.1
4.93	28.1	1.2	20.0	2.8	48.1
5.80	49.5	1.0	6.8	0.8	56.4
Cobalt					
4.02	1.8	0.1	105.0	1.6	106.8
3.64	13.3	0.8	92.2	1.0	105.5
4.94	27.1	1.0	79.0	1.1	106.1
5.71	40.8	1.3	66.6	0.9	107.4
5.88	55.6	2.0	52.8	2.0	108.4
6.34	74.4	2.3	40.4	2.2	114.8
6.81	86.7	2.3	28.8	1.6	115.5
6.54	102.2	2.1	15.2	1.0	117.3
6.55	120.8	2.0	0.1	0.1	120.8
Nickel					
3.54	2.0	4.1	111.9	2.6	113.87
5.44	9.1	1.4	99.5	2.4	108.58
4.68	23.8	2.0	85.6	2.3	109.38
5.96	36.6	1.4	74.2	0.7	110.75
6.44	50.4	1.7	60.7	0.8	111.07
6.99	41.9	2.6	46.4	1.3	88.21
7.3	66.8	2.8	34.6	2.9	101.44
7.38	71.9	3.9	22.8	1.6	94.71
7.2	77.8	5.6	9.1	4.2	86.93
Copper					
1.80			45.7	1.1	
1.94			46.6	0.7	
1.82			22.8	0.4	
1.96			24.3	0.7	
2.07			17.3	0.4	
2.17			11.7	0.3	
2.63			3.8	0.2	
2.32			6.5	0.2	

Table 7.20. Single metal extraction data for Zn(II), Co(II), Ni(II) and Cu(II) using 0.05 M 1-phenyl-3-methyl-4-[4-*t*-butylphenylaldenamine]-pyrazol-5-thione (**27**) in toluene. Aqueous data only for Cu(II).

pH	Organic (%)	Error (\pm x %)	Aqueous (%)	Error (\pm x %)	Mass Balance
Zinc					
3.38	1.3	0.2	106.7	5.8	108.0
4.10	10.5	1.0	97.8	5.2	108.4
4.41	22.5	1.9	82.7	3.1	105.2
4.46	34.1	1.7	70.6	2.9	104.7
4.65	47.4	3.5	55.8	5.7	103.2
4.86	60.5	4.0	46.9	5.8	107.4
5.03	71.5	4.8	34.5	3.3	106.0
5.34	84.9	4.7	21.8	2.2	106.7
4.56	96.8	6.2	8.4	0.9	105.2
7.39	105.8	6.7	0.1	0.2	105.8
Cobalt					
5.23	9.6	4.5	105.4	0.6	115.0
5.49	19.5	5.6	76.2	0.5	95.7
5.63	34.3	9.0	66.1	1.7	100.4
5.91	48.1	11.7	60.3	0.5	108.4
6.04	47.6	11.3	46.7	1.4	94.3
6.44	60.1	14.3	31.0	0.8	91.1
6.57	68.5	17.4	20.0	0.2	88.4
6.97	92.5	23.2	8.1	0.8	100.6
9.63	82.3	20.9	2.6	0.9	84.8
Nickel					
5.41	0.2	1.2	107.9	0.7	108.1
6.27	25.5	2.4	85.2	1.4	110.7
6.34	21.1	1.5	82.0	0.5	103.1
6.44	50.3	3.8	60.5	1.5	110.7
6.54	32.2	3.2	72.5	1.7	104.7
6.86	44.3	4.2	47.8	1.8	92.1
6.92	61.2	6.6	23.3	1.0	84.4
7.00	67.3	7.7	32.0	0.8	99.3
7.38	86.4	10.4	11.6	0.1	98.1
7.65	89.9	8.5	0.6	1.5	90.5
Copper					
1.93	66.8	6.9	31.1	1.3	97.9
1.95	59.8	5.3	30.3	1.5	90.1
1.97	69.3	3.5	24.7	2.3	94.0
2.00	77.6	7.1	21.6	2.0	99.2
2.00	73.0	8.0	17.0	1.3	89.9
2.17	84.7	7.5	13.8	1.0	98.5
2.31	89.9	6.4	8.7	0.6	98.7
2.54	100.1	7.3	4.7	0.4	104.8
3.16	106.1	8.9	0.7	0.1	106.7
2.44	65.5	4.0	0.1	0.1	65.6

Table 7.21. Single metal extraction data for Zn(II), Co(II), Ni(II) and Cu(II) using 0.05 M 1,3-dimethyl-4-[2-ethylhexylaldenamine]-pyrazol-5-thione (**29**) in toluene.

pH	Organic (%)	Error ($\pm x$ %)	Aqueous (%)	Error ($\pm x$ %)	Mass Balance
Zinc					
2.87	7.6	0.4	100.8	3.1	108.4
3.11	16.8	0.8	86.9	4.5	103.7
3.41	27.4	1.0	78.1	2.8	105.5
3.45	47.9	2.7	69.1	2.6	117.1
4.02	58.2	2.7	55.1	2.0	113.3
4.07	72.9	3.9	44.3	4.0	117.2
4.63	86.8	4.0	32.5	2.9	119.2
5.1	106.8	5.4	20.7	2.0	127.5
5.58	112.6	5.0	7.7	0.5	120.3
Nickel					
4.19	1.1	3.5	116.1	6.7	117.2
4.46	12.0	1.7	102.5	5.1	114.5
4.09	22.8	5.8	91.0	6.3	113.8
3.92	40.5	8.6	81.4	4.7	121.9
6.16	53.6	5.5	61.5	3.6	115.2
6.32	62.6	7.0	54.3	1.7	116.9
6.49	73.5	1.3	36.3	1.8	109.8
6.72	86.4	5.3	24.3	1.1	110.7
7.08	101.0	7.1	10.3	0.6	111.4
7.55	104.1	2.9	0.0	0.8	104.1

Table 7.22. Single metal extraction data for Zn(II) and Ni(II) using 0.05 M 1,3-dimethyl-4-[4-*t*-butylphenylaldenamine]-pyrazol-5-thione (**30**) in toluene.

pH	Organic (%)	Error ($\pm x$ %)	Aqueous (%)	Error ($\pm x$ %)	Mass Balance
5.48			76.8	4.5	
5.54			104.2	4.2	
5.81			67.5	4.7	
5.98			54.9	3.1	
6.02			89.6	7.3	
6.21			43.6	2.3	
6.33			30.7	2.5	
6.49			20.2	1.1	
6.96			6.3	5.4	
8.27			0.5	0.1	

Table 7.23. Single metal extraction data for Zn(II) using 0.05 M 1-phenyl-3-methyl-4-*t*-butylaldenamine-pyrazol-5-thione (**23**) in toluene. Aqueous data only.

Azopyrazolones.

pH	Organic (%)	Error (\pm x %)	Aqueous (%)	Error (\pm x %)	Mass Balance
Zinc					
5.05	0.8	0.1	98.8	11.5	99.6
6.04	59.8	0.2	40.9	3.2	100.8
6.22	60.0	0.6	39.4	2.8	99.5
5.94	65.0	0.6	34.7	2.8	99.7
6.17	51.6	0.3	50.8	4.0	102.4
6.45	83.8	0.3	15.5	0.6	99.3
6.39	70.2	0.4	28.6	1.1	98.8
6.61	80.1	0.4	22.8	1.3	102.9
6.42	71.3	0.6	25.4	0.8	96.7
6.65	89.6	7.1	13.7	1.1	103.3
6.9	82.5	5.2	10.3	0.6	92.8
6.99	71.5	6.5	9.4	0.1	80.9
8.70	33.0	1.3	0.9	0.1	34.0
Cobalt					
5.05	0.2	0.1	110.3	2.7	110.6
6.04	4.0	0.3	104.8	1.3	108.8
6.22	4.3	0.3	106.2	2.3	110.6
5.94	5.3	0.1	108.2	4.0	113.4
6.17	7.7	0.9	75.3	2.2	83.0
6.45	11.4	0.1	99.3	3.6	110.6
6.39	72.9	0.6	38.7	1.1	111.6
6.61	94.5	0.1	20.5	0.7	115.0
6.42	107.4	0.5	14.1	1.3	121.6
6.65	111.8	2.9	6.7	0.7	118.5
6.9	104.1	4.3	4.1	0.9	108.2
6.99	106.5	5.0	4.2	0.4	110.7
8.70	52.8	1.4	0.0	0.6	52.8
Nickel					
5.05	0.1	0.4	96.8	5.4	96.9
6.04	0.4	0.3	99.1	3.8	99.5
6.22	0.5	0.3	99.8	7.4	100.3
5.94	0.5	0.2	98.6	5.9	99.1
6.17	4.3	0.2	98.6	5.2	102.9
6.45	2.3	0.5	96.5	8.1	98.8
6.39	12.8	0.4	89.1	5.6	101.9
6.61	22.2	0.8	80.7	6.3	102.9
6.42	49.3	0.3	56.6	2.0	105.9
6.65	46.9	5.0	47.7	1.3	94.5
6.9	57.7	4.3	25.1	1.6	82.8
6.99	77.6	5.0	7.8	0.5	85.5
8.70	63.9	3.6	1.7	0.9	65.6

Table 7.24. Multi-metal extraction data for Zn(II), Co(II) and Ni(II) using 0.05 M 1-phenyl-3-methyl-4-phenylhydrazono-pyrazol-5-thione (**48**) in toluene.

pH	Organic (%)	Error (\pm x %)	Aqueous (%)	Error (\pm x %)	Mass Balance
Zinc					
4.98	0.8	0.1	103.3	7.0	104.1
5.87	23.1	0.2	72.6	10.4	95.7
6.53	39.5	0.1	48.0	3.4	87.5
6.64	39.1	0.2	45.7	1.5	84.8
6.60	45.1	0.5	40.3	2.4	85.4
6.72	50.5	0.3	50.1	4.4	100.6
6.84	56.8	0.6	28.6	2.4	85.4
6.94	53.1	0.3	19.5	1.1	72.7
7.14	56.4	0.3	7.2	0.8	63.6
7.30	53.1	3.2	6.5	0.2	59.6
7.03	46.4	1.9	10.3	1.1	56.7
7.15	47.7	2.6	6.7	0.5	54.5
8.25	49.0	2.6	0.0	0.3	49.0
Cobalt					
4.98	0.9	0.1	111.6	4.7	112.5
5.87	2.3	0.1	109.7	1.1	112.0
6.53	2.7	0.2	103.7	2.5	106.4
6.64	2.7	0.1	102.9	4.1	105.6
6.60	3.6	0.1	99.8	3.8	103.4
6.72	25.2	0.4	84.1	3.6	109.3
6.84	24.2	0.2	83.0	2.5	107.2
6.94	29.6	0.6	70.4	2.9	100.0
7.14	28.5	0.9	43.5	2.3	72.0
7.30	36.9	4.3	39.9	2.2	76.8
7.03	51.8	1.4	24.0	1.4	75.8
7.15	56.6	2.2	12.2	1.6	68.8
8.25	41.4	2.9	1.1	0.5	42.5
Nickel					
4.98	1.0	0.4	106.6	5.8	107.5
5.87	1.2	0.2	104.5	5.8	105.7
6.53	1.2	0.4	95.7	2.9	96.9
6.64	1.3	0.1	92.4	3.2	93.8
6.60	1.4	0.4	89.6	4.3	91.0
6.72	4.9	0.3	94.4	4.3	99.3
6.84	5.2	0.4	81.7	3.8	86.9
6.94	6.9	0.4	70.3	3.8	77.2
7.14	4.1	0.2	42.4	3.2	46.5
7.30	4.9	2.2	43.1	3.2	48.1
7.03	7.7	2.2	31.6	3.6	39.2
7.15	8.4	3.6	15.9	1.1	24.3
8.25	6.3	1.4	0.1	0.6	6.4

Table 7.25. Multi-metal extraction data for Zn(II), Co(II) and Ni(II) using 0.05 M 1-phenyl-3-methyl-4-[4-*t*-butylphenylhydrazono]-pyrazol-5-thione (**49**) in toluene.

pH	Organic (%)	Error (\pmx %)	Aqueous (%)	Error (\pmx %)	Mass Balance
4.49	0.9	1.6	101.4	2.2	102.3
4.33	11.7	1.9	79.8	4.7	91.5
5.15	25.9	3.1	90.9	1.0	116.8
5.38	41.5	4.6	66.5	3.6	107.9
5.52	60.3	6.0	54.8	2.9	115.0
5.55	77.6	7.5	41.8	1.7	119.4
6.10	87.4	9.9	30.2	1.2	117.6
6.13	106.8	12.1	17.5	0.9	124.3
6.17	113.7	15.7	4.6	0.3	118.3

Table 7.26. Single metal extraction data for Zn(II) using 0.05 M 1-phenyl-3-methyl-4-phenylhydrazono-pyrazol-5-thione (**48**) in toluene.

References.

1. W. Clegg, *Acta. Crystallogr.*, 1981, **A37**, 22.
2. G.M. Sheldrick, SHELXTL version 5, Siemens Analytical X-ray Instrument, Madison, Wisc., USA, 1995.
3. A. Altomare, M.C. Burla, M. Camalli, G. Cascarano, C. Giacovazzo, A. Guagliardi, G. Polidori, *J. Appl. Cryst.*, 1994, **27**, 435.
4. P.T. Beurskens, G. Beurskens, W.P. Bosman, R. de Gelder, S. Garcica-Granda, R.O. Gould, R. Israël, J.M.M. Smits, DIRDIF-96, Crystallography Laboratory, University of Nijmegen, The Netherlands, 1996.
5. R.H. Blessing, *Acta. Crystallogr.*, 1995, **A51**, 33.
6. R.H. Blessing, *J. Appl. Cryst.*, 1997, **30**, 421.
7. Microcal Origin 5.0 software, Inc.
8. Dr. Aid Bisson, personal communication, Avecia.